U.PORTO
FACULDADE DE CIÊNCIAS
UNIVERSIDADE DO PORTO

PhD

3rd CYCLE

FCUP
2026

U.PORTO

Conversion of Organic Waste into Multicolor Carbon Quantum Dots (CQDs) for use in Energy Efficient White LEDs (WLEDs)

Sónia Fernandes

FC

U.PORTO
FACULDADE DE CIÊNCIAS
UNIVERSIDADE DO PORTO

Conversion of Organic Waste into Multicolor Carbon Quantum Dots (CQDs) for use in Energy Efficient White LEDs (WLEDs)

Sónia Fernandes
Doctoral Program in Environmental Sciences and Technology
Department of Geosciences, Environment and Spatial Plannings
Faculty of Sciences of the University of Porto
2026

PhD

Conversion of Organic Waste into Multicolor Carbon Quantum Dots (CQDs) for use in Energy Efficient White LEDs (WLEDs)

Sónia Fernandes

Thesis carried out as part of the Doctoral Program in Environmental Sciences and Technology

Department of Geosciences, Environment and Spatial Plannings

2026

Supervisor
Luís Pinto da Silva, Assistant Professor, FCUP

Co-supervisor
Joaquim C. G. Esteves da Silva, Full Professor, FCUP

Dedicated to my family

Acknowledgements

I would like to express my sincere gratitude to the *Fundação Portuguesa para a Ciência e a Tecnologia* (FCT) for supporting my PhD through the fellowship 2021.05479.BD, funded by national resources from the Ministry of Education and Science.

I also acknowledge FCT for funding the R&D unit CIQUP (UID/00081/2025) and the Associate Laboratory IMS (LA/P/0056/2020), within which this research was conducted, as well as the Scientific Employment Stimulus (CEECINST/00069/2021) that supported Professor Dr. Luís Pinto da Silva.

Financial support from the projects FCT - 2023.13127.PEX, NORTE 2030 - RESTAURA (NORTE2030-FEDER-02704900), iChem4M (NORTE2030-FEDER-02706400), and AGRO-CIRN (NORTE2030-FEDER-02703200) is also gratefully acknowledged.

I would like to begin by expressing my deepest gratitude to my supervisor, Professor Dr. Luís Pinto da Silva, whose guidance, patience, and encouragement have been invaluable throughout this journey. I feel privileged to have learned so much under your mentorship, for your unwavering support, and for teaching me to approach every challenge with a positive mindset.

I am equally grateful to my co-supervisor, Professor Dr. Joaquim C. G. Esteves da Silva, for all the opportunities to learn and develop as part of your research group, for your guidance and leadership, and for fostering a stimulating environment that encouraged curiosity and continuous growth.

I would also like to thank CIQUP for providing an excellent research environment, access to resources, and support throughout my PhD.

I am especially thankful to my colleagues and fellow PhD students (Diana, Carla, Paulo, Ricardo, Jul, Hadi, and Archana). What started as professional collaboration soon grew into friendships that I deeply treasure. From stimulating discussions to shared moments of laughter and support, you have all been more than colleagues, Diana, Carla, Paulo, and Ricardo you have become a second family throughout this journey.

To my friends outside the lab, thank you for your constant encouragement and for reminding me that life exists beyond the pages of a thesis. The monthly dinners during my final year of the PhD were especially precious, protecting my mental well-being but

also gave me all the support I needed. Ana, Amanda, and Bia you believed in me even more than I did myself, and your friendship has meant more than words can convey.

Finally, I am profoundly grateful to my family. Your unconditional love, patience, and belief in me have been my constant source of strength. You have celebrated my successes, lifted me through challenges, and reminded me of the bigger picture when the path seemed uncertain. This thesis is as much yours as it is mine.

Resumo

A transição para sistemas energéticos mais sustentáveis exige o desenvolvimento de materiais e processos que conciliem o elevado desempenho funcional com o menor impacto ambiental. Neste contexto, os *carbon dots* (CDs) emergiram como nanomateriais luminescentes promissores, devido à sua fotoluminescência ajustável, estabilidade química, baixa toxicidade e potencial de síntese a partir de fontes de carbono abundantes e renováveis, incluindo resíduos orgânicos. Estas características tornam os CDs candidatos para aplicações relacionadas com iluminação, nomeadamente como componentes alternativos ou complementares em tecnologias de luz branca.

A presente tese de doutoramento investiga os CDs como materiais luminescentes sustentáveis, integrando avaliação do ciclo de vida (ACV), estratégias de síntese verde e estudos fundamentais de fotofísica. A tese segue uma abordagem baseada em artigos científicos e analisa os desafios-chave associados à produção de CDs, nomeadamente a sustentabilidade ambiental dos procedimentos de síntese, a valorização de resíduos como precursores de carbono e a compreensão das relações estrutura-propriedade que governam a fotoluminescência.

Numa primeira fase, é realizada uma ACV comparativa "*cradle-to-grave"* de seis procedimentos representativos de síntese "*bottom-up"*, incluindo estratégias convencionais e de elevado rendimento. Os resultados demonstram que rendimentos de síntese mais elevados não implicam necessariamente um melhor desempenho ambiental, uma vez que, os benefícios associados à eficiência do material podem ser compensados pelo aumento do consumo energético, complexidade do processo e utilização adicional de reagentes. O consumo de energia e a produção dos precursores foram identificados como os maiores contribuidores para os impactos ambientais, salientando a importância da simplicidade do processo e de condições energicamente eficientes.

Subsequentemente, desenvolve-se uma estratégia de síntese hidrotermal simples e ambientalmente benigna para a produção de CDs altamente fluorescentes a partir de diferentes resíduos orgânicos. A combinação de precursores derivados de resíduos com ácido cítrico e etilenodiamina permite alcançar uma dopagem de azoto consistente e a passivação superficial, resultando em rendimentos quânticos de fluorescência (QY_{FL}) superiores a 20% sob condições de reação suaves. Este trabalho demonstra que a valorização de resíduos e o elevado desempenho ótico podem ser

obtidos simultaneamente por meio da seleção racional de precursores e procedimentos de síntese simplificados.

Por fim, investiga-se a influência de precursores contendo enxofre em CDs dopados com azoto e azoto/enxofre. Os resultados evidenciam que a modulação da fluorescência é predominantemente dominada por efeitos de oxidação superficial, e não pela incorporação direta de enxofre, contribuindo para uma melhor compreensão dos mecanismos que controlam a emissão dos CDs e esclarecendo a influência de parâmetros de síntese relacionados com heteroátomos.

No seu conjunto, esta tese demonstra que é possível conciliar sustentabilidade ambiental, simplicidade de processo e elevado desempenho luminescente na conceção de CDs, estabelecendo bases sólidas para a sua futura aplicação em tecnologias de iluminação e fotónica sustentável.

Palavras-chave: *Carbon Dots*, nanomateriais sustentáveis, rendimento quântico de fluorescência, avaliação de ciclo de vida, síntese sustentável, valorização de resíduos, fotoluminescência, química de superfície, eficiência energética, LEDs de luz branca

Abstract

The transition towards more sustainable energy systems requires the development of materials and processes that combine high functional performance with reduced environmental impacts. In this context, carbon dots (CDs) have emerged as promising luminescent nanomaterials due to their tunable photoluminescence, chemical stability, low toxicity, and potential for synthesis from abundant and renewable carbon sources, including organic waste. These characteristics make CDs attractive candidates for lighting-related applications, particularly as alternative or complementary components in white light-emitting technologies.

This PhD thesis investigates CDs as sustainable luminescent materials by integrating life cycle assessment (LCA), green synthesis strategies, and fundamental photophysical studies. An article-based approach is adopted to address key challenges associated with CDs production, namely the environmental sustainability of synthesis routes, the use of waste-derived precursors, and the understanding of structure-property relationships governing photoluminescence.

First, a comparative cradle-to-grave LCA of six representative bottom-up synthesis routes is performed, encompassing both conventional and high-yield strategies. The results demonstrate that higher synthesis yields do not inherently lead to improved environmental performance, as gains in material efficiency are often offset by increased energy demand, process complexity, and reagent consumption. Energy use and precursor production are identified as the major contributors to environmental impacts, highlighting the importance of process simplicity and energy-efficient conditions.

Second, a facile and environmentally benign hydrothermal synthesis strategy is developed to produce brightly fluorescent CDs from a range of organic waste materials. By combining waste-derived precursors with citric acid and ethylenediamine, consistent nitrogen doping and surface passivation are achieved, enabling fluorescence quantum yields (QY_{FL}) exceeding 20% while maintaining mild reaction conditions. This work demonstrates that waste valorization and high optical performance can be simultaneously achieved through rational precursor selection and simplified synthesis procedures.

Finally, the role of sulfur-containing precursors in nitrogen- and nitrogen/sulfur-modified CDs is systematically investigated. The results reveal that fluorescence

modulation is primarily governed by surface oxidation effects rather than direct sulfur doping, providing new insights into the mechanisms controlling CDs photoluminescence and clarifying the influence of heteroatom-related synthesis parameters.

Overall, this thesis establishes an integrated framework for the sustainable design of CDs, demonstrating that environmental responsibility, process simplicity, and high luminescent performance can be jointly addressed. The findings contribute to the rational development of CDs as sustainable luminescent materials and provide a solid foundation for their future implementation in white light-emitting and related photonic technologies.

Keywords: Carbon Dots, sustainable nanomaterials, fluorescence quantum yield, Life Cycle Assessment, green synthesis, waste valorization, photoluminescence, surface chemistry, energy efficiency, white light-emitting technologies

Publications and Presentations of the Author Containing Work Related to this Thesis

The research work reported in this thesis was disseminated through oral and poster communications at scientific meetings and published in peer-reviewed international journals.

A. Published papers as first author

Sónia Fernandes, Joaquim C.G. Esteves da Silva, Luís Pinto da Silva, Life Cycle Assessment-Based Comparative Study between High-Yield and "Standard" Bottom-Up Procedures for the Fabrication of Carbon Dots, *Materials* **2022**, 15, 3446, DOI: https://doi.org/10.3390/ma15103446;

Sónia Fernandes, Manuel Algarra, Antonio Gil, Joaquim C.G. Esteves da Silva, Luís Pinto da Silva, Development of a Facile and Green Synthesis Strategy for Brightly Fluorescent Carbon Dots from Various Waste Materials, *ChemSusChem* **2025**, 18, DOI: https://doi.org/10.1002/cssc.202401702;

Sónia Fernandes, Manuel Algarra, Ana T.S.C. Brandão, Antonio Gil, Carlos M. Pereira, Joaquim C.G. Esteves da Silva, Luís Pinto da Silva, Insights into the role of common sulfur precursors in hydrothermally synthesized N,S-doped Carbon Dots: Fluorescence modulation *via* surface oxidation rather than sulfur doping, *Nanoscale* **2026**, 18, 9894-9907, DOI: https://doi.org/10.1039/d5nr05082k.

B. Published papers not as first author

Gabriela Rodríguez-Carballo, Ramón Moreno-Tost, Sónia Fernandes, Joaquim C.G. Esteves da Silva, Luís Pinto da Silva, Eulogio Castro Galiano, Manuel Algarra, Nitrogen doped carbon dots as a photocatalyst based on biomass. A life cycle assessment, *Journal of Cleaner Production* **2023**, 423, 138728, DOI: https://doi.org/10.1016/j.jclepro.2023.138728;

Carla M. Magalhães, Eduarda Ribeiro, Sónia Fernandes, Joaquim Esteves da Silva, Nuno Vale, Luís Pinto da Silva, Safety Evaluation of Carbon Dots in UM-UC-5 and A549 Cells for Biomedical Applications, *Cancers* **2024**, (16)9, 3332, DOI: https://doi.org/10.3390/cancers16193332.

C. Oral Communications as Presenting author

Sónia Fernandes, Joaquim C.G. Esteves da Silva, Luís Pinto da Silva (2023) Sustainable fabrication of fluorescent carbon quantum dots (CQDs), PhotoOnline' 2023, SP2P, Online Conference.

Sónia Fernandes, Joaquim C.G. Esteves da Silva, Luís Pinto da Silva (2023) Carbon Dots from organic waste: synthesis, characterization, and a comparative Life Cycle Assessment, XXVII Encontro Luso-Galego de Química, Porto, Portugal.

Sónia Fernandes, Joaquim C.G. Esteves da Silva, Luís Pinto da Silva (2024) Carbon Dots based on sustainable carbon precursors and their potential for sensing applications, The 1st International Online Conference on Photonics, Online Conference, Photonic, MDPI.

Sónia Fernandes, Joaquim C.G. Esteves da Silva, Luís Pinto da Silva (2025) Development of a Fabrication Strategy for Upcycling Organic Waste into Brightly Fluorescent Carbon Dots, XXIX Encontro Nacional da SPQ, Coimbra, Portugal.

Sónia Fernandes, Joaquim C.G. Esteves da Silva, Luís Pinto da Silva (2025) Sustainable Strategy for Upcycling Organic Waste into Highly Luminescent Carbon Dots, The 5th International Online Conference on Nanomaterials, Online Conference, MDPI.

Structure of the Thesis

This thesis is organized into three main sections: an introductory section, the body of the work, and a final section dedicated to conclusions and future perspectives. The core chapters of the thesis are structured around scientific articles published in peer-reviewed international journals.

Chapter 1 presents a comprehensive overview of the challenges associated with environmental sustainability in the context of the lighting sector and Carbon Dots (CDs). It addresses global climate change and the reduction of greenhouse gas (GHG) emissions within European climate and energy policy frameworks, emphasizing energy efficiency and renewable energy integration. The lighting sector is discussed with a focus on energy-efficient technologies, particularly light-emitting diodes (LEDs), their operating principles, and the limitations of conventional white LEDs based on blue chips and rare-earth phosphors, motivating alternative UV-LED-based approaches. Carbon dots (CDs) are then introduced as emerging sustainable nanomaterials, highlighting their key properties, bottom-up synthesis strategies, and the relevance of renewable and waste-derived carbon sources. The chapter also presents life cycle assessment (LCA) as a central tool for the environmental evaluation of nanomaterial synthesis.

The second section of the thesis comprises three chapters addressing different but complementary aspects of CDs development. Chapter 2 focuses on the LCA of bottom-up synthesis routes for CDs, presenting a comparative evaluation of conventional and high-yield approaches. This chapter identifies the main environmental hotspots and the key parameters governing the overall sustainability of CDs production. Chapter 3 addresses the development of green and facile synthesis strategies for CDs using waste-derived carbon precursors, with emphasis on precursor selection and the development of simple, energy-efficient, and environmentally benign routes for highly fluorescent CDs. Chapter 4 investigates the influence of sulfur-containing precursors on the structural and photophysical properties of N,S-doped CDs, contributing to a deeper understanding of heteroatom doping strategies and structure-property relationships.

The final section of the thesis summarizes the main conclusions drawn from the work developed, highlighting the principal scientific contributions of this research and outlining perspectives for future studies. In addition, the appendices include relevant works developed in collaboration with other researchers that complement and extend the core themes addressed in the thesis.

Table of Contents

List of Tables

List of Figures

List of Abbreviations

GHG	GREENHOUSE GAS
SDGs	SUSTAINABLE DEVELOPMENT GOALS
GSML	GLOBAL MEAN SEA LEVEL
UNFCCC	UNITED NATIONS FRAMEWORK CONVENTION ON CLIMATE CHANGE
IPCC	INTERGOVERNMENTAL PANEL ON CLIMATE CHANGE
CO_2	CARBON DIOXIDE
CH_4	METHANE
N_2O	NITROUS OXIDE
GMST	GLOBAL MEAN SURFACE TEMPERATURE
LAI	LEAF AREA INDEX
EDGAR	EMISSIONS DATABASE FOR GLOBAL ATMOSPHERIC RESEARCH
LULUCF	LAND USE, LAND USE CHANGE AND FORESTRY
EU27	EUROPEAN UNION WITH 27 MEMBERS STATES
NDCs	NATIONALLY DETERMINED CONTRIBUTIONS
EU ETS	EUROPEAN EMISSIONS TRADING SYSTEM
LED	LIGHT EMITTING DIODE
CFL	COMPACT FLUORESCENT LAMP
IL	INCANDESCENT LAMP
HL	HALOGEN LAMP
FL	FLUORESCENT LAMP
UV	ULTRAVIOLET (200-400 nm)
SSL	SOLID-STATE LIGHTING
RoHS	RESTRICTION OF HAZARDOUS SUBSTANCES
WLED	WHITE LIGHT-EMITTING DIODE
NUV	NEAR ULTRAVIOLET
CCT	CORRELATED COLOR TEMPERATURE
CRI	COLOR RENDERING INDEX
RGB	RED, GREEN, BLUE
LCA	LIFE CYCLE ASSESSMENT
REE	RARE-EARTH ELEMENT
WEEE	WASTE ELECTRICAL AND ELECTRONIC EQUIPMENT
UV-A	ULTRAVIOLET A (320-400 nm)

CDs	CARBON DOTS
QY_{FL}	FLUORESCENCE QUANTUM YIELD
EDA	ETHYLENEDIAMINE
PEI	POLYETHYLENIMINE
VOCs	VOLATILE ORGANIC COMPOUNDS
DESs	DEEP EUTECTIC SOLVENTS
PVP	POLYVINYLPYRROLIDONE
PMMA	POLYMETHYL METHACRYLATE
LCIA	LIFE CYCLE IMPACT ASSESSMENT
XPS	X-RAY PHOTOELCTRON SPECTROSCOPY
XRD	X-RAY DIFRACTION
AFM	ATOMIC FORCE MISCROSCOPY
CEMUP	MATERIALS CENTRE OF THE UNIVERSITY OF PORTO
FT-IR	FOURIER-TRANSFORM INFRARED SPECTROSCOPY
N-CDs	NIROGEN-DOPED CDs
N,S-CDs	NITROGEN, SULFUR-DOPED CDs
DLS	DYNAMIC LIGHT SCATTERING
EPR	ELECTRON PARAMAGNETIC RESONANCE

1. Introduction

1.1. Sustainability: Historical origins and conceptual framework

Industrialization in the eighteenth century marked a profound shift in the relationship between human societies and the natural environment, intensifying resource exploitation and environmental degradation. These transformations gradually prompted growing concern over the long-term consequences of human activities on natural systems. This awareness culminated in the United Nations Conference on the Human Environment, held in Stockholm from June 5 to 16, 1972, which led to the adoption of the Stockholm Declaration. Comprising 26 principles, the Declaration articulated a shared responsibility to protect and improve the human environment. Although it did not explicitly employ the term *sustainable development*, its emphasis on safeguarding the environment for present and future generations introduced the principle of intergenerational responsibility, thereby laying the conceptual foundations of sustainability.

Over the subsequent decades, sustainability has emerged as a central paradigm across scientific, political, and industrial domains, responding to the interconnected challenges of environmental degradation, social inequality, and economic growth. As a result, it has become a foundational framework underpinning contemporary discourse on environmental policy, development planning, and scientific research. The concept was formally articulated in the Brundtland Report [1], which defined *sustainable development* as “development that meets the needs of the present without compromising the ability of future generations to meet their own needs.”

Since then, sustainability has evolved into a multidimensional framework encompassing three interrelated and mutually reinforcing pillars (Figure 1): environmental integrity, social equity, and economic viability [2]. While this representation is widely used to illustrate the multidimensional nature of sustainability, it should be understood as a conceptual heuristic rather than a prescriptive model, as interactions and trade-offs among dimensions are context-dependent. These pillars function not only as normative guiding principles but also as analytical criteria for evaluating the long-term impacts of human activities on natural and social systems. The environmental dimension emphasizes the preservation of ecosystems, biodiversity, and the Earth’s life-supporting functions through responsible resource use and pollution reduction [3]. The social dimension focuses on equity, justice, and human well-being, including access to basic services, human rights, and the protection of cultural integrity

[4]. The economic dimension seeks to balance growth with efficiency and long-term resilience, promoting productive systems that are both regenerative and inclusive [5].

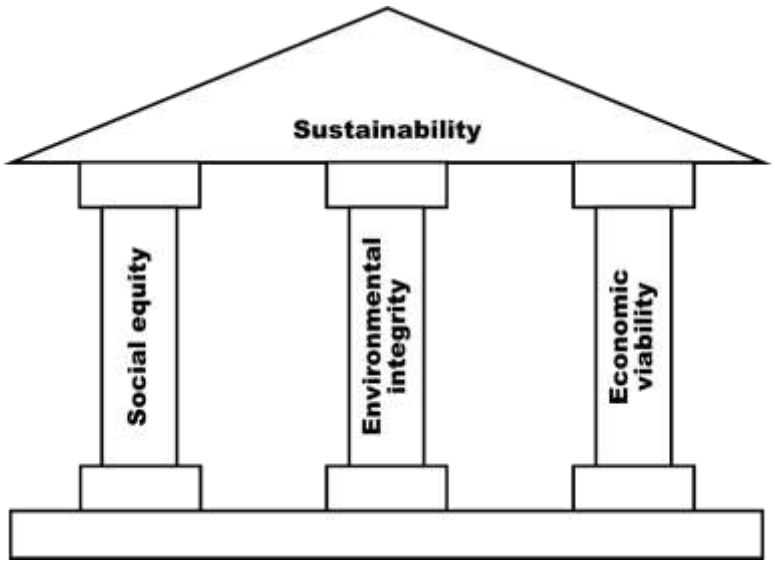

Figure 1. Conceptual representation of the three interrelated pillars of sustainability: environmental integrity, social equity, and economic viability. The model illustrates sustainability as a framework dependent on the balanced integration of these dimensions. Adapted from Purvis *et al.*, 2018 [2].

The urgency of integrating these dimensions has intensified in the context of accelerating environmental degradation, particularly climate change. Anthropogenic increases in greenhouse gas (GHG) emissions have disrupted the Earth's climate system, resulting in rising global temperatures, altered precipitation patterns, and an increased frequency and intensity of extreme weather events [6]. These changes pose significant risks not only to ecological stability but also to social and economic systems, disproportionately affecting vulnerable populations and regions [7].

In response to these challenges, sustainability has increasingly been translated into global policy frameworks aimed at operationalizing its principles. A major milestone in this process was the adoption of the United Nations 2030 Agenda for Sustainable Development, which established 17 Sustainable Development Goals (SDGs) as an integrated and universal roadmap for addressing environmental, social, and economic challenges [8]. The SDGs reflect the interdependent nature of sustainability objectives, providing a policy-oriented mechanism through which abstract principles are transformed into measurable targets and actions across multiple governance levels [9].

Despite its widespread adoption, sustainability remains a concept characterized by normative and conceptual ambiguity. It functions simultaneously as an analytical framework for understanding human-environment interactions and as a normative vision that articulates societal values and long-term development goals [10]. While normative

interpretations emphasize ethical considerations such as intergenerational justice and social equity, operational approaches seek to translate sustainability into indicators, assessment tools, and decision-making frameworks capable of guiding policy and practice [11].

The operationalization of sustainability is further complicated by the need to address multiple spatial and temporal scales. Sustainability challenges manifest differently at global, national, regional, and local scale, often involving trade-offs between short-term gains and long-term consequences [12]. Actions taken at one level may generate unintended effects at another, underscoring the importance of multi-level governance and systems-based approaches that account for cross-scale interactions and cumulative impacts [13].

Moreover, the integration of environmental, social, and economic objectives inherently involves tensions and trade-offs. Efforts to promote economic growth may conflict with environmental protection, while conservation measures can generate social or economic costs if not carefully designed [14]. Addressing these trade-offs requires governance frameworks capable of managing uncertainty, balancing competing objectives, and fostering inclusive and transparent decision-making processes [15]. Rather than seeking to eliminate trade-offs entirely, contemporary sustainability research emphasizes the importance of making them explicit and subject to deliberation, thereby enabling more informed, equitable, and resilient development pathways [16].

Thus, sustainability constitutes both an ethical imperative grounded in intergenerational responsibility and a practical framework for addressing the climate crisis. By integrating environmental limits with social needs and economic strategies, sustainability-oriented approaches enable the mitigation of GHG emissions, the enhancement of socio-ecological resilience, and the pursuit of development pathways that are viable, equitable, and consistent with the Earth's biophysical boundaries.

1.2. Climate change: Drivers, GHG emissions and sectorial contributions

This section introduces the scientific basis of climate change by synthesizing observational evidence, underlying physical mechanisms, and recent global, regional, and national GHG emission trends. The discussion is structured around four complementary perspectives: (1.2.1.) evidence of ongoing climate change, (1.2.2.) its primary causes and physical mechanisms, (1.2.3.) global and regional GHG emissions trends, providing a coherent framework for subsequent analysis of mitigation strategies,

and (1.2.4.) the policy context and the dominant role of the energy sector in shaping mitigation priorities.

1.2.1. Evidence of climate change

In the last decades, the Earth has experienced increasingly frequent and severe environmental disruptions, including rising sea levels, prolonged droughts, glacier retreat, and a growing incidence of extreme weather events. These phenomena are not isolated anomalies but indicators of a systemic shift in the global climate, which scientific consensus attributes primarily to anthropogenic activities since the Industrial Revolution, including fossil fuel combustion, deforestation, and rapid industrialization. In fact, the Industrial Revolution period was marked by rapid industrialization, population growth, and widespread deforestation, profoundly altering the chemical composition of the atmosphere and intensifying the Earth's natural greenhouse effect.

Observable impacts of climate change are already widespread. Global Mean Sea Level (GSML) rose by approximately 17 cm over the last 100 years (1920-2020) due to thermal expansion of warming oceans and accelerated melting of mountain glaciers and polar ice sheets, thereby increasing risks of coastal erosion, saltwater intrusion, and flooding [17-19]. At the same time, subtropical and Mediterranean regions have experienced longer and more intense droughts, as rising temperatures enhance evapotranspiration and modify precipitation patterns linked to oceanic circulation changes [20-22]. Glaciers worldwide are retreating at unprecedented rates. The Himalayas are a good example of this argument as it faces, ice mass losses of up to 25% over the past 30 years threatening freshwater availability for nearly two billion people downstream [23, 24]. These trends are compounded by the increasing frequency and intensity of extreme weather events, including more powerful hurricanes, record-breaking heatwaves, and heavy precipitation, fueled by warmer sea surfaces and greater atmospheric moisture content [21].

According to the Article 1 of the United Nations Framework Convention on Climate Change (UNFCCC) in 1992, Climate Change is "a change of climate which is attributed directly or indirectly to human activity that alters the composition of the global atmosphere, and which is in addition to natural climate variability observed over comparable time periods". Similarly, the Intergovernmental Panel on Climate Change (IPCC) describes Climate Change as a long-term alteration in the state of the climate, typically persisting for decades or longer, caused by natural variability or human influences that modifies the composition of the atmosphere [17].

1.2.2. Causes and mechanisms

Climate change is primarily driven by the intensification of greenhouse effect due to elevated concentrations of greenhouse gases in the atmosphere. Greenhouse effect is a natural mechanism in which GHG such as carbon dioxide (CO_2), methane (CH_4), nitrous oxide (N_2O) and water vapor due to their molecular structures can absorb and re-emit infrared radiation, maintaining Earth's surface temperature of circa 30°C warmer than it would be in their absence [25, 26]. However, since the mid-eighteenth century, large-scale combustion of fossil fuels, intensive agriculture, and deforestation to support human development have substantially amplified the greenhouse effect, creating an energy imbalance that drives global warming and associated climatic disruptions. Therefore, the enhancement of the greenhouse effect by anthropogenic greenhouse gas emissions is the principal driver of contemporary climate change.

Since the pre-industrial era, anthropogenic greenhouse gas emissions have markedly altered atmospheric composition with the increase of CO_2 from the combustion of coal, oil and natural gas, CH_4 from agricultural activities and fossil-fuel extraction, and N_2O from synthetic fertilizer application and industrial processes. Atmospheric concentrations of these GHGs have increased (Figure 2) from roughly 278.3 ppm (pre-industrial concentrations in 1750) to 420±0.1 ppm of CO_2 (a rise of 151%), 729.2 ppb to 1934±2 ppb (a 265% rise) of CH_4 and 270.1 ppb to 336.9±0.1 ppb (a 125% rise) of N_2O [21]. These elevated GHGs levels have driven an increase in Global Mean Surface Temperature (GMST) relative to pre-industrial levels, particularly in the period between 2011 to 2020 GMST was 1.09 (0.95 to 1.20)°C higher than 1850-1900 (period used as representative for pre-industrial conditions) [17].

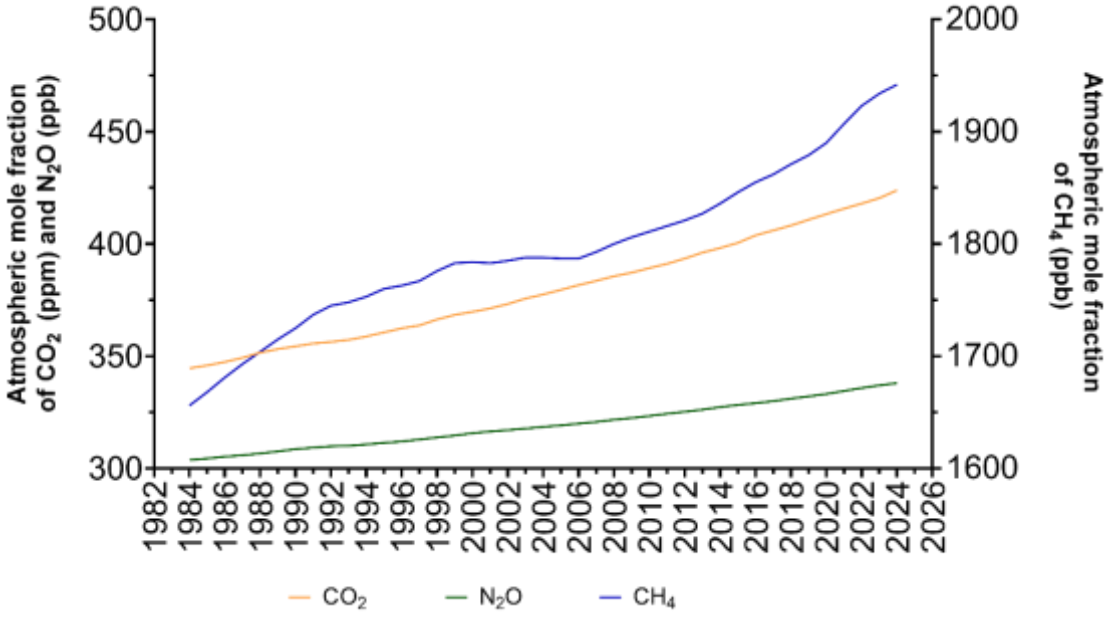

Figure 2. Annual mean globally averaged atmospheric mole fraction of CO_2, CH_4, and N_2O from 1984 to 2024. Data from World Data Centre for Greenhouse Gases (current state of GHGs) [27].

These warming trends are further amplified by several key climate feedback mechanisms. In fact, diminishing snow and ice cover reduces Earth's surface albedo, thereby enhancing solar radiation absorption and accelerating warming [17]. On the other hand, thawing permafrost in high-latitude regions releases previously sequestered CH_4 and CO_2, reinforcing GHGs load [17]. Adding to these, changes in anthropogenic land use such as large-scale deforestation and conversion of natural ecosystems to agricultural or urban land, degrade terrestrial carbon sinks and further exacerbate atmospheric GHGs accumulation [17, 22].

Despite natural processes contribute to the atmospheric GHGs load, such as volcanic degassing that releases about 0.13 Gt CO_2 yr^{-1} [28], and wetland biogenic emissions amount to roughly 200-300 Tg CH_4 yr^{-1} [29], their magnitude is minor compared to anthropogenic emissions.

It is also important to recognize that the natural greenhouse effect has been essential for maintaining habitable conditions on Earth over geological timescales, for example by trapping sufficient heat to sustain liquid water at the planet's surface. In addition, elevated atmospheric CO_2 concentrations can enhance plant photosynthesis and water-use efficiency, a phenomenon commonly referred to as the CO_2 fertilization effect.

Satellite observations combined with model analyses have revealed a persistent increase in global vegetation *"greenness"* detected as increases in leaf area index (LAI) across approximately 25-50% of the world's vegetated land surface. This trend has been largely attributed to rising atmospheric CO_2 concentrations, with CO_2 fertilization accounting for the dominant fraction (≈70%) of the observed greening during the period between 1980-2009 [30]. Elevated CO_2 concentrations also appear to increase forest water-use efficiency by reducing stomatal conductance relative to carbon uptake, consistent with fertilization responses reported in long-term ecosystem and tree-ring measurements [31].

However, the magnitude and persistence of the CO_2 fertilization effect are strongly constrained by nutrient availability (particularly, nitrogen and phosphorus), as well as by water stress and rising temperatures. As a result, this effect does not offset the broader ecological, climatic, and socio-economic risks associated with anthropogenic climate change. Observational and experimental evidence indicates that, although elevated CO_2 can stimulate plant productivity under certain conditions, the capacity of terrestrial ecosystems to function as a sustained net carbon sink depends on multiple interacting drivers. Consequently, any benefits associated with enhanced plant growth do not negate the adverse impacts of warming, increasing drought frequency, extreme climate events, and ongoing ecosystem degradation [32].

1.2.3. Global and regional GHG trends

According to the Emissions Database for Global Atmospheric Research (EDGAR), global GHG emissions reached 53.2 Gt CO_{2eq} in 2024, excluding Land Use, Land Use Change and Forestry (LULUCF), representing a 1.3% increase relative to 2023 [33]. In 2024 (Figure 3), the majority of global GHG emissions were dominated by fossil CO_2, representing 74.5% of total emissions, while CH_4 contributed to 17.9% of the total, N_2O to 4.8% and fluorinated gases to 2.8% [33].

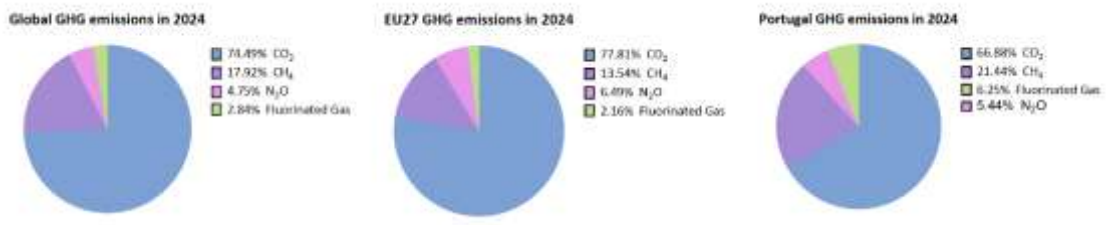

Figure 3. GHG emissions, comprising CO_2, CH_4, N_2O, and Fluorinated gas (F-gas) in 2024, from a global, European Union with 27 Member States (EU27), and Portugal perspective.

According to the trend of global GHG emissions from EDGAR, between 1990 and 2024, fossil CO_2 rose by 75% (from 22.7 to 39.6 Gt CO_{2eq}), CH_4 by 30% (from 7.3 to 9.5 Gt CO_{2eq}) and N_2O by 34.4% (from 1.9 to 2.5 Gt CO_{2eq}), while fluorinated gases experienced the most pronounced increase, surging by 310.4% (from 0.37 to 1.51 Gt CO_{2eq}). Over the same period, sectoral emissions evolved markedly with power industry increased by 104%, industrial combustion and processes by 93%, transport by 79%, fuel exploitation by 52%, waste by 46% and agriculture by 25%, while emissions from buildings declined by 4% (Figure 4).

On the other hand, the European Union with 27 Member States (EU27) recorded total GHG emissions of 3.2 Gt CO_{2eq} in 2024, reflecting a 1.8% decline from 2023 and a sustained downward trend since 1990. In 2024, CO_2 accounted for 77.8% of total EU27 emissions, CH_4 13.5%, N_2O 6.5%, and fluorinated gases 2.2% (Figure 3). Over the period 1990-2024, GHG emissions in EU27 have followed a steady downward trajectory over the past three decades with fossil CO_2 decreasing by 35.3% (from 3.8 to 2.5 Gt CO_{2eq}), CH_4 by 38.3% (from 0.69 to 0.43 Gt CO_{2eq}) and N_2O by 34.6% (from 0.31 to 0.21 Gt CO_{2eq}), whereas fluorinated gas emissions rose by 35.3% (from 0.05 to 0.07 Gt CO_{2eq}). Sectoral GHGs emissions in the EU27 between 1990 and 2024 declined several sectors, such as in power industry (55%), industrial combustion and processes (42%), buildings (39%), fuel exploitation (46%), agriculture (28%) and waste (31%), while transport increased by 21% (Figure 4).

Portugal's total GHGs emissions were 5.3 Gt CO_{2eq} in 2024, in which fossil CO_2 accounted for 66.9% of the national total, CH_4 for 21.4%, N_2O for 5.4% and fluorinated gases for 6.3% (Figure 3). Compared with GHGs emissions reported for the EU27 in 2024, Portugal shows a relatively larger contribution from CH_4 and fluorinated gases and a smaller share from CO_2. Portugal's GHG emissions from 1990 to 2024 indicates a decreasing in fossil CO_2 by 18.9% (from 43.9 to 35.6 Mt CO_{2eq}) and N_2O by 23.5% (from 3.8 to 2.9 Mt CO_{2eq}), although the increase in CH_4 by 14.4% (from 9.97 to 11.40 Mt CO_{2eq}), and fluorinated gases by 10079.0% (from 0.03 to 3.32 Mt CO_{2eq}). Portugal GHGs emissions trends between 1990-2024 shows an increased emissions rate in transport (75%), fuel exploitation (55%) and waste (28%), while decreasing in the power industry, industrial combustion and processes, agriculture and buildings by 69%, 15%, 14%, 9%, respectively (Figure 4). Unlike the EU27, where fuel exploitation and waste GHGs emissions decreased in the same period (1990-2024), these two sectors increased in Portugal.

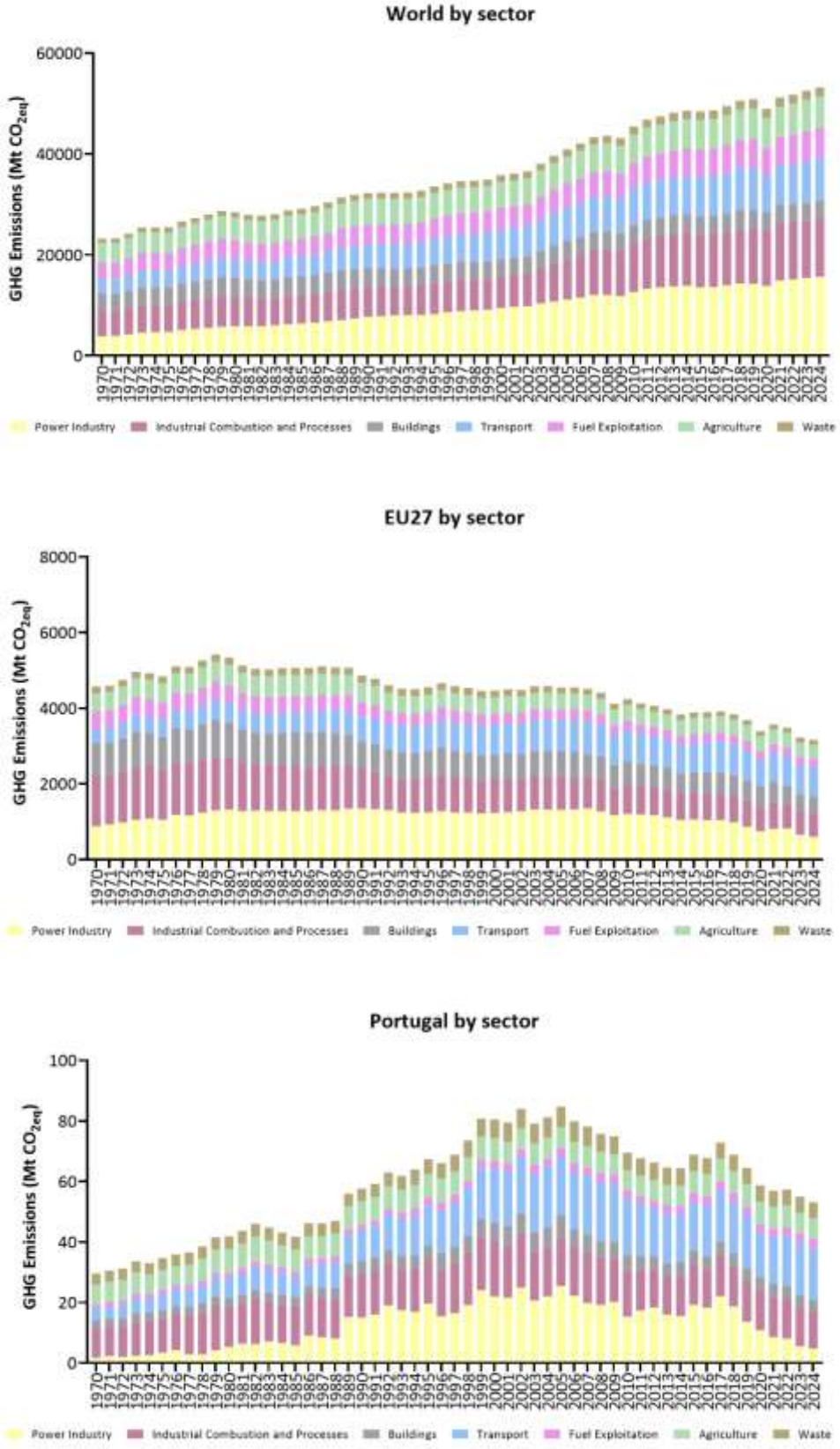

Figure 4. Sectorial GHG emissions from a global, EU27, and Portugal perspective.

Sectoral composition of CO_2, CH_4 and N_2O emissions in 2024 for the World, the EU27 and Portugal (Figure 5), allows to highlight the dominant source sectors and their implications for targeted mitigation strategies across global, regional and national scales. Global CO_2 emissions in 2024 totaled 39.6 Gt CO_{2eq} with the power industry (39.1%), industrial combustion and processes (24.4%) and transport (21.0%) as the main contributors. The EU27 totaled 2.5 Gt CO_{2eq}, dominated by transport (31.8%), power industry (23.9%) and industrial combustion and processes (20.8%). Portugal's CO_2 total was 35.6 Mt CO_{2eq}, with transport accounting for 48.0%, industrial combustion and processes 23.5% and power industry 13.0%. These sectoral patterns indicate that decarbonization of electricity generation and abatement in transport and industry are the highest-impact priorities at global and EU scales, while Portugal's mitigation potential is concentrated in the transport and industrial sectors. Global CH_4 in 2024 totaled 9.5 Gt CO_{2eq}, primarily from agriculture (45.4%) and fuel exploitation (33.9%), with waste contributing 17.3%. EU27 CH_4 emissions totaled 0.43 Gt CO_{2eq}, dominated by agriculture (54.9%) and waste (27.3%). Portugal's CH_4 total was 11.4 Mt CO_{2eq}, nearly evenly split between waste (44.8%) and agriculture (43.2%), with fuel exploitation at 8.4%. These results point to agricultural management and upstream methane controls in fossil-fuel systems as primary mitigation pathways, with waste-sector measures also important at national and regional scales. Global N_2O in 2024 totaled 2.5 Gt CO_{2eq}, with agriculture contributing 69.8% and industrial combustion and processes 12.0%. EU27 N_2O emissions totaled 0.21 Gt CO_{2eq}, with agriculture at 67.3% and industrial combustion and processes 16.7%. Portugal's N_2O total was 2.9 Mt CO_{2eq}, dominated by agriculture (63.2%), followed by industrial combustion and processes (15.4%) and waste (9.5%). Agricultural nitrogen management emerges as the clear priority for N_2O abatement across all regions, complemented by sector-specific industrial measures and improved waste handling.

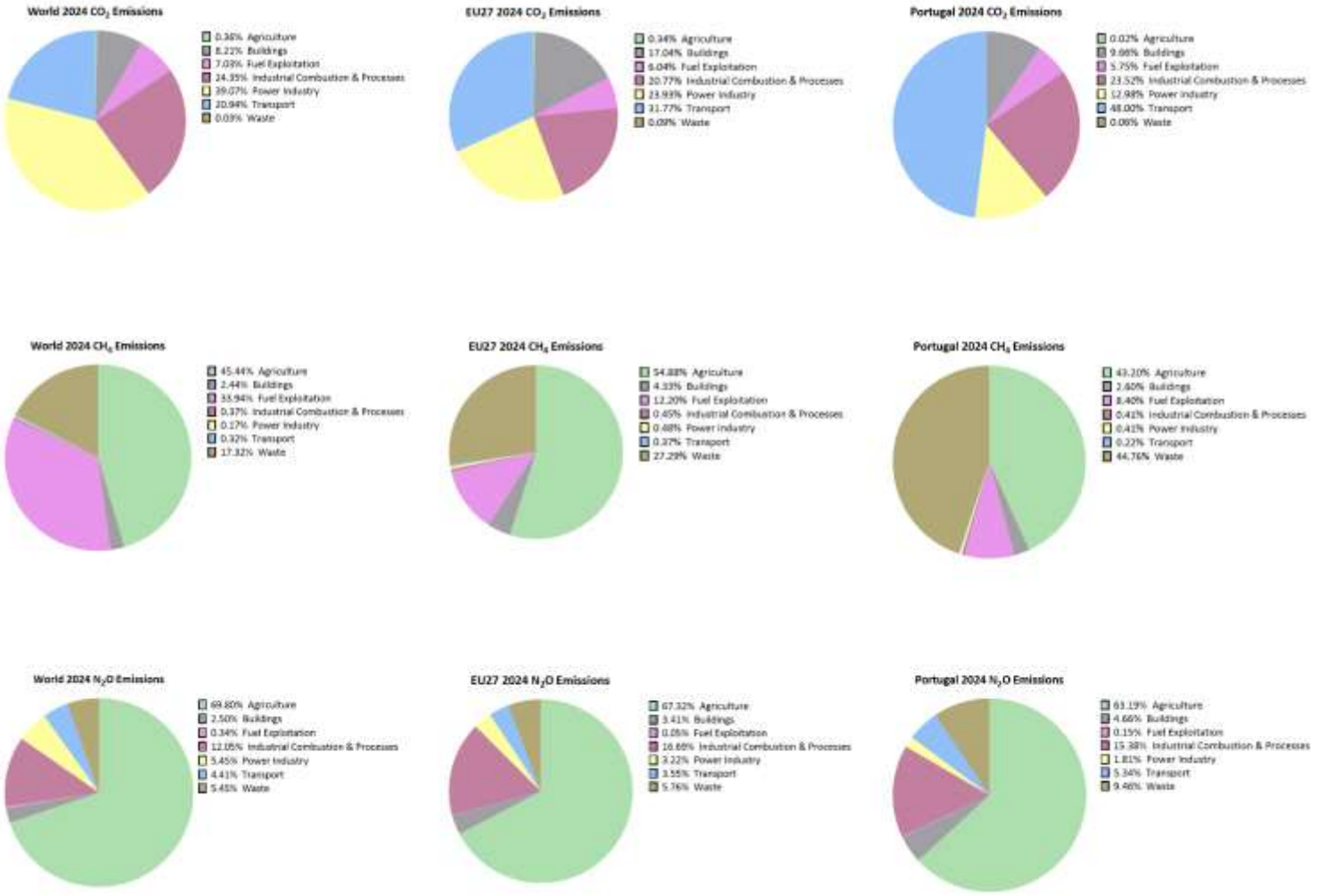

Figure 5. CO_2, CH_4, and N_2O emissions by sector in 2024 from a global, EU27, and Portugal perspective.

1.2.4. Policy context and energy sector dominance

Limiting global warming to 1.5°C demands rapid and deep reductions in anthropogenic GHG emissions in order to avoid escalating risks to ecosystems, human health and economic stability. In response to this challenge, governments have progressively established international climate policies and legally binding frameworks aimed at mitigating climate change. The Kyoto Protocol (1997) represented the first international agreement to set binding emission reduction targets for developed countries, laying the foundation for subsequent global climate governance. This effort was significantly strengthened by the Paris Agreement (2015), under which 196 Parties committed to holding the increase in global average temperature below 2°C above pre-industrial levels, while pursuing efforts to limit warming to 1.5°C through nationally determined contributions (NDCs).

At the European level, the European Climate Law (Regulation EU 2021/1119) legally binds the European Union to achieve climate neutrality by 2050 and establishes a binding target of at least a 55% net reduction in GHG emissions by 2030 compared to 1990 levels. These objectives are supported by a comprehensive policy framework, notably the EU Emissions Trading System (EU ETS; Directive 2003/87/EC), which caps emissions from power generation and energy-intensive industries through a market-based mechanism design to promote cost-effective decarbonization. The implementation of these instruments has contributed to a sustained decline in europe GHG emissions over the past three decades, as previously illustrated (Figure 4).

A comparison of sectoral GHG emission shares in 2024 (Figure 6) reveals marked differences between global and European emission profiles. Globally, emissions are dominated by the power industry (29.3%) and industrial combustion and processes (21.6%), highlighting electricity decarbonization and industrial efficiency as the highest-impact mitigation priorities. In contrast, Europe shows a comparatively larger contribution from transport (EU27: 25.0%; Portugal: 32.4%), alongside significant emissions from industrial combustions and processes (EU27: 19.5%; Portugal: 22.9%). These differences suggests that mitigation strategies policies should focus on transport electrification, modal shift, freight efficiency and vehicle fleet renewal, complemented by industrial process electrification and heat efficiency to achieve major national and regional reductions.

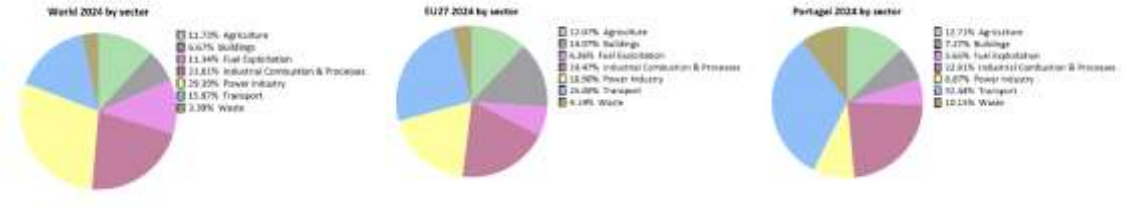

Figure 6. Sectorial GHG emissions in 2024 from a global, EU27, and Portugal perspective.

EDGAR (database used for GHG emissions) developed by the European Commission's Joint Research Centre, follows the methodological and sectoral framework of the Intergovernmental Panel on Climate Change (IPCC) for greenhouse gas inventories. This database, as we saw previously, reports activity-based sectors such as power industry, fuel exploitation, transport, buildings, industrial combustion and processes, agriculture, and waste, which correspond to the broader IPCC inventory categories. Within the IPCC framework , the "Energy sector" encompasses all emissions from fuel combustion (across power generation, transport, buildings, and industry) together with fugitive emissions from fuel extraction, processing, and distribution [6, 17, 19].

To quantify the contribution of energy-related activities to total GHG emissions using the EDGAR database, it is necessary to aggregate the categories power industry, fuel exploitation, transport, buildings, and industrial combustion. Collectively, these sectors encompass emissions arising from fuel combustion and fugitive processes, corresponding to the energy sector as defined in the IPCC greenhouse gas inventory framework. This aggregation approach enables a consistent and comprehensive estimation of energy-related GHG emissions, ensuring methodological coherence between EDGAR and IPCC datasets and providing a robust analytical basis for cross-scale comparisons of global, regional, and national emission profiles [6, 33]. Based on this methodological alignment, the energy sector emerges as by far the dominant source of anthropogenic GHG emissions worldwide, reflecting the pervasive role of fossil-fuel combustion and related processes in powering modern economies and driving climate change. The IPCC's integrated accounting of direct combustion and fugitive emissions thus provides a holistic perspective on the climate impact of energy production and use, underpinning both global and regional mitigation assessments.

Based on this harmonized approach, the energy sector emerges as the dominant source of anthropogenic GHG emissions worldwide. In 2024, energy-related activities accounted for approximately 75.5% of global emissions, 74.6% in the EU27, and 63.0% in Portugal, as estimated from EDGAR data reported in million tonnes of CO_2 equivalent.

These clearly underscore the central role of energy system transformation in achieving climate mitigation targets.

Consequently, the targeted deployment of proven, high-efficiency technologies offers substantial potential for reducing emissions across the dominant sectors. In the power sector, priority actions include the expansion of renewable energy generation, enhanced grid flexibility, and energy storage deployment. In industry, key measures comprise process electrification, high-efficiency heat pumps, waste-heat recovery, and material-efficiency strategies. In transport, accelerated vehicle electrification, expansion of public transport systems, and optimization of freight logistics are essential. Across all sectors, the large-scale adoption of high-efficiency lighting technologies, such as light-emitting diodes (LEDs) combined with smart control systems, can deliver immediate and cost-effective emission reductions.

1.3. Energy sector, energy mix and efficiency: the role of sustainable lighting

1.3.1. Energy consumption, sustainability and the role of lighting

Sustainability has become one of the most critical global challenges of the twenty-first century, demanding decisive action across all areas of human activity [34]. As the primary consumers and polluters of the planet, societies must rethink how energy is produced, managed, and consumed to ensure a responsible and resilient future [35, 36]. Sustainability considerations now extend across multiple sectors (residential [37, 38], commercial [39], industrial [40, 41], transportation [42], education [43], and leisure [44]), and all of which require strategies to reduce overall energy use [45] and to promote environmentally responsible design and resource management [46]. However, given that a substantial portion of global energy consumption still relies on fossil resources [47], strengthening the role of renewable energy systems remains essential for mitigating environmental impacts [48]. In this context, examining the energy sector, its evolving energy mix, and the increasing importance of energy efficiency is fundamental to advancing sustainability and achieving long-term climate goals.

As we approach in 2024, the battle against climate change continues to intensify, with reducing GHG emissions taking center stage across all sectors of the global economy. According to the International Energy Agency [49], the energy sector remains the dominant source of anthropogenic emissions, responsible for around 73% of total global GHG emissions. Within this sector, the lighting industry has become a focal point

for efforts to reduce energy consumption and associated emissions, particularly due to its high demand for electricity.

Lighting accounts for an estimated 19% of global electricity consumption [50-52], making it a main area for improving efficiency. With increasing urbanization and the growing demand for artificial lighting, reducing the carbon footprint of lighting systems has become critical. Fortunately, advancements in lighting technologies, particularly in energy-efficient lighting and renewable energy integration, present substantial opportunities to mitigate emissions. The widespread adoption of more efficient lighting solutions, coupled with a transition to renewable energy sources, has the potential to transform the sector.

1.3.2. Evolution of lighting technologies and energy efficiency

In recent years, the lighting industry has undergone a transformation with the widespread adoption of energy-efficient lighting technologies. Among the key innovations are Light Emitting Diodes (LEDs), Compact Fluorescent Lamps (CFLs), and High-Efficiency Halogen Lamps. Each of these technologies has contributed to reducing energy consumption and emissions compared to traditional incandescent and fluorescent lighting.

Thus, the lighting sector faces both challenges and opportunities in achieving greater energy efficiency and emissions reductions. The shift from traditional lighting technologies to more energy-efficient alternatives, such as LEDs, combined with the integration of renewable energy sources, has the potential to significantly transform how we consume energy and contribute to emissions. The evolution of lighting technologies over the decades has played a key role in this transition.

The development of lightbulbs and lighting technologies extends over more than a century, with successive innovations not only improving energy efficiency but also changing the way cities and industries consume electricity. From the invention of the incandescent bulb to the introduction of fluorescent lamps and the more recent rise of LEDs (Table 1), each major technological advancement has contributed to reducing energy consumption and, by extension, GHG emissions.

Light Sources	Luminous Efficacy (lm/W)	Lifetime (h)
Incandescent Lamp (IL)	5-20	~1,000
Halogen Lamp (HL)	15-25	2,000-4,000
Compact Fluorescent Lamp (CFL)	50-70	8000-15,000
Fluorescent Lamp (FL)	60-100	10,000-20,000
Light Emitting Diodes (LEDs)	120-220	25,000-50,000

Table 1. Typical performance ranges of major lighting technologies in terms of luminous efficacy and operational lifetime. Values represent approximate ranges reported in the literature and may vary depending on lamp design, operating conditions, and technological generation [53-57].

The incandescent lamp (IL), invented by Thomas Edison in 1879, represented the first mass-accessible widely adopted form of electric lighting [58]. Its operation is based on resistive heating of a tungsten filament to incandescence, producing electromagnetic radiation of which only a small fraction lies within the visible spectrum [58, 59]. Classical studies in lighting engineering demonstrate that less than 10% of the electrical energy consumed by incandescent lamps is converted into visible light, with the remainder (90%) dissipated as heat due to the predominantly infrared emission of the filament [59, 60]. As a consequence, incandescent lamps exhibit low luminous efficacy, commonly 5 to 20 lumens per watt (lm/W), and a limited operational lifetime of approximately 1,000 hours, making them less sustainable compared to modern alternatives [57, 61].

The pursuit of improved energy efficiency led to the development and commercialization of fluorescent lamps (FL) in the early 20th century (1930) as a major advancement over incandescent lighting technology [59, 62]. These lamps operate through an electric discharge in low-pressure mercury (Hg) vapor inside the bulb, which emits ultraviolet (UV) radiation that is subsequently converted into visible light by a phosphor coating on the inner surface of the lamp [53]. Compared with incandescent lamps, fluorescent lamps achieve significantly higher luminous efficacies, typically ranging from 50 to over 100 lm/W, enabling substantial reductions in electricity consumption for equivalent light output [63]. In addition, fluorescent lamps offer significantly longer operational lifetimes (up to 10 times longer) than IL, typically ranging from 8,000 to 20,000 hours, while also consume approximately 65% less energy for the same luminous output [53, 64]. Nevertheless, the presence of Hg within the lamp remains a significant environmental concern, as Hg can be released if lamps are broken or improperly disposed of, posing ecological and health risks and requiring careful end-of-life management [65, 66].

In the 1950s, halogen lamps (HL) were introduced as an improved variant of conventional incandescent technology, incorporating halogen gases such as iodine or bromine to initiate a regenerative cycle that reduces filament evaporation and extends service life [53, 67]. Despite modest gains in efficacy compared to traditional incandescent bulbs, halogen technology still suffers substantial thermal losses and does not approach the energy efficiency of discharge or solid-state sources [53].

By the 1990s, compact fluorescent lamps (CFLs) became widely adopted as an energy-efficient alternative to incandescent bulbs, which apply the same operating principles as linear fluorescent lamps in a compact form factor suitable for residential and commercial lighting. CFLs consume significantly less energy (≈75% savings) and deliver substantially longer lifetimes compared to incandescent sources, although their mercury content poses challenges for safe handling, disposal, and recycling [53, 68]. Despite their energy advantages over incandescent and halogen lamps, CFLs still have lower efficacy and performance limitations relative to emerging technologies.

1.3.3. Solid-state lighting and the rise of LEDs

Lighting is a fundamental component of modern society, with a direct impact on global energy consumption, environmental sustainability, and quality of life. As referred, conventional lighting technologies (including IL, FL, CFL, and HL) have historically dominated illumination applications. Nevertheless, these technologies are intrinsically limited by low energy conversion efficiency, significant thermal losses, reduced operational lifetime, and, in the case of discharge-based lamps, the presence of environmentally hazardous materials such as mercury [54, 69, 70]. Consequently, a considerable fraction of the electrical energy consumed by these light sources is dissipated as heat rather than converted into useful visible radiation.

To overcome these limitations, solid-state lighting (SSL) has emerged as a disruptive lighting paradigm. In SSL devices, electrical carriers are injected into semiconductor materials in the solid phase, where radiative recombination directly generates photons, eliminating the inefficiencies associated with thermal radiation and gas discharge mechanisms [71, 72]. This approach enables substantially higher efficiency, improved reliability, compact device architectures, and precise optical control. Among SSL technologies, LEDs have become the most mature and widely adopted solution [73].

Early generations of LEDs were inherently monochromatic, emitting narrow spectral bands in colors such as red, yellow, and green, which limited their applications primarily to indicator lights and signaling devices [72-75]. Subsequent advances in

semiconductor materials, epitaxial growth, and device engineering (particularly, the development of efficient blue and ultraviolet LEDs) enabled the realization of multi-color and white-light emission [70, 74]. White LEDs are typically achieved either by combining multiple monochromatic emitters or, more commonly, by using blue LEDs coupled with wavelength-converting phosphor materials that produce broadband visible spectra.

Modern LEDs are semiconductor optoelectronic devices that convert electrical energy directly into light through radiative electron-hole recombination under forward bias [70, 74, 76-78]. The emission wavelength is fundamentally determined by the bandgap energy of the semiconductor, allowing intrinsic color tunability without external filters. Compared with conventional lighting technologies (IL, FL, CFL, and HL), LEDs offer superior luminous efficacy (exceeding 200 lm/W), long operational lifetimes often exceeding 25,000-50,000 hours, low operating voltage, fast switching speeds, high mechanical robustness, and excellent dimming capability [53-56, 74]. In addition, LEDs provide high color rendering index values, a wide range of correlated color temperatures, and compatibility with digital control and wireless communication systems [54, 70].

From an environmental and regulatory perspective, LEDs are mercury-free, emit negligible ultraviolet radiation, and comply with international environmental standards such as Restriction of Hazardous Substances (RoHS) directives, making them a sustainable alternative to legacy lighting technologies [54, 74]. As a result of these advantages, inefficient lighting sources have been progressively phased out in many regions, accelerating the global transition toward LED-based illumination.

1.3.4. Fundamentals of LEDs operation

Given the central role of LEDs in contemporary solid-state lighting and their evolution from monochromatic emitters to multi-color and white-light sources, a detailed understanding of their operating principles is essential. The following section therefore presents the fundamental mechanisms governing LEDs operation, including carrier injection, radiative recombination, and light generation processes.

An LED’s light generation is governed by the physics of a semiconductor p–n junction, as observed in Figure 7 [79-81]. An LED consists of p-type and n-type semiconductor regions brought into intimate contact, forming a junction that enables controlled carrier injection and radiative recombination. The n-type region is doped with donor impurities such as phosphorus or arsenic, which supply excess electrons as majority carriers. Conversely, the p-type region is doped with acceptor atoms such as boron or gallium, creating vacant electronic states known as holes [79, 80]. At the interface between the p-type and n-type regions, electrons diffuse from the n-side into

the p-side and recombine with holes. This diffusion leaves behind fixed ionized donor and acceptor atoms, forming a depletion region devoid of free carriers. The resulting spatial charge separation generates an internal electric field and a built-in potential that inhibits further carrier diffusion under equilibrium conditions [79, 80]. When a forward bias voltage is applied across the junction, the built-in potential barrier is reduced and the depletion region narrows, allowing electrons and holes to be injected into the active region. In direct-bandgap semiconductor materials commonly used in LEDs, such as gallium nitride (GaN), indium gallium nitride (InGaN), and aluminum gallium indium phosphide (AlGaInP), these carriers recombine radiatively. During this recombination process, the energy difference between the conduction band and the valence band is released in the form of photons [81-83].

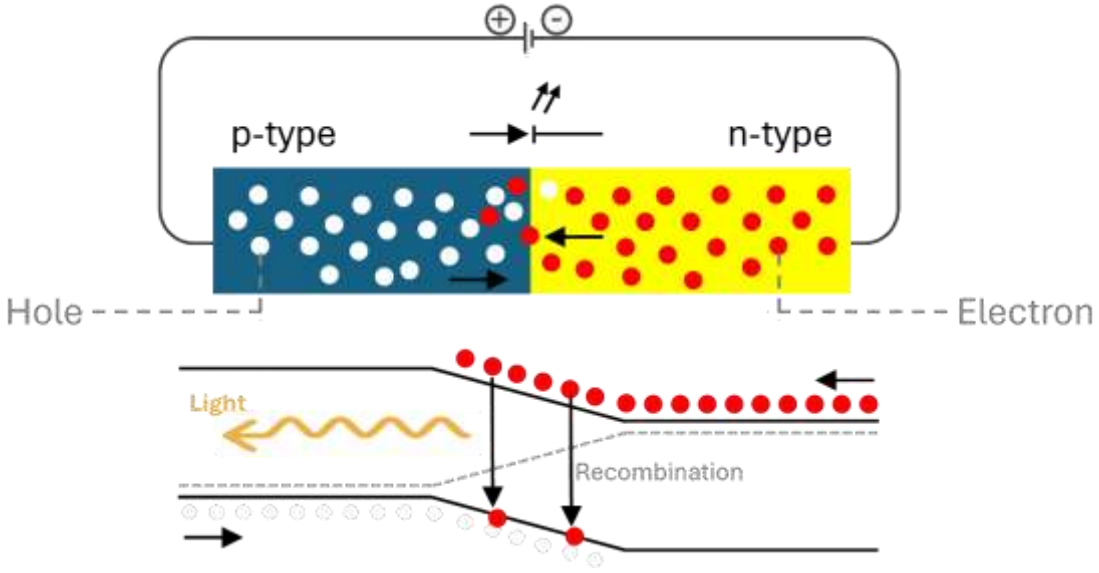

Figure 7. Schematic representation of physics of a semiconductor p–n junction to generate LED's light.

The emission wavelength of a LED is fundamentally determined by the bandgap energy of the semiconductor material forming the active region [79, 81, 82]. LEDs are commonly fabricated using III-V compound semiconductors, whose direct bandgap enables efficient radiative recombination. Materials such as gallium arsenide (GaAs), gallium phosphide (GaP), GaN, InGaN, and AlGaInP are widely employed to cover emission wavelengths ranging from the infrared to the visible spectrum, e.g. GaAs for infrared (~870 nm), GaP for green (~555 nm), and InGaN for blue (~450 nm) [79-82].

The relationship between the bandgap energy (E_g) and the emitted photon wavelength (λ) is given by

$$E_{photon} = E_g = h\upsilon = \frac{hc}{\lambda}$$

where h is Planck's constant, c is the speed of light in vacuum, and υ is the photon frequency [79, 82]. This equation illustrates that materials with larger bandgap energies emit higher-energy (shorter-wavelength) photons, corresponding to blue or ultraviolet light, whereas materials with smaller bandgaps emit lower-energy (longer-wavelength) photons in the red or infrared region.

1.3.5. White Light-Emitting Diodes (WLEDs)

While conventional LEDs emit light at a single wavelength determined by the semiconductor bandgap, their inherent monochromatic emission limits their use for general illumination. To overcome this, white light-emitting diodes (WLEDs) were developed (Figure 8), either through spectral conversion using phosphor layers or by optically mixing multiple LED colors, enabling broad-spectrum, energy-efficient lighting suitable for residential, commercial, and industrial applications or by UV or near-UV (NUV) LEDs to pump multiple phosphors [73, 79, 81, 84, 85].

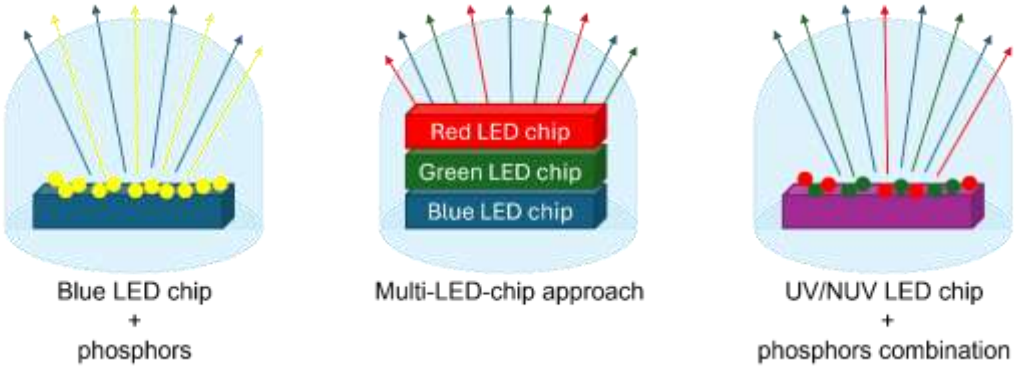

Figure 8. Schematic representation of WLED architecture: three dominant ways.

Phosphor-converted WLEDs are the most widespread method, in which a blue or near-ultraviolet LED chip excites luminescent materials that down-convert part of the emitted energy into longer wavelengths [73]. The phosphor absorbs part of the blue emission and re-emits at longer wavelengths (yellow to red), producing a mixture of transmitted blue and converted yellow light perceived as white [86, 87]. Commercial WLEDs typically use a blue InGaN LED coupled with cerium-doped yttrium aluminum garnet (YAG:Ce^{3+}) phosphor to achieve broadband output, with the correlated color temperature (CCT) and color rendering index (CRI) tuned through phosphor composition, layer thickness, or particle concentration [73, 81, 87]. In fact, manufacturers

can tune the CCT across a range from cool white (~6500 K) to warm white (~2700 K) [73, 88]. Despite its commercial dominance, phosphor conversion exhibits intrinsic efficiency losses due to the Stokes shift and produces spectral peaks rather than a continuous spectrum, which can limit color rendering [73, 86, 87]. Environmental concerns also arise from the use of rare-earth elements such as cerium, whose extraction and processing are energy-intensive [70].

A second approach (RGB mixed WLEDs) employs the RGB mixing, in which discrete red, green, and blue LED chips are combined optically to produce white light by combining multiple monochromatic emissions [85, 86]. This method allows independent adjustment of each primary LED's intensity, enabling dynamic CCT tuning and potentially higher CRI compared with single-phosphor LEDs. However, these systems require more complex driving electronics, precise optical alignment, and careful thermal management to maintain color stability and uniform illumination [84-86]. RGB WLEDs are therefore more commonly applied in displays, stage lighting, and specialized illumination, where dynamic color control is critical.

A third strategy involves UV or near-ultraviolet LEDs pumping multiple phosphors, each emitting at different visible wavelengths [73, 86, 87]. By combining emissions from several phosphors, a more continuous white spectrum can be achieved with higher CRI compared with single phosphor systems. This approach provides a compromise between the simplicity of phosphor conversion and the spectral control of RGB mixing [87, 89].

Emerging technologies, such as quantum dot conversion layers and hybrid architectures, are also being investigated to further optimize white spectra, color quality, and tunability [70, 89].

1.3.6. Environmental performance and life cycle impacts of LEDs

The widespread adoption of LEDs, including WLEDs, has significantly mitigated the environmental concerns associated with conventional lighting technologies. Owing to their high luminous efficacy, long operational lifetimes, and absence of mercury, LEDs significantly reduce electricity consumption and GHGs emissions compared with incandescent and fluorescent lamps [84]. Life Cycle Assessments (LCA) studies consistently demonstrate that the use phase dominates the overall environmental footprint of LED lighting systems, as electricity consumption over tens of thousands of operating hours remains the primary contributor to total impacts, particularly when electricity is generated from fossil-based sources [90, 91]. The elimination of mercury

further minimizes toxic waste during both use and disposal, representing a clear advantage over fluorescent technologies [84, 92].

Despite these pronounced use-phase benefits, upstream (production) and downstream (end-of-life) impacts remain significant. LEDs manufacturing and material supply chains rely on a complex combination of critical and scarce elements, including III-V semiconductors materials such as gallium (Ga), indium (In), arsenic (As), as well as rare-earth elements (REEs) such as yttrium (Y), cerium (Ce), and europium (Eu), which are widely used in phosphor-converted WLEDs [92]. Characterization studies of end-of-life LEDs lamps confirm the presence of a broad range of valuable and potentially hazardous elements, including Ce, Ga, Y, As, lead (Pb), silver (Ag), and gold (Au), distributed across different device components, thereby posing environmental and health risks if improperly managed [93]. The extraction and refining of these materials are energy-intensive processes and may generate toxic by-products such as arsenic trioxide and hydrofluoric acid, which can lead to soil and water contamination, particularly in regions associated with REE mining and processing [94]. In addition, some REEs used in LED phosphors are classified as critical raw materials, owing to supply risks and strong geopolitical concentration of production [94]. Life-cycle impact-based assessments further indicate that, for certain metals, LEDs may exhibit higher resource depletion and toxicity potentials per unit mass than incandescent lamps, even when normalized over their extended service lifetime [95].

Manufacturing-phase impacts are also non-negligible. Comparative LCA studies examining the fabrication of WLEDs (including sapphire substrate production, epitaxial growth, phosphor integration, and electronic packaging) show that although LEDs outperform conventional lighting technologies in overall environmental performance, material extraction and component manufacturing contribute a growing share of total impacts as electricity grids progressively decarbonize [90, 91]. Under low-carbon electricity scenarios, the relative importance of the production phase increases, shifting the environmental burden upstream.

End-of-life management presents further challenges. As LED adoption continues to grow, waste electrical and electronic equipment (WEEE) streams are becoming enriched with LED components containing critical and precious materials. Detailed compositional analyses highlight both the recycling potential and the technical complexity associated with recovering rare earths and metals from spent LED lamps [93, 96]. Current recycling practices are constrained by the small size, material heterogeneity, and strong encapsulation of LED components, which limit economic feasibility and result

in low recovery rates, with a substantial fraction of materials still ending up in landfills or incineration pathways [92, 93].

Overall, while LEDs and WLEDs represent a major advancement toward sustainable lighting, future environmental improvements will depend increasingly on material efficiency, circular design strategies, and advanced recycling technologies, rather than further gains in operational efficiency alone. Integrating eco-design principles, improving material recovery routes, and reducing dependence on critical raw materials are therefore essential to fully realize the long-term sustainability potential of solid-state lighting technologies [90, 94, 96].

Future sustainability improvements in solid-state lighting will depend less on further gains in operational efficiency (which is already approaching fundamental limits) and increasingly on materials recovery, green chemistry, spectral optimization, and circular design strategies. While LEDs and WLEDs have drastically reduced energy consumption and GHGs emissions compared with conventional lighting technologies, emerging challenges related to spectral quality, material sustainability, and human health impacts must be addressed to ensure long-term environmental sustainability in lighting systems.

1.3.7. Addressing false white light in LEDs: spectral, biological, and visual perspectives

A key concern associated with many phosphor-converted WLEDs is the phenomenon commonly referred to as “false white light”. In blue-chip-based WLEDs, white light is produced by combining a strong blue emission peak with a broad yellow phosphor band rather than a continuous, sunlight-like spectrum. This spectral imbalance can degrade color rendering and visual comfort and has raised concerns that extend beyond aesthetics to include biological and physiological effects [85].

Blue-enriched white light has been shown to exert a disproportionate influence on circadian rhythms and melatonin suppression, particularly when exposure occurs during evening or nighttime hours. Experimental studies demonstrate that short-wavelength light in the blue region (~450-480 nm) strongly stimulates intrinsically photosensitive retinal ganglion cells, leading to circadian phase shifts and sleep disturbances [97]. In addition, high-intensity blue light has been associated with glare, visual discomfort, and increased light pollution, affecting both human well-being and ecological systems [98].

As a result, contemporary lighting research and practice increasingly emphasize spectral tuning, optical diffusion, and appropriate luminaire shielding to mitigate the adverse effects of blue-enriched white light while maintaining high luminous efficacy [98]. These strategies aim to balance energy efficiency with visual comfort and biological compatibility, particularly in residential, healthcare, and urban environments.

Beyond spectral management, alternative white-light generation approaches are being explored. One promising approach involves near-ultraviolet (NUV or UV-A) LEDs combined with multi-phosphor systems, which can produce broadband white light with improved spectral continuity and reduced blue intensity peaks. Compared with conventional blue-chip WLEDs, UV-excited phosphor systems offer enhanced color rendering and greater flexibility in spectral design engineering, potentially alleviating circadian and visual concerns associated with blue-enriched white light [86].

1.3.8. Emerging alternatives and transition toward Carbon Dots

More recently, CDs have emerged as a highly promising class of photoluminescent nanomaterials for next-generation solid-state lighting applications. CDs exhibit strong and tunable emission under UV or near-UV excitation and can operate efficiently in the solid state. Compared with conventional rare-earth-based phosphors, CDs offer several advantages, such as low toxicity, abundant precursor materials, chemical stability, and potentially lower environmental impact during synthesis [99]. Importantly, recent advances demonstrate that solid-state CDs can generate broadband emission suitable for high-quality white light, reducing reliance on critical rare-earth elements and enabling more sustainable WLED architectures [99].

Although challenges remain regarding long-term photostability, thermal robustness, and large-scale manufacturing, CDs represent a promising pathway toward healthier spectral profiles and reduced material criticality in future lighting systems. Their integration with UV-LED platforms may enable white lighting solutions that simultaneously address energy efficiency, environmental sustainability, and human-centric lighting requirements.

In summary, while LEDs and WLEDs have already transformed global lighting by substantially improving energy efficiency and operational lifetime, current research increasingly emphasizes spectral quality, material sustainability, and human-centric lighting considerations. Addressing challenges associated with blue-enriched white light, critical material dependence, and end-of-life management remains essential. In this context, emerging approaches such as UV-excited architectures and CDs-based wavelength converters have attracted growing research interest as potential pathways

toward spectrally improved and more sustainable white lighting systems, although further validation at the system and life-cycle levels is still required [84, 86, 92, 99].

1.4. Carbon Dots as emerging sustainable luminescent nanomaterials

1.4.1. Definition, properties and applications of Carbon Dots

Carbon Dots (CDs) are a type of fluorescent carbon-based nanomaterial with a near-spherical shape, an amorphous or nanocrystalline core, and a functionalized surface where different functional groups such as alcohols, amines, and carboxylic acids can be found [100-102]. These nanomaterials were first reported in 2004 by Xu *et al*. as carbon nanoparticles isolated as a by-product during the synthesis of single-walled carbon nanotubes [103], and were subsequently named in 2006 by Sun *et al*. [104], attracting sustained interest from the scientific community since then.

Beyond CDs, carbon-based nanomaterials comprise a broad and diverse family that has been extensively studied in recent years as potential substitutes for traditionally used materials, owing to the superior properties enabled by their nanoscale structure. This class includes single-walled [105] and multi-walled [106] carbon nanotubes, nanodiamonds [107], nanofibers [108], graphene [109], buckminsterfullerene [110], and CDs [100, 111-115]. While bulk carbon is a black, water-insoluble material that does not exhibit photoluminescence, its nanosized forms display markedly different physicochemical properties, making them suitable for a wide range of advanced applications.

Based on their structural features, CDs exhibit a range of highly desirable properties, including low-cost production, high fluorescence quantum yield (QY_{FL}) [111, 116], broadband absorption [117], good water solubility [118], high photo- and chemical stability [119, 120], biocompatibility [121], and low toxicity [122]. Given these properties, it is not surprising that CDs have attracted increasing interest from the research community and have been widely investigated for a broad range of applications, such as in sensing/biosensing [111, 123-127], bioimaging [128-131], photocatalysis [132-134], light-emitting devices [135-138], drug delivery systems [139, 140], solar cells [141, 142], and photodynamic and phototherapeutic applications [143-146]. Overall, these diverse studies demonstrate the versatility of CDs and their potential for applications ranging from optoelectronics to biomedical technologies.

1.4.2. Synthetic approaches and precursor diversity

Regarding their production, CDs can be synthesized through a wide range of methodologies that are generally classified into two main categories, top-down and bottom-up approaches (Figure 9).

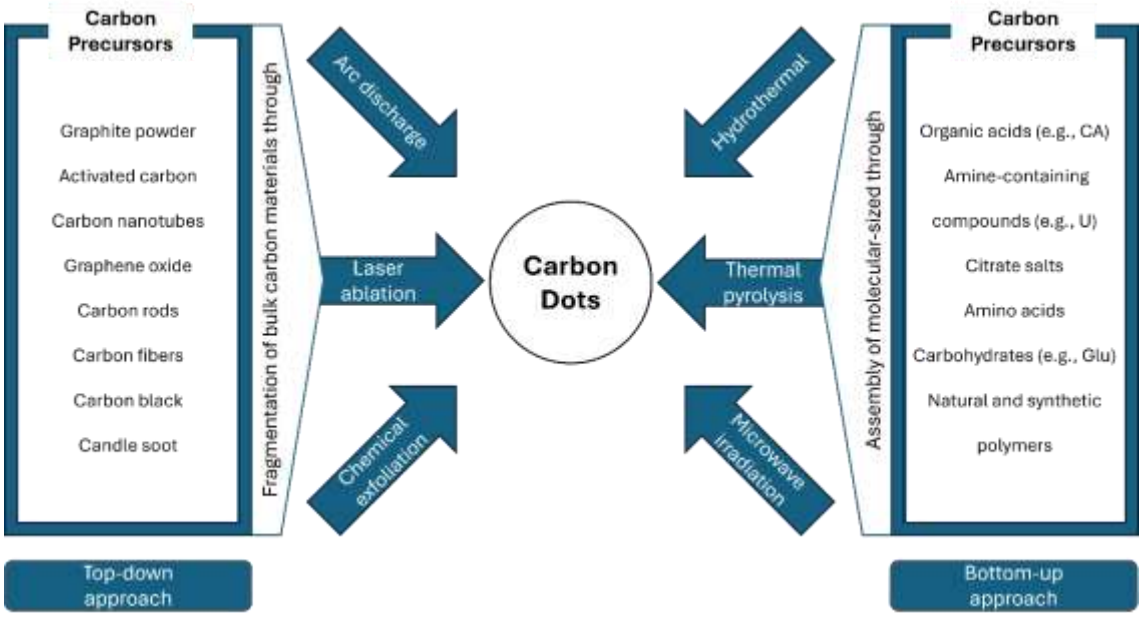

Figure 9. Schematic representation of top-down and bottom-up approaches.

Top-down routes involve the fragmentation of bulk carbon materials, such as graphite, activated carbon, carbon fibers, carbon nanotubes and coal, into nanoscale structures [147], and typically require expensive equipment and labor-intensive processes, including arc-discharge [148], laser ablation [149], chemical exfoliation [150], ultrasonic treatment [151], and electrochemical shocking [152].

On other hand, bottom-up approaches are based on the assembly of molecular-sized carbon precursors into larger nanostructures [147] and are generally considered low-cost and environmentally friendly strategies, including hydrothermal and solvothermal treatments, thermal pyrolysis, and microwave irradiation. Although top-down and bottom-up strategies for CDs synthesis have been widely investigated, they present inherent advantages and limitations that affect their applicability.

Top-down approaches are often associated with the production of CDs with relatively well-defined structures and potential scalability; however, their limited ability to modulate surface chemistry and structural diversity can restrict their versatility [153]. In contrast, bottom-up methods, despite being challenged by the formation of side products and the need for additional purification steps [153, 154], provide greater flexibility through

one-pot surface functionalization and access to a broader range of structures and functionalities compared to top-down routes, whose products frequently resemble the structure of the starting materials [154]. These features have contributed to the increasing preference for bottom-up strategies, particularly solvothermal methods, which are typically simpler, faster, and more cost-effective, owing to their low cost, process simplicity, and general use of non-toxic materials [155]. Nevertheless, limitations related to low synthetic yields and time-consuming purification steps remain significant challenges for large-scale production, motivating the development of alternative bottom-up approaches with improved scalability [156].

Among the various bottom-up routes, microwave irradiation and hydrothermal treatment of solutions containing molecular carbon sources are the most commonly employed methods, with heteroatom-containing precursors, such as nitrogen- and sulfur-based compounds, being incorporated when heteroatom doping is desired [157-160].

Another attractive characteristic of CDs is the wide diversity of carbon precursors that can be employed for their production, encompassing both bulk carbon materials traditionally used in top-down approaches and a broad variety of molecular carbon sources in bottom-up strategies. These precursors include commercially available chemical reagents as well as natural resources, reflecting the versatility of CDs and the broad range of synthesis methodologies available for their preparation. The literature reports the use of a broad spectrum of carbon precursors, encompassing both bulk carbon materials traditionally used in top-down approaches and a rich variety of molecular carbon sources in bottom-up strategies. As refer above, in top-down routes, CDs are derived from large carbonaceous substrates such as graphite powder, activated carbon, carbon nanotubes, graphene oxide, carbon rods, carbon fibers, carbon black and related materials (candle soot), where the precursor influences the structural and surface features of the resulting nanoparticles [161-166]. On the other hand, bottom-up approaches offer a significantly broader chemical space of carbon precursors, relying on the carbonization or polymerization of small molecules and natural or synthetic macromolecules which enable significant flexibility in tuning the structural and optical properties of the resulting nanomaterials [167-169].

Common small precursors include organic acids (e.g. citric acid, ascorbic acid, tartaric acid, succinic acid, maleic acid, and acrylic acid); amine-containing compounds (e.g. urea and p-/o-/m-phenylenediamine); citrate salts (e.g. sodium, calcium); amino acids (e.g. histidine, cysteine, serine), carbohydrates (e.g. glucose, sucrose, fructose and other sugars) [168, 170-172]. In addition, natural polymers and biomass, such as

lignin, chitosan, xylan, egg white, peanut shells, corn stover, eucalyptus leaves, sawdust, spent coffee grounds, cork powder, onion peel, and orange peel, as well as synthetic polymers, including polyethyleneimine, polyamidoamine, polyacrylic acid, polyvinyl alcohol, polyacrylamide, polyethylene glycol, and polypropylene, have also been employed as carbon sources [116, 173-176].

The extensive diversity of carbon precursors reported for the synthesis of CDs largely arises from sustained efforts to overcome intrinsic limitations associated with low synthetic yields and modest QY_{FL}, challenges that have been recognized since the earliest studies on these nanomaterials [103, 104, 177, 178]. Since the first reports on CDs, these two parameters (synthesis yield and QY_{FL}) have represented key obstacles to their development. Specifically, these parameters reflect different aspects of CDs performance: synthesis yield corresponds to the amount of material obtained relative to the initial carbon precursor, whereas the QY_{FL} is defined as the ratio between emitted and absorbed photons. In the earliest studies, CDs were commonly obtained as minor by-products or via poorly controlled carbonization routes, resulting in low production yields and weak photoluminescence, with QY_{FL} typically below 10% [103, 104].

In this context, top-down approaches are generally associated with higher synthesis yields and improved scalability; however, they offer limited control over particle morphology, size distribution, surface chemistry, and emissive states, often resulting in CDs with modest QY_{FL} [179-181]. On the contrary, bottom-up strategies, despite commonly suffering from lower synthetic yields, provide access to a broad chemical space through the use of diverse molecular precursors, enabling fine control over carbonization pathways, surface states, and electronic structure [179-181]. This versatility makes bottom-up approaches particularly effective for tuning the photophysical properties of CDs and optimizing QY_{FL} through rational precursor selection and controlled carbonization pathways. As a result, more recent studies have demonstrated substantial improvements in fluorescence efficiency, with optimized systems achieving QY_{FL} exceeding 50% through careful precursor selection and reaction control [182, 183]. Nevertheless, the simultaneous achievement of high synthesis yield and QY_{FL} remains a central challenge in CDs research, thereby motivating continued efforts focused on precursor engineering, heteroatom doping, and solvent effects.

1.4.3. Heteroatom doping strategies for improved photoluminescence in Carbon Dots

One of the key limitations, as refer above, during the early development of CDs was their inherently low QY_{FL} (typically below ≈ 1%) due to non-radiative recombination

pathways and surface defects that quench fluorescence [184]. Surface modification, passivation techniques and heteroatom doping have been extensively employed to improve fluorescence efficiency [184]. Surface functionalization, achieved by regulating the nature and distribution of functional groups on the CDs surface, enables the modulation of surface states that govern emission and facilitates interactions with functional molecules or polymeric species, thereby influencing both optical properties and application-specific performance [185]. Despite its effectiveness, surface passivation often involves time-consuming procedures and the use of organic reagents or catalysts that may be cytotoxic and environmentally hazardous [160].

Consequently, heteroatom doping has emerged as a particularly attractive alternative [160]. Chemical doping is defined as the intentional incorporation of heteroatoms into the carbon framework during synthesis, has proven particularly powerful in regulating the electronic structure of CDs. By altering charge distribution, energy-level alignment, and defect density, heteroatom doping can suppress non-radiative recombination pathways and promote radiative transitions, leading to substantial improvements in QY_{FL} [184, 186]. A broad range of heteroatoms, including nitrogen (N), sulfur (S), boron (B), phosphorus (P), selenium (Se), tellurium (Te), silicon (Si), and halogens, has been successfully introduced into CDs, demonstrating the generality of this approach for tuning photophysical behaviour [114, 157, 185, 187, 188].

Heteroatom-doped CDs can be mono- or co-doped, with co-doping exploiting synergistic interactions between multiple heteroatoms, giving rise to modified electronic structures that are particularly favourable for enhanced fluorescence emission [189]. Furthermore, heteroatom doping can be broadly divided into non-metal and metal doping. Non-metal dopants (N, S, and B) are especially attractive due to their atomic sizes being comparable to that of carbon, which facilitates uniform incorporation into the carbon lattice and relatively straightforward synthesis [185]. Metal doping, by contrast, introduces ions (such as Na^{+}, Fe^{3+}, Cu^{2+} and Zn^{2+}) with partially filled or vacant orbitals, enabling more pronounced modulation of electronic states, energy gaps, and charge density distribution, thereby offering additional opportunities for tuning the optoelectronic properties of CDs [185].

Although metal ions can effectively modulate the electronic structure and optical properties of CDs due to their multiple available orbitals and larger atomic radii, their incorporation often suffers from non-uniform doping due to lattice mismatch with carbon, leading to limited structural control. Moreover, concerns related to cytotoxicity and environmental impact have further restricted the widespread use of metal-doped CDs

[160, 190]. As a result, metal ion doping has received comparatively less attention, and non-metal heteroatom doping has emerged as the preferred strategy for tuning the photophysical properties of CDs. In particular, doping with elements such as N, S, P and B has been shown to modify electronic states, enhance emissive properties, and improve QY_{FL} by reducing non-radiative recombination pathways [114, 157, 187, 188].

Among the several heteroatoms employed for the doping of CDs, N and S have emerged as key strategies for the enhancement of CDs photoluminescence [191]. Nitrogen is the most commonly used, largely due to the abundance of N-containing precursors and the relatively simple incorporation into the carbon framework [153]. N-doping has been consistently shown to enhance the photoluminescence properties of CDs by modifying their electronic structure and surface states. Owing to its five valence electrons and an atomic radius comparable to carbon, N can form stable covalent bonds with the carbon lattice while introducing lone-pair electrons that facilitate charge transport and promote radiative recombination, ultimately improving fluorescence efficiency [183, 192, 193]. Despite these well-documented benefits, the precise mechanisms governing N-induced blue- or red-shifts in absorption and emission remain an active topic of investigation, with studies suggesting that even hybridization of frontier orbitals at edge N-doping sites leads to a blue shift, whereas uneven orbital hybridization results in a red shift [194, 195]. Sulfur is the second most frequently employed heteroatom dopant for CDs [153]. In contrast to nitrogen, sulfur doping primarily introduces sulfur-related emissive or trap states that can capture photoexcited electrons, thereby altering the electronic structure and modulating the photoluminescence behavior of the nanomaterials [191]. In many systems, S incorporation has been associated with bathochromic shifts in absorption and emission bands, often resulting in red-shifted emission and improved QY_{FL} [160, 196]. The incorporation of N and S not only improves optical performance but also expands potential applications of CDs in areas such as electronics, optoelectronics, catalysis, and energy storage, since the lone pair electrons introduced by these heteroatoms act synergistically, increasing the electron density and promoting radiative recombination, thereby enhancing the QY_{FL} and enabling tunable emission across a range of wavelengths [160].

Doping with N and S induces structural modifications, producing additional electron pairs, new defect sites and active centers that significantly boost fluorescence efficiency [160, 197-199]. Due to their comparable atomic sizes (the radius of C: 0.77, N: 0.75) and similar electronegativity values (C: 2.55, N: 2.75, S: 2.58), these heteroatoms can be incorporated into CDs structures, refining their optical and electronic properties [197]. In particular, nitrogen doping enhances fluorescence intensity by introducing

reactive functional groups (-OH, -COOH, -N=C, -CN, -NH_2) and modifying surface states [160, 198]. In CDs synthesis, commonly used nitrogen sources include urea, ethylenediamine (EDA), ammonia, phenylenediamine, polyethylenimine (PEI) and melamine [200-203]. Usually, the most sulfur dopants employed are sodium thiosulfate ($Na_2S_2O_3$), sulfuric acid (H_2SO_4), and sodium sulfide [158, 159, 187, 196, 204].

1.4.4. Solvent effects and photophysical tunning

In addition to heteroatom doping and precursor selection, the choice of solvent and reaction medium constitutes a critical factor in tailoring the optical properties of CDs. These properties are primarily governed by their electronic structure, surface chemistry, and particle size, which are, in turn, strongly influenced by the synthesis conditions and post-synthetic modifications. Although CDs generally exhibit comparable photophysical behavior, variations in absorption and emission profiles arise from differences in functional groups, synthetic routes, dopant incorporation, precursor identity, and the surrounding chemical environment [205, 206].

CDs possess intrinsic photophysical properties, enabling them to absorb and emit light across a broad spectral range [207]. Typically, CDs exhibit strong absorption in the ultraviolet (UV) region (200-400 nm) with a tail extending to the visible range (400-700 nm) [147, 182, 207]. The absorption spectra of CDs are generally governed by electronic transitions arising from both the carbon core and surface states, with π-π* transitions associated with sp^2-hybridized aromatic domains (C=C bonds) and n-π* transitions primarily involving surface carbonyl and nitrogen-containing groups (C=O and C=N), as well as other oxygen-containing functionalities [153, 182, 208]. As illustrated in Figure 10, the absorption can be divided into multiple bands: Band I (π-π*), Band II (n-π*), and Bands III-V, corresponding to transitions involving the carbon core and surface states, including heavily graphitic nitrogen and oxygen-related groups [207]. The surface state transitions contribute to a red shift in the absorption and emission spectra, which is key for tuning the optical properties of CDs.

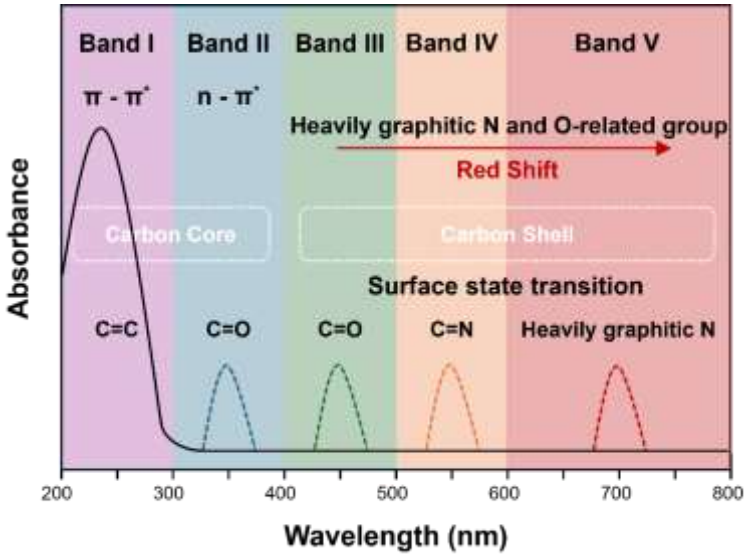

Figure 10. Schematic representation of the absorption bands of CDs, showing π-π* (Band I) and n-π* (Band II) transitions associated with the carbon core, as well as surface state transitions (Bands III-V) involving C=O, C=N, and heavily graphitic nitrogen and oxygen-containing groups. Adapted from [207].

CDs are renowned for their tunable photoluminescence, which is highly influenced by their synthesis procedures, precursors, and surface chemistry [181, 209]. They can emit across a wide spectral range, from blue to red, although blue and green emissions are most common [102, 153, 184]. The emission spectra of CDs are generally broad and roughly symmetrical, often exhibiting large Stokes shifts compared with organic dyes [184]. In many cases, fluorescence exhibits excitation wavelength-dependent behavior, with emission maxima red-shifting as the excitation wavelength increases [102, 184, 209]. This dependence has been attributed to size heterogeneity, diverse surface functional groups, quantum confinement effects, and different emissive surface traps [153, 184, 209]. Conversely, CDs with uniform size and well-passivated surfaces can exhibit excitation-independent emission [102, 209]. Additional factors such as particle size, morphology, internal structure, and chemical composition further modulate photoluminescence properties [184, 209]. Despite extensive studies, the precise mechanisms governing photoluminescence in CDs remain under debate, with evidence pointing to contributions from edge and surface defects, surface defect states, and molecular or molecule-like states, reflecting the complex interplay between the carbon core and surface functional groups [209].

Solvent effects play a critical role in modulating the photoluminescence of CDs by influencing both ground and excited electronic states through dielectric interactions, hydrogen bonding, and polarity-dependent stabilization of dipoles [210-212]. Beyond modulating the emission of pre-formed CDs, the choice of reaction solvent can strongly

influence the carbonization pathways and surface chemistry during synthesis, altering the formation of emissive centers, surface states, and structural domains in the carbon core [213]. Variations in solvent polarity and proticity have been shown to induce significant shifts in emission maxima, modify fluorescence intensities and QY_{FL}, as these properties depend on the interaction of solvent molecules with surface functional groups and defect sites that act as emissive centers [210, 211]. For example, CDs dispersed in polar solvents often exhibit red-shifts in emission compared with less polar solvents, which is attributed to enhanced stabilization of excited states and solvation of surface emissive sites [211, 212]. Solvent-dependent photoluminescence behavior has been observed in both aprotic and protic systems, highlighting the role of non-specific dipole-dipole interactions and specific hydrogen bonding in modulating the energies of surface states [210, 212]. Moreover, solvents can indirectly affect photoluminescence by influencing carbonization kinetics and surface passivation during synthesis, thus modulating the formation and distribution of emissive centers [210, 212]. Comprehensive reviews further highlight solvent-dependent emission tuning as a key strategy for achieving multicolor and high-efficiency CDs [214]. Collectively, these studies demonstrate that solvent engineering is a powerful approach for tuning the emission wavelength, QY_{FL}, and solvatochromic behavior of CDs, enabling applications in multicolor imaging, sensing, and other optoelectronic technologies [210-212, 214].

1.4.5. Sustainability challenges and Life Cycle Assessment

However, while solvent engineering has proven to be a highly effective strategy for tuning the photophysical properties of CDs, it also raises important environmental and sustainability concerns. Many conventional organic solvents frequently employed in both the synthesis and post-synthetic characterization of CDs (includes toluene, dichloromethane, N,N-dimethylformamide, and other volatile organic compounds (VOCs)) are derived from non-renewable fossil resources and exhibit high volatility, toxicity, and environmental persistence [215, 216]. These solvents contribute not only to hazardous emissions and waste streams during laboratory or industrial-scale syntheses, but also generate environmental and health risks when used in post-synthetic studies, such as solvatochromic measurements and photophysical testing [215-217]. They can pose occupational health risks through inhalation and dermal exposure, with potential effects ranging from respiratory irritation to neurotoxicity and reproductive harm, while their poor biodegradability, formation of secondary pollutants, and bioaccumulation can adversely impact aquatic and terrestrial ecosystems [216, 217]. Furthermore, the widespread use of these solvents amplifies their environmental footprint, highlighting the

inherent trade-offs between achieving optimal material properties and ensuring sustainability [215, 216].

These challenges have driven a growing emphasis on green chemistry principles, including the development and adoption of eco-friendly alternative solvents derived from renewable feedstocks or designed for reduced toxicity and improved biodegradability, such as aqueous media, bio-derived solvents, and Deep Eutectic Solvents (DESs) [218-220]. Nevertheless, the adoption of these alternatives requires careful evaluation of their compatibility with photophysical tuning of CDs and their overall environmental profiles [219, 220]. Thus, addressing solvent sustainability is essential not only for mitigating the ecological and health risks associated with CDs synthesis and characterization, but also for enabling comprehensive Life Cycle Assessments (LCA) that account for upstream and downstream impacts (Figure 11), ultimately guiding the design of truly sustainable nanomaterials aligned with long-term environmental and regulatory goals.

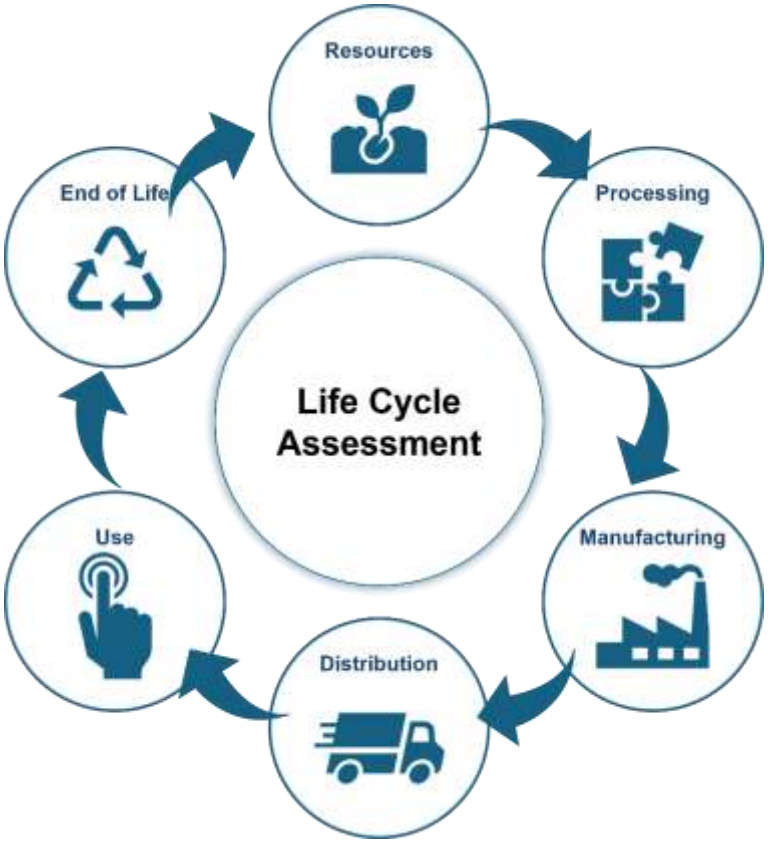

Figure 11. Schematic representation of Life Cycle Assessment approach.

As a direct consequence of the environmental and health concerns associated with solvent-intensive synthetic and characterization protocols, the synthesis of CDs and other engineered nanomaterials has increasingly been evaluated through an LCA framework. Recent LCA studies have demonstrated that solvent selection, energy

demand, and waste generation constitute major contributors to the overall environmental footprint of CDs production, in many cases exceeding the impacts associated with precursor materials themselves [221-223]. These findings have prompted the development of greener synthesis strategies, including the use of benign solvents, solvent-free approaches, and renewable carbon sources, in accordance with green chemistry principles [168, 174, 223, 224].

Despite the considerable technological and application potential of CDs, uncertainty remains regarding which synthetic strategies optimize both performance and environmental sustainability, largely due to the limited availability of systematic comparative data on the environmental impacts of alternative synthesis routes [225]. Several stages of nanomaterial production have been identified as environmentally relevant or impact-intensive [226], and previous investigations indicate that the choice of reagents, solvent systems, and energy inputs can disproportionately contribute to the life-cycle environmental burden of nanomaterials [221, 222]. Consequently, large-scale or industrial synthesis routes must be carefully evaluated to ensure that improvements in QY_{FL}, optical properties, or scalability are not offset by increased environmental impact [227].

In this context, LCA provides a robust, quantitative, and standardized methodology for assessing environmental impacts across all stages of a material's life cycle, from raw material extraction through synthesis, use, and end-of-life stages [228-230]. LCA has been successfully applied to a wide range of engineered nanomaterials, including TiO_2 nanoparticles, silver and copper nanoparticles, carbon nanotubes, magnetic nanoparticles, and CDs, providing insights into environmental hotspots and dominant impact drivers within their production chains [157, 222, 231-242]. By enabling comparative evaluation of alternative synthesis pathways and the identification of key contributors to environmental impacts such as GHGs emissions, energy consumption, water use, and toxicity LCA represents a critical decision-support tool for guiding the development of cleaner, more sustainable, and industrially scalable nanomaterial synthesis strategies.

LCA studies focusing on the synthesis of CDs have consistently identified the carbon precursor as one of the main contributors to the overall environmental impacts associated with their production [157, 227, 241]. This conclusion holds across different bottom-up synthesis routes and carbon sources, including widely used commercial precursors such as citric acid [157, 227, 241]. Since many commonly employed organic precursors are industrially produced chemicals, their use and/or synthesis is frequently

associated with high economic costs and potential risks to the environment and human health [243]. Consequently, the selection of the carbon precursor plays a central role in the development of more sustainable CDs synthesis strategies.

1.4.6. Sustainable carbon precursors and waste valorization

Although CDs can be synthesized from a wide range of organic molecules through simple solvothermal, hydrothermal, thermal, or microwave-assisted processes without sophisticated equipment [168, 169, 208, 244], sustainability considerations increasingly motivate the use of renewable and waste-derived precursors. Biomass and organic residues are particularly attractive due to their abundance, low cost, renewability, and potential for waste valorization within a circular economy framework [168, 244]. In fact, different researchers have already studied the fabrication of CDs from different types of waste and renewable carbon sources, such as fruits, biomass, residues, and others [200, 244-253]. Despite these promising results, CDs obtained from these carbon sources have been shown to present relatively low QY_{FL} values, typically below 20% [200, 247, 250-252]. To overcome this limitation, strategies such as heteroatom doping and surface functionalization have been widely adopted, leading to substantial improvements in fluorescence efficiency [243, 254].

All following examples involve hydrothermal synthesis of CDs from various natural precursors, highlighting the versatility of this approach in producing fluorescent nanomaterials. Hydrothermally synthesized CDs from natural fruit sources have demonstrated variable QY_{FL} depending on the precursor, presence of dopants, purification, and reaction conditions. For instance, CDs derived from pear fruit and watermelon juice exhibited QY_{FL} of approximately 10%, both with purification and in the absence of N-dopant [247]. In contrast, CDs synthesized from *Citrus aurantium* and pineapple juices without purification and nitrogen doping achieved slightly higher QY_{FL} of 13% (after 12 h reaction) and 10%, respectively [250, 251]. Other biomass-derived precursors, such as dwarf banana peel, fruit extracts, red onion peel, and *eucalyptus twigs*, yielded CDs with QY_{FL} 23%, 9%, 12%, and 2-10% (without purification but in the presence of nitrogen dopants including ammonia, EDA, and ammonium chloride), respectively [200, 248, 255, 256]. Notably, CDs obtained from orange juice in combination with EDA reached a QY_{FL} of 31.7% after purification, although requiring an extended hydrothermal treatment of 11 h [249]. These examples illustrate that a wide range of low-value organic wastes can serve as effective carbon sources for luminescent nanomaterials.

1.4.6.1. Corn Stover

Among agricultural residues, corn stover (comprising the leaves, stalks, and cobs remaining after corn harvest) represents a particularly significant and underutilized biomass resource. Global corn production is currently on the order of 1 billion tons per year, with a harvest index between 47% and 56%, meaning that roughly half of the above-ground biomass remains as residue [257]. Corn stover alone can reach an estimated 1.66 billion tons annually worldwide, however less than 10% is currently utilized, with only a small fraction directed toward industrial applications [258, 259]. The majority of corn stover is either left unused or openly burned, leading to wasted resources and environmental pollution [258]. The valorization of such abundant residues as carbon precursors for CDs synthesis therefore represents a highly promising strategy to reduce waste, lower environmental impacts, and support sustainable nanomaterial production.

Overall, LCA-based analyses clearly highlight the importance of precursor selection in minimizing the environmental footprint of CDs production. The use of abundant biomass and organic waste streams as carbon sources offers a viable pathway toward more sustainable CDs synthesis, particularly when integrated into well-designed processes that balance material performance with environmental responsibility, while maintaining functional optical properties required for practical applications.

1.5. Multicolor Carbon Dots in White LEDs

CDs have emerged as highly promising luminescent nanomaterials for WLEDs due to their tunable photoluminescence, low toxicity, and excellent optical stability. In WLED architectures, CDs function primarily as down-conversion phosphors: upon excitation by UV or blue LED chips, they efficiently convert high-energy photons into visible light (Figure 12). By employing either single-component CDs with broad emission spectra or blends of CDs emitting in complementary regions (e.g., blue, green, and red), a continuous emission across the visible spectrum can be achieved, enabling the generation of high-quality white light with superior CRI and tunable CCT [260].

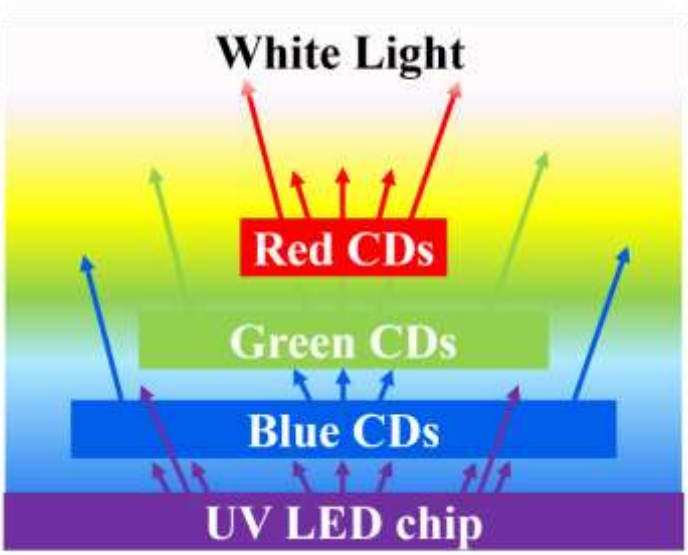

Figure 12. Schematic representation of WLEDs using multicolor CDs.

For device integration, CDs are typically embedded within optically transparent polymeric matrices, such as polyvinylpyrrolidone (PVP) or polymethyl methacrylate (PMMA), which provide uniform dispersion, mechanical stability, and enhanced spectral homogeneity. Optimization of the excitation wavelength, emission balance, and matrix-CDs interactions is critical to maximize luminous efficacy and spectral characteristics. Multicolor CDs-based WLEDs have been reported to exhibit CRIs exceeding 90, while single-component systems with broad emission spectra can simplify device fabrication and reduce inter-component spectral gaps [261, 262].

Recent studies demonstrate that WLEDs incorporating CDs can achieve both high luminous efficiency and spectral quality, highlighting their potential as sustainable alternatives to conventional rare-earth phosphors and heavy-metal quantum dots. Ongoing challenges include improving long-term operational stability under continuous electroluminescence and enhancing photon conversion efficiency, which remain a central objective in the development of high-performance solid-state lighting devices [263].

Therefore, the integration of CDs into WLEDs presents a promising strategy for the development of high-efficiency, environmentally friendly solid-state lighting, warranting further investigation into their optical performance and device stability.

1.6. Objectives

The transition towards more sustainable energy systems requires not only improvements in energy efficiency but also the development of materials and processes with reduced environmental footprints. In this context, CDs have emerged as promising luminescent nanomaterials due to their tunable photoluminescence, chemical stability, and potential for synthesis from abundant and renewable carbon sources, including organic waste.

Despite their growing relevance, important challenges remain regarding the environmental sustainability of CDs synthesis routes and the understanding of how synthesis parameters and precursor chemistry influence their optical performance. Many reported fabrication strategies rely on energy-intensive conditions, complex processing steps, or poorly understood structure-property relationships, limiting their scalability and sustainable implementation.

The overall objective of this PhD thesis is to investigate CDs as sustainable luminescent materials for potential application in WLEDs technologies by integrating LCA, green synthesis strategies, and fundamental studies of photoluminescence modulation.

To achieve this goal, the thesis addresses the following specific objectives:

I. To perform a life cycle assessment-based comparison of conventional and high-yield bottom-up synthesis routes for CDs, identifying environmental hotspots and evaluating whether increased synthesis yield effectively translates into improved environmental performance.
II. To develop and assess facile and environmentally benign synthesis strategies for producing brightly fluorescent CDs from waste-derived carbon sources, focusing on the role of precursor selection and synthesis conditions in achieving high photoluminescence efficiency.
III. To elucidate the influence of sulfur-containing precursors on the photoluminescent behavior of nitrogen- and nitrogen/sulfur-modified CDs, clarifying the mechanisms underlying fluorescence modulation, particularly the relative roles of surface oxidation and heteroatom incorporation.

1.7. Scope of the Thesis

This thesis focuses on the sustainability-oriented development and analysis of CDs as luminescent nanomaterials, integrating environmental assessment, green synthesis, and photophysical investigation. The scope is deliberately limited to bottom-up approaches, with particular emphasis on routes compatible with mild conditions, reduced energy demand, and the use of renewable or waste-derived carbon precursors.

From an environmental perspective, the work adopts a life cycle thinking approach, using LCA to evaluate synthesis-related impacts and to identify key parameters governing the environmental performance of CDs production. The scope of the LCA is restricted to the synthesis stage and associated end-of-life scenarios, as downstream device integration is beyond the boundaries of this study.

From a materials science perspective, the thesis addresses the relationship between precursor chemistry, surface structure, and photoluminescent behavior, with particular attention to nitrogen- and sulfur-related effects. The work aims to elucidate fluorescence modulation mechanisms rather than to maximize device-level performance.

While the potential application of CDs in WLEDs technologies motivates this research, the thesis does not include the fabrication or optimization of complete WLED devices. Instead, it provides the environmental, synthetic, and photophysical foundations necessary to support future integration of CDs into lighting systems.

Accordingly, the scope of this thesis is confined to establishing design principles for sustainable and high-performance CDs, balancing material functionality with environmental responsibility, rather than addressing large-scale manufacturing or commercial deployment.

2. Life Cycle Assessment as a pathway to sustainable Carbon Dots synthesis

2.1. **Article I**: Life Cycle Assessment-Based Comparative Study between High-Yield and “Standard” Bottom-Up Procedures for the Fabrication of Carbon Dots

Sónia Fernandes, Joaquim C. G. Esteves da Silva, and Luís Pinto da Silva

2.1.1. Contextualization and author contributions

CDs are widely synthesized through bottom-up approaches, including hydrothermal, microwave-assisted, and thermal treatments of small organic precursors [157, 168, 244, 264]. These methods are popular due to their simplicity and versatility; however, they generally exhibit low material efficiency, with synthesis yields often below 10 wt.% [157, 264]. Such low yields raise concerns regarding resource utilization, scalability, and environmental sustainability.

To overcome these limitations, several strategies have been developed to achieve higher yields. Representative approaches include salt-assisted thermal treatments and multi-step processes, such as the hydrothermal conversion of biomass-derived hydrochar followed by oxidative processing to obtain CDs, with reported yields ranging from 20-40 wt.% [264, 265]. Comparative studies suggest that these high-yield strategies can improve material efficiency, although potential environmental trade-offs remain [226].

Nevertheless, higher yields do not automatically translate into better environmental performance. High-yield routes often require longer reaction times, higher energy input, and additional chemical reagents, increasing process complexity. Previous LCA studies on nanomaterials have consistently shown that synthesis-related inputs, particularly energy demand and chemical use, tend to dominate overall environmental impacts, potentially offsetting the benefits associated with improved material efficiency [221, 222, 226, 227].

Within this context, this work [224] systematically evaluates the environmental sustainability of six representative CDs synthesis routes, encompassing both conventional bottom-up methods (hydrothermal, microwave-assisted, and thermal) and high-yield multi-step strategies [157, 168, 226, 244, 264, 265]. Multiple life cycle impact assessment (LCIA) methodologies (ReCiPe, Greenhouse Gas Protocol, AWARE, and

USEtox) were applied to capture a broad range of environmental impact categories and critically assess the trade-offs between synthesis yield, process complexity, and environmental performance.

I developed the comparative LCA framework, establishing the system boundaries and functional unit, and compiled and analysed the corresponding life cycle inventory data. The results were interpreted with particular emphasis on the relationship between synthesis yield and environmental impacts, under the supervision of Professor Dr. Luís Pinto da Silva. I also prepared the initial manuscript draft, which was subsequently reviewed and refined by Professor Dr. Luís Pinto da Silva and Professor Dr. Joaquim C. G. Esteves da Silva.

materials

MDPI

Article

Life Cycle Assessment-Based Comparative Study between High-Yield and "Standard" Bottom-Up Procedures for the Fabrication of Carbon Dots

Sónia Fernandes [1], Joaquim C. G. Esteves da Silva [1,2] and Luís Pinto da Silva [1,2,*]

[1] Chemistry Research Unit (CIQUP), Institute of Molecular Sciences (IMS), Faculty of Sciences of University of Porto, R. Campo Alegre 697, 4169-007 Porto, Portugal; soniaf91991@gmail.com (S.F.); jcsilva@fc.up.pt (J.C.G.E.d.S.)
[2] LACOMEPHL GreenUPorto, Department of Geosciences, Environmental and Territorial Planning, Faculty of Sciences of University of Porto, R. Campo Alegre 697, 4169-007 Porto, Portugal
* Correspondence: luis.silva@fc.up.pt

Abstract: Carbon dots (CDs) are carbon-based nanomaterials with remarkable properties that can be produced from a wide variety of synthesis routes. Given that "standard" bottom-up procedures are typically associated with low synthesis yields, different authors have been trying to devise alternative high-yield fabrication strategies. However, there is a doubt if sustainability-wise, the latter should be really preferred to the former. Herein, we employed a Life Cycle Assessment (LCA) approach to compare and understand the environmental impacts of high-yield and "standard" bottom-up strategies, by applying different life cycle impact assessment (LCIA) methods. These routes were: (1) production of hydrochar, via the hydrothermal treatment of carbon precursors, and its alkaline peroxide treatment into high-yield CDs; (2) microwave treatment of carbon precursors doped with ethylenediamine; (3) and (6) thermal treatment of carbon precursor and urea; (4) hydrothermal treatment of carbon precursor and urea; (5) microwave treatment of carbon precursor and urea. For this LCA, four LCIA methods were used: ReCiPe, Greenhouse Gas Protocol, AWARE, and USEtox. Results identified CD-5 as the most sustainable synthesis in ReCiPe, Greenhouse Gas Protocol, and USEtox. On the other hand, in AWARE, the most sustainable synthesis was CD-1. It was possible to conclude that, in general, high-yield synthesis (CD-1) was not more sustainable than "standard" bottom-up synthesis, such as CD-5 and CD-6 (also with relatively high-yield). More importantly, high-yield synthesis (CD-1) did not generate much lower environmental impacts than "standard" approaches with low yields, which indicates that higher yields come with relevant environmental costs.

Keywords: life cycle assessment; carbon dots; bottom-up synthesis; high-yield synthesis; sustainability

Citation: Fernandes, S.; Esteves da Silva, J.C.G.; Pinto da Silva, L. Life Cycle Assessment-Based Comparative Study between High-Yield and "Standard" Bottom-Up Procedures for the Fabrication of Carbon Dots. *Materials* **2022**, *15*, 3446. https://doi.org/10.3390/ma15103446

Academic Editor: Gueorgui Gueorguiev

Received: 29 March 2022
Accepted: 5 May 2022
Published: 11 May 2022

1. Introduction

Carbon Dots (CDs) consist of fluorescent nanomaterials based on carbon. These possess a near-spherical shape and have either an amorphous or nanocrystalline core and a surface where different functional groups (alcohols, amines, and carboxylic acids, for example) can be found [1–3].

CDs possess various attractive features, such as strong luminescence [4,5], good physical–chemical and photochemical stability [6–8], water solubility [6], biocompatibility [9–11] and low toxicity [5]. These remarkable characteristics have attracted the research community, which is focused on developing several practical applications for CDs, such as in light-emitting devices [12–14], sensing [14–18], bioimaging [19–21], photocatalysis [22], drug delivery [23], solar cells [24] and in photodynamic therapy [25,26]. Beyond this, CDs can be synthesized using a wide variety of precursors without sophisticated equipment through different bottom-up strategies, such as solvothermal, hydrothermal, thermal, or

microwave treatment of organic molecules [24,27–31]. While CDs can be generated from a wide variety of organic molecules as carbon sources, most of them can be expensive, as well as cause significant challenges to the environment and human health due to their use and/or synthesis [32].

One problem very present in CD development is related to their very low synthesis yields, which are generally equal to or below ~10% [33–35]. This can impair the production of CDs on a large-scale, as well as their future industrial applications. However, this problem can be solved if a way is found to convert the large amounts of solid carbon material, which are a major by-product of current synthesis strategies, into CDs.

As a matter of fact, some authors are already focusing on this topic [36] and they were able to produce CDs in high yield, achieving a synthesis yield of circa 20–40%. Despite these good results, the importance of these studies in the development of new CDs is still not validated in terms of efficiency, sustainability, and potential environmental impacts. To establish a suitable synthetic strategy for the sustainable fabrication of nanomaterials it is crucial to know this type of information, especially when the fabrication stage of nanomaterials was identified as an environmental concern [37]. In fact, some studies have defined that, during the life cycle of nanomaterials, the reagents and the energy required for the synthesis can contribute considerably to the environmental impacts [38,39]. In this sense, it is fundamental that before moving on to the industrial production of nanomaterials, the available synthesis routes are evaluated regarding their environmental impacts and sustainability to achieve the best alternatives for cleaner production.

Thus, our goal is to assess the environmental impacts associated with different synthesis route strategies of CDs, including high-yield and "standard" bottom-up synthesis. The "standard" bottom-up syntheses are related to either thermal or microwave-based heating of smaller organic molecules in powder form (calcination) or in solution (hydrothermal or solvothermal). These types of approaches can achieve a wide range of synthesis yields, albeit typically with lower yields. On the other hand, high-yield synthesis adds complexity to the synthesis procedures to ensure higher synthesis yields, by different approaches such as using a mixture of salts during thermal treatment, [40] or performing a subsequent alkaline peroxide treatment of the solid carbon by-product [36]. According to a previous study [41] that compared two high-yield syntheses, it was concluded that the procedure of an alkaline peroxide treatment of hydrochar [36] was more sustainable than a thermal treatment of carbon precursors mixed in a eutectic mixture of salts [40]. For this reason, the present work used the study [36] as the representative high-yield synthesis with the best environmental performance. In their turn, three studies [27,29,33] were considered where different "standard" bottom-up procedures (hydrothermal, microwave, and calcination) were performed. To achieve this aim, a life-cycle assessment (LCA) approach in order to quantify the environmental impacts of a given system during its life cycle [42–44] will be employed. Our LCA study will consider different parameters to evaluate the environmental impacts of the syntheses, for this, four distinct life cycle impact assessment (LCIA) methods will be used that specifically assess general parameters, CO_2 emissions, water consumption, and toxicity. This tool (LCA) has already been used to evaluate the environmental impacts related to different types of engineered nanomaterials, such as carbon nanotubes [45–48], copper nanoparticles [49], graphene oxide [50], silver nanoparticles [39,51], nanocellulose [52], TiO_2 nanoparticles [53], and even CDs [27,29,33,41,54]. Therefore, we expect to identify the synthesis route that is more sustainable and the most crucial parameters associated with the environmental impacts. More importantly, we want to evaluate if the higher synthesis yields of high-yield synthesis [36,40] can offset the expected higher environmental impacts associated with their complexity and added steps of high-yield synthesis, or if the simplicity of "standard" bottom-up procedures can lead to lower environmental impacts that can justify sustainability-wise lower synthesis yields.

2. Materials and Methods

The experimental section in this study is divided into four subsections: Scope and System Boundaries (2.1), Synthesis Routes (2.2), Life Cycle Inventory Data (2.3), and Environmental Impact Assessment (2.4).

2.1. Scope and System Boundaries

The present study consists of a cradle-to-grave LCA that aims for the evaluation of potential environmental impacts through their quantification and comparison, the assessment of the differences between these six types of CDs syntheses using different methods in these analyses, as well as the evaluation of two types of disposal scenarios. For this work, the laboratory-scale manufacturing stage of target nanoparticles was considered, as well as the direct emissions from CD production and indirect impacts related to the upstream resource extraction and energy generation.

This study uses six different synthesis routes for the fabrication of CDs [27,29,33,36] that englobe high-yield synthesis and different "standard" bottom-up synthesis strategies such as hydrothermal, microwave-assisted, and calcination, which are described in detail below (Scheme 1).

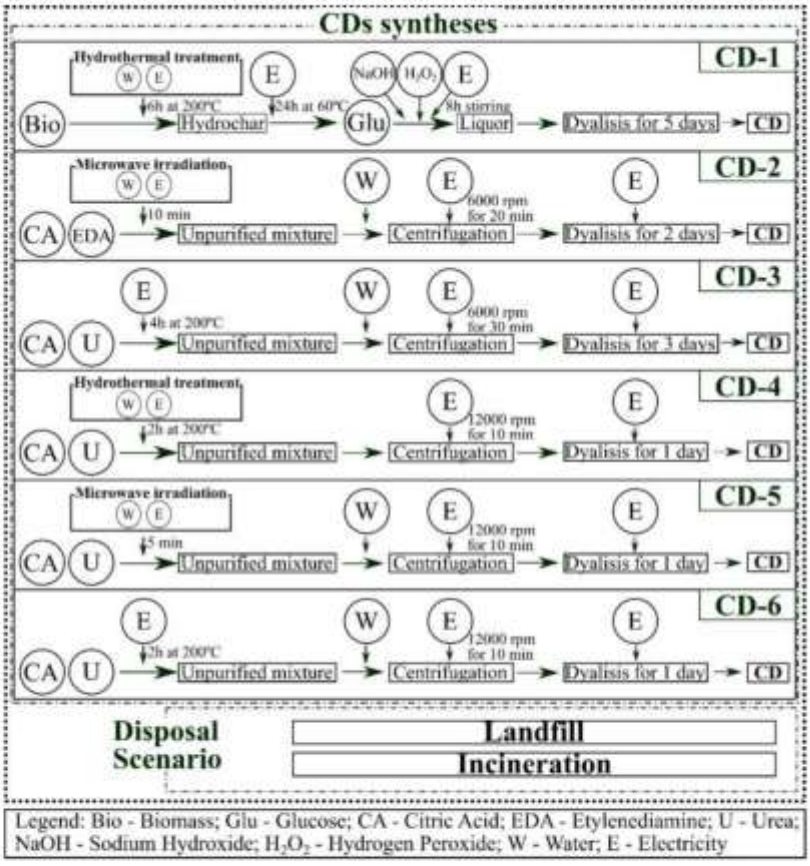

Scheme 1. Diagram for the six routes of Carbon Dot (CD) production and two disposal scenarios.

For this work, the environmental impacts were analyzed by using a weight-based functional unit of 1 kg, which means that 1 kg of produced CDs was considered. In this sense, it is possible to compare an equivalent amount of nanomaterials through the synthesis yield [55,56]. The synthesis yield of each CD under study can be viewed in Table 1.

Table 1. Synthesis yield of each CD under study.

CDs	Synthesis Yield (wt. %)	References
CD-1	40.1	[36]
CD-2	7.3	[33]
CD-3	9.85	[27]
CD-4	1.8	[29]
CD-5	28.5	[29]
CD-6	26.9	[29]

2.2. Synthesis Routes

In this study, as mentioned above, six different syntheses of CDs [27,29,33,36] were compared, in which the used materials and electricity can be viewed in Table S1. CDs 1, 2, 3, 4, 5, and 6 produced by the synthesis are named CD-1, CD-2, CD-3, CD-4, CD-5, and CD-6, respectively. CD-1 [36] is used as a representative for high-yield synthesis, while other CDs are employed as representatives for different approaches of "standard" bottom-up methods.

The synthesis route for CD-1 begins with hydrothermal treatment of glucose for 6 h at 200 °C. Posteriorly, it follows the centrifugation to separate the suspension and the obtained hydrochar. This was then dried for 24 h at 60 °C in an oven. Finally, an alkaline peroxide treatment of the dried hydrochar was performed for 8 h, in which the hydrochar was dispersed into diluted NaOH solution as H_2O_2 was added. Then, this mixture was stirred for 8 h at room temperature and the pure CDs were obtained after 5-day dialysis to remove salts and other molecular impurities [36].

In CD-2 [33], the synthesis route begins with mixing 0.5 g of citric acid (CA) and 556 µL of Ethylenediamine (EDA) in 5 mL of deionized water. Then, a microwave treatment of this solution was performed for 10 min. Posteriorly, to remove unsuspended and insoluble aggregates, the synthesized CDs were suspended in water, and then the solution was purified by centrifugation for 20 min at 6000 rpm to eliminate impurities. Finally, the sample was redispersed in 10 mL of deionized water and then purified by dialysis for 48 h. The purified sample was dried at 80 °C to evaporate the water of the sample.

In the synthesis route for CD-3 [27], 2.5 g of citric acid and urea (U) was prepared with a proportion of 3:1 in a beaker. Then, this mixture was heated for 4 h at 200 °C in an oven. Later, the synthesized CDs were suspended in water and then the solution was purified by centrifugation for 30 min at 6000 rpm to eliminate impurities. Finally, the CDs were purified by dialysis for three days and then the sample was freeze-dried, in which the resulting powder was stored for further use.

For CD-4 [29], the synthesis route begins with mixing 0.75 g of CA and 0.25 g of U in 5 mL of deionized water. Then, this mixture was placed in a Teflon-lined reactor and was heated for 2 h at 200 °C in an oven. Posteriorly, the synthesized CDs were suspended in 5 mL of deionized water and purified by centrifugation for 10 min at 12,000 rpm to remove impurities. Finally, the sample was purified through a 24 h dialysis process.

In CD-5 [29], the synthesis begins by mixing 0.75 g of CA and 0.25 g of U in 5 mL of deionized water. Then, this mixture was placed in a glass beaker and subjected to a microwave treatment for 5 min. Later, the synthesized CDs were suspended in 5 mL of deionized water and purified by centrifugation for 10 min at 12,000 rpm to remove impurities. Lastly, the sample was purified through a dialysis process for 24 h.

In the synthesis route for CD-6 [29], 0.75 g of CA and 0.25 g of U were mixed in a glass Petri box and heated for 2 h at 200 °C in an oven. Then, the synthesized CDs were suspended in 5 mL of deionized water and purified by centrifugation for 10 min

at 12,000 rpm to remove impurities. Finally, the sample was purified through a 24 h dialysis process.

2.3. Life Cycle Inventory Data

The evaluation of environmental impacts of CDs syntheses was based on inventory data from laboratory-scale synthesis procedures, the foreground data. This consists of raw materials (chemicals) and electricity (heating plate, oven, microwave, and centrifuge) used in the synthesis procedures (primary data). The foreground system included in this study was modeled from the data present in the Ecoinvent® 3.5 database, where GLO stands for global, RER for regional market for Europe, and RoW for Rest-of-World. In this sense, the amount of chemicals and electricity used, as well as the data used from Ecoinvent® 3.5 database are described in Table S1.

According to the Ecoinvent® 3.5 database, for electricity, the dataset used is related to the available electricity data on the medium voltage level in Europe in 2014. The electricity considered, as referred above, consists of what is used in the heating plate, oven, microwave, and centrifuge. For CD-2, CD-3, CD-4, CD-5, and CD-6 the above were considered as the equipment identified in the studies [27,29,33]. On the other hand, in CD-1, since the authors of this study did not identify the used equipment, we decided to apply standard plates and ovens. In this sense, the Normax Nx1200 Analogical magnetic stirrer with heating was considered, which has a power consumption of 500 W. The oven considered was the DRY-Line® Prime from VWR, with 12 A and a power supply in AC (single phase) of 230 V, which can achieve with a maximum power factor (1) a power consumption maximum of 2760 W. In CD-3, for dialysis, the heating plate referred to above was considered, and was also considered as the equipment used for the centrifugation in CD-2, CD-4, CD-5, and CD-6.

Regarding the disposal scenarios and the Ecoinvent® 3.5 database, two possible scenarios were considered, incineration and landfill.

2.4. Environmental Impact Assessment

This LCA study used a cradle-to-grave approach, from the production of precursor materials to the disposal scenario, also including the fabrication of CDs. The environmental impacts were modeled by four different LCIA methods, ReCiPe 2016 V1.03 endpoint method, Greenhouse Gas Protocol V1.02 method, AWARE (Available Water Remaining) V1.02 method, and USEtox 2 V1.00 method. This LCA study was performed with SimaPro 9.0.0.48 software.

ReCipe 2016 method, Hierarchist version [56] evaluates the environmental impacts in three categories of potential impacts (Human Health, Ecosystems, and Resources), which posteriorly are subdivided into subcategories. In the Human Health (HH) category, Global Warming–Human Health (GW–HH), Stratospheric ozone depletion (SO), Ionization Radiation (IR), Ozone formation–Human Health (OF), Fine Particulate Matter formation (FPM), Human Carcinogenic toxicity (HC), Human Non-Carcinogenic toxicity (HNC) and Water Consumption–Human Health (WC–HH) were assessed. On the other hand, in the Ecosystems ®category, the potential environmental impacts evaluated were Global Warming–Terrestrial Ecosystems (GW–TE), Global Warming–Freshwater Ecosystems (GW–FE), Ozone Formation–Terrestrial Ecosystems (OF–TE), Terrestrial acidification (TA), Freshwater Eutrophication (FE), Marine Eutrophication (ME), Terrestrial EcoToxicity (TET), Freshwater EcoToxicity (FET), Marine EcoToxicity (MET), Land Use (LU), Water Consumption–Terrestrial Ecosystem (WC–TE) and Water Consumption–Aquatic Ecosystems (WC–AE). Lastly, in the Resourc®(R) category, Mineral Resource scarcity (MR) and Fossil Resource scarcity (FR) were assessed.

The Greenhouse Gas Protocol method evaluates the CO_2 emissions through four categories, Fossil CO_2, Biogenic CO_2, CO_2 from land transformation, and CO_2 uptake. In Fossil CO_2, the fossil-based carbon, more specifically the carbon originating from fossil fuels is assessed. On the other hand, in the Biogenic CO_2 category, the biogenic carbon is

considered, which is the carbon originating from biogenic sources. In the CO_2 from land transformation category, only the direct impacts are assessed and, in turn, in the carbon uptake category, the carbon dioxide stored in plants and trees as they grow is considered.

The AWARE method assesses the water consumption impact in an LCA, more specifically it considers the potential of water deprivation, either to humans or ecosystems.

Finally, the USEtox 2 method evaluates the human and ecotoxicological impacts of chemicals in two categories, Human Health and Ecosystems. In the Human Health category, Human toxicity, cancer and Human toxicity, non-cancer are assessed. On the other hand, in the Ecosystems category, freshwater ecotoxicity is considered.

3. Results and Discussion

This section is divided into four subsections related to the methods used in the present LCA: ReCiPe method (3.1), Greenhouse Gas Protocol method (3.2), AWARE method (3.3), and USEtox method (3.4).

In this LCA, a comparison of potential environmental impacts, considering a weight-based functional unit of 1 kg of CDs was performed. However, our intention was to compare, in each method, the contributions of the different impact categories of the input involved in each synthesis and with each other. In this sense, it is not intended to make quantitative appreciations of the environmental impacts of each material input. As indicated before, CD-1 is used as a representative for high-yield synthesis, while CD-2 to CD-6 are representatives of different alternatives for "standard" bottom-up methods. More importantly, these latter CDs represent a wide range of synthesis yields (Table 1).

3.1. Impact Assessment by ReCiPe Method

The individual results regarding the associated environmental impacts obtained for CD-1, CD-2, CD-3, CD-4, CD-5, and CD-6 can be viewed in Figure S1. According to the input of each synthesis under the study, it was possible to verify that the major contributor in all subcategories was CA for CD-4 (Figure S1D) with environmental impacts varying between 67 and 99%. However, for the remaining syntheses in almost all the subcategories, electricity was the higher contributor in CD-1 (with contributions between 56 and 96%), CA was responsible for most of the impacts in CD-2 (between 41 and 94%), CD-3 (between 53 and 95%), CD-5 (between 48 and 95%), and CD-6 (between 54 and 95%). In this sense, for CD-1 (Figure S1A), the carbon precursor (glucose) constitutes the highest contribution to environmental impacts (circa 61%) in Marine Eutrophication (ME) and Land Use (LU). In CD-2 (Figure S1B), electricity was the major contributor (circa 49%) in Ionizing Radiation (IR) and EDA was responsible for most of the impacts in ME and Fossil Resource scarcity (FR), contributing by approximately 63% and 67%, respectively. For CD-3 (Figure S1C) and CD-6 (Figure S1F), electricity was the highest contributor to IR and Freshwater Eutrophication (FE), being responsible for circa 80% (CD-3: 84% and CD-6: 83%) and 50% (CD-3: 52% and CD-6: 51%) of impacts. In CD-5 (Figure S1E), electricity was responsible for most of the impacts in the IR subcategory, contributing to 82% of the environmental impacts. It is worth mentioning that for this CD, in the FE subcategory, CA and electricity have similar contributions to the environmental impacts, with 48% and 47%, respectively. On the other hand, for all the syntheses in the study, water appears to have quite negligible impacts in almost all the subcategories. In CD-1, hydrogen peroxide also seems to have negligible environmental impacts.

The comparison of associated environmental impacts for the six syntheses can be observed in Figure 1, in which all environmental impact subcategories are included in only three main categories (Human Health, Ecosystems, and Resources). The first conclusion was that synthesis 5 (CD-5) is associated with lower environmental impacts and synthesis 4 (CD-4) with the highest impacts. In this sense, it is possible to understand that hydrothermal treatment has more impacts than microwave treatment. However, in CD-1 (in which hydrothermal treatment was also performed), the environmental impacts are expressively lower than in CD-4. This can be attributed to the distinct synthesis yields, which are 40.1%

for CD-1 and 1.8% for CD-4. It is worth mentioning that, only in CD-2 is it possible to observe expressively higher impacts in the Resources category than in the other categories (difference of 12% and 14% of impacts, respectively, with Human Health and Ecosystems). One possible explanation for this can be attributed to EDA, which as we mentioned above, is the highest contributor in the FR subcategory, one of the two subcategories that are included in the Resources category.

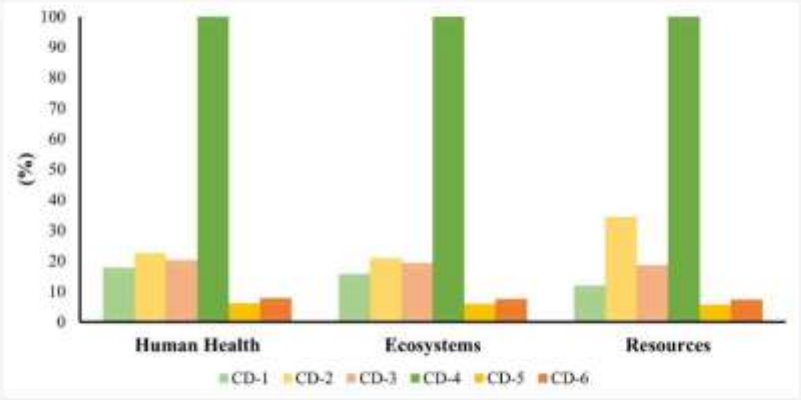

Figure 1. Relative environmental impacts of syntheses under study, applying ReCiPe method. Green scale refers to hydrothermal treatments; Yellow scale refers to microwave-assisted treatments; Orange scale refers to calcination treatments.

It was also possible to observe from the previous figure that CD-1 does not have a lower environmental impact when compared to CD-2 and CD-3. However, there is a significant difference between the synthesis yield of these syntheses (Table 1). In this sense, it was verified that, between CD-1 and CD-2, the differences in potential impacts were 5% in Human Health and Ecosystems, and 22% in Resources. On the other hand, the variations in the contributions were 2% in Human Health, 4% in Ecosystems, and 7% in Resources, between CD-1 and CD-3. The major differences in amounts of inputs of these syntheses were in water and energy, in which CD-1 used less water than CD-2 and CD-3 (CD-1: 24.9 kg; CD-2: 77.9 kg; CD-3: 101.5 kg), and higher electricity in CD-1 when compared to the other syntheses (CD-1: 146.8 kWh; CD-2: 24.2 kWh; CD-3: 46.09 kWh). Considering the energy inputs to perform CD-1 it was verified that the higher input is related to the hydrothermal treatment and the drying process (82.8 kWh) by the oven. For the stirring step and dialysis, only 4 kWh and 60 kWh were needed. On the other hand, in CD-2 and CD-3, the higher energy input is related to dialysis (CD-2: 24 kWh; CD-3: 36 kWh). The remaining inputs are related to microwave (0.12 kWh) and centrifuge (0.06 kWh) in CD-2, and to the oven (10 kWh) and centrifuge (0.09 kWh) in CD-3. Thus, these smaller differences in potential environmental impacts between high-yield synthesis and "standard" bottom-up syntheses with low yield (less than 10%) suggest that the first may not offset the higher yield. Nevertheless, given that CD-1 spends a significant amount of energy when drying with an oven, employing a less energy-consuming strategy for this step might reduce the associated environmental costs in a relevant manner.

Once our LCA considers a cradle-to-grave approach, it is important to evaluate disposal scenarios of the synthesized CDs. These scenarios intend to assess a more advanced stage of the life cycle of these CDs, considering either incineration or landfill disposal.

In incineration, for each synthesis, it was possible to understand that the synthesis has more environmental impacts than the disposal scenario in all the subcategories (Figure S2). Thus, the potential impacts of synthesis vary between 91–100% for CD-1, 90–100% for CD-2, 89–100% for CD-3, 97–100% for CD-4, 71–100% for CD-5, and 76–100% for CD-6. It

is worth mentioning that the incineration scenario has quite negligible impacts with the exception of the FET, MET, and HNC subcategories in CD-1 (respectively, 9%, 9%, and 7%), CD-2 (respectively, 10%, 9%, and 6%), CD-3 (respectively, 11%, 10%, and 7%), and CD-4 (respectively, 3%, 3%, and 2%). On the other hand, the exceptions for CD-5 and CD-6 were the GW–HH (2% for both CDs), GW–TE (2% for both CDs), GW–FE (2% for both CDs), SO (CD-5: 2%), FET (CD-5: 29% and CD-6: 24%), MET (CD-5: 27% and CD-6: 22%), HC (CD-5: 4% and CD-6: 3%), and HNC (CD-5: 20% and CD-6: 16%) subcategories.

Comparing all the syntheses (Figure 2) for the incineration scenario it was possible to understand that CD-5 is associated with lower environmental impacts and CD-4 with the highest impacts. Once again, it is possible to verify that CD-2 has higher impacts in the Resources category than the other categories (differences of 12% with HH and 14% with E).

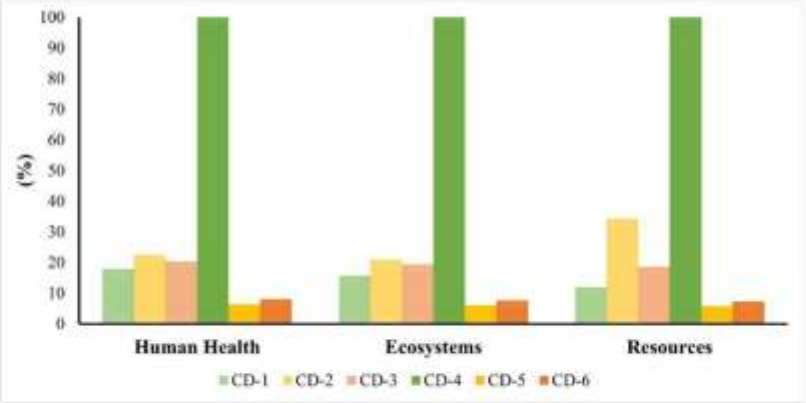

Figure 2. Relative environmental impacts of syntheses under study for incineration disposal scenario, applying ReCiPe method. Green scale refers to hydrothermal treatments; Yellow scale refers to microwave-assisted treatments; Orange scale refers to calcination treatments.

For the landfill scenario, it was also verified that the synthesis is responsible for more impacts than the disposal scenario in all the syntheses under study (Figure S3). In this sense, the synthesis potential environmental impacts vary between 87–100% for CD-1, 85–100% for CD-2, 84–100% for CD-3, 96–100% for CD-4, 61–100% for CD-5, and 67–100% for CD-6. For all the syntheses it was possible to understand that the disposal scenario has quite negligible impacts with some exceptions. In CD-1 and CD-3, these were in ME (CD-1: 4% and CD-3: 3%), FET (CD-1: 14% and CD-3: 16%), MET (CD-1: 13% and CD-3: 15%), and HNC (CD-1: 12% and CD-3: 13%). On the other hand, for CD-2 and CD-4, the exceptions were in FET (CD-2: 15% and CD-4: 4%), MET (CD-2: 14% and CD-4: 4%), and HNC (CD-2: 11% and CD-4: 3%). Finally, GW–HH (3% for both CDs), GW–TE (3% for both CDs), GW–FE (3% for both CDs), ME (CD-5: 9% and CD-6: 7%), FET (CD-5: 39% and CD-6: 33%), MET (CD-5: 38% and CD-6: 32%), HC (CD-5: 2%), and HNC (CD-5: 33% and CD-6: 28%) were the exceptions in CD-5 and CD-6.

For the landfill scenario, considering all the syntheses (Figure 3), it was possible to corroborate once again that CD-5 has the lowest environmental impacts and CD-4 is related to the highest impacts. In this disposal scenario, it also verifies that CD-2 has higher impacts in the Resources category than the others.

For a better understanding of the relative environmental impacts of different disposal scenarios, we compared the environmental impacts for CD-5 (the route with lower impacts) when considering both incineration and landfill. It was observed that incineration has slightly lower impacts than landfill in the three main categories (Figure S4). However, the evaluation of the subcategories allows understanding that incineration has significantly lower impacts in ME, FET, MET, and HNC with differences of 9%, 15%, 15%, and 17%,

respectively (Figure 4). It is worth mentioning that, in the Resources category (MR and FR subcategories), landfill and incineration have almost the same environmental impacts.

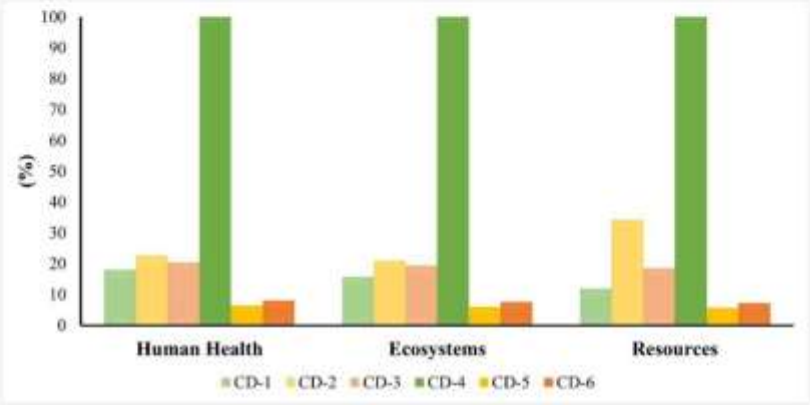

Figure 3. Relative environmental impacts of syntheses under study for landfill disposal scenario, applying ReCiPe method. Green scale refers to hydrothermal treatments; Yellow scale refers to microwave-assisted treatments; Orange scale refers to calcination treatments.

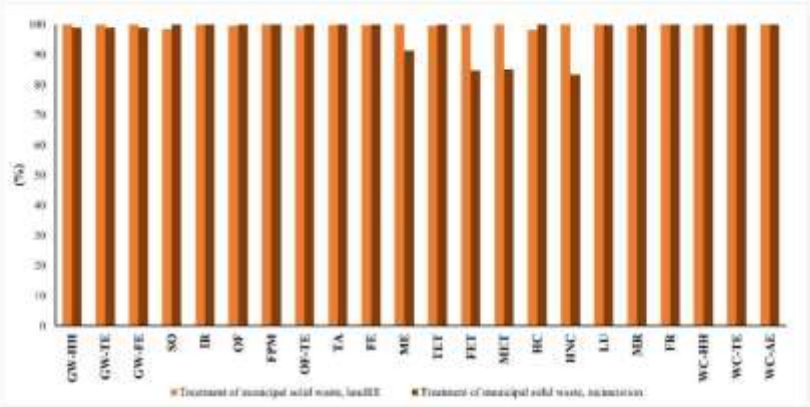

Figure 4. Comparative relative environmental impacts of CD-5 for incineration and landfill disposal scenario, applying ReCiPe method.

3.2. *Impact Assessment by Greenhouse Gas Protocol Method*

The individual results regarding the associated environmental impacts obtained for all the syntheses with the Greenhouse Gas Protocol method can be observed in Figure S5. It can be seen that, when considering each input of the syntheses under study, the major contributor to the environmental impacts was electricity in CD-1 (with contributions of between 55 and 97%) and CA in CD-2 (contributions varying from 50–92%), CD-3 (contributions varying from 51–93%), CD-4 (contributions varying from 83–99%), CD-5 (contributions varying from 56–94%), and CD-6 (contributions varying from 53–93%). It is worth mentioning that in CD-1 (Figure S5A), the contributions of electricity and glucose are slightly similar (differences of 10%) in the CO_2 uptake category. In CD-2 (Figure S5B), electricity and EDA have a slightly higher contribution to the impacts in the Fossil and Biogenic CO_2 categories, in which EDA is higher in the first and electricity in the second

category. On the other hand, in CD-3 (Figure S5C), electricity has a greater impact on Biogenic CO_2 than in the other three categories but is still smaller than CA (a difference of 4%). Finally, in CD-4, CD-5, and CD-6, electricity has a higher impact on Biogenic CO_2 (CD-4: 5%, CD-5: 42% and CD-6: 45%) and urea in Fossil CO_2 (CD-4: 15%, CD-5 and CD-6: 12%), with CA still being responsible for most impacts in both categories. It is important to note that, the relative contributions of water in all the syntheses and hydrogen peroxide in CD-1 appear to be quite negligible.

The comparison of all the syntheses (Figure 5) allowed us to understand that CD-5 is associated with lower environmental impacts and CD-4 has the highest impacts, which also permitted us to verify that the hydrothermal treatment has more impacts than the microwave treatment. Despite a hydrothermal treatment being performed in CD-1, the potential impacts were significantly lower than in CD-4 due to the differences in the synthesis yield. It is noteworthy that the environmental impacts for CD-1 were considerably higher in the Biogenic CO_2 category and drastically lower in CO_2 uptake. This analysis also allowed us to understand that the Biogenic CO_2 category in this method is a key category in CD syntheses since the relative impacts were higher when compared with the other categories, mainly in CD-1 (differences between 24% and 36%).

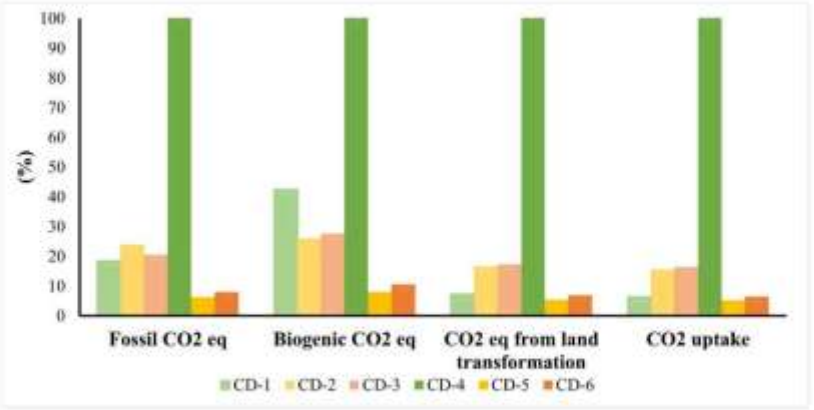

Figure 5. Relative environmental impacts of syntheses under study, applying Greenhouse Gas Protocol method. Green scale refers to hydrothermal treatments; Yellow scale refers to microwave-assisted treatments; Orange scale refers to calcination treatments.

To evaluate the entire life cycle of the synthesized CDs an assessment of incineration and landfill disposal scenarios was carried out.

For the incineration scenario, the results obtained for each synthesis can be observed in Figure S6. This analysis also allowed us to understand that the synthesis has more environmental impacts than the disposal scenario. The contributions of the synthesis vary between 91–100% in CD-1 (Figure S6A), 85–100% in CD-2 (Figure S6B), 86–100% in CD-3 (Figure S6C), 96–100% in CD-4 (Figure S6D), 64–100% in CD-5 (Figure S6E), and 70–100% in CD-6 (Figure S6F). In this sense, the impacts of incineration are quite negligible with the exception of Biogenic CO_2 in CD-1 (9%), CD-2 (15%), CD-3 (14%), CD-4 (4%), CD-5 (2%), and CD-6 (2%). Fossil CO_2 is also an exception in CD-5, with contributions of 36%, and in CD-6 with 30%.

Comparing all the syntheses for the incineration scenario (Figure 6) it was possible to verify that CD-5 has lower environmental impacts and CD-4 is associated with the highest impacts, as we observed in the ReCiPe method. It was possible to observe that, for all the CDs, in the Biogenic CO_2 category the impacts are higher when compared with the other categories. These differences are expressively higher in CD-1, in which the contributions rise between 26% and 38%. That allowed us to understand that in this method the Biogenic

CO_2 was a key category in CD syntheses, since the impacts of incineration have greater contributions, mainly in CD-1.

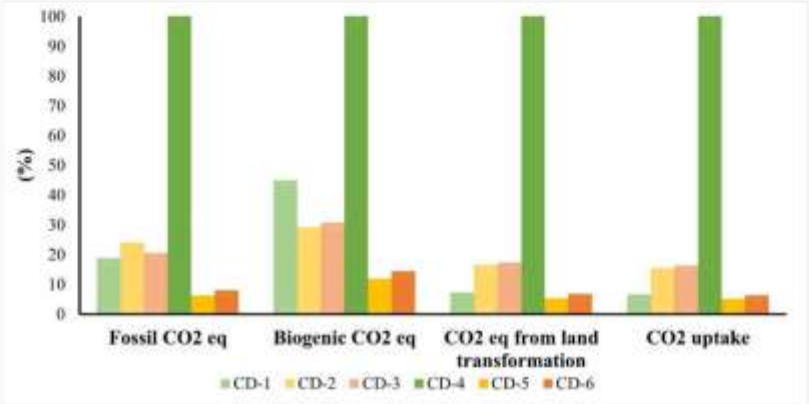

Figure 6. Relative environmental impacts of syntheses under study for incineration disposal scenario, applying Greenhouse Gas Protocol method. Green scale refers to hydrothermal treatments; Yellow scale refers to microwave-assisted treatments; Orange scale refers to calcination treatments.

On the other hand, for the landfill disposal scenario, the results obtained can be observed in Figure S7. It was possible to observe that, once again, the synthesis has higher impacts than the disposal scenario. Thus, the environmental impacts of synthesis range between 91–100% in CD-1 (Figure S7A), 86–100% in CD-2 (Figure S7B), 87–100% in CD-3 (Figure S7C), 96–100% in CD-4 (Figure S7D), 66–100% in CD-5 (Figure S7E), and 72–100% in CD-6 (Figure S7F). As a result, the contributions of the landfill scenario are quite negligible with the exception of Biogenic CO_2 in all the syntheses (CD-1: 9%, in CD-2: 14%, in CD-3: 13%, in CD-4: 4%, in CD-5: 35%, and in CD-6: 29%).

The comparison of all the syntheses for the landfill disposal scenario (Figure 7) allowed us to understand that CD-5 has minor impacts and CD-4 has the highest environmental impacts. It is worth mentioning that, once again, in all the syntheses of CDs, the impacts were higher in the Biogenic CO_2 category, especially in CD-1.

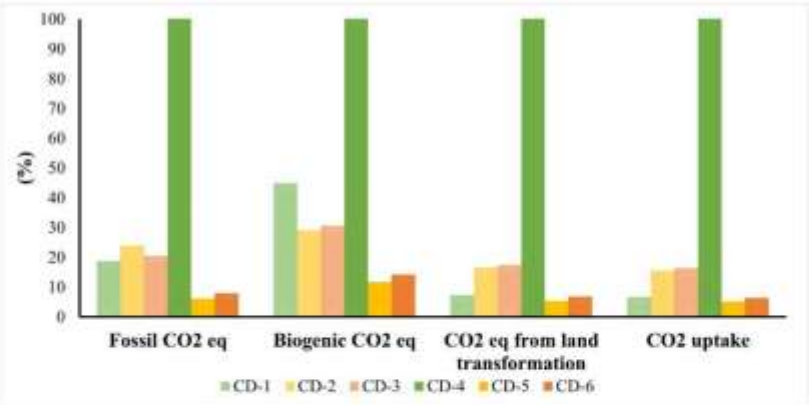

Figure 7. Relative environmental impacts of syntheses under study for landfill disposal scenario, applying Greenhouse Gas Protocol method. Green scale refers to hydrothermal treatments; Yellow scale refers to microwave-assisted treatments; Orange scale refers to calcination treatments.

Considering the synthesis with lower impacts (CD-5), the disposal scenarios that were more sustainable were evaluated (Figure 8). In this sense, we verify that for CO_2 from land transformation and CO_2 uptake categories, the contributions of landfill and incineration have the same environmental impacts. However, in Fossil and Biogenic CO_2, the landfill has slightly lower impacts than incineration (a difference of 2%). According to the previous method (ReCiPe), it was verified that for the Human Health and Ecosystem categories, incineration has slightly lower impacts. This allowed us to conclude that, for CD-5, the landfill has minor environmental impacts on CO_2 emissions (Fossil and Biogenic) and incineration has lower impacts on Human Health and Ecosystems.

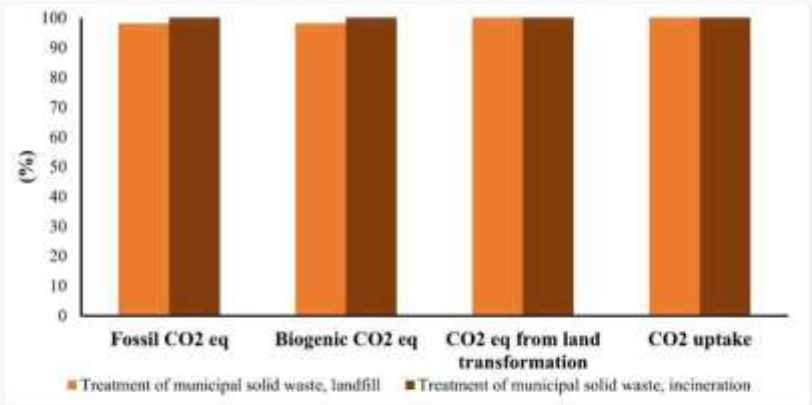

Figure 8. Relative environmental impacts of CD-5 for incineration and landfill disposal scenario, applying Greenhouse Gas Protocol method.

3.3. *Impact Assessment by AWARE Method*

The results obtained by this method for each synthesis under study can be observed in Figure S8. It was possible to observe that for water use, the major contributor was electricity in CD-1 (with contributions of 76%) and CA in the remaining syntheses (CD-2: 78%, CD-3: 80%, CD-4: 84%, CD-5: 81%, and CD-6: 80%). In relation to the other synthesis inputs, it was possible to verify a trend (from the highest to the lowest contributor) of electricity > glucose > NaOH > H_2O_2 > H_2O in CD-1 (Figure S8A), CA > EDA > electricity > H_2O in CD-2 (Figure S8B), CA > urea > electricity > H_2O in CD-3 (Figure S8C), CA > urea > H_2O > electricity in CD-4 (Figure S8D), and CA > urea > electricity > H_2O in CD-5 (Figure S8E) and CD-6 (Figure S8F). In general, it was possible to understand that CD-2, CD-3, CD-5, and CD-6 appear to have a similar trend, in which we have a carbon precursor as the higher contributor, followed by the N-containing small organic molecules (EDA or urea) and then, electricity and water. It is worth mentioning that in CD-4 and CD-6, water appears to have negligible impacts (less than 1%).

Comparing all the syntheses under study (Figure 9), the first conclusion was that CD-1 is associated with lower environmental impacts and CD-4 with the highest impacts. These synthesis routes performed a hydrothermal treatment of the precursors, and the major difference is that CD-1 consists of a high-yield synthesis. Furthermore, the carbon precursor in these syntheses is different (CD-1: glucose and CD-4: citric acid), which can also explain the difference (97%) in the potential environmental impacts. It is worth mentioning that this method allowed us to understand that, when we focus on the potential of water deprivation, the high-yield synthesis (CD-1) is more sustainable.

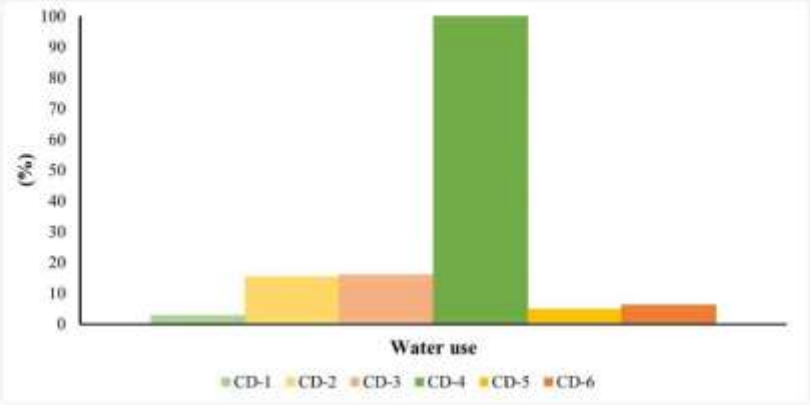

Figure 9. Relative environmental impacts of all syntheses under study, applying AWARE method. Green scale refers to hydrothermal treatments; Yellow scale refers to microwave-assisted treatments; Orange scale refers to calcination treatments.

The contribution of incineration and landfill disposal scenarios to the water consumption of the synthesized CDs was also evaluated.

For each synthesis under study, the analysis of the incineration scenario can be observed in Figure S9. In all the synthesized CDs, the synthesis was responsible for most of the environmental impacts, meaning the disposal scenario contributions were negligible. This method allowed us to understand that, for water use, the synthesis has an expressively higher contribution than incineration (CD-1: 99.81%, CD-2: 99.96%, CD-3: 99.97%, CD-4: 99.99%, CD-5: 99.89%, and CD-6: 99.91%).

Comparing all the syntheses for the incineration scenario (Figure 10), we concluded that CD-1 has lower environmental impacts and CD-4 is associated with higher impacts. These syntheses have a difference of 97% in the potential impacts, despite both having a hydrothermal approach.

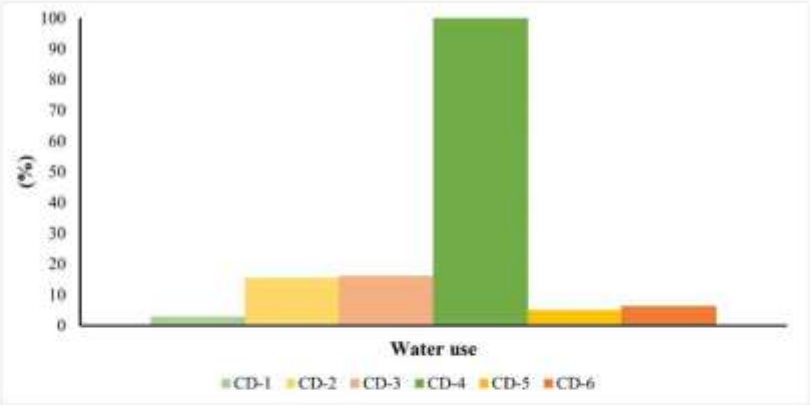

Figure 10. Relative environmental impacts of all the syntheses under study for incineration disposal scenario, applying AWARE method. Green scale refers to hydrothermal treatments; Yellow scale refers to microwave-assisted treatments; Orange scale refers to calcination treatments.

The evaluation of the landfill scenario of each synthesis under study can be observed in Figure S10. It was possible to conclude that, in all synthesized CDs, the contributions of the

disposal scenario were quite negligible, meaning the synthesis step had more environmental impacts. In this sense, the synthesis was responsible for 99.95% in CD-1 (Figure S10A), 99.99% in CD-2 (Figure S10B), CD-3 (Figure S10C) and CD-4 (Figure S10D), 99.97% in CD-5 (Figure S10E), and 99.98% in CD-6 (Figure S10F).

In the evaluation of the landfill scenario, a comparison of all the syntheses under study was also performed (Figure 11). That allowed us to conclude that in this scenario CD-1 is also related to lower impacts and CD-4 with higher environmental impacts. Thus, this shows once again the sustainability of CD-1 regarding water deprivation.

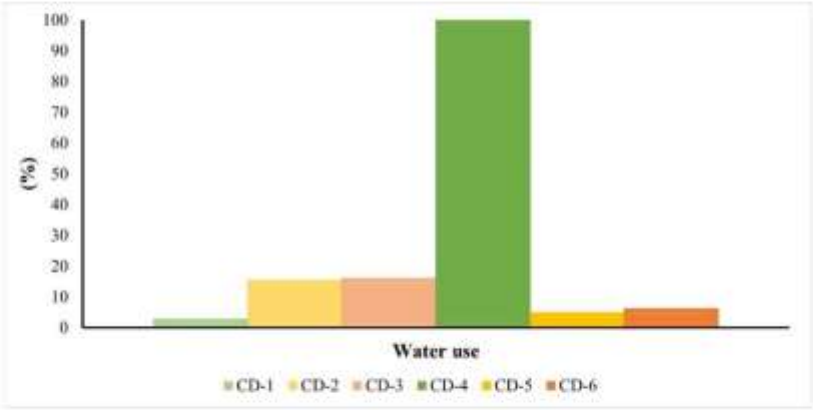

Figure 11. Relative environmental impacts of all syntheses for landfill disposal scenario, applying AWARE method. Green scale refers to hydrothermal treatments; Yellow scale refers to microwave-assisted treatments; Orange scale refers to calcination treatments.

According to the synthesis with lower impacts in this method, an evaluation of the disposal scenario (Figure 12) was performed. This analysis permitted us to conclude that no significant differences exist between the disposal scenarios, despite landfill having slightly lower environmental impacts than incineration (a difference of 0.14%). Therefore, as verified in the previous method (Greenhouse Gas Protocol method), the landfill scenario appears to be more sustainable regarding CO_2 emissions and water consumption.

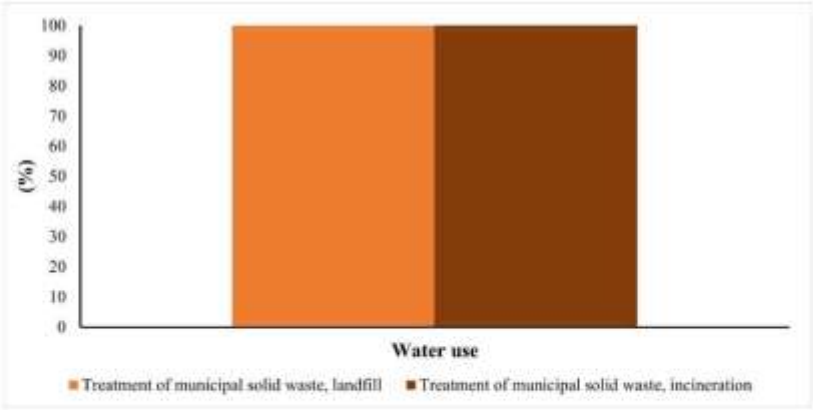

Figure 12. Relative environmental impacts of CD-1 for incineration and landfill disposal scenario, applying AWARE method.

3.4. Impact Assessment by USEtox Method

The assessment of human and ecotoxicological impacts for each synthesis under study can be observed in Figure S11. This allowed us to conclude that the major contributor was electricity in CD-1 (with contributions between 80 and 93%) and CA in the remaining syntheses (CD-2: 44–61%, CD-3: 52–67%, CD-4: 87–93%, CD-5: 56–71%, and CD-6: 54–69%). In CD-1 (Figure S11A), it was possible to observe that glucose has the highest contribution to the Human Toxicity non-cancer category, being responsible for 16% of the impacts (a difference of 13% when compared to the other subcategories). For CD-2 it was verified that the highest contributor is not completely isolated from the other inputs, especially from EDA in Human Health (differences of 12%). It is still worth mentioning that, in this synthesis, EDA has a higher impact than electricity. In CD-3, a similitude of potential environmental impacts between CA and electricity exists in the Human Toxicity cancer subcategory (difference of 10%). For CD-4 (Figure S11D), in all subcategories, urea has more environmental impacts than electricity. On the contrary, in CD-3 (Figure S11C), CD-5 (Figure S11E) and CD-6 (Figure S11F), electricity was responsible for more environmental impacts than urea in all the subcategories. It is noteworthy that water appears to have quite negligible environmental impacts in all the syntheses, as compared with hydrogen peroxide in CD-1.

The comparison of all syntheses under study (Figure 13) allowed us to conclude that CD-5 is associated with lower impacts and CD-4 with the highest environmental impacts. Thus, this method observed that, for toxicological impacts of chemicals, CD-5 appears to be more sustainable than the other syntheses, as we observed in the ReCiPE and Greenhouse Gas Protocol method.

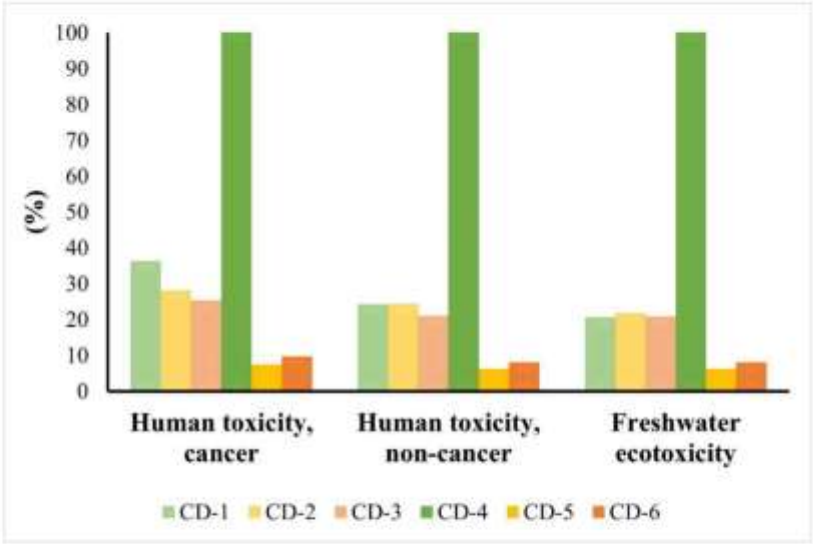

Figure 13. Relative environmental impacts of all syntheses under study, applying USEtox method. Green scale refers to hydrothermal treatments; Yellow scale refers to microwave-assisted treatments; Orange scale refers to calcination treatments.

For this method, the incineration and landfill disposal scenarios of the synthesized CDs were evaluated.

The results obtained for incineration in each synthesis under study can be observed in Figure S12. It was possible to observe that the synthesis was responsible for more environmental impacts than the disposal scenario. In this sense, the contributions of the

synthesis varied between 94–99% in CD-1 (Figure S12A) and CD-3 (Figure S12C), 95–99% in CD-2 (Figure S12B), 99–100% in CD-4 (Figure S12D), 83–96% in CD-5 (Figure S12E), and 86–97% in CD-6 (Figure S12F). Thus, the potential impact of incineration appears to be quite negligible, especially in the Human Toxicity cancer subcategory for CD-1, CD-2, and CD-4 (contributions less than 1%). However, for CD-4, in the Human Toxicity non-cancer subcategory the impacts were also less than 1%. For CD-3, it was observed that the impacts were lower in the Human Health category (i.e., human toxicity with cancer and human toxicity without cancer subcategories) than in Freshwater ecotoxicity. It is worth mentioning that for CD-5 and CD-6, in all subcategories, the environmental impacts of incineration were lower, when compared with the previous syntheses. On the other hand, for CD-5 and CD-6, the difference in potential impacts between Human Health and Ecosystems was higher. That is expressively evident in the Freshwater ecotoxicity subcategory, in which incineration was responsible for 17% and 14% of environmental impacts, respectively, in CD-5 and in CD-6.

Comparing all the syntheses for the incineration scenario (Figure 14), it was possible to understand that CD-5 has lower environmental impacts and CD-4 has higher impacts. Furthermore, CD-1, CD-2, and CD-3 have higher impacts in the Human Health category than in the Ecosystem category. It is worth mentioning that CD-1 has expressively higher impacts on Human toxicity with cancer, with differences of 12% and 15% when compared to Human toxicity without cancer and Freshwater ecotoxicity, respectively. This allowed us to conclude that CD-1 presents less sustainability when we assessed the ecotoxicity of chemicals. That can be explained due to the alkaline peroxide treatment performed in this synthesis route.

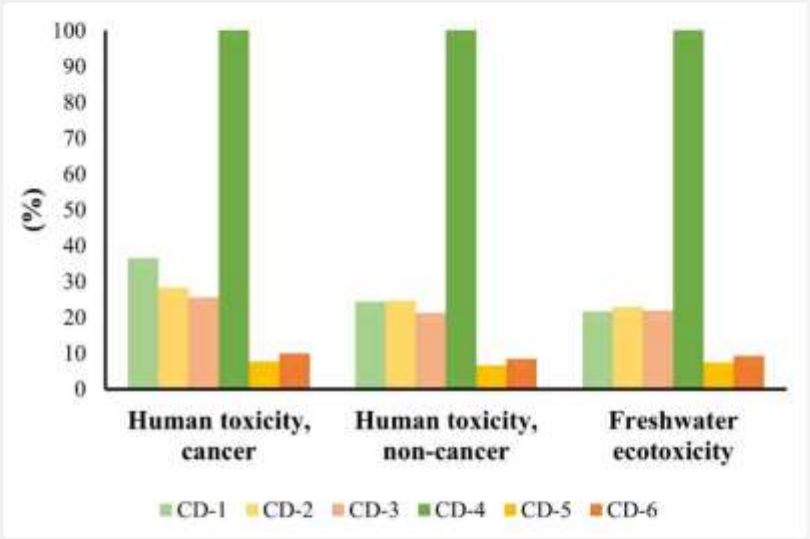

Figure 14. Relative environmental impacts of all the syntheses under study for incineration disposal scenario, applying USEtox method. Green scale refers to hydrothermal treatments; Yellow scale refers to microwave-assisted treatments; Orange scale refers to calcination treatments.

On the other hand, the analysis of the landfill disposal scenario of each synthesized CD can be observed in Figure S13. It was possible to understand that, once again, the synthesis scenario is associated with higher environmental impacts than the disposal scenario. In this sense, the contributions of synthesis vary between 91–100% in CD-1 (Figure S13A), 92–99% in CD-2 (Figure S13B) and in CD-3 (Figure S13C), 98–100% in CD-4 (Figure S13D), 76–98% in CD-5 (Figure S13E), and 81–98% in CD-5 (Figure S13F). It is noteworthy that, in CD-1, CD-2,

and CD-3, the impacts of the landfill scenario were quite negligible in the Human Toxicity with cancer subcategory. Whereas in the remaining subcategories the contributions were responsible for more than 2% of impacts. In CD-4, the contributions of the landfill category appear to be very insignificant in both subcategories of the Human Health category (less than 0.5% of impacts). Finally, in CD-5 and CD-6, the environmental impacts of the disposal scenario were lower in all subcategories when compared with the other synthesis. However, the difference in impacts between the Human Health subcategories and Ecosystems was higher than in the other syntheses. This is expressively evident in freshwater, where the contributions were 24% and 19% of impacts in CD-5 and CD-6, respectively.

The evaluation of all the syntheses in respect of the landfill scenario (Figure 15) allowed us to understand that CD-5 has lower impacts and CD-4 was associated with higher environmental impacts. Once again, it was verified that CD-1, CD-2, and CD-3 have higher impacts on Human Health than in the Ecosystem category. This is expressively evident in CD-1, where differences between both subcategories of Human Health and the Human toxicity, cancer with Freshwater ecotoxicity were 12% and 14%, respectively. Thus, once again, when we compared the impacts of CD-1 considering the other methods, it was concluded that CD-1 presents less sustainability related to the ecotoxicity of chemicals.

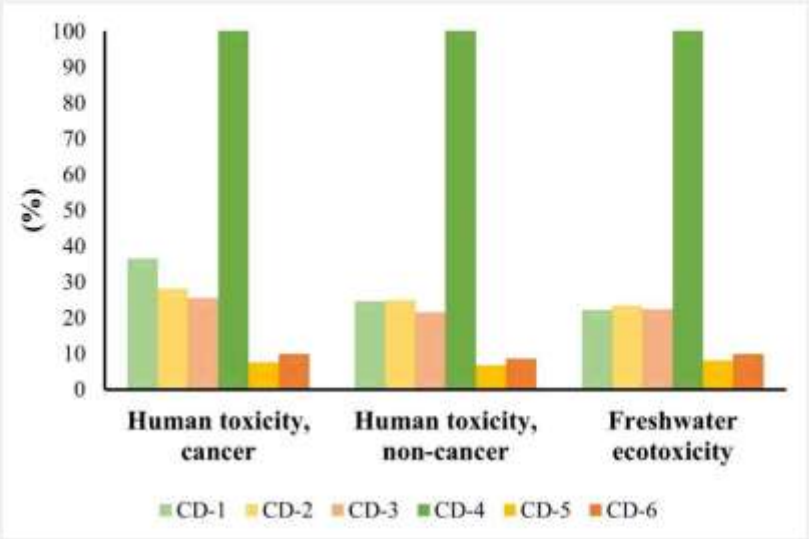

Figure 15. Relative environmental impacts of all syntheses for landfill disposal scenario, applying USEtox method. Green scale refers to hydrothermal treatments; Yellow scale refers to microwave-assisted treatments; Orange scale refers to calcination treatments.

Considering the synthesis with lower impacts in this method (CD-5), we verified that the incineration scenario has slightly lower environmental impacts than the landfill scenario (a difference of 0.9% for Human Health and 8.1% for Ecosystems), as is noted in Figure 16. This was also seen for the ReCiPe method. However, it was observed that in the Human Health category, incineration has lower impacts on human toxicity without cancer and higher impacts on human toxicity with cancer.

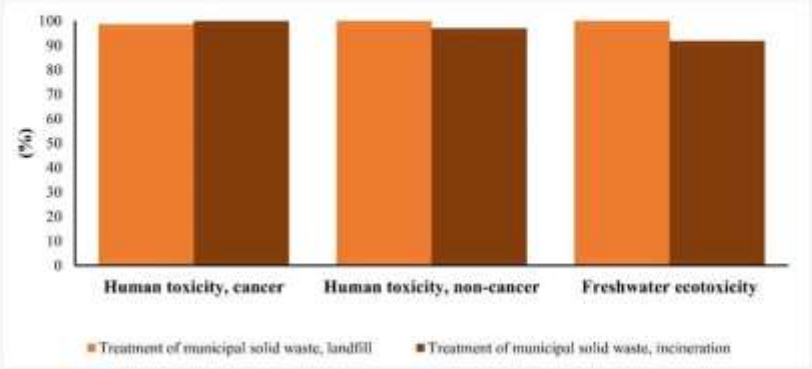

Figure 16. Relative environmental impacts of CD-5 for incineration and landfill disposal scenario, applying USEtox method.

4. Conclusions

The present work allowed us to conclude that CD-5 has lower environmental impacts when analyzed using the ReCiPe, Greenhouse Gas Protocol, and USEtox LCIA methods. On the other hand, in the AWARE method, the most sustainable synthesis was CD-1. Nonetheless, in all the methods, CD-4 has a higher environmental impact.

According to the disposal scenario, for CD-5, it was verified that incineration has slightly lower impacts than the landfill scenario in the ReCiPe and USEtox methods. On the contrary, in the Greenhouse Gas Protocol, the landfill scenario has lower impacts than incineration. In the AWARE method, for CD-1, it was shown that no significant differences exist between both disposal scenarios with landfill being somewhat more sustainable than incineration.

In the ReCiPe method, CD-1 was associated with lower impacts than CD-4 (despite both performing a hydrothermal treatment), which can be explained due to the difference in the synthesis yields. Additionally, in the three analyses (synthesis, incineration, and landfill) performed, it was verified that CD-2 has higher impacts in the Resources category.

In the Greenhouse Gas Protocol, considering all the subcategories, it was noted that the impacts in CD-1 were higher in Biogenic CO_2 and lower in CO_2 uptake. Beyond this, Biogenic CO_2 appears to be a key category in this method, since the environmental impacts were higher in all synthesized CDs.

In the AWARE method, we verified that the synthesis routes where a hydrothermal treatment was performed (CD-1 and CD-4) were either the most sustainable (CD-1) or were responsible for higher impacts (CD-4). This could be explained by the distinct synthesis yields and carbon precursor used in the synthesis or the huge input of water in CD-4. It is worth mentioning that CD-1 was more sustainable in water deprivation.

In USEtox, the analysis of the disposal scenario showed that CD-5 and CD-6 have lower environmental impacts when compared to the remaining syntheses. However, in CD-5 and CD-6, the difference in potential environmental impacts between the two main categories (Human Health and Ecosystems) was higher than in the other syntheses. Beyond this, the impacts of incineration and landfill in CD-1 were higher in Human Health, and ecotoxicity cancer than in the other subcategories. Due to the higher impacts of CD-1 in comparison with the other methods, it was concluded that CD-1 presents less sustainability related to the ecotoxicity of chemicals.

In short, we concluded that, for CD-5, landfill has minor environmental impacts on CO_2 emissions (Fossil and Biogenic) and incineration has lower impacts in the Human Health and Ecosystems categories (ReCiPe and USEtox methods).

In general, it is possible to conclude that high-yield synthesis (CD-1) is not associated with lower potential impacts than some "standard" bottom-up syntheses, such as CD-5

and CD-6. Actually, in three of the methods used (ReCiPe, Greenhouse Gas Protocol, and USEtox), despite the difference of 12–13% in the synthesis yield between CD-5, CD-6, and CD-1, the impacts were lower for the "standard" bottom-up synthesis. More importantly, in terms of sustainability, CD-1 is not so much "greener" than CD-2 and CD-3, which are "standard" bottom-up syntheses with low yields (CD-2: 7.3% and CD-3: 9.85%). In this sense, it was concluded that current high-yield procedures may not yet be readily-available alternatives for cleaner production, since higher synthesis yields appear to come with higher environmental costs. Nevertheless, the higher impacts associated with higher synthesis yields appear to come from increased consumption of electricity associated with the hydrothermal and drying processes. Thus, if electricity consumption could be reduced in those steps, these new strategies could indeed be more suitable choices for producing CDs in a more environmentally friendly way.

Supplementary Materials: The following supporting information can be downloaded at: https://www.mdpi.com/article/10.3390/ma15103446/s1, Table S1. Inventory of raw materials for each CD under study, in which quantities are referred to as 1 kg of CD; Figure S1. Relative environmental impacts of the synthesis under study applying the ReCiPe endpoint method. (A) CD-1; (B) CD-2, (C) CD-3; (D) CD-4, (E) CD-5 and (F) CD-6. The abbreviations are explained in Section 2.4; Figure S2. Relative environmental impacts of the synthesis under study and the disposal scenario of incineration, applying the ReCiPe endpoint method. (A) CD-1; (B) CD-2, (C) CD-3; (D) CD-4, (E) CD-5 and (F) CD-6. The abbreviations are explained in Section 2.4; Figure S3. Relative environmental impacts of the synthesis under study and the disposal scenario of landfill, applying the ReCiPe endpoint method. (A) CD-1, (B) CD-2, (C) CD-3, (D) CD-4, (E) CD-5, and (F) CD-6. The abbreviations are explained in Section 2.4; Figure S4. Relative environmental impacts of CD-5 for incineration and landfill disposal scenario, applying the ReCiPe method; Figure S5. Relative environmental impacts of syntheses under study, applying the Greenhouse Gas Protocol method. (A) CD-1, (B) CD-2, (C) CD-3, (D) CD-4, (E) CD-5, and (F) CD-6; Figure S6. Relative environmental impacts of syntheses under study for the incineration disposal scenario, applying the Greenhouse Gas Protocol method. (A) CD-1, (B) CD-2, (C) CD-3, (D) CD-4, (E) CD-5, and (F) CD-6; Figure S7. Relative environmental impacts of syntheses under study for the landfill disposal scenario, applying the Greenhouse Gas Protocol method. (A) CD-1, (B) CD-2, (C) CD-3, (D) CD-4, (E) CD-5, and (F) CD-6; Figure S8. Relative environmental impacts of syntheses under study, applying the AWARE method. (A) CD-1, (B) CD-2, (C) CD-3, (D) CD-4, (E) CD-5, and (F) CD-6; Figure S9. Relative environmental impacts of syntheses under study for the incineration disposal scenario, applying the AWARE method. (A) CD-1, (B) CD-2, (C) CD-3; (D) CD-4, (E) CD-5 and (F) CD-6; Figure S10. Relative environmental impacts of syntheses under study for the landfill disposal scenario, applying the AWARE method. (A) CD-1, (B) CD-2, (C) CD-3, (D) CD-4, (E) CD-5, and (F) CD-6; Figure S11. Relative environmental impacts of syntheses under study, applying the USEtox method. (A) CD-1, (B) CD-2, (C) CD-3, (D) CD-4, (E) CD-5, and (F) CD-6; Figure S12. Relative environmental impacts of syntheses under study, for the incineration disposal scenario, applying the USEtox method. (A) CD-1, (B) CD-2, (C) CD-3, (D) CD-4, (E) CD-5, and (F) CD-6; Figure S13. Relative environmental impacts of syntheses under study, for the landfill disposal scenario, applying the USEtox method. (A) CD-1, (B) CD-2, (C) CD-3, (D) CD-4, (E) CD-5, and (F) CD-6.

Author Contributions: Conceptualization, L.P.d.S.; investigation, S.F.; writing—original draft preparation, S.F.; writing—review and editing, L.P.d.S. and J.C.G.E.d.S.; visualization, S.F.; supervision, L.P.d.S. and J.C.G.E.d.S.; funding acquisition, L.P.d.S. and J.C.G.E.d.S. All authors have read and agreed to the published version of the manuscript.

Funding: "Fundação para a Ciência e Tecnologia" (FCT, Portugal) is acknowledged for the funding project PTDC/QUI-QFI/2870/2020, R&D Units CIQUP (UIDB/00081/2020) and GreenUPorto (UIDB/05748/2020), and Associated Laboratory IMS (LA/P/0056/2020). Luís Pinto da Silva acknowledges funding from the FCT under the Scientific Employment Stimulus (2021.00768.CEECIND). Sónia Fernandes also acknowledges the FCT for funding her Ph.D. grant (2021.05479.BD).

Acknowledgments: The Laboratory for Computational Modeling of Environmental Pollutants-Human Interactions (LACOMEPHI) is acknowledged.

Conflicts of Interest: The authors declare no conflict of interest.

References

1. Esteves da Silva, J.C.G.; Gonçalves, H.M. Analytical and bioanalytical applications of carbon dots. *TrAC Trends Anal. Chem.* **2011**, *30*, 1327–1336. [CrossRef]
2. Wang, R.; Lu, K.Q.; Tang, Z.R.; Xu, Y.J. Recent progress in carbon quantum dots: Synthesis, properties and applications in photocatalysis. *J. Mater. Chem. A* **2017**, *5*, 3717–3734. [CrossRef]
3. Zhou, J.; Zhou, H.; Tang, J.; Deng, S.; Yan, F.; Li, W.; Qu, M. Carbon dots doped with heteroatoms for fluorescent bioimaging: A review. *Microchim. Acta* **2017**, *184*, 343–368. [CrossRef]
4. Xiong, Y.; Schneider, J.; Ushakova, E.V.; Rogach, A.L. Influence of molecular fluorophores on the research field of chemically synthesized carbon dots. *Nano Today* **2018**, *23*, 124–139. [CrossRef]
5. Wang, R.; Gao, Z.; Gao, G.; Wo, Y.; Wang, Y.; Shen, G.; Cui, D. Systematic safety evaluation on photoluminescent carbon dots. *Nanoscale Res. Lett.* **2013**, *8*, 122. [CrossRef] [PubMed]
6. Lim, S.Y.; Shen, W.; Gao, Z. Carbon quantum dots and their applications. *Chem. Soc. Rev.* **2015**, *44*, 362–381. [CrossRef] [PubMed]
7. Kozák, O.; Datta, K.K.R.; Greplová, M.; Ranc, V.; Kašlík, J.; Zbořil, R. Surfactant derived amphiphilic carbon dots with tunable photoluminescence. *J. Phys. Chem. C* **2013**, *117*, 24991–24996. [CrossRef]
8. Sendão, R.M.S.; Crista, D.M.A.; Afonso, A.C.P.; Martínez de Yuso, M.V.; Algarra, M.; Esteves da Silva, J.C.G.; Pinto da Silva, L. Insight into the hybrid luminescence showed by carbon dots and molecular fluorophores in solution. *Phys. Chem. Chem. Phys.* **2019**, *21*, 20919–20926. [CrossRef]
9. Baker, S.N.; Baker, G.A. Luminescent carbon nanodots: Emergent nanolights. *Angew. Chem. Int. Ed. Eng.* **2010**, *49*, 6726–6744. [CrossRef]
10. Sun, Y.P.; Zhou, B.; Lin, Y.; Wang, W.; Fernando, K.A.; Pathak, P.; Meziani, M.J.; Harruff, B.A.; Wang, X.; Wang, H.; et al. Quantum-sized carbon dots for bright and colorful photoluminescence. *J. Am. Chem. Soc.* **2006**, *128*, 7756–7757. [CrossRef]
11. Vale, N.; Silva, S.; Duarte, D.; Crista, D.M.A.; Pinto da Silva, L.; Esteves da Silva, J.C.G. Normal breast epithelial MCF-10A cells to evaluate the safety of carbon dots. *RSC Med. Chem.* **2021**, *12*, 245–253. [CrossRef] [PubMed]
12. Wang, C.; Hu, T.; Chen, Y.; Xu, Y.; Song, Q. Polymer-assisted self-assembly of multicolor carbon dots as solid-state phosphors for fabrication of warm, high quality, and temperature-responsive white-light-emitting devices. *ACS Appl. Mater. Interfaces* **2019**, *11*, 22332–22338. [CrossRef]
13. Wang, Y.; Wang, K.; Han, Z.; Yin, Z.; Zhou, C.; Du, F.; Zhou, S.; Chen, P.; Xie, Z. High color rendering index trichromatic white and red LEDs prepared from silane functionalized carbon dots. *J. Mater. Chem. C* **2017**, *5*, 9629–9637. [CrossRef]
14. Qiao, G.; Chen, G.; Wen, Q.; Liu, W.; Gao, J.; Yu, Z.; Wang, Q. Rapid conversion from common precursors to carbon dots in large scale: Spectral controls, optical sensing, cellular imaging and LEDs application. *J. Colloid Interface Sci.* **2020**, *580*, 88–98. [CrossRef] [PubMed]
15. Crista, D.M.A.; Mello, G.P.C.; Shevchuk, O.; Sendão, R.M.S.; Simões, E.F.C.; Leitão, J.M.M.; Pinto da Silva, L.; Esteves da Silva, J.C.G. 3-Hydroxyphenylboronic acid-based carbon dot sensors for fructose sensing. *J. Fluoresc.* **2019**, *29*, 265–270. [CrossRef]
16. Afonso, A.C.P.; Correia, A.S.; Duarte, D.; Brandão, A.T.S.C.; de Yuso, M.d.V.M.; Jiménez-Jiménez, J.; Vale, N.; Pereira, C.M.; Algarra, M.; Pinto da Silva, L. An Active Surface Preservation Strategy for the Rational Development of Carbon Dots as pH-Responsive Fluorescent Nanosensors. *Chemosensors* **2021**, *9*, 191. [CrossRef]
17. Mello, G.P.C.; Simões, E.F.C.; Crista, D.M.A.; Leitão, J.M.M.; Pinto da Silva, L.; Esteves da Silva, J.C.G. Glucose sensing by fluorescent nanomaterials. *Crit. Rev. Anal. Chem.* **2019**, *49*, 542–552. [CrossRef]
18. Simões, E.F.C.; Pinto da Silva, L.; Esteves da Silva, J.C.G.; Leitão, J.M.M. Hypochlorite fluorescence sensing by phenylboronic acid-alizarin adduct based carbon dots. *Talanta* **2020**, *208*, 120447. [CrossRef]
19. Kang, Y.F.; Li, Y.H.; Fang, Y.W.; Xu, Y.; Wei, X.M.; Yin, X.B. Carbon quantum dots for zebrafish fluorescence imaging. *Sci. Rep.* **2015**, *5*, 11835. [CrossRef]
20. Bogireddy, N.K.; Lara, J.; Fragoso, L.R.; Agarwal, V. One-step hydrothermal preparation of highly stable N-doped oxidized carbon dots for toxic organic pollutants sensing and bioimaging. *Chem. Eng. J.* **2020**, *401*, 126097. [CrossRef]
21. Ding, Y.; Tan, W.; Zheng, X.; Ji, X.; Song, P.; Bao, L.; Zhang, C.; Shang, J.; Qin, K.; Wei, Y. Serratia marcescens-derived fluorescent carbon dots as a platform toward multi-mode bioimaging and detection of p-nitrophenol. *Analyst* **2020**, *146*, 683–690. [CrossRef] [PubMed]
22. Li, D.; Huang, J.; Li, R.; Chen, P.; Chen, D.; Cai, M.; Liu, H.; Feng, Y.; Lv, W.; Liu, G. Synthesis of a carbon dots modified g-C_3N_4/SnO_2 Z-scheme photocatalyst with superior photocatalytic activity for PPCPs degradation under visible light irradiation. *J. Hazard. Mater.* **2021**, *401*, 123257. [CrossRef] [PubMed]
23. Hettiarachchi, S.D.; Graham, R.M.; Mintz, K.J.; Zhou, Y.; Vanni, S.; Peng, Z.; Leblanc, R.M. Triple conjugated carbon dots as a nano-drug delivery model for glioblastoma brain tumors. *Nanoscale* **2019**, *11*, 6192–6205. [CrossRef] [PubMed]
24. Yan, L.; Yang, Y.; Ma, C.Q.; Liu, X.; Wang, H.; Xu, B. Synthesis of carbon quantum dots by chemical vapor deposition approach for use in polymer solar cell as the electrode buffer layer. *Carbon* **2016**, *109*, 598–607. [CrossRef]
25. He, H.; Zheng, X.; Liu, S.; Zheng, M.; Xie, Z.; Wang, Y.; Yu, M.; Shuai, X. Diketopyrrolopyrrole-based carbon dots for photodynamic therapy. *Nanoscale* **2018**, *10*, 10991–10998. [CrossRef] [PubMed]
26. Knoblauch, R.; Geddes, C.D. Carbon nanodots in photodynamic antimicrobial therapy: A review. *Materials* **2020**, *13*, 4004. [CrossRef] [PubMed]

27. Crista, D.M.A.; El Mragui, A.; Algarra, M.; Esteves da Silva, J.C.G.; Luque, R.; Pinto da Silva, L. Turning spent coffee grounds into sustainable precursors for the fabrication of carbon dots. *Nanomaterials* **2020**, *10*, 1209. [CrossRef]
28. Zhou, Y.; Liyanage, P.Y.; Geleroff, D.L.; Peng, Z.; Mintz, K.J.; Hettiarachchi, S.D.; Pandey, R.R.; Chusuei, C.C.; Blackwelder, P.L.; Leblanc, R.M. Photoluminescent carbon dots: A mixture of heterogeneous fractions. *ChemPhysChem* **2018**, *19*, 2589–2597. [CrossRef]
29. Crista, D.M.A.; Esteves da Silva, J.C.G.; Pinto da Silva, L. Evaluation of different bottom-up routes for the fabrication of carbon dots. *Nanomaterials* **2020**, *10*, 1316. [CrossRef]
30. Zhou, D.; Wang, Y.; Tian, P.; Jing, P.; Sun, M.; Chen, X.; Xu, X.; Li, D.; Mei, S.; Liu, X.; et al. Microwave-assisted heating method toward multicolor quantum dot-based phosphors with much improved luminescence. *ACS Appl. Mater. Interfaces* **2018**, *10*, 27160–27170. [CrossRef]
31. Tripathi, K.M.; Sonker, A.K.; Bhati, A.; Bhuyan, J.; Singh, A.; Singh, A.; Sarkar, S.; Sonkar, S.K. Large-scale synthesis of soluble graphitic hollow carbon nanorods with tunable photoluminescence for the selective fluorescent detection of DNA. *New J. Chem.* **2016**, *40*, 1571–1579. [CrossRef]
32. Zhang, B.; Liu, Y.; Ren, M.; Li, W.; Zhang, X.; Vajtal, R.; Ajayan, P.M.; Tour, J.M.; Wang, L. Sustainable synthesis of bright green fluorescent nitrogen-doped carbon quantum dots from alkali lignin. *ChemSusChem* **2019**, *12*, 4202–4210. [CrossRef] [PubMed]
33. Christė, S.; Esteves da Silva, J.C.G.; Pinto da Silva, L. Evaluation of the environmental impact and efficiency of N-doping strategies in the synthesis of carbon dots. *Materials* **2020**, *13*, 504. [CrossRef] [PubMed]
34. Tan, J.; Zou, R.; Zhang, J.; Li, W.; Zhang, L.; Yue, D. Large-scale synthesis of N-doped carbon quantum dots and their phosphorescence properties in polyurethane matrix. *Nanoscale* **2016**, *8*, 4742–4747. [CrossRef] [PubMed]
35. Yang, Y.; Cui, J.; Zheng, M.; Hu, C.; Tan, S.; Xiao, Y.; Yang, Q.; Liu, Y. One-step synthesis of amino-functionalized fluorescent carbon nanoparticles by hydrothermal carbonization of chitosan. *Chem. Commun.* **2012**, *48*, 380–382. [CrossRef]
36. Jing, S.; Zhao, Y.; Sun, R.C.; Zhong, L.; Peng, X. Facile and high-yield synthesis of carbon quantum dots from biomass-derived carbons at mild condition. *ACS Sustain. Chem. Eng.* **2019**, *7*, 7833–7843. [CrossRef]
37. Pourzahedi, L.; Eckelman, M.J. Comparative life cycle assessment of silver nanoparticles synthesis routes. *Environ. Sci. Nano* **2015**, *2*, 361–369. [CrossRef]
38. Eckelman, M.J.; Zimmerman, J.B.; Anastas, P.T. Toward green Nano, E-factor analysis of several nanomaterial syntheses. *J. Ind. Ecol.* **2008**, *12*, 316–328. [CrossRef]
39. Bafana, A.; Kumar, S.V.; Temizel-Sekeryan, S.; Dahoumane, S.A.; Haselbach, L.; Jeffryes, C.S. Evaluating microwave-synthesized silver nanoparticles from silver nitrate with life cycle assessment techniques. *Sci. Total Environ.* **2018**, *636*, 936–943. [CrossRef]
40. Li, L.; Lu, C.; Li, S.; Liu, S.; Wang, L.; Cai, W.; Xu, W.; Yang, X.; Liu, Y.; Zhang, R. A high-yield and versatile method for the synthesis of carbon dots for bioimaging applications. *J. Mater. Chem. B* **2017**, *5*, 1935. [CrossRef]
41. Fernandes, S.; Esteves da Silva, J.C.G.; Pinto da Silva, L. Comparative life cycle assessment of high-yield synthesis routes for carbon dots. *NanoImpact* **2021**, *23*, 100332. [CrossRef]
42. Ramos, A.; Teixeira, C.; Rouboa, A. Assessment study of an advanced gasification strategy at low temperature for syngas generation. *Int. J. Hydrogen Energy* **2018**, *43*, 10155–10166. [CrossRef]
43. Ramos, A.; Teixeira, C.; Rouboa, A. Environmental analysis of waste-to-energy—A Portuguese case study. *Energies* **2018**, *11*, 548. [CrossRef]
44. Hischier, R.; Walser, T. Life cycle assessment of engineered nanomaterials: State of the art and strategies to overcome existing gaps. *Sci. Total Environ.* **2012**, *425*, 271–282. [CrossRef]
45. Upadhyayula, V.; Meyer, D.E.; Curran, M.A.; Gonzalez, M.A. Life cycle assessment as a tool to enhance the environmental performance of carbon nanotube products: A review. *J. Clean. Prod.* **2012**, *26*, 37–47. [CrossRef]
46. Celik, I.; Mason, B.E.; Phillips, A.B.; Heben, M.J.; Apul, D. Environmental impacts from photovoltaic solar cells made with single walled carbon nanotubes. *Environ. Sci. Technol.* **2017**, *51*, 4722–4732. [CrossRef]
47. Teah, H.Y.; Sato, T.; Namiki, K.; Asaka, M.; Feng, K.; Noda, S. Life cycle greenhouse gas emissions of long and pure carbon nanotubes synthesized via onsubstrate and fluidized-bed chemical vapor deposition. *ACS Sustain. Chem. Eng.* **2020**, *8*, 1730–1740. [CrossRef]
48. Temizel-Sekeryan, S.; Wu, F.; Hicks, A.L. Global scale life cycle environmental impacts of single- and multi-walled carbon nanotube synthesis processes. *Int. J. Life Cycle Assess.* **2021**, *26*, 656–672. [CrossRef]
49. Pu, Y.; Tang, F.; Adam, P.M.; Laratte, B.; Ionescu, R.E. Fate and characterization factors of nanoparticles in seventeen subcontinental freshwaters: A case study on copper nanoparticles. *Environ. Sci. Technol.* **2016**, *50*, 9370–9379. [CrossRef]
50. Deng, Y.; Li, J.; Qiu, M.; Yang, F.; Zhang, J.; Yuan, C. Deriving characterization factors on freshwater ecotoxicity of graphene oxide nanomaterial for life cycle impact assessment. *Int. J. Life Cycle Assess.* **2016**, *22*, 222–236. [CrossRef]
51. Temizel-Sekeryan, S.; Hicks, A.L. Global environmental impacts of silver nanoparticle production methods supported by life cycle assessment. *Resour. Conserv. Recycl.* **2020**, *156*, 1046762. [CrossRef]
52. Piccinno, F.; Hischier, R.; Seeger, S.; Som, C. Predicting the environmental impact of a future nanocellulose production at industrial scale: Application of the life cycle assessment scale-up framework. *J. Clean. Prod.* **2018**, *174*, 283–295. [CrossRef]
53. Fernandes, S.; Esteves da Silva, J.C.G.; Pinto da Silva, L. Life cycle assessment of the sustainability of enhancing the photodegradation activity of TiO_2 with metal doping. *Materials* **2020**, *13*, 1487. [CrossRef] [PubMed]

54. Sendão, R.; Martínez de Yuso, V.M.; Algarra, M.; Esteves da Silva, J.C.G.; Pinto da Silva, L. Comparative life cycle assessment of bottom-up synthesis routes for carbon dots derived from citric acid and urea. *J. Clean. Prod.* **2020**, *254*, 120080. [CrossRef]
55. Feijoo, S.; González-García, S.; Moldes-Diz, Y.; Vazquez-Vazquez, C.; Feijoo, G.; Moreira, M.T. Comparative life cycle assessment of different synthesis routes of magnetic nanoparticles. *J. Clean. Prod.* **2017**, *143*, 528–538. [CrossRef]
56. Huijbregts, M.A.J.; Steinmann, Z.J.N.; Elshout, P.M.F.; Stam, G.; Verones, F.; Vieira, M.; Zipj, M.; Hollander, A.; van Zelm, R. ReCiPe2016: A harmonized life cycle impact assessment method at midpoint and endpoint level. *Int. J. Life Cycle Assess.* **2017**, 22, 138. [CrossRef]

2.1.2. Supporting Information

Supplementary Materials

Table S1. Inventory of raw materials for each CD under study, in which quantities are referred to 1 kg of CD.

Ecoinvent® 3.5 database	CD-1	CD-2	CD-3	CD-4	CD-5	CD-6
Glucose {GLO}|market for glucose| APOS, S	2.49 kg					
Sodium hydroxide, without water, in 50% solution state {GLO}|market for| APOS, S	1.49 kg					
Hydrogen peroxide, without water, in 50% solution state {GLO}|market for| APOS, S	0.239 kg					
Citric Acid {GLO}|market for| APOS, S		7.2 kg	7.61 kg	50 kg	2.4 kg	3 kg
Ethylenediamine {RER}| market for| APOS, S		7.2 kg				
Urea, as N {GLO}| market for| APOS, S			2.54 kg	16 kg	0.8 kg	1 kg
Water, deionized, from tap water, at user {Europe without Switzerland}| market for water, deionized, from tap water, at user| APOS, S	24.9 kg	77.9 kg	101.5 kg	330 kg	20 kg	20 kg
Electricity, medium voltage {RER}|market group for| APOS, S	146.8 kWh	24.2 kWh	46.09 kWh	17 kWh	12 kWh	17 kWh

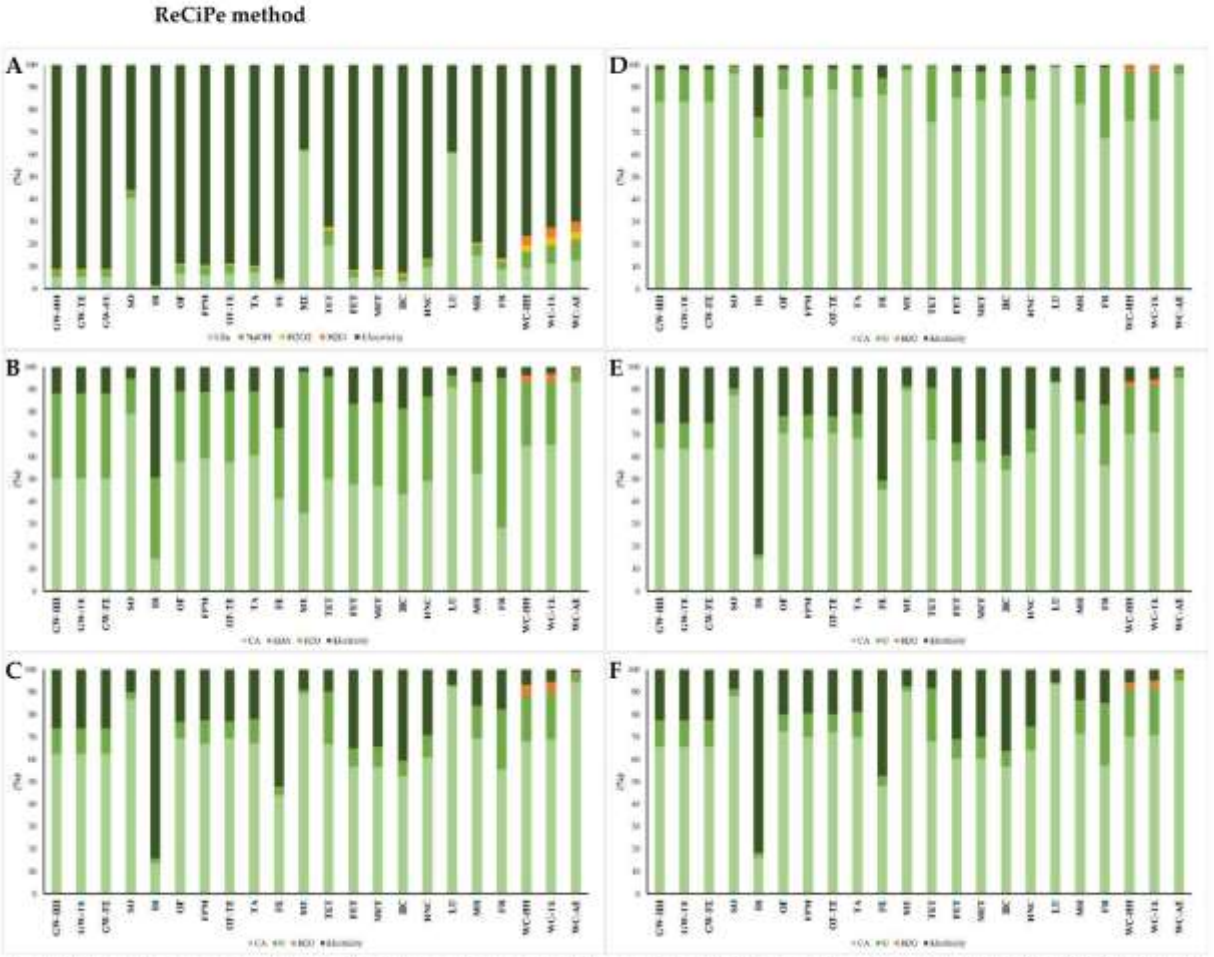

Figure S1. Relative environmental impacts of the synthesis under study applying ReCiPe endpoint method. (**A**) CD-1; (**B**) CD-2, (**C**) CD-3; (**D**) CD-4, (**E**) CD-5 and (**F**) CD-6. The abbreviations are explained in Section 2.4.

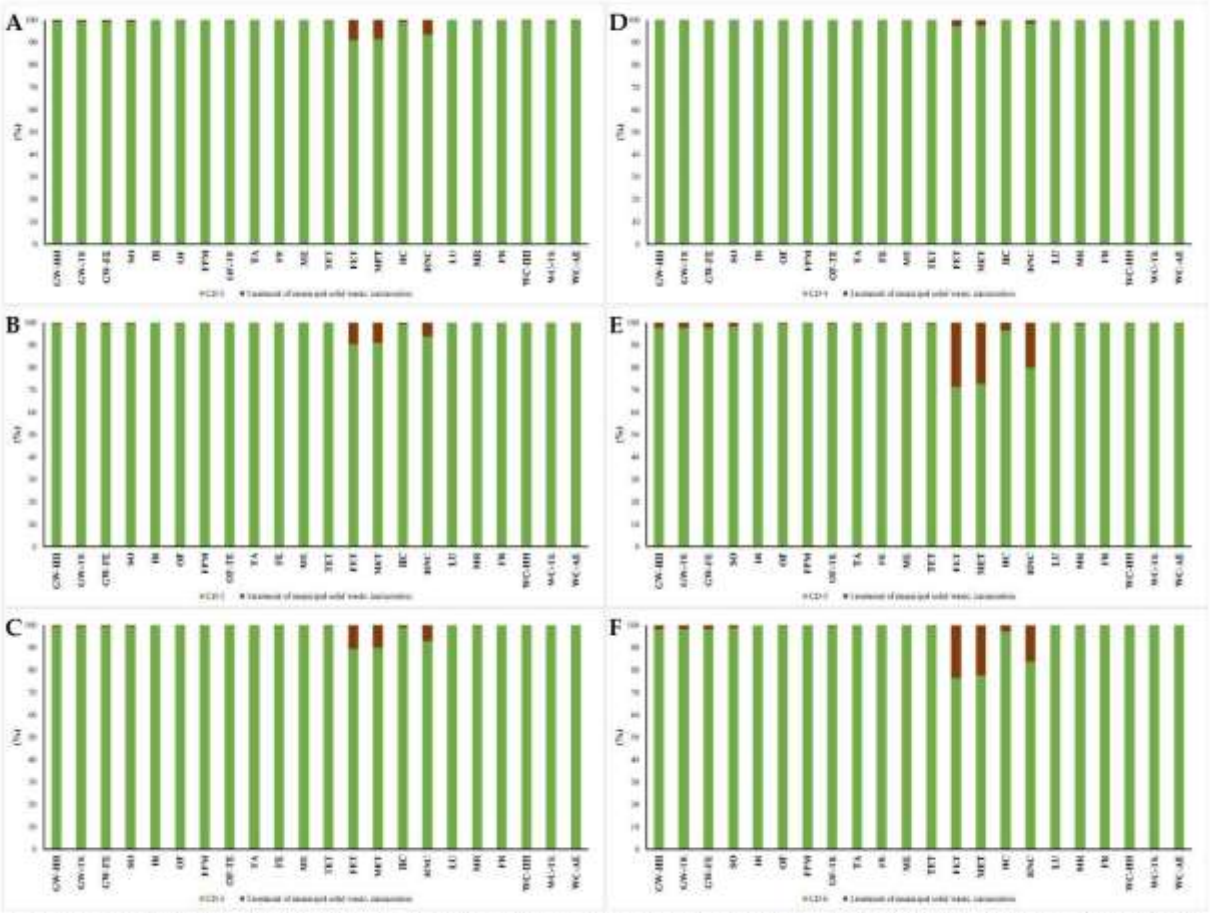

Figure S2. Relative environmental impacts of the synthesis under study and the disposal scenario of incineration, applying ReCiPe endpoint method. (**A**) CD-1; (**B**) CD-2, (**C**) CD-3; (**D**) CD-4, (**E**) CD-5 and (**F**) CD-6. The abbreviations are explained in Section 2.4.

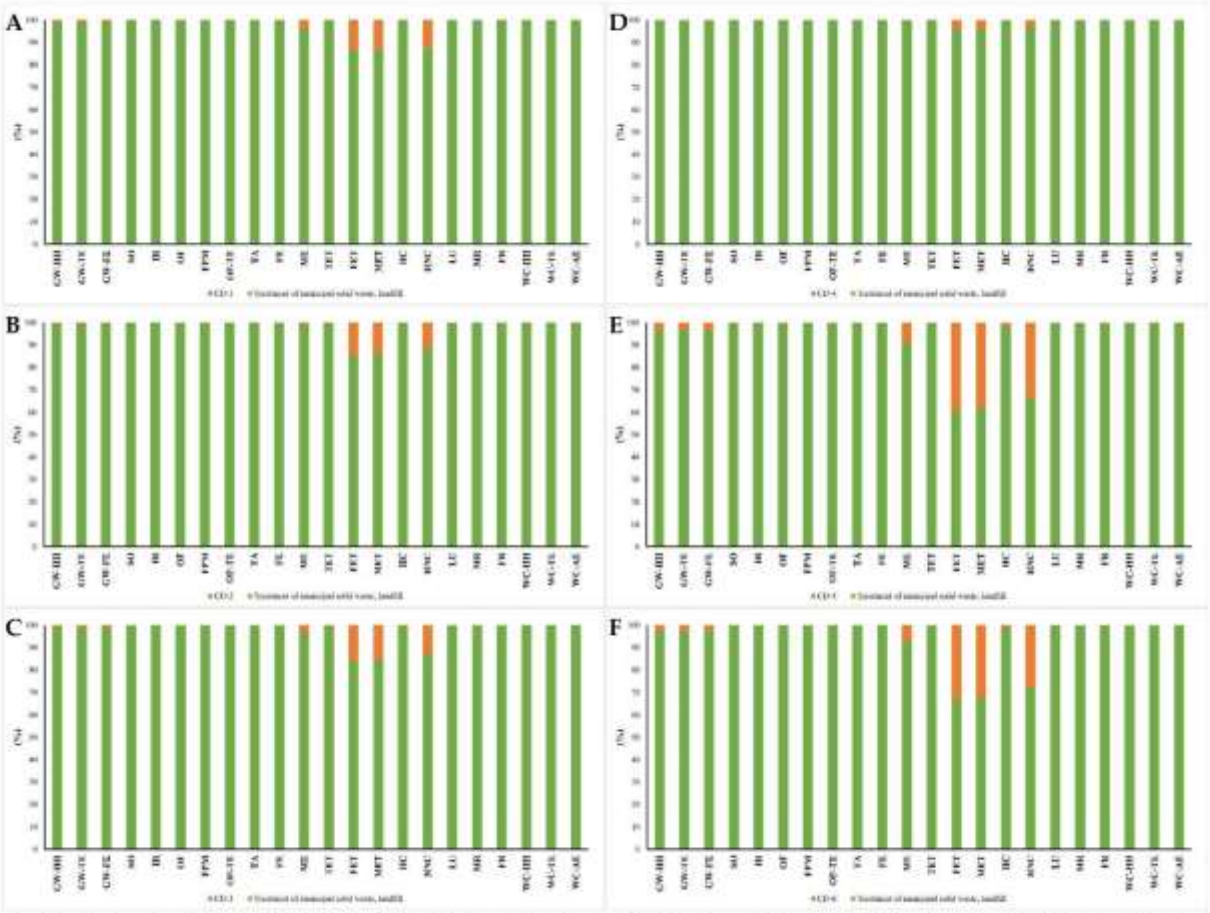

Figure S3. Relative environmental impacts of the synthesis under study and the disposal scenario of landfill, applying ReCiPe endpoint method. (**A**) CD-1; (**B**) CD-2, (**C**) CD-3; (**D**) CD-4, (**E**) CD-5 and (**F**) CD-6. The abbreviations are explained in Section 2.4

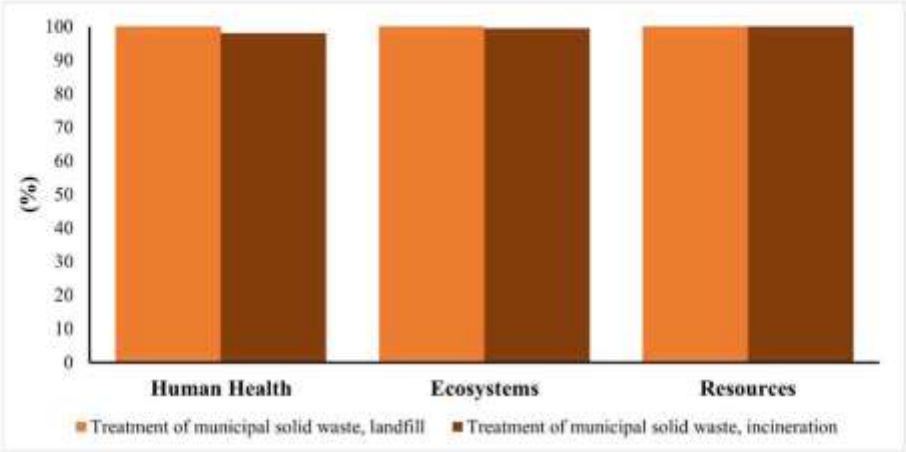

Figure S4. Relative environmental impacts of CD-5 for incineration and landfill disposal scenario, applying ReCiPe method.

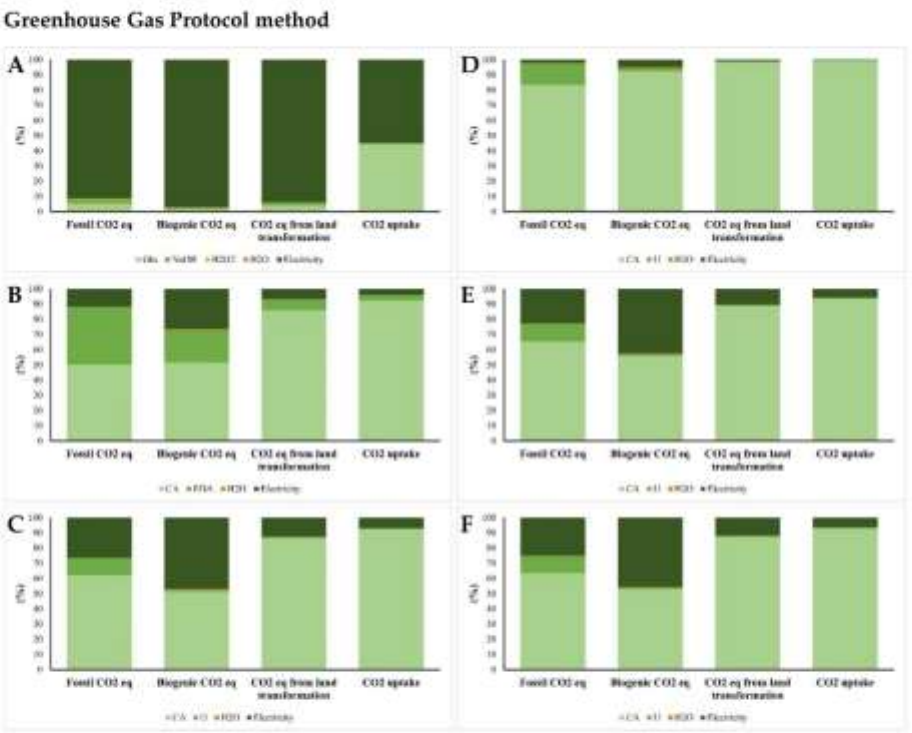

Figure S5. Relative environmental impacts of syntheses under study, applying Greenhouse Gas Protocol method. (**A**) CD-1; (**B**) CD-2, (**C**) CD-3; (**D**) CD-4, (**E**) CD-5 and (**F**) CD-6.

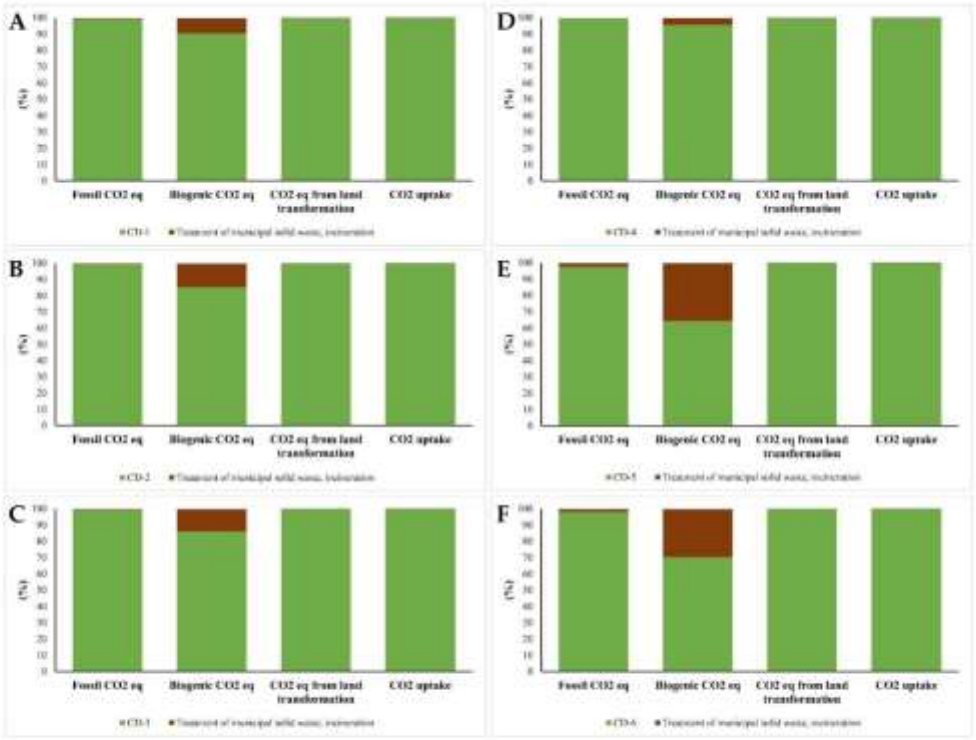

Figure S6. Relative environmental impacts of syntheses under study for incineration disposal scenario, applying Greenhouse Gas Protocol method. (**A**) CD-1; (**B**) CD-2, (**C**) CD-3; (**D**) CD-4, (**E**) CD-5 and (**F**) CD-6.

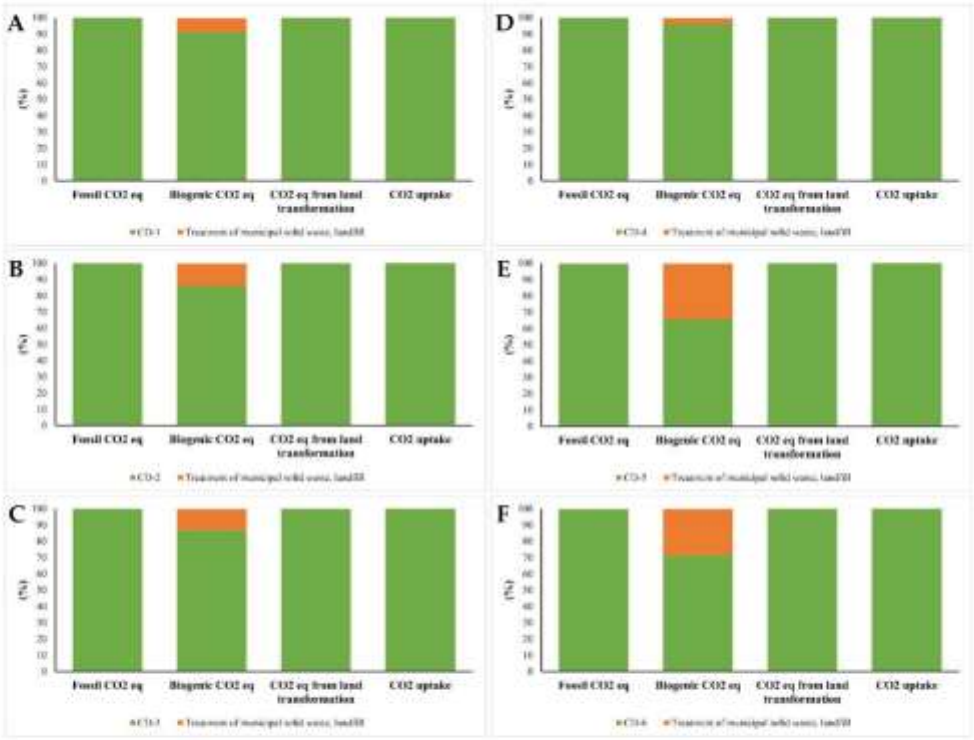

Figure S7. Relative environmental impacts of syntheses under study for landfill disposal scenario, applying Greenhouse Gas Protocol method. (**A**) CD-1; (**B**) CD-2, (**C**) CD-3; (**D**) CD-4, (**E**) CD-5 and (**F**) CD-6.

AWARE method

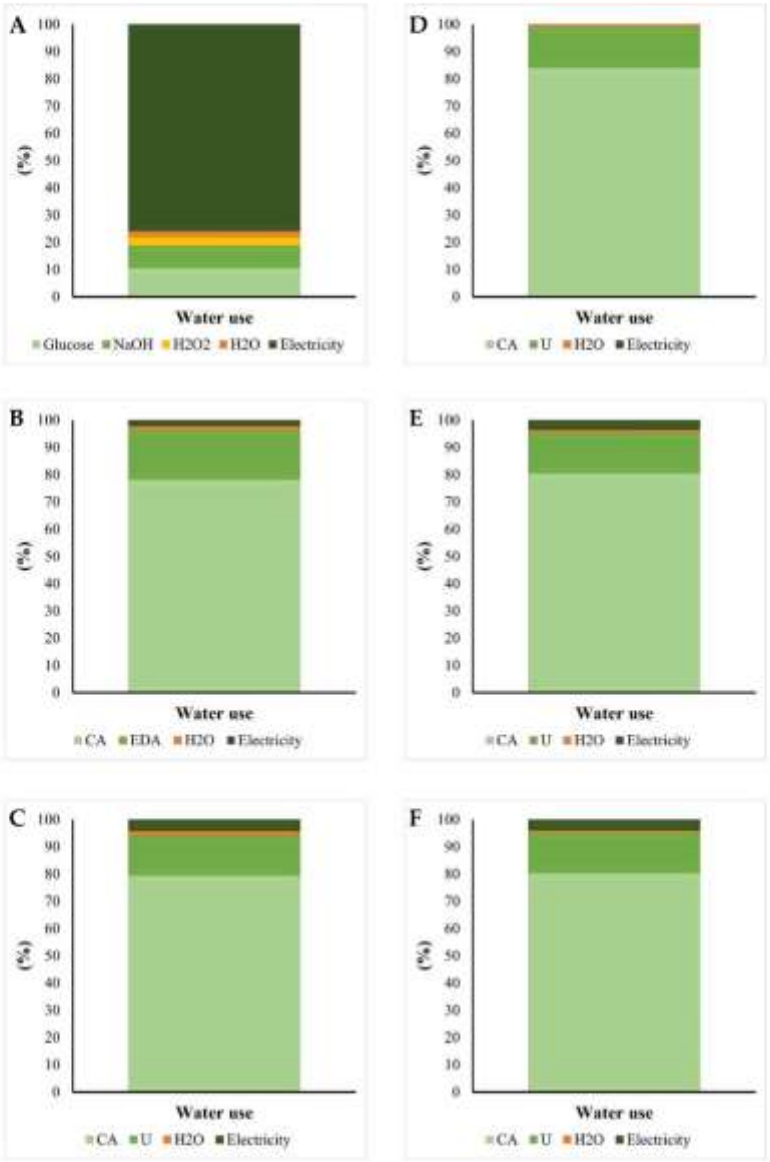

Figure S8. Relative environmental impacts of syntheses under, applying AWARE method. (**A**) CD-1; (**B**) CD-2, (**C**) CD-3; (**D**) CD-4, (**E**) CD-5 and (**F**) CD-6.

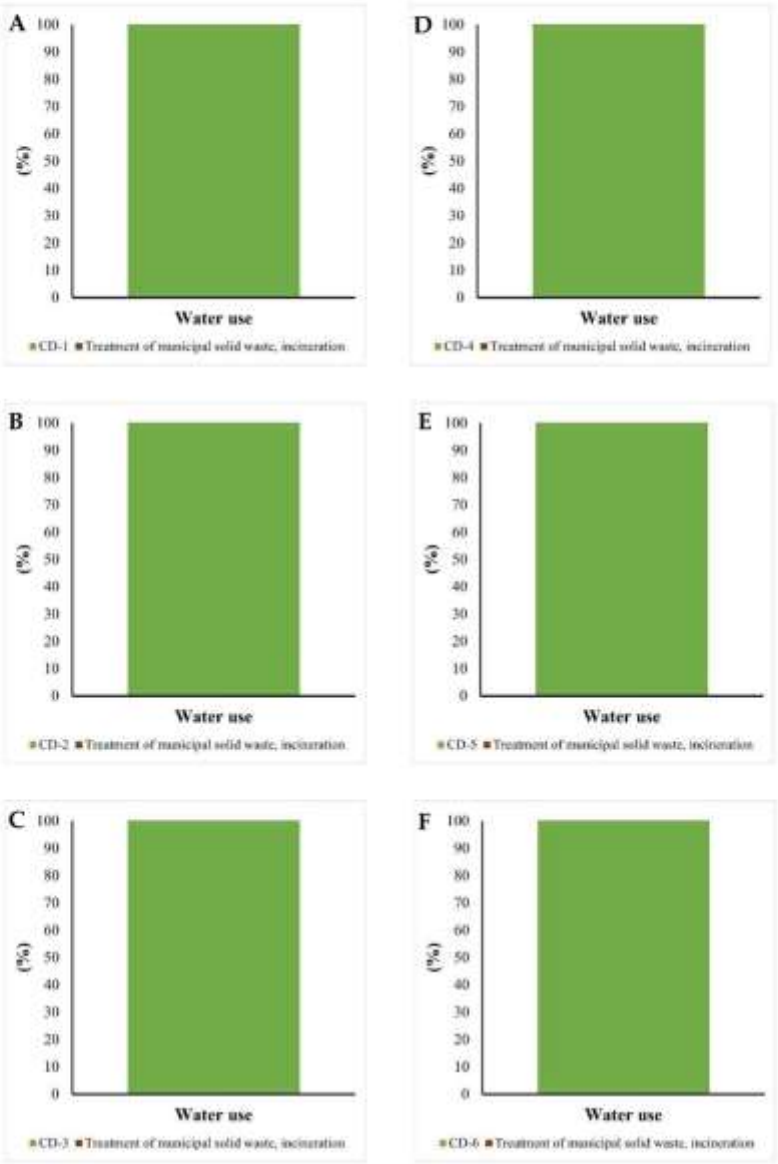

Figure S9. Relative environmental impacts of syntheses under for incineration disposal scenario, applying AWARE method. (**A**) CD-1; (**B**) CD-2, (**C**) CD-3; (**D**) CD-4, (**E**) CD-5 and (**F**) CD-6.

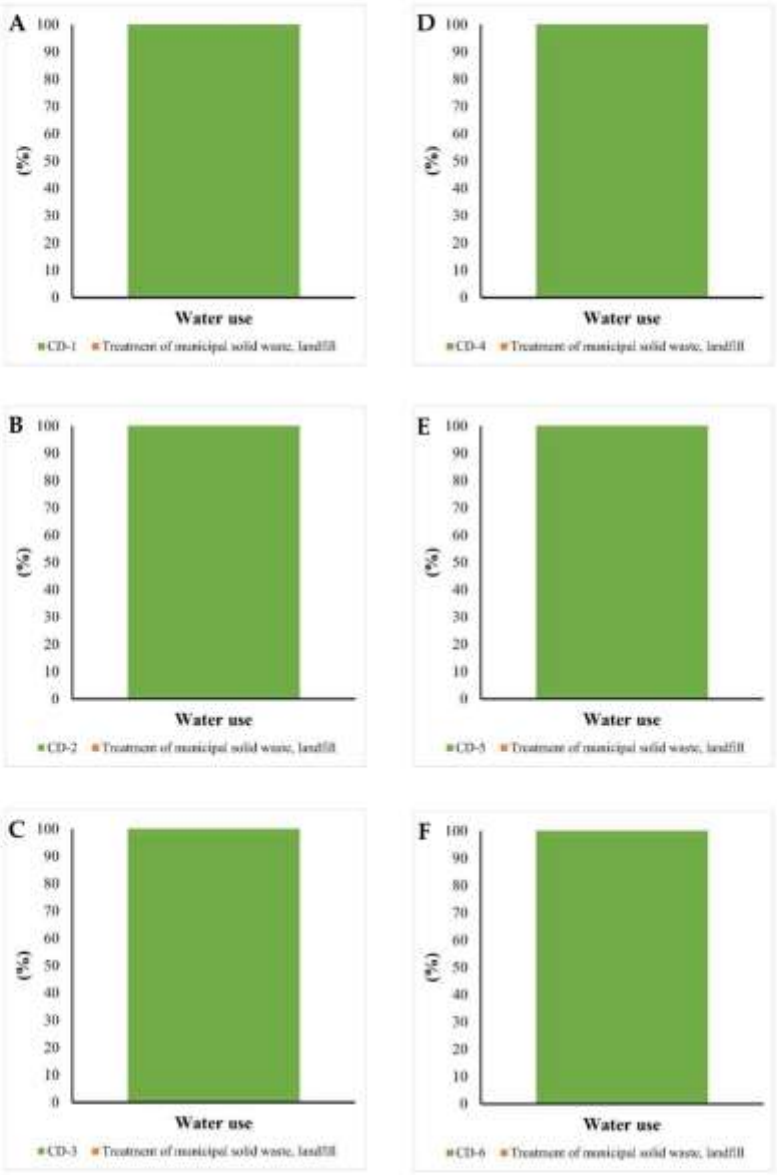

Figure S10. Relative environmental impacts of syntheses under for landfill disposal scenario, applying AWARE method. (**A**) CD-1; (**B**) CD-2, (**C**) CD-3; (**D**) CD-4, (**E**) CD-5 and (**F**) CD-6.

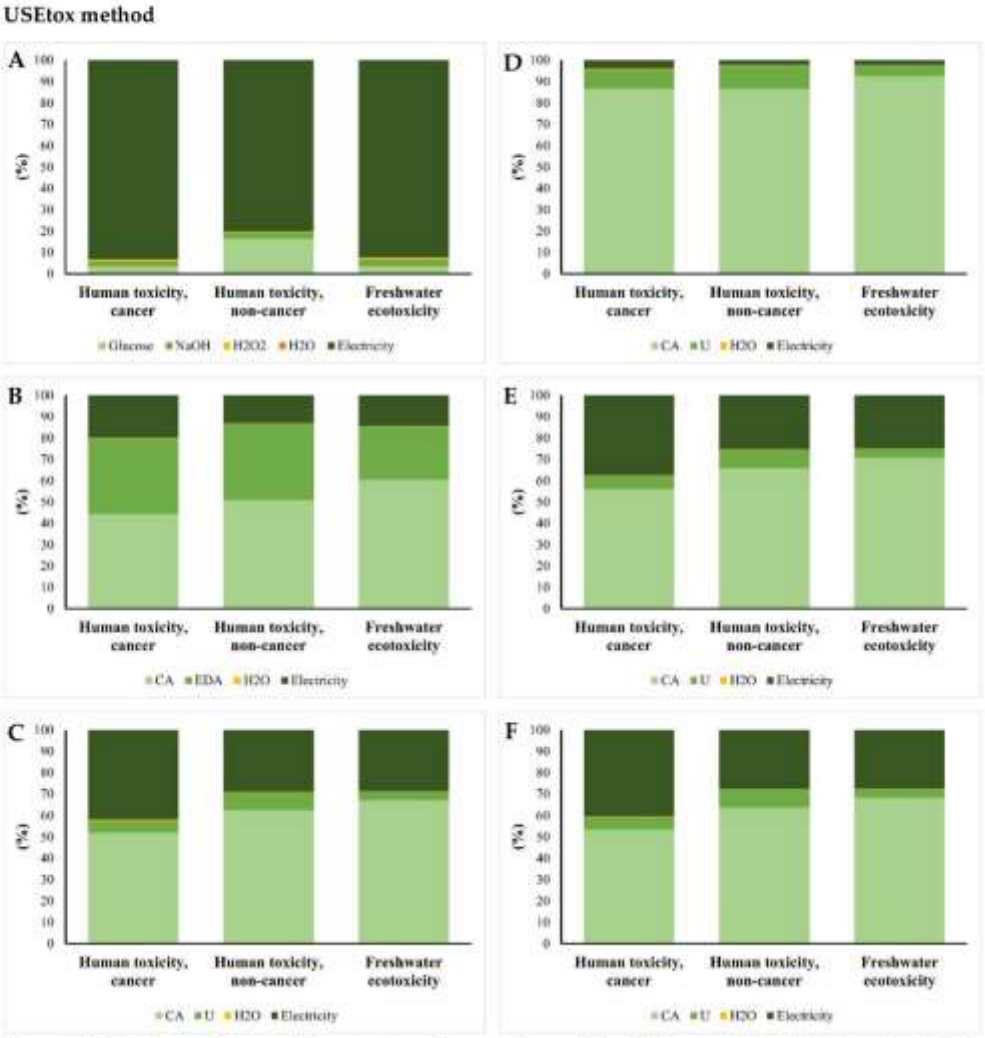

Figure S11. Relative environmental impacts of syntheses under, applying USEtox method. (**A**) CD-1; (**B**) CD-2, (**C**) CD-3; (**D**) CD-4, (**E**) CD-5 and (**F**) CD-6.

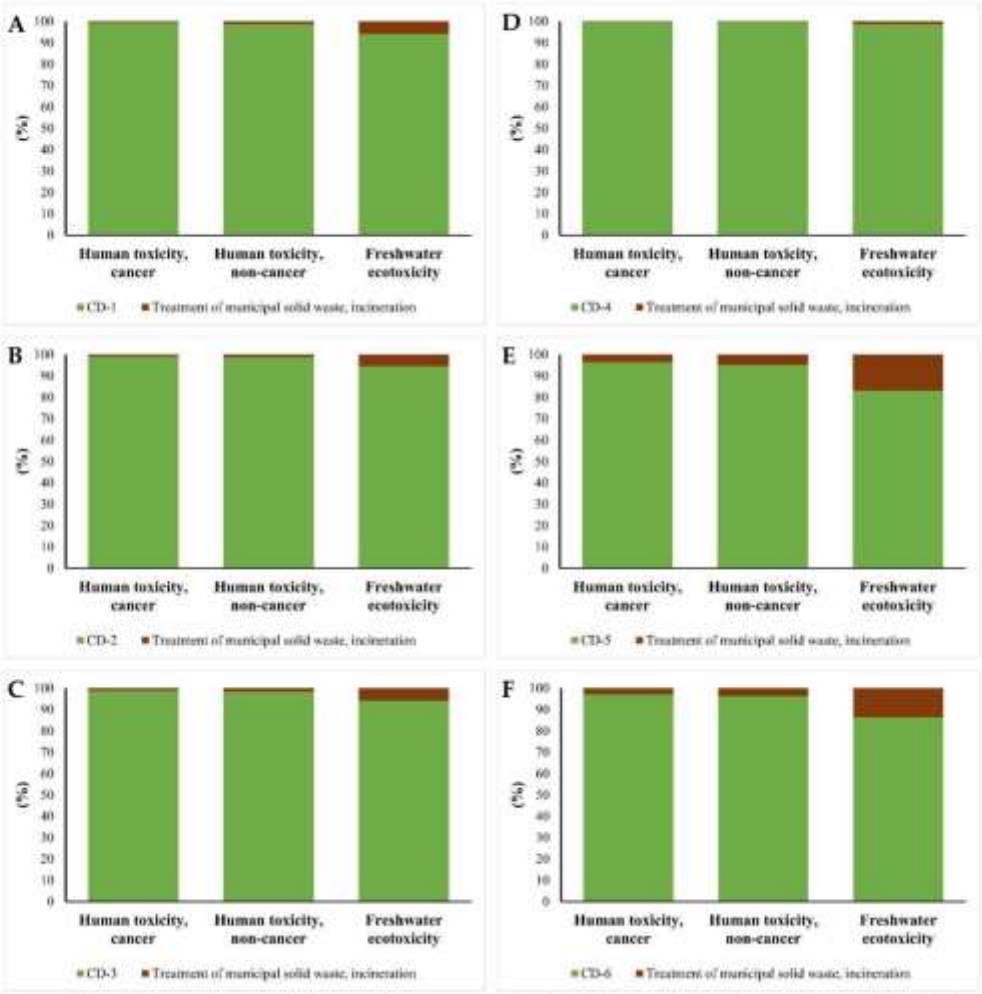

Figure S12. Relative environmental impacts of syntheses under for incineration disposal scenario, applying USEtox method. (**A**) CD-1; (**B**) CD-2, (**C**) CD-3; (**D**) CD-4, (**E**) CD-5 and (**F**) CD-6.

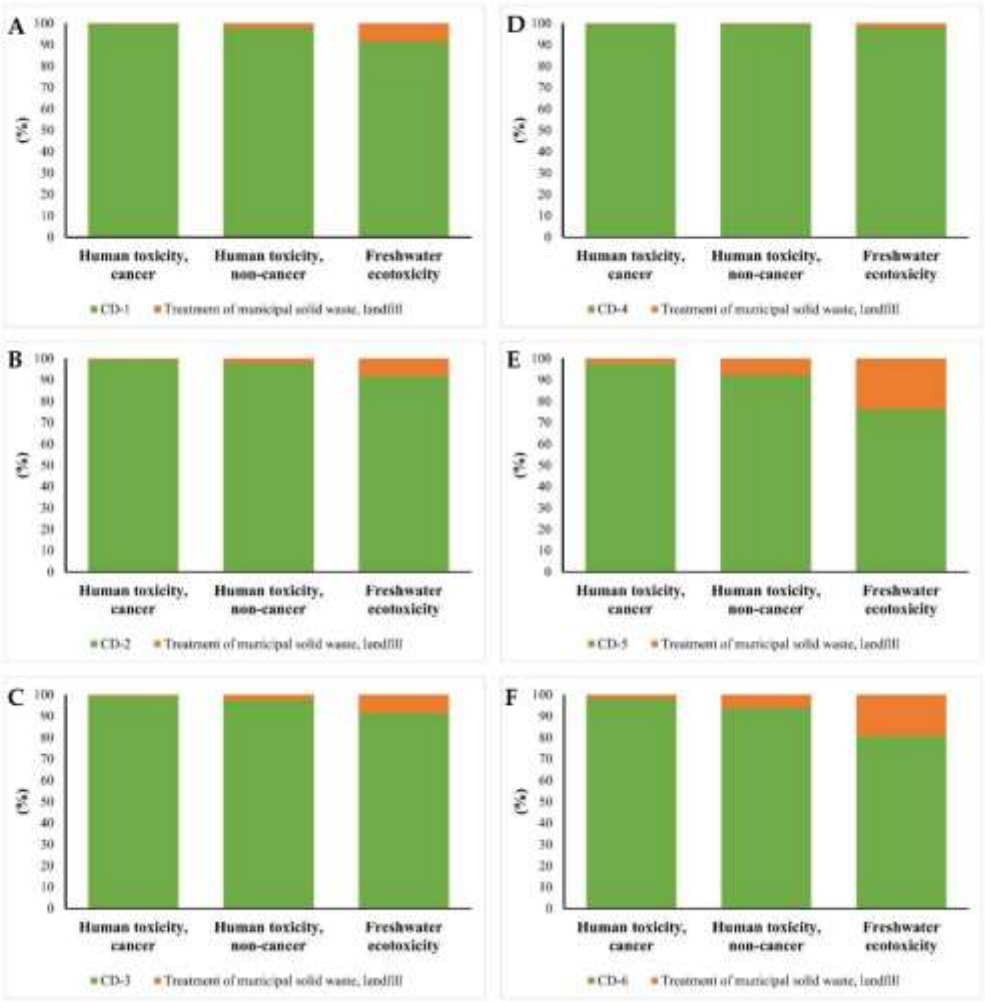

Figure S13. Relative environmental impacts of syntheses under for landfill disposal scenario, applying USEtox method. (**A**) CD-1; (**B**) CD-2, (**C**) CD-3; (**D**) CD-4, (**E**) CD-5 and (**F**) CD-6.

2.1.3. Conclusion

This study presents a comparative LCA of six representative synthesis routes for CDs, enabling a systematic evaluation of high-yield and conventional bottom-up fabrication strategies. Adopting a cradle-to-grave perspective and a mass-based functional unit of 1 kg of produced CDs, the analysis provides a detailed understanding of the environmental trade-offs associated with synthesis yield, energy demand, and process complexity.

The results demonstrate that synthesis yield alone is not a reliable indicator of environmental sustainability in CDs production. While high-yield strategies enhance material efficiency, their potential benefits are frequently offset by higher energy consumption, longer reaction times, and increased use of chemical reagents. Across most impact categories, energy and carbon precursor were identified as the dominant contributors to the overall environmental footprint.

Evaluation using the ReCiPe, Greenhouse Gas Protocol, and USEtox methods, the microwave-assisted synthesis based on citric acid and urea (CD-5) consistently exhibited the lowest overall environmental impacts, while the hydrothermal route with very low yield (CD-4) was associated with the highest impacts. Although the high-yield synthesis route (CD-1) significantly reduced environmental burdens when compared to low-yield hydrothermal synthesis, it did not systematically outperform simpler “standard” bottom-up approaches that combine moderate-to-high yields with lower energy requirements.

End-of-life scenarios, including incineration and landfill disposal, contributed only marginally to the total impacts, indicating that sustainability improvements should primarily focus on the synthesis stage. Interestingly, the AWARE method highlighted a different trend, identifying the high-yield route as the most favorable regarding water deprivation potential. This result underscores the importance of assessing multiple environmental dimensions, as conclusions on sustainability may vary depending on the selected impact category.

Consistently with these results, a previous study [227] has also shown that increased yields do not necessarily reduce environmental impacts, with precursor selection, energy consumption, and process complexity remaining key drivers of environmental performance.

Overall, these results emphasize the importance of a life cycle perspective when evaluating CDs synthesis strategies. Sustainability claims based solely on yield may be

misleading, and integrated assessments that consider both material efficiency and process-related environmental burdens are essential for informed decision-making. This work establishes a methodological and empirical foundation for subsequent studies in this thesis, which further explore sustainable synthesis pathways, precursor selection, and design strategies for CDs targeting lighting applications. In line with these findings, complementary work (Appendix 1) has further explored the environmental performance of waste-derived CDs, reinforcing the importance of precursor selection and process design in shaping the sustainability profile of CDs production.

In conclusion, higher synthesis yields do not inherently lead to improved environmental performance. In many cases, the increased energy demand and process complexity associated with high-yield strategies offset the advantages of enhanced material efficiency. Consequently, relatively simple bottom-up routes that achieve moderate-to-high yields while maintaining manageable energy and reagent requirements may offer the most environmentally balanced options for CDs production, although the optimal choice ultimately depends on the specific objectives and conditions of the production process.

3. Conversion of organic waste into multicolor CDs

3.1. **Article II**: Development of a Facile and Green Synthesis Strategy for Brightly Fluorescent Carbon Dots from Various Waste Materials

Sónia Fernandes, Manuel Algarra, Antonio Gil, Joaquim Esteves da Silva, and Luís Pinto da Silva

3.1.1. Contextualization and author contributions

CDs have emerged as a versatile class of carbon-based nanomaterials due to their tunable photoluminescence, high photostability, low toxicity, and broad applicability in sensing, bioimaging, optoelectronics, and lighting-related technologies [101, 177, 178]. These properties, combined with their potential for synthesis from abundant and renewable carbon sources, make CDs particularly attractive within the framework of sustainable nanomaterials development.

In recent years, increasing attention has been directed toward the use of biomass residues and organic waste as carbon precursors for CDs synthesis, aiming to reduce environmental impacts while promoting waste valorization within a circular economy perspective [243, 244, 264]. However, the heterogeneous composition of waste-derived feedstocks often leads to significant variability in the optical properties of the resulting CDs. In particular, waste-based CDs frequently exhibit limited fluorescence quantum yields (QY_{FL}), restricting their use in high-performance optical applications.

Against this background, the central objective of this work [116] was to develop a generic, reproducible, and environmentally responsible synthesis strategy capable of converting a wide range of organic waste materials into brightly fluorescent CDs with QY_{FL} values exceeding 20%. Achieving high photoluminescence efficiency while maintaining sustainability constraints remains a major challenge, as improvements in emission intensity are often associated with harsher reaction conditions, increased energy consumption, or more complex multistep procedures.

To address this challenge, a facile and green hydrothermal synthesis route was developed, combining waste-derived carbon sources with citric acid as a co-carbon precursor and ethylenediamine as a nitrogen dopant. This approach enables controlled carbonization, nitrogen incorporation, and surface passivation under mild reaction

conditions, while preserving a high degree of flexibility with respect to precursor selection. Importantly, the procedure was designed to be broadly applicable to different waste streams, rather than optimized for a single feedstock, thereby supporting the development of a versatile and scalable synthesis platform.

Within the scope of this thesis, this study complements the life cycle-oriented assessment presented in the previous work (Article I) by highlighting precursor selection and waste valorization as critical design parameters for sustainable CDs synthesis. In combination, these studies aim to contribute to the development of CDs that reconcile high optical performance with environmentally responsible fabrication strategies.

I was responsible for the synthesis of all CDs and for the optical characterization, LCA, and data analysis associated with this study, under the supervision of Professor Dr. Luís Pinto da Silva. X-ray photoelectron spectroscopy (XPS) and X-ray diffraction (XRD) analyses were performed by the research group of Dr. Manuel Algarra (University of Malaga). Atomic force microscopy (AFM) measurements were conducted at CEMUP (Materials Centre of the University of Porto), while Fourier-Transform Infrared spectroscopy (FT-IR) and zeta potential measurements were carried out by me in collaboration with the laboratory Lab&Services (Chemistry and Biochemistry Department of the Faculty of Sciences of Porto University) team, particularly Cláudia Alves.

The interpretation and discussion of all experimental results, including structural, chemical, optical, and environmental data, were carried out by me under the supervision of Professor Dr. Luís Pinto da Silva. I prepared the initial manuscript draft, which was subsequently reviewed and refined by Professor Dr. Luís Pinto da Silva, Professor Dr. Joaquim C. G. Esteves da Silva, Dr. Manuel Algarra, and Dr. Antonio Gil.

Check for updates

ChemSusChem

Research Article
doi.org/10.1002/cssc.202401702

Chemistry Europe
European Chemical Societies Publishing

www.chemsuschem.org

Development of a Facile and Green Synthesis Strategy for Brightly Fluorescent Carbon Dots from Various Waste Materials

Sónia Fernandes,[a] Manuel Algarra,[b] Antonio Gil,[b] Joaquim Esteves da Silva,[a] and Luís Pinto da Silva*[a]

Carbon dots (CDs) are fluorescent carbon-based nanomaterials with remarkable properties, making them more attractive than traditional fluorophores. Consequently, researchers focused on their development and application in fields such as sensing and bioimaging. One potential advantage of employing CDs is using organic waste as carbon precursors in their synthesis, providing a pathway for waste upcycling for a circular economy. However, waste-based CDs often have low fluorescence quantum yields (QY_{FL}), limiting their practical applications. So, there is a need for a well-defined strategy to consistently produce waste-based CDs with appreciable QY_{FL}, irrespective of the starting waste material. Herein, we developed a fabrication strategy based on the hydrothermal treatment of waste materials, using citric acid as a co-carbon precursor and ethylenediamine as N-dopant. This strategy was tested with various materials, including corn stover, spent coffee grounds, cork powder, and sawdust. The results showed consistently appreciable QY_{FL}, reaching up to ~40%. A Life Cycle Assessment (LCA) study demonstrated that producing these waste-based CDs has lower environmental impacts compared to CDs made solely from commercial reagents. Thus, we have established a framework for the environmentally friendly production of CDs by upcycling different waste materials without significant sacrifices in performance (QY_{FL}).

Introduction

Carbon dots (CDs) are fluorescent carbon-based nanoparticles, which are known for having good stability, water-solubility, and being biocompatible.[1,2] Due to these properties, they have been studied for use in applications as diverse as bioimaging, sensing, and phototherapies, among others.[2–20]

CDs can be produced via either top-down or bottom-up approaches. The former involves the breakdown of large graphite materials,[21] while the latter consists of producing larger nanoparticles from smaller organic molecules.[22–24] Bottom-up routes are typically preferred, as they are commonly considered to be a low-cost and environmentally friendly strategy to produce CDs.[21,25,26] CDs produced from top-down approaches can also present relatively low fluorescence quantum yields (QY_{FL}).[2]

Moreover, various precursors can be used to produce CDs when following bottom-up routes.[27–30] However, when devising different production strategies, it is crucial to consider their environmental impact and ensure their sustainability. This aspect is even more critical with engineered nanomaterials, including CDs, as their production processes have been recognized as being of environmental concern.[31–33]

Life cycle assessment (LCA) is an approach capable of measuring the environmental impacts of a given system or product during its entire life cycle.[34–36] In fact, it has been used previously to investigate the environmental impacts of synthesizing CDs.[23,27,37–39] More relevantly, these LCA studies have indicated that the carbon precursor is the main contributor to the environmental impacts that result from the production of CDs.[23,27,37–39] This finding has been consistent, being common to various bottom-up processes and different carbon precursors (including commonly employed ones, such as citric acid, or CA).[23,27,37–39] Notably, typical carbon precursors of CDs are commercial chemicals, such as acids, carbohydrates, and other more complex compounds.[23,27,37–39]

Thus, reducing the amount of carbon used or replacing typical carbon precursors in synthesizing CDs is essential to minimize their environmental impact. Interestingly, CDs can also be produced using different types of organic waste and biomass as carbon precursors instead of commercial chemicals.[22] Given this, the focus should be reducing or replacing commercial precursors using organic waste.

In fact, different researchers have already studied the fabrication of CDs from different types of waste and renewable carbon sources, such as fruits, biomass, residues, and others.[28,40–43] However, CDs obtained from these carbon sources have been shown to present relatively low QY_{FL} values, typically below 20%.[42,44,45–48] This is problematic because typical applications in which CDs are used require as high of a QY_{FL} value as

[a] Chemistry Research Unit (CIQUP), Department of Geosciences, Environment and Spatial Plannings, Faculty of Sciences, Institute of Molecular Sciences (IMS), University of Porto, Porto, Portugal
[b] Department of Science, Public University of Navarre INAMAT - Institute for Advanced Materials and Mathematics, Pamplona, Spain
Correspondence: Luís Pinto da Silva, Chemistry Research Unit (CIQUP), Department of Geosciences, Environment and Spatial Plannings, Faculty of Sciences, Institute of Molecular Sciences (IMS), University of Porto, R. Campo Alegre s/n, Porto 4169-007, Portugal.
Email: luis.silva@fc.up.pt

Supporting Information for this article is available on the WWW under https://doi.org/10.1002/cssc.202401702

ChemSusChem
Research Article
doi.org/10.1002/cssc.202401702
Chemistry Europe
European Chemical Societies Publishing

possible. So, current examples are reducing environmental impacts by sacrificing the performance of CDs, meaning that using these nanomaterials is not viable for practical applications in which strong luminescence is needed.

Thus, there is a need to develop novel and cleaner strategies for producing CDs that do not sacrifice their performance. That is, there is a need for fabrication strategies that reduce the amount of commercial chemicals by incorporating organic waste while consistently producing CDs that retain appreciable QY_{FL} values (higher than 20%), irrespective of the selected waste material.

Herein, we aim to optimize a bottom-up route in which different CDs can be produced from diverse types of waste material while consistently obtaining higher QY_{FL} values. More specifically, it will establish a framework to produce different waste-based CDs with strong enough fluorescence for future application-oriented research while allowing for waste upcycling in a circular economy approach.

We successfully developed CDs from different waste materials (corn stover, sawdust, cork powder, and spent coffee grounds), which showed appreciable fluorescence (up to ~40%), higher than found in existing literature. LCA studies highlighted that introducing waste as co-carbon precursors decreased the environmental impacts of the synthesis process over corresponding routes involving only commercial chemicals. The CDs were also thoroughly characterized by AFM, XPS, DLS, FTIR, XRD, UV-Vis, and fluorescence spectroscopy.

Results and Discussion

Preparation of CDs

This study employed a hydrothermal approach to synthesize CDs due to requiring mild experimental conditions and being easy to operate, low cost, and secure. It also allows for one-pot synthesis for heterogeneous reactions.[93] The Supporting Information details the experimental procedures and steps to optimize reaction conditions. In short, all CDs were produced via a hydrothermal approach, with a final reaction volume of 10 mL of NaOH 0.01 M solution used for all synthesis. The reaction mixtures were always placed in a 25 mL Teflon-lined reactor with a stainless-steel shell. Different reaction parameters were changed: amount and identity of carbon precursor; identity and amount of N-dopant; reaction time and temperature. The resulting solutions were then subjected to centrifugation and dialysis for purification.

Initially, we attempted to synthesize CDs using only waste materials as carbon precursors (Figure S1 and Table S1). We tested 9 types of organic waste, including corn stover, orange peels, spent coffee grounds, and sawdust.

Subsequently, instead of exclusively using organic waste, we modified traditional hydrothermal routes with a carbon precursor and an N-dopant molecule. CA is arguably the most common among traditional carbon precursors. Specifically, we aimed to reduce the amount of CA by incorporating waste materials as co-carbon precursors. This approach allows the upcycling of waste while decreasing the use of CA, which is a relevant endeavor as previous studies have identified commercial carbon precursors (including CA) as the main contributors to the environmental impacts of the synthesis of CDs.[23,27,37–39]

Initial optimization of reaction conditions was performed by investigating the effect of different parameters, such as the addition of N-dopant, the ratio of N-dopant:carbon precursors, the identity of N-dopant, and reaction temperature (Table S2), as described in the Supporting Information. In this analysis, we employed corn stover as reference waste material. We chose corn stover as it is one of the most abundant agricultural wastes, and it is ubiquitous around the world. Despite this, corn stover is typically discarded, as it has no relevant valuable end application.

The final step in this optimization process was to evaluate the effect of the reaction time. To this end, we performed 4 additional syntheses with increasing reaction times (Table 1 and Scheme 1): 4 hours, 8 hours, 16 hours, and 24 hours ($CS\text{-}CDs_{4hr}$, $CS\text{-}CDs_{8hr}$, $CS\text{-}CDs_{16hr}$, and $CS\text{-}CDs_{24hr}$, respectively). The experimental conditions are defined in Table 1.

Introducing waste materials as carbon precursors, with the consequent reduction of commercial chemicals, is a relevant research topic for upcycling waste in a circular economy approach. However, this introduction is only worth pursuing if the performance and environmental impacts of the resulting nanomaterials are not significantly worse than those produced only from commercial chemicals.

Table 1. Synthesis parameters, emission (λ_{em}) and excitation (λ_{ex}) wavelength maxima, QY_{FL} and synthesis yield of CDs performed at different reaction times.

CDs	Corn Stover (g)	Citric Acid (g)	Ethylenediamine (g)	Reaction Time (h)	λ_{em} (nm)	λ_{ex} (nm)	QY_{FL} (%)	Synthesis Yield (%)
$CS\text{-}CDs_{4h}$	0.075	0.075	0.15	4	445	355	9.9	8.4
$CS\text{-}CDs_{8h}$	0.075	0.075	0.15	8	440	350	39.3	6.9
$CS\text{-}CDs_{16h}$	0.075	0.075	0.15	16	440	350	38.9	6.2
$CS\text{-}CDs_{24h}$	0.075	0.075	0.15	24	440	355	33.1	5.5
CDs_{4h}	-	0.15	0.15	4	440	350	65.0	3.9
CDs_{8h}	-	0.15	0.15	8	440	350	66.4	2.4
CDs_{16h}	-	0.15	0.15	16	440	350	66.4	1.5
CDs_{24h}	-	0.15	0.15	24	440	350	65.2	4.5

ChemSusChem
Research Article
doi.org/10.1002/cssc.202401702
Chemistry Europe
European Chemical Societies Publishing

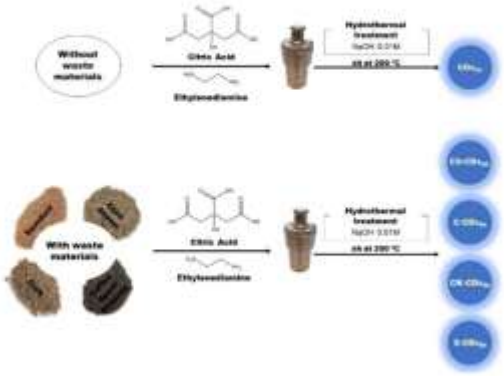

Scheme 1. Scheme of CDs synthesis. xh refers to different reaction times applied to the synthesis (4, 8, 16, and 24 h). CS-CDs$_{xh}$ and CDs$_{xh}$ refer to CDs with and without corn stover at several reaction times, as mentioned in Table 1. C-CDs$_{8h}$, CK-CDs$_{8h}$, and S-CDs$_{8h}$ refer to CDs from spent coffee grounds, cork powder, and sawdust.

To evaluate this, we have then synthesized four additional CDs using only CA and ethylenediamine (EDA) in a mass ratio of 1:1 and with increasing reaction times (Scheme 1): CDs$_{4h}$, CDs$_{8h}$, CDs$_{16h}$, and CDs$_{24h}$ (the other synthesis parameters are the same as for CS-CDs$_{xh}$). By not using corn stover as a co-carbon precursor, the amount of CA used for CDs$_{xh}$ is double that used for CS-CDs$_{xh}$.

It should be noted that the objective of this work is not the development of one single CDs from organic waste with appreciable fluorescence. Instead, it is to develop a synthesis approach in which waste-based CDs can be produced consistently with appreciable QY$_{FL}$ (higher than 20%), irrespective of the type of waste material used as starting material/co-carbon precursor.

With this approach, researchers could have a framework to develop novel and different CDs in a more environmentally friendly way and in a circular economy approach without sacrificing the performance of CDs in terms of QY$_{FL}$ (essential for most of the practical applications in which CDs could be applied). Furthermore, establishing a reliable synthesis process with lower environmental impacts for CDs while ensuring consistently high fluorescence is essential for future application-oriented research. Tuning the properties/reactivity of CDs toward specific applications could be done by selecting waste materials with specific compositions. Thus, while this study does not present specific examples of practical applications, it was performed to provide a foundation for future studies in which CDs are applied in sensing, imaging, light-emitting devices, etc.

To demonstrate the reliability and consistency of our synthesis approach, we have used it to produce 3 additional waste-based CDs, by changing only the identity of the waste material (Scheme 1). Namely, spent coffee grounds, cork powder, or sawdust (C-CDs$_{8h}$, CK-CDs$_{8h}$, and S-CDs$_{8h}$, respectively).

Characterization of CDs

2D excitation-emission contour plots (EECP) were measured for each CDs using only waste materials as precursors (Figure S1), which showed a similar fluorescence profile between the samples. Namely, all CDs presented a well-defined luminescent center with an emission maximum of about 440 nm. However, the QY$_{FL}$ was below 1.4% for all syntheses (Table S1), suggesting that solely using organic waste is not a consistently effective method for producing CDs with significant fluorescence. As a result, we explored an alternative synthesis strategy in which we combined a carbon precursor and an N-dopant molecule.

Reaction conditions were evaluated, such as the addition of N-dopant (Figure S2), the ratio of N-dopant:carbon precursors (Figure S3A and S3B), the identity of N-dopant (Figure S4A and S4B), and reaction temperature (Figure S4A and S4 C). This optimization allowed us to identify EDA as a suitable N-dopant. The mass ratio of N-dopant:carbon precursor ratio was set to 1:1, with CA and corn stover being used as co-carbon precursors in a 1:1 mass ratio (meaning a 50% reduction of CA by using organic waste as a co-carbon precursor).

The obtained EECPs for CS-derived CDs (Figure 1 and Figure S5) present a single luminescent center with an emission maximum at ~440 nm and an excitation maximum at ~350 nm. There are differences in fluorescence intensities between CDs, consistent with their respective QY$_{FL}$ (Table 1). There are also relatively small differences in the emission and excitation maxima for the different CS-CDs (Table 1). Thus, the reaction time has limited influence on this type of CDs' emission and excitation wavelength.

The absorption spectra of these CDs showed that for CS-CDs$_{8h}$, CS-CDs$_{16h}$, and CS-CDs$_{24h}$, there is an absorption band with a peak at about 350 nm (associated with to n→π* transitions) and a small shoulder at ≈238 nm (Figure S6A). Absorption spectra for CS-CDs$_{4h}$ (Figure S6A) exhibit a shoulder at around 275 nm, attributed π→π* transitions.[23,51–53] Interestingly, for CS-CDs$_{4h}$, the band at 350 nm is almost nonexistent. This means that the reaction has some effect on the structure of the synthesized CDs. Regarding QY$_{FL}$ (Table 1), we observed a quite relevant increase from 9.9% at 4 hours to 39.3% at 8 hours. Further increases in reaction time started to decrease the QY$_{FL}$, down to 33.1%, which is still a significant value. These values are encouraging as CDs obtained from different biomass/organic waste had previously been showing QY$_{FL}$ below 20%.[42–44,46–48]

So, we successfully produced CDs with appreciable fluorescence by incorporating corn stover as a co-carbon precursor while reducing the amount of commercial carbon precursor.

The EECPs obtained for CDs without waste materials (CDs$_{xh}$) are presented in Figures 1 and Figure S7. They present a well-defined luminescent center with an emission maximum of ~440 nm and an excitation maximum of ~350 nm. These EECPs are like those obtained for corn stover-based CDs (Figure 1). This result is of note as the similarity between EECPs could mean that the different CS-CDs$_{xh}$ and CDs$_{xh}$ nanoparticles are all being produced from just CA and EDA, with corn stover not

ChemSusChem
Research Article
doi.org/10.1002/cssc.202401702
Chemistry Europe
European Chemical Societies Publishing

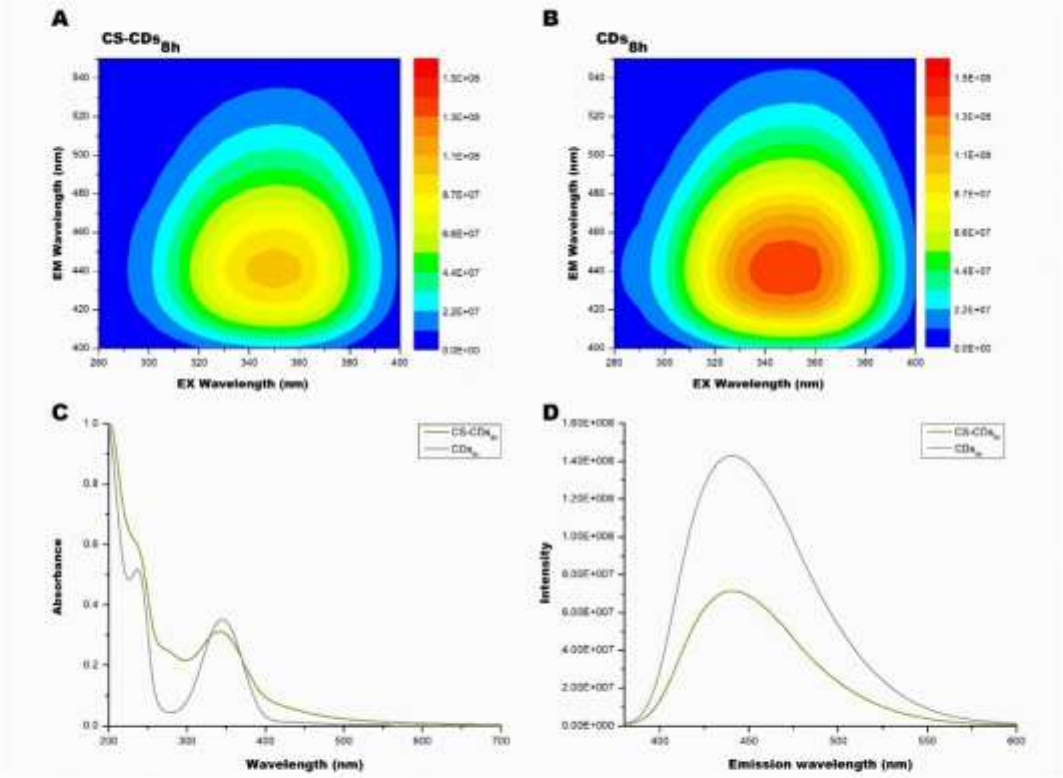

Figure 1. Optical characterization of CS-CDs$_{8h}$ and CDs$_{8h}$. EECPs of CS-CDs$_{8h}$ (A) and CDs$_{8h}$ (B). Absorption (C) and emission (D) spectra. In emission spectra, the excitation wavelength was 350 nm. Water was the solvent used in all analyses.

being incorporated in the CDs despite its addition to the reaction mixtures for the former.

However, further analysis does not support the notion that both CS-CDs$_{xh}$ and CDs$_{xh}$ are the same CA:EDA-based CDs. For one, the synthesis yields (Table 1) are higher for CS-CDs$_{xh}$ than for CDs$_{xh}$. The synthesis yields for the former also decrease with increasing reaction time, a relationship not fully observed for the latter.

More relevant are the differences in QY_{FL} between CS-CDs$_{xh}$ and CDs$_{xh}$ (Table 1 and Figure S8). While the maximum QY_{FL} for CS-CDs$_{xh}$ is 39.3%, we measured a maximum value of 66.4% for CDs$_{xh}$. Moreover, while the QY_{FL} for CS-CDs$_{xh}$ varied between 9.9% and 39.3%, there was just a variation of ~1% for CDs$_{xh}$ in the same time range. Thus, the QY_{FL} is quite dependent on the reaction time for CS-CDs$_{xh}$, while being essentially independent of this parameter for CDs$_{xh}$. These relevant differences can be ascribed to the introduction of corn stover as a co-carbon precursor, as the properties of CDs can vary greatly when changing precursors and dopants.[27,54] The absorption spectra of CDs$_{xh}$ (Figure S6B) are composed of a well-defined band and shoulder at ≈350 nm and ≈238 nm, respectively. These can be attributed to the n→π* transition at the edge of the carbon lattice and π→π* transition of the C=C bond, respectively.[23,51–53] By comparing these spectra with those for CS-CDs$_{xh}$ (Figure S6A), we can see that the overall shape of the spectra is different between the two sets of nanoparticles. The shape of the spectra of CS-CDs$_{xh}$ also varies relevantly with reaction time, which is not the case for CDs$_{xh}$. It should be noted that, at the same mass concentration, the absorbance measured for the latter increases with reaction time, which is not the case for the former. Thus, these results show relevant differences between CS-CDs$_{xh}$ and CDs$_{xh}$ (Figure 1C), further highlighting the effects of corn stover as a co-carbon precursor.

Emission spectra (Figure 1D) were also measured for CS-CDs$_{8h}$ (corn stover-based CDs with higher QY_{FL}) and CDs$_{8h}$ (non-corn stover-based CDs obtained at the same reaction time). A single band with monomodal behavior was obtained for both, with differences in fluorescence intensity (Figures 1 and Figure S9). The similarity can be explained by the fact that despite the former including a different co-carbon precursor, both CDs are prepared from CA and EDA. Thus, some similarity between their properties is to be expected.

To gain further insight into the characteristics of CS-CDs, and how they differ from CA:EDA-only CDs, we proceeded to

ChemSusChem
Research Article
doi.org/10.1002/cssc.202401702
Chemistry Europe
European Chemical Societies Publishing

their analysis by AFM, XPS, FTIR, DLS, and XRD. In this analysis, we have focused on CS-CDs_{6h} as representative corn stover-based CDs, due to it presenting the highest QY_{FL}. CDs_{6h} was also analyzed to understand better how the absence of corn stover affects the CDs.

AFM determined the average particle sizes of CS-CDs_{6h} and CDs_{6h}: 1.14 ± 0.25 nm and 5.41 ± 1.57 nm, respectively (Figure 2A and B). There is a significant difference between the sizes of the two CDs ($p < 0.05$), which further highlights that these should not be the same type of CA:EDA-based particles.

Another potential question regarding our results could be if the synthesis including corn stover could produce two types of CDs: one from CA and EDA (with this being the highest emitting CDs), and one from corn stover (with participation or not of CA and/or EDA). We do not think that the data support this hypothesis, but instead, our initial one in which the introduction of corn stover produces only one type of CDs from corn stover:CA:EDA. For one, analysis of the size distribution of both CS-CDs_{6h} and CDs_{6h} (Figure 2A and B) shows a homogenous distribution for both but without overlap, as the sizes are centered around ~1 and ~5 nm (respectively). Thus, CS-CDs_{6h} appears to be composed of a single population of nanoparticles, but with relevantly different sizes from CDs_{6h}. Furthermore, the EECP (Figure 1A and B) and emission spectrum (Figure 1D) measured for CS-CDs_{6h} showed a monomodal behavior. Thus, there is no evidence for the co-existence of two types of particles.

XPS spectroscopy was performed to understand the surface composition of these two CDs (Figure S10). As expected, the measured XPS atomic composition reveals that both CDs are mostly composed of C (~70–74%). More specifically, the chemical surface composition of CS-CDs_{6h} is 70.0% C, 18.5% O, and 11.6% N. CDs_{6h} presents a surface comprising 74.4% C, 15.5% O, and 10.1% N (Table S3). These results suggest that including corn stover results in similar N-doping efficiency while enhancing the incorporation of O heteroatoms and decreasing the C content.

High-resolution spectra for the C 1*s*, N 1*s*, and O 1*s* levels were obtained for the samples. The respective deconvolution, chemical state, and quantitative analysis were performed to identify the functional groups present in the CDs' surface (Figure 2C–H).[55,56]

The C 1*s* spectrum of CS-CDs_{6h} splits into three peaks with binding energies of 285.0 eV, 286.4 eV, and 288.2 eV. These can be attributed to C–C/C=C, C–N/C–O/C–OH/C–O–C, and N–C=O/C=O/C–OH, respectively.[21,23] By its turn, the C 1*s* spectra for CDs_{6h} yield four peaks with binding energies of 285.0 eV, 286.4 eV, 287.7 eV, and 288.6 eV. The peak at 287.7 eV can be attributed to C=O/C–C_x[23] with the other peaks being already mentioned above.

On the other hand, the N 1*s* spectrum of CS-CDs_{6h} reveals two peaks at 400 eV and 401.8 eV, ascribed to -NH_2/N–H/C–N-C and N–H, respectively.[21,23] For CDs_{6h}, deconvolution of N 1*s* spectra shows two peaks at binding energies of 399.98 eV and 401.3 eV that result in amide carbonyl groups (–CH_2/-NH_2) and amide carbonyl groups (–N–C=O), respectively.

Finally, the CS-CDs_{6h} deconvolution of the O 1*s* spectrum results in two peaks, with binding energies of 531.4 eV and 532.9 eV, which result from C=O and C–OH/C–O–C/C–O groups, respectively.[21,23] Otherwise, for CDs_{6h}, the O 1*s* spectra split into three peaks with binding energies of 531.1 eV, 532.2 eV, and 533.5 eV. The C=O contribution at 531.1 eV results from carbonyl and carboxylate groups, while the peak at 532.2 is attributed to C–OH/C–O–C. This shows that the surface is dominated by the carbonyl group up to 2.5 times, indicating the high level of the oxidation process. Finally, the peak at 533.5 eV can be attributed to C–O.

These results show differences in surface composition between the studied CDs, which may explain the different QY_{FL} between them while showing the impact of adding corn stover to the reaction mixture.[57–59]

ζ potential measurements of these CDs (Figure S11) yielded values of −9.1 mV for CS-CDs_{6h} and −8.0 mV for CDs_{6h}.

FT-IR spectra are shown in Figure 2I. Both samples presented a broad absorption band from 2500–3500 cm^{-1} that clearly demonstrates overlapping O–H and N–H stretching vibration modes.[21,60] Besides, there are bands located at ≈1653, ≈1527/1546 (CDs_{6h}/CS-CDs_{6h}), ≈1390/1395 (CDs_{6h}/CS-CDs_{6h}), and ≈1052/1045 (CDs_{6h}/CS-CDs_{6h}) cm^{-1} that can be assigned to C=O, N–H, C–N stretching, and C–O–H bending vibration modes, respectively.[21,60] C=C and C–O–C stretching vibration modes were identified at ≈1477 and ≈1219 cm^{-1} for CS-CDs_{6h}.[21,60] These results are in line with the XPS results. It should be highlighted that there are some relevant differences between relative band intensities, which further indicates the disparity between the surface composition of the studied CDs.

Finally, the XRD spectra of both CDs (CS-CDs_{6h} and CDs_{6h}) displayed a non-crystalline character, with the CDs presenting an amorphous structure (Figure 2J).

So, the obtained results demonstrate that we successfully used corn stover as a carbon precursor for producing waste-based CDs with strong fluorescence. However, our objective was not to produce one specific waste-based CDs, but instead to develop a synthesis strategy to produce CDs from different waste materials that consistently show appreciable fluorescence. To demonstrate the validity of our approach (Scheme 1), we have then analyzed CDs produced from other waste materials (Table 2): spent coffee grounds (C-CDs_{6h}), cork powder (CK-CDs_{6h}), and sawdust (S-CDs_{6h}).

The obtained EECPs (Figure 3A–C) for these CDs present a similar fluorescence profile to corn stover-based CDs, with emission and excitation maximums at ~440 and ~350 nm, respectively. The absorption spectra of these new CDs can be found in Figure 3D. They consist of a band with a peak at ≈350 nm and a small shoulder at ≈238 nm that can be attributed to n→π* and π→π* transitions, respectively.[7–10] Compared to CS-CDs_{6h}, the most similar nanoparticles appear to be S-CDs_{6h}.

Consistent with our expectations, all CDs presented relevant QY_{FL} values (Table 2). Specifically, 35.9% for S-CDs_{6h}, 24.7% for C-CDs_{6h}, and 21.8% for CK-CDs_{6h}. Thus, this synthesis approach produces CDs from waste with relevant QY_{FL}, irrespective of the starting waste material. This demonstrates the validity of the

ChemSusChem
Research Article
doi.org/10.1002/cssc.202401702
Chemistry Europe
European Chemical Societies Publishing

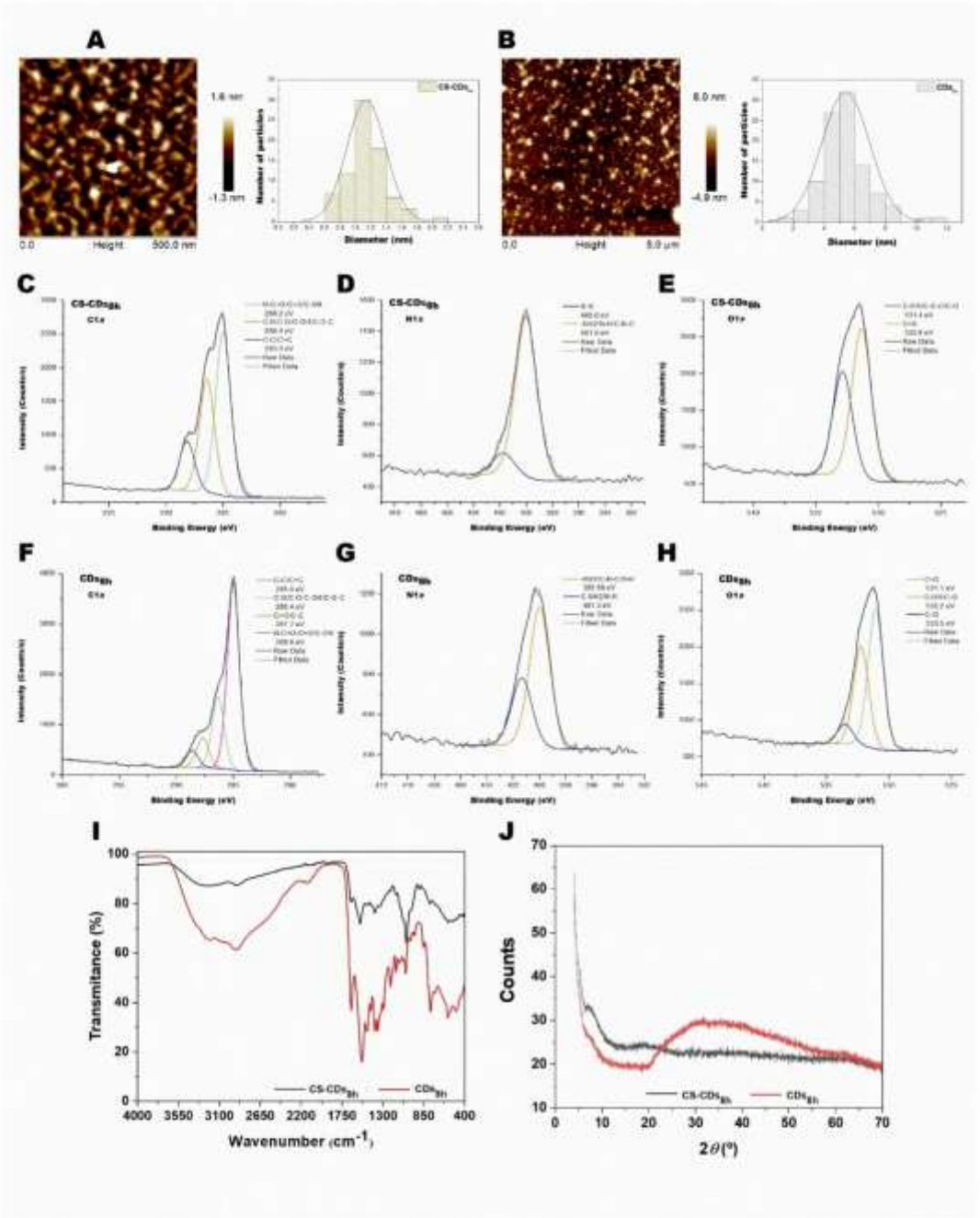

Figure 2. CS-CDs_{Bh} and CDs_{Bh} characterization. AFM of CS-CDs_{Bh} (A) and CDs_{Bh} (B). XPS core level spectra of CS-CDs_{Bh}: C 1*s* (C), N 1*s* (D), and O 1*s* (E); and of CDs_{Bh}: C 1*s* (F), N 1*s* (G), O 1*s* (H). FT-IR spectra (I) and XRD spectra (J) of CS-CDs_{Bh} (black) and CDs_{Bh} (red).

ChemSusChem
Research Article
doi.org/10.1002/cssc.202401702
Chemistry Europe
European Chemical Societies Publishing

Table 2. Emission (λ_{em}) and excitation (λ_{ex}) wavelength maxima, QY_{FL} and synthesis yield of $C\text{-}CDs_{8h}$, $CK\text{-}CDs_{8h}$ and $S\text{-}CDs_{8h}$.

CDs	λ_{em} (nm)	λ_{ex} (nm)	QY_{FL} (%)	Synthesis Yield (%)
$C\text{-}CDs_{8h}$	440	355	24.7	6.7
$CK\text{-}CDs_{8h}$	440	350	21.8	4.0
$S\text{-}CDs_{8h}$	440	350	35.9	4.2

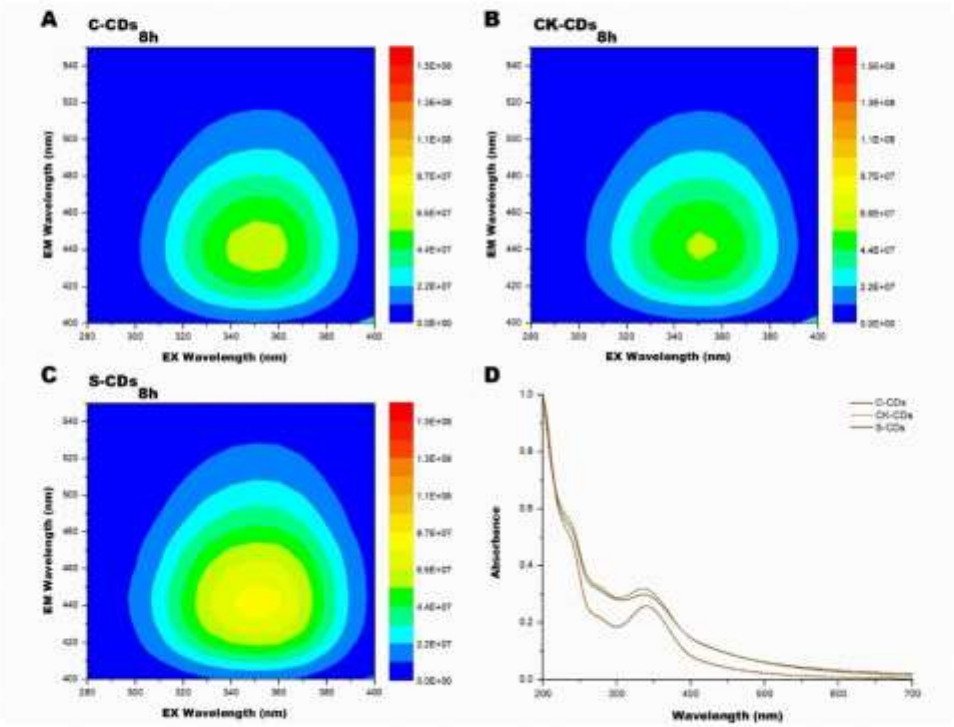

Figure 3. EECPs of spent coffee grounds (A), cork powder (B), and sawdust-based CDs (C). Absorption spectra of $C\text{-}CDs_{8h}$, $CK\text{-}CDs_{8h}$ and $S\text{-}CDs_{8h}$ (D). Water was the solvent used in all analyses.

presented synthesis strategy toward the consistent production of waste-based CDs with appreciable fluorescence. It should be noted that $CS\text{-}CDs_{8h}$ still presents the highest QY_{FL} among waste-based CDs.

It should also be highlighted that these results do not support the possibility that CDs produced in reaction mixtures containing waste would only originate from reactions between CA and EDA (with waste material not participating). That is, if the obtained CDs were only similarly generated from CA:EDA (and waste was not a relevant factor), we would expect similar QY_{FL} for all and not variations from 21.8% to 39.3%.

Life Cycle Assessment

While the results presented in the previous section are promising, one should always assess the environmental impacts of a new synthesis strategy. This is particularly true for nanomaterials, as their production has been identified as being of environmental concern.[31,32]

Given this, we have performed an LCA study about the synthesis processes for the 4 corn stover-based CDs highlighted in the previous section: $CS\text{-}CDs_{4h}$, $CS\text{-}CDs_{8h}$, $CS\text{-}CDs_{16h}$, and $CS\text{-}CDs_{24h}$. This cradle-to-gate study, in which laboratory data was scaled up to an industrial level (by considering the production of 100 L), was made with the assumption that, with the goal being the commercial use of CDs, scaled-up data would be more relevant and representative than information on a purely laboratory scale. This was performed by considering the scale-

ChemSusChem
Research Article
doi.org/10.1002/cssc.202401702
Chemistry Europe
European Chemical Societies Publishing

up framework developed by Piccinno et al.,[39] as described in more detail in the Supporting Information.

This LCA study was started by considering a volume-based functional unit (FU) of 100 L. Our intention was not to make quantitative appreciations of the environmental impacts of each material input but rather to compare the contributions of the different impact categories from the input involved in each synthesis with each other.

The individual results of corn stover-based CDs (Figure S12) demonstrated that, for all of them, the major contributor toward its associated environmental impacts is EDA (in terms of endpoint indicators: Human Health, Ecosystems, and Resources), with CA also being a relevant contributor. In terms of midpoint indicators, EDA is also the highest contributor to most of the different categories, except for Stratospheric Ozone Depletion (SO), Land Use (LU), and Water Consumption – Human Health (WC-HH). In these cases, CA is associated with more environmental impacts.

When comparing the impacts of each synthesis (Figure S13A), we can observe that the relative environmental impacts increase with an increasing reaction time for the three considered categories. This increase can be attributed to two factors: the increased amount of electricity required for the longer reaction times and the fact that increasing the reaction time appears to decrease the synthesis yield of the studied CDs (Table 1), resulting in a lower CDs' production yield for the same volume.

We have also compared the environmental impacts of the four CDs by considering a function-based FU (Supporting Information and Figure S13B). Using a function-based FU is important to evaluate if better performances in the use stage offset higher environmental impacts resulting from production stages. Given the relevance of the QY_{FL} for various typical applications for which CDs are tested,[7,10,14,15,17] and its previous use in this manner,[23,28,37–39] we have chosen this parameter as the basis for our selected function-based FU (Supporting Information section 1.5.1).

Interestingly, a function-based FU significantly changes all categories' results (Figure S13B). The increased reaction times are not translated into higher relative environmental impacts. The CD associated with higher impacts is CS-CDs_{4h}, presenting a considerably higher relative impact than the other three CDs. The relative distribution of the four CDs indicates that the higher QY_{FL} values offset the higher impacts resulting from electricity and lower yields. In fact, CS-CDs_{8h} presents the lower relative impacts while presenting the higher QY_{FL}. Thus, this CDs can present appreciable fluorescence with lower environmental impacts.

An LCA study was also performed to understand the environmental impacts of producing CDs from commercial reagents (CDs_{ca}). We have found that the highest contributor in the Human Health and Ecosystems categories is generally CA, while EDA is the highest contributor in the Resources category (Figure S14). This differs from corn stover-based CDs, in which the highest contribution was from EDA for the three studied categories (Figure S12). These results align with the literature, in which the commercial chemicals used as carbon precursors (including CA) are the main responsible for the environmental impacts of producing CDs.[23,39] So, reducing the use of CA is supported as the key approach to reducing these impacts. The contribution of electricity is relatively small, consistent with previous studies that show that the contribution of electricity decreases with scaling-up.[39]

There are no significant differences when comparing these CDs when using FU of either 100 L or based on the QY_{FL} (Figure S15). CDs_{24h} is associated with the lowest environmental impacts, whereas CDs_{16h} is associated with the highest. It is worth mentioning that the differences in relative environmental impacts between CDs_{24h} and CDs_{4h} are lower than 4% (in both comparisons).

So, our results indicate that we could produce CDs using waste (corn stover) that still presents appreciable QY_{FL}, in contrast to CDs produced solely by organic waste. This is a relevant development toward upcycling waste into nanotechnological solutions. However, it is a fact that corresponding corn-stover-free CDs still present higher QY_{FL} than CS-CDs_{8h} (Table 1). Thus, it is essential to verify if the incorporation of corn stover is still environmentally beneficial for the synthesis process when considering their relative performance in terms of QY_{FL}.

To that end, we have compared the environmental impacts associated with the production of CS-CDs_{8h} (corn stover-based CDs with the highest QY_{FL}) and the four CDs produced solely from CA and EDA (Table 1). This study only considered a function-based FU (Supporting Information). The results are presented in Figure 4.

The results indicate that using corn stover as a co-carbon precursor does result in a synthesis process with lower environmental impacts. When comparing CS-CDs_{8h} with CDs_{8h} (same reaction time, but in the presence or absence of corn stover, respectively), the relative environmental impacts of CS-CDs_{8h} are 30% lower than those of CDs_{8h}. Even when comparing CS-CDs_{8h} with the CDs produced without corn stover with lower impacts (CDs_{24h}), the latter is associated with lower relative environmental impacts. Regarding individual contributors, EDA

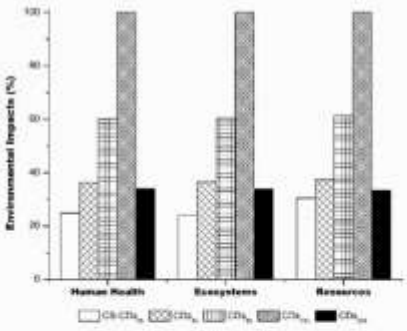

Figure 4. Comparison of relative environmental impacts of CS-CDs_{8h} with CDs without corn stover (CDs_{ca}) using a QY_{FL}-based FU.

ChemSusChem
Research Article
doi.org/10.1002/cssc.202401702
Chemistry Europe
European Chemical Societies Publishing

is the major contributor in the Resources category for all five CDs (Figure S12B and Figure S14). However, there are relevant differences in the Human Health and Ecosystems categories.

For CS-CDs$_{ox}$, the major contributor in the three categories is EDA (Figure S12B), while for the four non-corn stover-based CDs, the highest contributor is CA (Figure S14). These results show that using waste material reduces the impacts associated with using commercial reagents as a carbon precursor. Thus, this LCA study shows that the QY_{FL} of CS-CDs$_{ox}$ is still high enough for their synthesis processes to have lower environmental impacts than those of CDs$_{ox}$.

An additional LCA study was conducted considering the synthesis of the C–CDs$_{ox}$, CK-CDs$_{ox}$, and S-CDs$_{ox}$ (Figure S16). This allowed us to observe that, as seen for CS-CDs$_{ox}$, EDA is the major contributor to the environmental impacts in all endpoint indicators (Human Health, Ecosystems, and Resources). This shows that CDs synthesized using waste as a co-carbon precursor reduce the environmental impacts of the commercial carbon precursor.

When comparing the CS-CDs$_{ox}$, C–CDs$_{ox}$, CK-CDs$_{ox}$, and S-CDs$_{ox}$ using a volume-based FU of 100 L (Figure S17A), we observe that CS-CDs$_{ox}$ and S-CDs$_{ox}$ present the lowest and highest relative environmental impacts, respectively. CS-CDs$_{ox}$ and C–CDs$_{ox}$ have almost the same environmental impacts (a difference of less than 1%). When considering a function-based FU involving QY_{FL}, it is possible to conclude that corn-stover-based CDs still present the lowest relative environmental impacts (Figure S17B). Finally, the associated impacts of cork-based CDs were increased.

Comparison with other Biomass/Waste-Based CDs

Thus, we have shown that this synthesis approach consistently results in waste-based CDs with appreciable QY_{FL}, irrespective of the starting waste material. Regarding the environmental impacts of the production step, we have also demonstrated the advantages of adding waste as a co-carbon precursor to CA and EDA.

At this stage, it is important to compare the QY_{FL} of produced CDs with values obtained by other organic waste/biomass-based CDs already presented in the literature (Table 3).

From Table 3 we can conclude that the CDs obtained with this procedure present higher QY_{FL} than basically all their counterparts from other works.[42–49] This is especially true for CDs based on corn stover (39.3%) and sawdust (35.9%), the waste-CDs with the highest QY_{FL}.

It is also worth noting that the CDs with higher QY_{FL} from other reports (entries 2, 4, and 8) have reaction times between 11 and 24 hours, whereas our process occurs in only 8 hours, saving time and energy. Finally, several published works, including entries with higher QY_{FL} (4 and 8), did not include dialysis or chromatography as a purification technique. However, it is known that the synthesis of CDs can also generate fluorescent molecules that should be removed from solution by either dialysis or chromatography. By performing neither, the QY_{FL} presented in those studies may be impacted by fluorescent impurities.

Thus, our approach allowed the production of different waste-based CDs with better performance, in terms of QY_{FL}, than existing literature.

Table 3. Comparison of different hydrothermal treatment methods for the production of CDs with biomass or organic waste as (co)-carbon precursor.

CDs	Carbon precursor	Nitrogen Dopant	Temperature (°C)	Reaction Time (H)	Dialysis or chromatography	QY_{FL} (%)	Reference
1	Pear fruit	-	180	6	Yes	10.8	[42]
2	Dwarf banana peel	ammonia	200	24	No	23	[43]
3	*C. retusus* fruit extract	ammonia	180	6	No	9	[44]
4	Orange juice	EDA	200	11	Yes	31.7	[45]
5	*Citrus aurantium*	-	130	12	No	13.3	[46]
6	Pineapple juice	-	150	3	No	10.1	[47]
7	Watermelon juice	-	180	3	Yes	10.6	[48]
8	Lemon juice	-	240	12	No	21	[49]
9	Red onions peel	EDA	120	2.5	No	12	[61]
10	*Eucalyptus* twigs	ammonium chloride	180	4	No	2–10	[62]
9	Corn stover/citric acid	EDA	200	8	Yes	39.3	This work
10	Spent Coffee Grounds/citric acid	EDA	200	8	Yes	24.7	This work
11	Cork powder/citric acid	EDA	200	8	Yes	21.8	This work
12	Sawdust/citric acid	EDA	200	8	Yes	35.9	This work

ChemSusChem | Research Article
doi.org/10.1002/cssc.202401702
Chemistry Europe
European Chemical Societies Publishing

Conclusions

In this work, we aimed to develop a more environmentally friendly production strategy for waste-based CDs, consistently with appreciable QY_{FL} and irrespective of the selected waste material. This was achieved by developing a strategy based on the hydrothermal treatment of waste material and CA as co-carbon precursors while employing EDA as the N-dopant. CDs were produced from different waste carbon sources, such as corn stover, spent coffee grounds, cork powder, and sawdust, with appreciable QY_{FL} values being consistently obtained (up to ~40%). An LCA study demonstrated that the production of CDs from waste material, with our approach, is associated with lower environmental impacts than the production of corresponding CA:EDA-only CDs. The waste-based CDs reported in this work showed a generally better fluorescent performance than other reports concerning organic waste/biomass-based CDs. Thus, this work provides the framework for consistently producing CDs with high QY_{FL} and from different types of waste in a manner that favors a circular economy.

Acknowledgments

"Fundação para a Ciência e Tecnologia" (FCT, Portugal) is acknowledged for the funding of R&D Units CIQUP (UIDB/00081/2020 and UIDP/00081/2020), project 2023.13127.PEX and Associated Laboratory IMS (LA/P/0056/2020). Luís Pinto da Silva acknowledges funding from the FCT under the Scientific Employment Stimulus (CEECINST/00069/2021). Sónia Fernandes also acknowledges the FCT for funding her Ph.D. grant (2021.05479.BD). We also acknowledge the laboratory Lab&Services of the Chemistry and Biochemistry Department of the Faculty of Sciences of Porto University (FCUP | DQB), and CEMUP (Materials Centre of the University of Porto). Manuel Algarra thanks to projects MCIN/AEI/10.13039/501100011033 through the project PID2021-122613OB-I00.

Conflict of Interests

The authors declare no conflict of interest.

Data Availability Statement

The data that support the findings of this study are available in the supplementary material of this article.

Keywords: Carbon dots · Organic waste · Life cycle assessment · Fluorescence · Waste upcycling

[1] S. Dua, P. Kumar, B. Pani, A. Kaur, M. Khanna, G. Bhatt, *RSC Adv.* **2023**, *13*, 13845–13861.
[2] J. Liu, R. Li, B. Yang, *ACS Cent. Sci.* **2020**, *6*, 2179–2195.
[3] D. M. A. Crista, G. P. C. Mello, O. Shevchuk, R. M. S. Sendao, E. F. C. Simoes, J. M. M. Leitao, L. P. da Silva, J. C. G. Esteves da Silva, *J. Fluoresc.* **2019**, *29*, 265–270.
[4] Q. Liu, Z. Dong, A. Hao, X. Guo, W. Dong, *Talanta* **2021**, *221*, 121372.
[5] L. Yan, Y. Yang, C.-Q. Ma, X. Liu, H. Wang, B. Xu, *Carbon* **2016**, *109*, 598–607.
[6] Y. Wang, K. Wang, Z. Han, Z. Yin, C. Zhou, F. Du, S. Zhou, P. Chen, Z. Xie, *J. Mater. Chem. C* **2017**, *5*, 9629–9637.
[7] C. Wang, T. Hu, Y. Chen, Y. Xu, Q. Song, *ACS Appl. Mater. Interfaces* **2019**, *11*, 22332–22338.
[8] E. F. C. Simoes, L. Pinto da Silva, J. C. G. Esteves da Silva, J. M. M. Leitao, *Talanta* **2020**, *208*, 120447.
[9] Y. Qiu, D. Gao, H. Yin, K. Zhang, J. Zeng, L. Wang, L. Xia, K. Zhou, Z. Xia, Q. Fu, *Sens. Actuators B Chem.* **2020**, *324*, DOI: 10.1016/j.snb.2020.128722.
[10] G. Qiao, G. Chen, Q. Wen, W. Liu, J. Gao, Z. Yu, Q. Wang, *J. Colloid Interface Sci.* **2020**, *580*, 88–98.
[11] G. P. C. Mello, E. F. C. Simoes, D. M. A. Crista, J. M. M. Leitao, L. Pinto da Silva, J. C. G. Esteves da Silva, *Crit. Rev. Anal. Chem.* **2019**, *49*, 542–552.
[12] D. Li, J. Huang, R. Li, P. Chen, D. Chen, M. Cai, H. Liu, Y. Feng, W. Lv, G. Liu, *J. Hazard Mater.* **2021**, *401*, 123257.
[13] R. Knoblauch, C. D. Geddes, *Materials (Basel)* **2020**, *13*, DOI: 10.3390/ma13184004.
[14] Y. F. Kang, Y. H. Li, Y. W. Fang, Y. Xu, X. M. Wei, X. B. Yin, *Sci. Rep.* **2015**, *5*, 11835.
[15] S. D. Hettiarachchi, R. M. Graham, K. J. Mintz, Y. Zhou, S. Vanni, Z. Peng, R. M. Leblanc, *Nanoscale* **2019**, *11*, 6192–6205.
[16] H. He, X. Zheng, S. Liu, M. Zheng, Z. Xie, Y. Wang, M. Yu, X. Shuai, *Nanoscale* **2018**, *10*, 10991–10998.
[17] Y. Ding, W. Tan, X. Zheng, X. Ji, P. Song, L. Bao, C. Zhang, J. Shang, K. Qin, Y. Wei, *Analyst* **2021**, *146*, 683–690.
[18] N. K. R. Bogireddy, J. Lara, L. R. Fragoso, V. Agarwal, *Chem. Eng. J.* **2020**, *401*, DOI: 10.1016/j.cej.2020.126097.
[19] B. Hu, K. Huang, B. Tang, Z. Lei, Z. Wang, H. Guo, C. Lian, Z. Liu, L. Wang, *Nanomicro Lett.* **2023**, *15*, 217.
[20] X. Shen, Z. Wang, H. Guo, Z. Lei, Z. Liu, L. Wang, *Small* **2023**, *19*, e2303156.
[21] T. T. A. Do, K. Wicaksono, A. Soendoro, T. Imae, M. J. Garcia-Celma, S. Grijalvo, *J. Funct. Biomater.* **2022**, *13*, DOI: 10.3390/jfb13040219.
[22] B. K. John, T. Abraham, B. Mathew, *J. Fluoresc.* **2022**, *32*, 449–471.
[23] S. Christé, J. C. G. Esteves da Silva, L. Pinto da Silva, *Materials (Basel)* **2020**, *13*, DOI: 10.3390/ma13030504.
[24] H. Zhang, H. Guo, D. Li, Y. Zhang, S. Zhang, W. Kang, C. Liu, W. Le, L. Wang, D. Li, B. Dai, *Nat. Commun.* **2024**, *15*, 2980.
[25] Y. Wang, A. Hu, *J. Mater. Chem. C* **2014**, *2*, DOI: 10.1039/c4tc00988f.
[26] P. G. Luo, F. Yang, S.-T. Yang, S. K. Sonkar, L. Yang, J. J. Broglie, Y. Liu, Y.-P. Sun, *RSC Adv.* **2014**, *4*, DOI: 10.1039/c3ra47683a.
[27] D. M. A. Crista, J. C. G. Esteves da Silva, L. Pinto da Silva, *Nanomaterials (Basel)* **2020**, *10*, DOI: 10.3390/nano10071316.
[28] D. M. A. Crista, A. El Mragui, M. Algarra, J. C. G. Esteves da Silva, R. Luque, L. Pinto da Silva, *Nanomaterials (Basel)* **2020**, *10*, DOI: 10.3390/nano10061209.
[29] Y. Zhou, P. Y. Liyanage, D. L. Geleroff, Z. Peng, K. J. Mintz, S. D. Hettiarachchi, R. R. Pandey, C. C. Chusuei, P. L. Blackwelder, R. M. Leblanc, *ChemPhysChem* **2018**, *19*, 2589–2597.
[30] D. Zhou, Y. Wang, P. Tian, P. Jing, M. Sun, X. Chen, X. Xu, D. Li, S. Mei, X. Liu, W. Zhang, R. Guo, S. Qu, H. Zhang, *ACS Appl. Mater. Interfaces* **2018**, *10*, 27160–27170.
[31] L. Pourzahedi, M. J. Eckelman, *Environ. Sci. Nano.* **2015**, *2*, 361–369.
[32] M. J. Eckelman, J. B. Zimmerman, P. T. Anastas, *J. Ind. Ecol.* **2008**, *12*, 316–328.
[33] A. Bafana, S. V. Kumar, S. Temizel-Sekeryan, S. A. Dahoumane, L. Haselbach, C. S. Jeffryes, *Sci. Total Environ.* **2018**, *636*, 936–943.
[34] A. Ramos, C. A. Teixeira, A. Rouboa, *Int. J. Hydrogen Energy* **2018**, *43*, 10155–10166.
[35] A. Ramos, C. Afonso Teixeira, A. Rouboa, *Energies* **2018**, *11*, DOI: 10.3390/en11030548.
[36] R. Hischier, T. Walser, *Sci. Total Environ.* **2012**, *425*, 271–282.
[37] R. Sendão, M. M. Yuso, M. Algarra, J. C. G. Esteves da Silva, L. Pinto da Silva, *J. Clean. Prod.* **2020**, *254*, DOI: 10.1016/j.jclepro.2020.120080.
[38] S. Fernandes, J. C. G. Esteves da Silva, L. Pinto da Silva, *Materials (Basel)* **2022**, *15*, DOI: 10.3390/ma15103446.
[39] S. Fernandes, J. C. G. Esteves da Silva, L. Pinto da Silva, *NanoImpact* **2021**, *23*, 100332.

ChemSusChem
Research Article
doi.org/10.1002/cssc.202401702
Chemistry Europe
European Chemical Societies Publishing

[40] Y. Xie, D. Cheng, X. Liu, A. Han, *Sensors (Basel)* **2019**, *19*, DOI: 10.3390/s19143169.
[41] M. Algarra, L. Orfão, C. S. Alves, R. Moreno-Tost, M. S. Pino-González, J. Jiménez-Jiménez, E. Rodríguez-Castellón, D. Eliche-Quesada, E. Castro, R. Luque, *ACS Sustainable Chem. Eng.* **2019**, *7*, 10493–10500.
[42] J. R. Bhamore, S. Jha, R. K. Singhal, T. J. Park, S. K. Kailasa, *J. Mol. Liq.* **2018**, *264*, 9–16.
[43] R. Atchudan, T. N. J. I. Edison, S. Perumal, N. Muthuchamy, Y. R. Lee, *Fuel* **2020**, *275*, DOI: 10.1016/j.fuel.2020.117821.
[44] R. Atchudan, T. N. J. I. Edison, D. Chakradhar, S. Perumal, J. J. Shim, Y. R. Lee, *Sens. Actuators B Chem.* **2017**, *246*, 497–509.
[45] Z. Li, Y. Zhang, Q. Niu, M. Mou, Y. Wu, X. Liu, Z. Yan, S. Liao, *J. Lumin.* **2017**, *187*, 274–280.
[46] A. M. Senol, E. Bozkurt, *Microchem. J.* **2020**, *159*, DOI: 10.1016/j.microc.2020.105357.
[47] S. Sharma, A. Umar, S. K. Mehta, S. K. Kansal, *Ceram. Int.* **2017**, *43*, 7011–7019.
[48] M. Lu, Y. Duan, Y. Song, J. Tan, L. Zhou, *J. Mol. Liq.* **2018**, *269*, 766–774.
[49] B. T. Hoan, T. T. Thanh, P. D. Tam, N. N. Trung, S. Cho, V.-H. Pham, *Mater. Sci. Eng. B* **2019**, *251*, DOI: 10.1016/j.mseb.2019.114455.
[50] H. K. M. Ng, G. K. Lim, C. P. Leo, *Microchem. J.* **2021**, *165*, DOI: 10.1016/j.microc.2021.106116.
[51] W. Kasprzyk, T. Swiergosz, S. Bednarz, K. Walas, N. V. Bashmakova, D. Bogdal, *Nanoscale* **2018**, *10*, 13889–13894.
[52] Y. Hu, J. Yang, J. Tian, J. S. Yu, *J. Mater. Chem. B* **2015**, *3*, 5608–5614.
[53] J. Schneider, C. J. Reckmeier, Y. Xiong, M. von Seckendorff, A. S. Susha, P. Kasák, A. L. Rogach, *J. Phys. Chem. C* **2017**, *121*, 2014–2022.
[54] J. Fan, L. Kang, X. Cheng, D. Liu, S. Zhang, *Nanomaterials (Basel)* **2022**, *12*, DOI: 10.3390/nano12244473.
[55] H. Guo, J. Raj, Z. Wang, T. Zhang, K. Wang, L. Lin, W. Hou, J. Zhang, M. Wu, J. Wu, L. Wang, *Small* **2024**, e2311132, DOI: 10.1002/smll.202311132.
[56] H. Guo, L. Zhou, K. Huang, Y. Li, W. Hou, H. Liao, C. Lian, S. Yang, D. Wu, Z. Lei, Z. Liu, L. Wang, *Adv. Funct. Mater.* **2024**, DOI: 10.1002/adfm.202402650.
[57] M. Lei, Y. Xie, L. Chen, X. Liu, Y. Yang, J. Zheng, Q. Li, *RSC Adv.* **2022**, *12*, 27431–27441.
[58] Y. Park, J. Yoo, B. Lim, W. Kwon, S. W. Rhee, *J. Mater. Chem. A* **2016**, *4*, 11582–11603.
[59] K. Yuan, X. Zhang, R. Qin, X. Ji, Y. Cheng, L. Li, X. Yang, Z. Lu, H. Liu, *J. Mater. Chem. C* **2018**, *6*, 12631–12637.
[60] M. B. Prado, N. T. Truong, A. K. Wanekaya, *Sens. Actuators Rep.* **2023**, *6*, DOI: 10.1016/j.snr.2023.100165.
[61] H. Salimi Shahraki, Qurtulen, A. Ahmad, *Inorg. Chem. Commun.* **2023**, *150*, DOI: 10.1016/j.inoche.2023.110514.
[62] D. P. Damera, R. Manimaran, V. V. Krishna Venuganti, A. Nag, *ACS Omega* **2020**, *5*, 19905–19918.
[63] J. R. Lakowicz, *Principles of Fluorescence Spectroscopy*, Springer New York, NY, New York **2006**, XXVI, 954.
[64] A. T. R. Williams, S. A. Winfield, J. N. Miller, *Analyst* **1983**, *108*, 1067–1071.
[65] W. Melhuish, *J. Phys. Chem* **1961**, *65*, DOI: 10.1021/j100820a009.
[66] S. Feijoo, S. González-García, Y. Moldes-Diz, C. Vazquez-Vazquez, G. Feijoo, M. T. Moreira, *J. Clean. Prod.* **2017**, *143*, 528–538.
[67] M. A. J. Huijbregts, Z. J. N. Steinmann, P. M. F. Elshout, G. Stam, F. Verones, M. Vieira, M. Zijp, A. Hollander, R. van Zelm, *Int. J. Life Cycle Assess.* **2016**, *22*, 138–147.
[68] F. Piccinno, R. Hischier, S. Seeger, C. Som, *J. Clean. Prod.* **2016**, *135*, 1085–1097.
[69] H. K. Sadhanala, S. Pagidi, A. Gedanken, *J. Mater. Chem. C* **2021**, *9*, 1632–1640.
[70] J. Liao, Z. Cheng, L. Zhou, *ACS Sustainable Chem. Eng.* **2016**, *4*, 3053–3061.
[71] Y. Deng, J. Qian, Y. Zhou, Y. Niu, *RSC Adv.* **2021**, *11*, 10922–10928.
[72] A. Wang, F. Kang, Z. Wang, Q. Shao, Z. Li, G. Zhu, J. Lu, Y. Y. Li, *Adv. Sustain. Syst.* **2018**, *3*, DOI: 10.1002/adsu.201800132.
[73] A. Gouda, J. Manioudakis, R. Naccache, F. Soavi, C. Santato, *Adv. Sustain. Syst.* **2021**, *5*, DOI: 10.1002/adsu.202100152.
[74] D. Crista, M. Algarra, M. V. Martinez de Yuso, J. C. G. Esteves da Silva, L. Pinto da Silva, *J. Mater. Chem. B* **2023**, *11*, 1131–1143.
[75] J. Zhou, H. Zhou, J. Tang, S. Deng, F. Yan, W. Li, M. Qu, *Mikrochim. Acta.* **2016**, *184*, 343–368.
[76] Z. Ruan, X. Wang, Y. Liu, W. Liao, in *Integrated Processing Technologies for Food and Agricultural By-Products* (Eds.: Z. Pan, R. Zhang, S. Zicari), Academic Press, **2019**, pp. 59–72.
[77] S. Kim, B. E. Dale, *Biomass Bioenergy* **2004**, *26*, 361–375.
[78] W. Zhao, Y. Cui, X. Sun, H. Wang, X. Teng, *Sci. Total Environ.* **2021**, *758*, 143883.
[79] T. Wang, H. Luo, X. Jing, J. Yang, M. Huo, Y. Wang, *Molecules* **2021**, *26*, DOI: 10.3390/molecules26051246.
[80] M. Zhang, X. Long, Y. Ma, S. Wu, *Opt. Mater.* **2023**, *135*, DOI: 10.1016/j.optmat.2022.113311.
[81] B. Vercelli, R. Donnini, F. Ghezzi, A. Sansonetti, U. Giovanella, B. La Ferla, *Electrochim. Acta.* **2021**, *387*, DOI: 10.1016/j.electacta.2021.138557.
[82] C. Olla, A. Cappai, S. Porcu, L. Stagi, M. Fantauzzi, M. F. Casula, F. Mocci, R. Corpino, D. Chiriu, P. C. Ricci, C. M. Carbonaro, *Nanomaterials (Basel)* **2023**, *13*, DOI: 10.3390/nano13081344.
[83] *W. M. Haynes, D. R. Lide, T. J. Bruno (Eds.) Atomic, Molecular, and Optical Physics in Handbook Of Chemistry and Physics*, CRC Press, Boca Raton, 95th Ed. **2014–2015**, ISBN-13: 978-1-4822-0868-9 (eBook - PDF).
[84] X.-Y. Jiao, L.-s. Li, S. Qin, Y. Zhang, K. Huang, L. Xu, *Colloids Surf., A* **2019**, *577*, 306–314.

Manuscript received: July 31, 2024
Accepted manuscript online: September 2, 2024
Version of record online: December 4, 2024

3.1.2. Supporting Information

ChemSusChem

Supporting Information

Development of a Facile and Green Synthesis Strategy for Brightly Fluorescent Carbon Dots from Various Waste Materials

Sónia Fernandes, Manuel Algarra, Antonio Gil, Joaquim Esteves da Silva, and Luís Pinto da Silva*

Supporting information

Development of a Facile and Green Synthesis Strategy for Brightly Fluorescent Carbon Dots from Various Waste Materials

Sónia Fernandes, Manuel Algarra, Antonio Gil, Joaquim Esteves da Silva and Luís Pinto da Silva*

Table of Contents

1. Experimental Section/Methods

1.1. Waste material

Corn stover was collected at an agriculture field in Mindelo, Vairão (Vila do Conde) that belongs to Porto University. First, this material was washed with deionized water to remove the contaminants and then dried at 50 ºC in a DRY- Line® Prime oven from VWR until it was completely dry. Afterward, it was crushed using a Laarmann CM50 mill with a sieve size of 0.5 mm trapezoidal. Finally, the crushed biomass from corn (corn stover) was stored in a freezer at -80 ºC to prevent the growth of microorganisms. Organic waste from tea was acquired after letting lemon and ginger tea bags from Portuguese Continente supermarket, for 5 minutes in boiled water. The contents of the bags were subsequently collected. Spent coffee grounds were collected after using a coffee capsule of Ardenza type from Dolce Gusto. Tea and coffee residues were placed in glass beakers and left at room temperature until they were completely dry. They were then stored at -80 ºC. Undifferentiated forest biomass, sawdust and cork were supplied by different Portuguese companies. These materials were dried for 24 hours at 105 ºC in a DRY- Line® Prime oven from VWR, and then stored in a freezer at -80 ºC. Organic waste from onion and orange were domestic organic residues that were dried at room temperature for 1 day and then crushed using a Laarmann CM50 mill with a sieve size of 0.5 mm trapezoidal and stored at -80 ºC. Biomass from eucalyptus leaves (*Eucalyptus globulus*) was obtained from local plantations in Portugal and then washed with deionized water to remove the contaminants. Later, these leaves were dried at room temperature and ground until a fine powder was obtained. Finally, this biomass was also stored in a freezer at -80 ºC.

1.2. CDs synthesis

All CDs were produced via a hydrothermal approach in which synthesis conditions were varied (such as carbon precursor, identity of nitrogen dopant, precursors quantities, reaction time, and temperature). A final volume of 10 mL of NaOH 0.01 M solution was used throughout all the syntheses. The mixture of precursors was placed in a 25 mL Teflon-lined reactor with a stainless-steel shell from Cambridge Energy Solutions (CES) and then heated in a D-6450 Hanau oven from Heraeus. Afterwards, the resulting CDs solution was placed for 20 minutes in a sonicator from VWR, type USC100TH (ultrasonic cleaner). Later, the sample was centrifuged for 30 minutes at 6000 rpm through a MIKRO 220R from Hettich to remove suspended particles. The precipitate was discarded and the supernatant was further purified. Namely, the CDs were submitted to dialysis for 24 hours, using a Float-A-Lyzer®G2 Dialysis Device, MWCO: 3500 Da. The commercial chemicals that were used were citric acid anhydrous (99%), ethylenediamine (≥99%), urea, and sodium hydroxide (≥97%), from Sigma-Aldrich.

The first CDs were synthesized via hydrothermal treatment (200 ºC for 4 hours) using 0.3 g of different organic waste such as corn stover, biomass, tea, coffee, cork, sawdust, onion peel, orange peel, and eucalyptus (CS-CDs, B-CDs, T-CDs, C-CDs, CK-CDs, S-CDs, OnP-CDs, OrP-CDs, E-CDs, respectively).

For the following synthesis, a commercial carbon precursor (CA – citric acid) and/or an N-dopant (U – urea or EDA – ethylenediamine) was added. The heating stage lasted 4 hours at 200 ºC. In a first approach, for a final weight of 0.3 g of precursors, urea ($CDs_{1:0:1}$) was added to corn stover, with a mass ratio of 1:1 (0.15 g each). Secondly, we added citric acid and corn stover as co-carbon precursors, while using urea as the N-dopant. This was done considering a mass ratio (CS:CA:U) of 1:1:1 ($CDs_{1:1:1}$) and 0.5:0.5:1 ($CDs_{0.5:0.5:1}$). In the first case, 0.15 g of each precursor were used, while in the second, 0.075 g of each co-carbon precursors were added to 0.15 g of U. Finally, for 0.3 g of precursors, the CDs were synthesized using 0.15 g of citric acid and 0.15 g of N-dopants (either urea or ethylenediamine). In this case, citric acid and U/EDA CDs were synthesized at 200 ºC for 4 hours ($CDs_{0:1:1\_U}$ and $CDs_{0:1:1\_EDA}$, respectively. Similarly, an additional citric acid and U CD was prepared at 180 ºC for 4 hours.

Considering a carbon/nitrogen ratio of 1:1 and using EDA as the N-dopant, CDs using a conjugation of corn stover and citric acid as co-carbon precursors (CS-CDs_{eth}) or using only citric acid (CDs_{eth}) were prepared at 200 ºC with reaction times of 4, 8, 16 and 24 hours.

1.3. CDs characterization

Fluorescence measurements were collected with Horiba Jobin Yvon Fluoromax-4 spectrofluorometer, using a standard 10 mm fluorescence quartz cell. The fluorescence spectra were obtained with slits widths of 2 nm.

Absorbance spectra were acquired with a UV-3100PC spectrophotometer from VWR, using quartz cells.

AFM analysis was conducted using the tapping mode in a Veeco Metrology Multimode/Nanoscope IVA. For this analysis was used a silica plate to deposit the sample for analysis and an AFM TESP-SS cantilever (curvature radius of 2 nm). Samples were prepared via drop evaporation of a diluted CDs solution and NanoScope was the software used for the AFM data analysis. Particle size measurements were made based on the height of the particles and the average size was calculated by averaging the measurements of 100 individual particles.

ζ Potential measurements were performed in a polycarbonate Omega Cuvette with a particle analyzer Anton Paar LitesizerTM 500.

X-ray photoelectron spectroscopy (XPS) data were acquired with a Kratos Axis Ultra HSA, using monochromatic Al-Kα radiation with a hemispherical multichannel detector (90 W and 15 kV). To prepare the samples, a droplet of CDs solution was deposited onto a silicon wafer and left to dry until it formed a uniform layer. Analysis and quantification of spectra were made using the CasaXPS software and as a reference to obtain the binding energy values was consider the carbon C 1*s* signal at 285.0 eV, applying Gauss-Lorentz curves and Shirley-type background.

Fourier transform infrared (FT-IR) spectroscopy was performed with PerkinElmer Spectrum Two (ATR module) FT-IR spectrometer, using Spectrum software. FT-IR-ATR technique was accomplished with 4 scans per spectrum and a wavenumber range of 4000-400 cm-1.

Laboratory X-ray powder diffraction (XRPD) patterns were collected on a PANanalytical EMPYREAN automated diffractometer. The powder patterns were recorded using the PIXcel 3D detector in Bragg-Brentano reflection configuration. A step size of 0.017° (2θ) was used, and the patterns were recorded between 5 and 70 in 2θ. The total measuring time for recording the patterns was 60 minutes.

1.4. Fluorescence Quantum Yield Determination

A standard procedure [1, 2] was followed to determine the Fluorescence Quantum Yield (QY_{FL}). This procedure involved comparing the integrated luminescence intensities and absorbance values of the samples (CDs) with a reference fluorophore (quinine sulfate). QY_{FL} is calculated according to the following equation: Grad refers to the gradient from the plot of integrated fluorescence intensity versus absorbance, and **η** is the refractive index.

$$QY_{FL}(\%) = QY_{FL_{reference}} \times \frac{Grad_{sample}}{Grad_{reference}} \times \frac{\eta^2_{sample}}{\eta^2_{reference}} \times 100$$

In this study, quinine sulfate (QS) was chosen as the reference fluorophore, with a QY_{FL} of 0.54 [3]. QS is a typical choice as a reference for the determination of QY_{FL} for CDs, given that it absorbs at the chosen excitation wavelength and emits in a similar region to typical CDs (including the ones analyzed here). The refractive index used for the reference was 1.33 (0.1M H_2SO_4) and 1.34 (water), respectively [4, 5]. QY_{FL} determination assays were performed by considering different solutions of increasing concentration for each sample (including solvent blank). First, the absorbance at the excitation wavelength was recorded for all samples. The same excitation wavelength (350 nm) was used for all. The recorded absorbances did not exceed 0.1. The fluorescence spectra of the same studied solutions were recorded, and the integrated fluorescence intensities (the area of the spectra) were calculated. All the fluorescence spectra were recorded with constant slit width. Finally, for each sample, it was plotted a graph of integrated fluorescence intensity as a function of absorbance at the excitation wavelength. This produces a straight line: the slope is $Grad_{sample/reference}$, and the intercept is zero."

1.5. Life Cycle Assessment

The experimental section of the LCA study is divided into four sub-sections: goal and scope definition (1.5.1), life cycle inventory data (1.5.2), life cyle impact assessment (1.5.3), and scale-up (1.5.4), as described below.

1.5.1. Goal and Scope Definition

This LCA study aims to evaluate and compare the potential environmental impacts of each synthesis by using a cradle-to-gate approach. To this end, a scale-up modelling of the laboratory-scale synthesis procedures was made in which two bottom-up procedures for CDs production were considered. These synthesis routes differ in the carbon precursors used. The first type used a waste material (corn stover, coffee, cork, and sawdust) and a commercial chemical reagent (citric acid) as co-carbon precursors. The second type only considers citric acid as the carbon precursor (Scheme S1). The present LCA study focus on the industrial manufacturing stage of target nanoparticles by scaling up the synthesis of CDs at a laboratory scale. It considers either the direct emissions resulting from CDs production, as well as the indirect impacts associated with upstream resource extraction and energy generation.

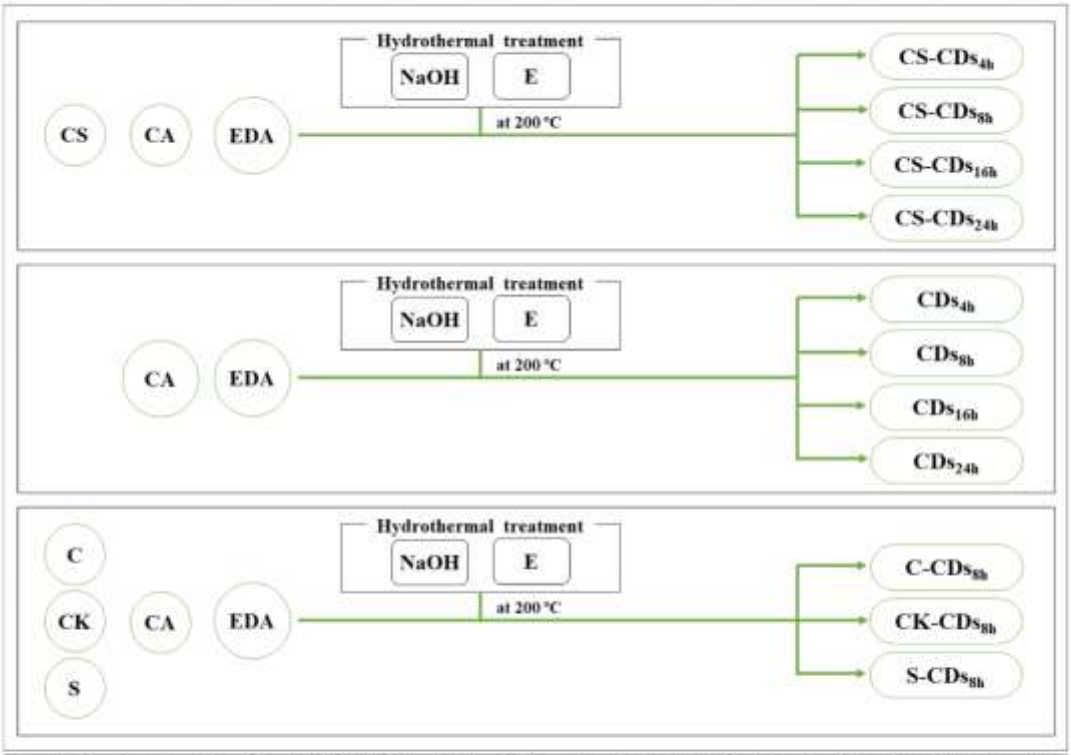

Legend: CS – Corn Stover; CA – Citric Acid; EDA – Ethylenediamine; NaOH – Sodium hydroxide 0.01M solution; C – Coffee; CK – Cork; S – Sawdust; E – Electricity.

Scheme S1. Diagram for the Carbon Dots syntheses.

Thus, in a first stage, the environmental impacts were analyzed and compared using a volume-based functional unit of 100 L to allow the comparison of an equivalent quantity of nanomaterial [6, 7]. This was determined by the scale-up of the laboratory-scale manufacturing considering a batch reactor of 100 L, which is specified in section 1.5.4. A volume-based functional unit of 100 L was considered once the energetic consumption of equipment used at a laboratory scale may not be adjusted to the quantities of CDs produced. Therefore, it is more pertinent to evaluate data at an industrial scale when assessing the potential commercial of CDs production. In a later stage, it was consider a different functional unit by normalizing the impacts based on the fluorescence quantum yield (QY_{FL}) of the CDs under study, thus considering the functional benefits of the synthesized nanomaterials,. It is important to consider that the evaluation of potential environmental impacts using a volume-based functional unit may not account scenarios where the synthesis method requires more resources that posteriorly could be justified in the use stage. Thus, QY_{FL} was selected as the normalization factor since the QY_{FL} is a relevant property in several CDs applications, such as light-emitting devices, photocatalysis, and sensing [8]. In this sense, adhering to a standard practice, the QY_{FL} was established as the framework for a functional unit (FU) aiming to assess the performance of the CDs, which has been previously applied in LCA studies of CDs [9, 10]. The FU used in this LCA study is related to the highest QY_{FL} of CDs under study and then compared to each CD, leading to a factor calculated as follows:

$$\frac{QY_{FL_{reference}}}{QY_{FL}}$$

1.5.2. Life Cycle Inventory

The assessment of potential environmental impacts linked to the synthesis of CDs was conducted using inventory data obtained from laboratory-scale synthesis procedures (foreground data) found in the Ecoinvent® 3.9.1 database. This foreground system consists of raw materials (chemicals) and electricity (oven referred to in section 1.2) used in the synthetic procedures. For the study of CDs, the synthesis procedure consists of a hydrothermal-based treatment of the precursors in a NaOH solution for a

specified reaction time. Centrifugation and dialysis steps were the same for all CDs, so they were not considered since they should have provided the same potential environmental impacts for all procedures. Thus, the foreground system consists of the electricity and the production of chemicals (CA, EDA, NaOH solution, and deionized water) used as raw materials in the manufacture of CDs. The environmental impacts associated with the production of the used waste materials were not considered, as these waste materials are produced irrespectively of their potential subsequent use as carbon precursors for CDs. Their production results entirely as a by-product/waste from other industries and would not be avoided either way. Thus, their relative environmental impacts were attributed to the industry that generated them, and not to the production of CDs.

In this LCA study, the processes and chemicals were modelled with the following data present in the Ecoinvent® 3.9.1 database (GLO standing for global, RER for regional market for Europe, and PT for Portugal): citric acid {GLO}| market for| cut-off, S; ethylenediamine {RER}| market for ethylenediamine| cut-off, S; sodium hydroxide, without water, in 50% solution state{GLO}| market for sodium hydroxide, without water, in 50% solution state| cut-off, S; water, deionized, {Europe without Switzerland}| market for water, deionized| cut-off, S; electricity, medium voltage {PT}| market for electricity, medium voltage| cut-off, S. The dataset for electricity in Portugal describes the available electricity data on the medium voltage level in 2014 (Ecoinvent® 3.9.1 database).

1.5.3. Life Cycle Impact Assessment

As referred above, the present LCA study consists on a cradle-to-gate study concerning stages from the precursors fabrication to the CDs production. In this sense, SimaPro 9.5.0.0 software was used to performed this LCA study, and on the other hand ReCiPe 2016 V1.08 endpoint method, Hierarchist version [11] was used to model the potential environmental impacts. Considering the most widely accepted policy principles related to the time frame and plausibility of impact mechanisms to deal with uncertainties and assumptions it was adopted the scientific consensus model of the Hierarchist perspective. This method evaluates three endpoint indicators: Human Health, Ecosystems, and Resources, in which each one evaluates different midpoint indicators. Human Health midpoint indicators are Fine Particulate Matter formation (FPM), Global Warming – Human Health (GW–HH), Human Carcinogenic toxicity (HC), Human Non-Carcinogenic toxicity (HNC), Ionization Radiation (IR), Ozone formation – Human Health (OF), Stratospheric ozone depletion (SO), and Water Consumption – Human Health (WC–HH). In Ecosystems were assessed the subcategories: Freshwater Eutrophication (FE), Freshwater EcoToxicity (FET), Global Warming – Freshwater Ecosystems (GW–FE), Global Warming – Terrestrial Ecosystems (GW–TE), Land Use (LU), Marine Eutrophication (ME), Marine EcoToxicity (MET),Ozone Formation – Terrestrial Ecosystems (OF–TE), Terrestrial acidification (TA), Terrestrial EcoToxicity (TET), Water Consumption – Aquatic Ecosystems (WC–AE), and Water Consumption – Terrestrial Ecosystem (WC–TE). Midpoint indicators of Resources are Mineral Resource scarcity (MR) and Fossil Resource scarcity (FR).

1.5.4. Scale-up

By implementing a volume base functional unit of 100 L, this LCA study effectively addresses specific uncertainties linked to the industrial production of CDs. For that, the laboratory results were successfully scaled up to an industrial level by extrapolating the framework developed by Piccinno et al. [12]. The quantities of precursors used (citric acid, EDA, NaOH solution) were linearly increased to 100 L (processing quantity). On the other hand, the electricity was scaled based on the work referred above, which determined the energy required for the heating. The heating energy required for the synthesis is determined by the equation:

$$Q_{react} = \frac{Q_{heat} + Q_{loss}}{\eta_{heat}} = \frac{C_p \times m_{mix} \times (T_r - T_0) + A \times \frac{k_a}{s} \times (T_r - T_{out}) \times t}{\eta_{heat}}$$

In which, Cp (J/K/kg), mmix (kg), Tr (K), T_0 (K), T_{out} (K), A (m^2), ka (W/m+K), s (m), t (h), and ηheat (%) are respectively the specific heat capacity of the main solvent, the mass of the reaction mixture, the reaction temperature, the starting temperature, the temperature outside the reactor, the surface area of the reactor, the thermal conductivity of the insulation material, the thickness of the insulation, the time of the reaction, and the efficiency of the heating device [12]. It is worth mentioning that were considered the values suggested by [12], Cp parameter for the solvent refers to water, and the remaining parameters were obtained from the CDs synthesis.

2. Results

2.1. Characterization of CDs produced

2.1.1. CDs from different organic waste

Previous LCA studies of CDs syntheses have identified the carbon precursor, typically a commercial chemical reagent, as one of the major contributors to their environmental impacts [9, 10, 13-15]. So, replacing these commercial chemical reagents with waste materials as the carbon precursor could reduce the environmental impacts resulting from the CDs synthesis. Considering this, we have synthesized a series of CDs via hydrothermal treatment from different waste materials as precursors: corn stover, biomass, tea, spent coffee grounds, cork powder, sawdust, onion peel, orange peel, and eucalyptus biomass (CS-CDs, B-CDs, T-CDs, C-CDs, CK-CDs, S-CDs, OnP-CDs, OrP-CDs, and E-CDs, respectively).

2D excitation-emission contour plots (EECP) were measured for each CDs (Figure S1), which showed a similar fluorescence between the samples. Namely, all CDs presented a well-defined luminescent center with an emission maximum at about 440 nm. However, all the CDs presented negligible QY_{FL} values in a range between 0.5% and 1.4% (Table S1), which are too low for in the typical applications for CDs. Moreover, the fact that all waste-derived CDs presented negligible QY_{FL} suggests that using waste materials by themselves might not be enough to produce CDs with an adequate fluorescence. Given this, we optimized the synthesis procedure by investigating different parameters, such as the carbon precursor and dopant, their respective ratios, and the temperature and duration of the synthesis.

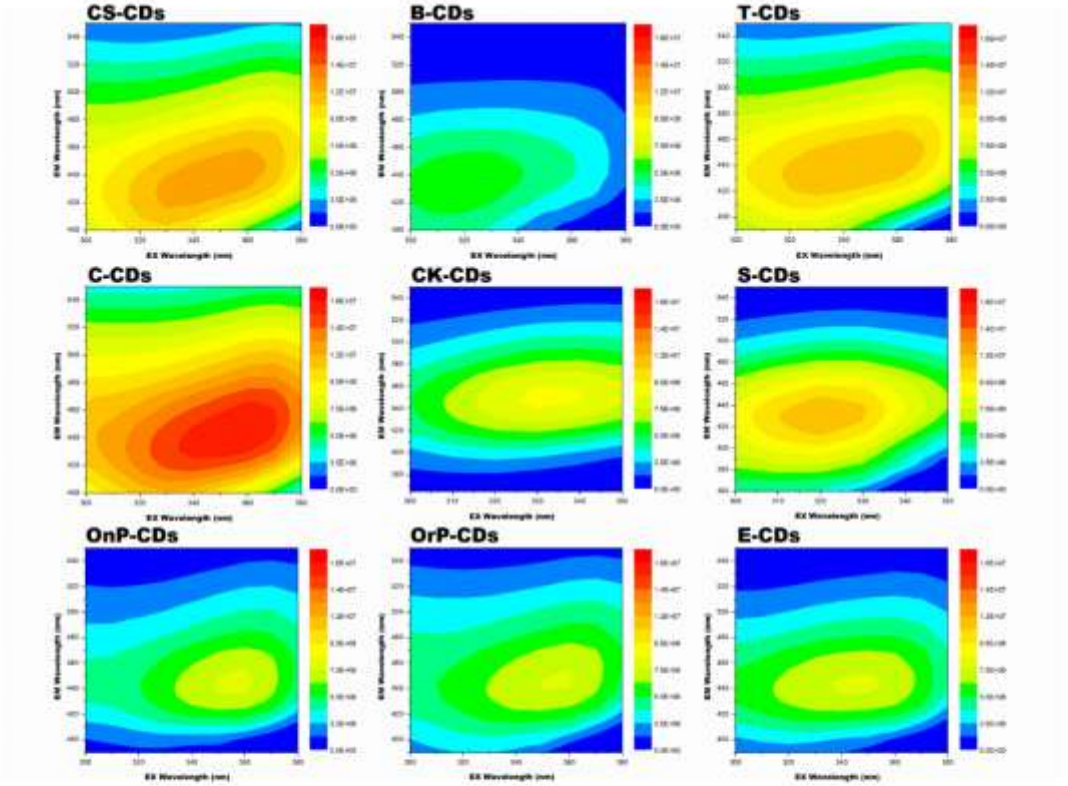

Figure S1. EECPs of CDs with corn stover (CS-CDs), biomass (B-CDs), tea (T-CDs), coffee (C-CDs), cork (CK-CDs), sawdust (S-CDs), onion peel (OnP-CDs), orange peel (OrP-CDs), and Eucalyptus (E-CDs). Water was the solvent used in all analyses.

Table S1. Fluorescence Quantum Yield (QY_{FL}) of Carbon Dots from different organic waste.

Organic Waste	CDs	QY_{FL} (%)
Corn Stover	CS-CDs	1.1
Biomass	B-CDs	0.6
Tea	T-CDs	1.2
Coffee	C-CDs	1.4
Cork	CK-CDs	0.6
Sawdust	S-CDs	1.2
Onion Peel	OnP-CDs	0.5
Orange Peel	OrP-CDS	0.9
Eucalyptus	E-CDs	0.6

2.1.2. Initial optimization of CDs synthesis from Corn Stover

The previously shown results indicated that just replacing commercial chemical reagents with waste materials as carbon precursors was not enough to obtain CDs with high QY_{FL} values. So, our aim shifted from replacing commercial reagents altogether to reducing their use on the process by conjugating them with waste materials as co-carbon sources.

Typical synthesis procedures of CDs include both a carbon precursor and a heteroatom-dopant. The use of this type of dopants allows the incorporation of chosen heteroatoms (such as N, S, B, and P) into the structure of CDs. This is a commonly employed strategy to improve the fluorescent properties of this type of nanomaterials [16-18]. Among heteroatom-doping strategies, the use of N-dopants is arguably the most frequent [19-21], as carbon and nitrogen have comparable sizes and nitrogen atoms offer five valence electrons to form bonds with carbon atoms [22]. Given this, the next step of this study was to produce CDs via hydrothermal treatment using mixtures of carbon precursors and N-dopants, in which waste material is introduced as a co-carbon precursor, thus reducing the need of commercial reagents.

In this optimization step, corn stover was used as the waste material. It was one of the materials that resulted in the highest QY_{FL} in the previous section and, more importantly, it is a highly relevant, but underused, agricultural waste. Worldwide, corn production is circa 1 billion tons, with corn stover consisting being around half the weight of the aboveground part of the corn [23]. Moreover, less than 10% of corn stover is utilized (i.e., less than 1% is processed for industrial production and approximately 5% is used in animal feed and livestock bedding) [24, 25]. Thus, most of the corn stover remains unused, being either discarded or burned directly, meaning that the resource is wasted and the environment polluted [24, 25].

The first step of the synthesis optimization was made by preparing CDs ($CS\text{-}CDs_{1:0:1}$) from corn stover (as a carbon precursor) and a commercial N-dopant (urea) in a 1:1 mass ratio. This synthesis was made with the objective of seeing if adding an N-dopant to the synthesis is enough to obtain a higher QY_{FL} without introducing commercial reagents as co-carbon precursors. The second step consisted on the synthesis of other CDs ($CS\text{-}CDs_{1:1:1}$) in which citric acid was added to corn stover and urea as an addition carbon precursor. This mixture presented a mass ratio of 1:1:1 (corn stover: citric acid: urea). This was followed by the synthesis of another CDs ($CS\text{-}CDs_{0.5:0.5:1}$), in which the mass ratio of corn stover and citric acid was half of that of urea. This was made to verify if reducing the amount of commercial reagents by adding corn stover as a co-carbon precursor while maintaining a 1:1 ratio of carbon precursors:urea was possible without limiting the obtained QY_{FL} significantly.

The EECP for $CS\text{-}CDs_{1:0:1}$ (Figure S2) was similar to that of the CDs produced from corn stover (CS-CDs, Figure S1), presenting an emission wavelength maximum at ~435 nm. More relevantly, the QY_{FL} of $CS\text{-}CDs_{1:0:1}$ is just as negligible (0.5%, Table S2). This indicates that introducing N-dopant alone to a synthesis using only waste material as the carbon precursor is not a promising strategy to increase the QY_{FL}.

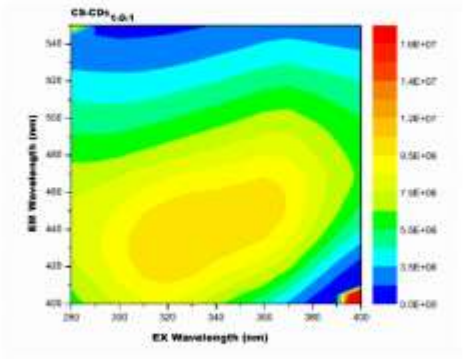

Figure S2. EECP of CD with corn stover and urea (CS-CDs$_{1:0:1}$). Water was the solvent used in all analyses.

Table S2. QY_{FL} of CDs with the addition of another carbon precursor (citric acid) and/or nitrogen dopant (urea or EDA: ethylenediamine).

CDs	Corn Stover (g)	Citric Acid (g)	Urea (g)	EDA (g)	Temperature (°C)	QY_{FL} (%)
CS-CDs$_{1:0:1}$	0.15	-	0.15	-	200	0.5
CS-CDs$_{1:1:1}$	0.15	0.15	0.15	-	200	7.3
CS-CDs$_{0.5:0.5:1}$	0.075	0.075	0.15	-	200	13.0
CDs$_{0:1:1_U}$	-	0.15	0.15	-	200	23.2
CDs$_{0:1:1_EDA}$	-	0.15	-	0.15	200	65.0
CDs$_{0:1:1_180}$	-	0.15	0.15	-	180	24.4

The analysis of both CS-CDs$_{1:1:1}$ and CS-CDs$_{0.5:0.5:1}$ was performed to verify if the introduction of a commercial reagent (even in reduced amounts) allowed an increased QY_{FL}. Here, citric acid (as carbon precursor) and urea (as N-dopant) were used given their frequent use in the synthesis of CDs [13, 14, 26]. The EECPs (Figure S3) for these CDs showed a similar emission wavelength maximum at ~440 nm, with excitation at both ~310 and ~365 nm. Interestingly, CS-CDs$_{1:1:1}$ showed more intense emission when excited at ~365 nm, while CS-CDs$_{0.5:0.5:1}$ presented more intense emission with excitation at ~310 nm. Furthermore, we did see increased values of QY_{FL} with the introduction of citric acid. CS-CDs$_{1:1:1}$ and CS-CDs$_{0.5:0.5:1}$ presented QY_{FL} of 7.3% and 13.0%, respectively (Table S2).

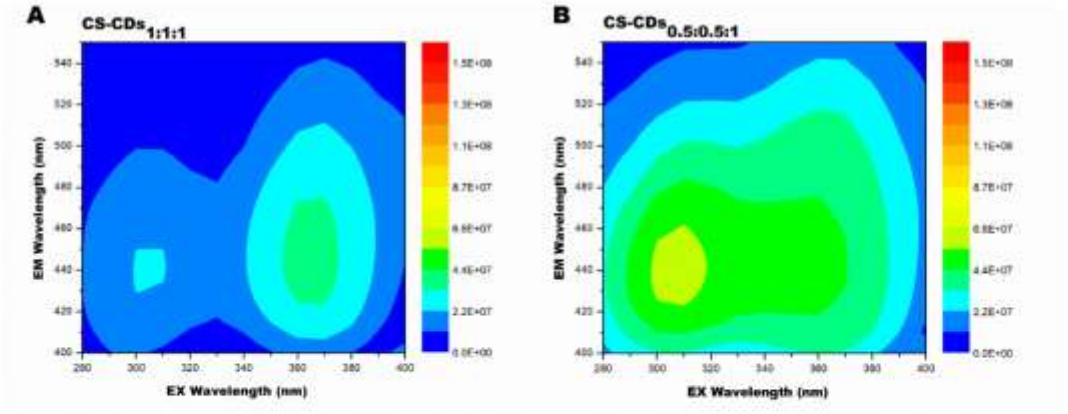

Figure S3. EECPs of CDs with corn stover, citric acid, and urea in a mass ratio of 1:1:1 (CS-CDs$_{1:1:1}$) and 0.5:0.5:1 (CS-CDs$_{0.5:0.5:1}$). Water was the solvent used in all analyses.

While still relatively low, these values of QY_{FL} show the potential of optimization using a mixture of co-carbon precursors comprised of waste material, commercial reagent, and N-dopant. That the highest QY_{FL} was obtained with a lower amount of citric acid was also promising.

Given that the highest QY_{FL} was obtained with a corn stover:citric acid:urea ratio of 0.5:0.5:1, this means that the best overall carbon precursor:N-dopant ratio was 1:1. Citric acid was found to enhance the obtained QY_{FL}, and so, its inclusion as a co-carbon precursor in subsequent synthesis should be explored. Base on that, we subsequently tried to investigate the impact of different N-dopants, urea ($CDs_{0:1:1\_U}$ and $CDs_{0:1:1\_180}$) and ethylenediamine ($CDs_{0:1:1\_EDA}$) and the influence of different synthesis temperatures, 200ºC ($CDs_{0:1:1\_U}$ and $CDs_{0:1:1\_EDA}$) and 180ºC ($CDs_{0:1:1\_180}$), in the synthesis. The experimental conditions are described in Table S2. In order to understand the effects of these parameters without limiting ourselves to the results of a single waste material (corn stover), these syntheses were performed using citric acid and N-dopants. This combination of citric acid and N-dopants is very common in the literature and can be considered representative of CDs in general [13-15, 26-31].

The EECPs obtained for these CDs showed some differences depending on the N-dopant (Figure S4). Namely, the CDs obtained from urea ($CDs_{0:1:1\_U}$ and $CDs_{0:1:1\_180}$) showed the same emission maximums with an excitation wavelength maximum below 300 nm, irrespective of the reaction temperature. These CDs displayed more than one luminescent center, with the same emission wavelength. As for $CDs_{0:1:1\_EDA}$, it showed a similar emission wavelength maximum, presenting just one well-defined luminescent center with a red-shifted excitation, when compared with urea-based CDs. More relevant were the obtained QY_{FL} (Table S2). All QY_{FL} were significantly higher than those measured before. Urea-based CDs presented QY_{FL} between 23 and 24% for the tested temperatures, with the negligible difference in terms of QY_{FL} suggesting that temperature is a reaction parameter with less potential in terms of optimization. Interestingly, using EDA as an N-dopant increased the obtained QY_{FL} to 65.0%, indicating that EDA should be preferred as an N-dopant in subsequent synthesis.

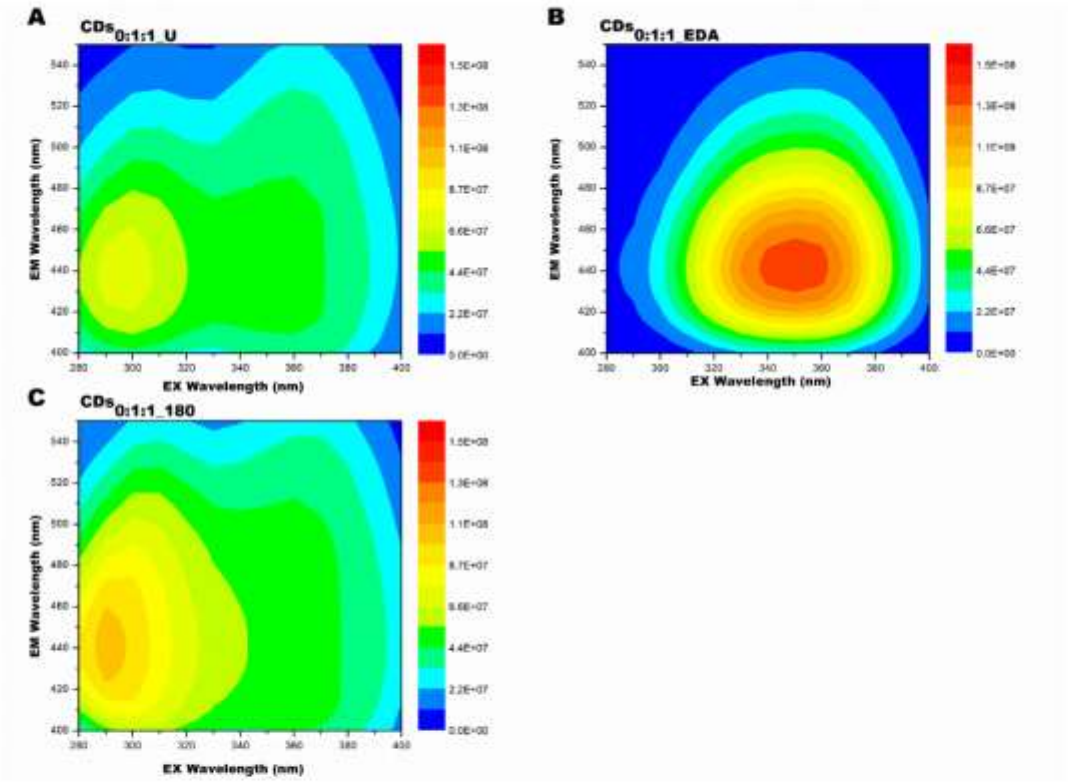

Figure S4. EECPs of CDs with citric acid and N-dopants (U: urea, or EDA: ethylenediamine) at 200 ºC (respectively, $CDs_{0:1:1\_U}$ and $CDs_{0:1:1\_EDA}$), as well as CDs with citric acid and urea at 180 ºC ($CDs_{0:1:1\_180}$). Water was the solvent used in all analyses.

2.1.3. Carbon Dots with and without corn stover

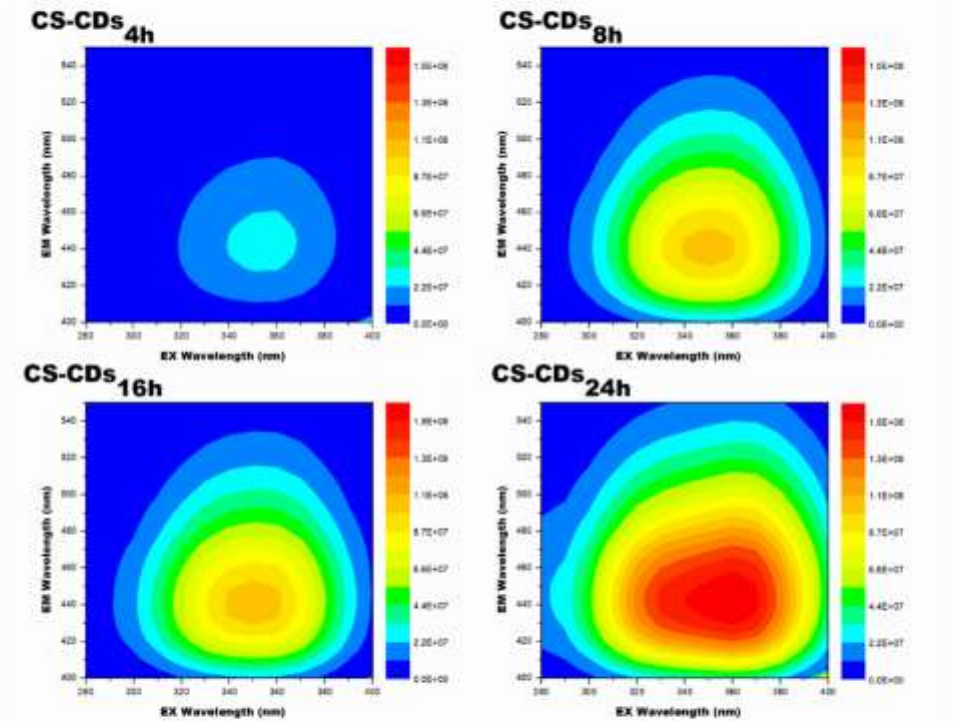

Figure S5. EECPs of CDs with corn stover at different reaction times, 4h ($CS\text{-}CDs_{4h}$), 8h ($CS\text{-}CDs_{8h}$), 16h ($CS\text{-}CDs_{16h}$), and 24h ($CS\text{-}CDs_{24h}$). Water was the solvent used in all analyses

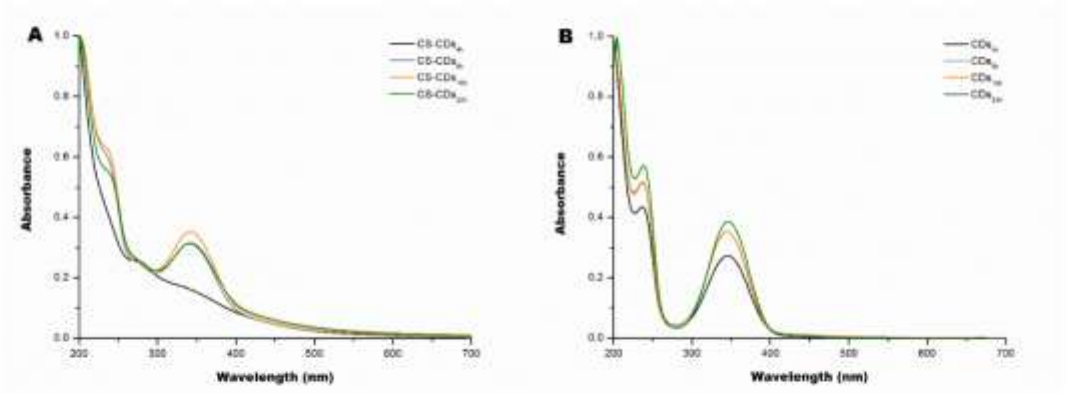

Figure S6. Absorption spectra of CDs with corn stover (A) and without corn stover (B), increasing reaction time. Water was the solvent used in all analyses.

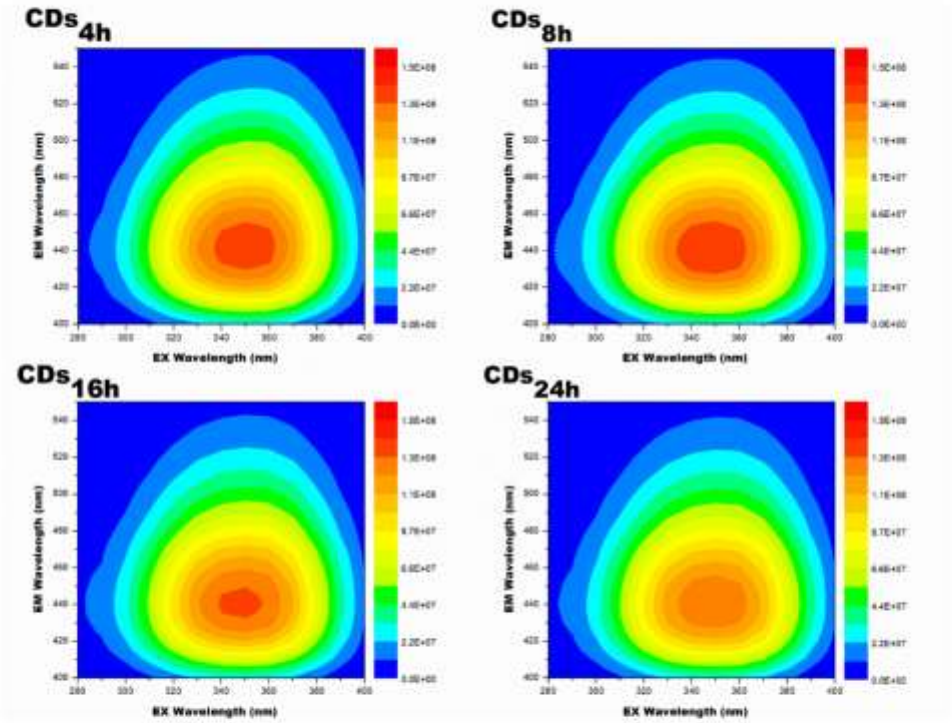

Figure S7. EECPs of CDs with corn stover at different reaction times, 4h (CDs_{4h}), 8h (CDs_{8h}), 16h (CDs_{16h}), and 24h (CDs_{24h}). Water was the solvent used in all analyses.

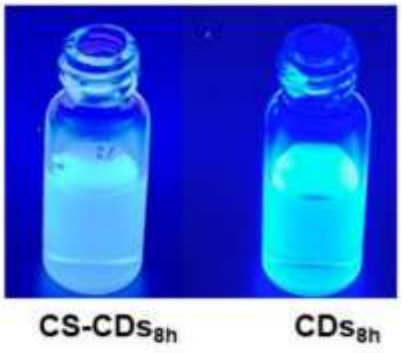

Figure S8. Aqueous solutions of CS-CDs_{8h} and CDs_{8h} (0.5 mg/mL), under blacklight irradiation.

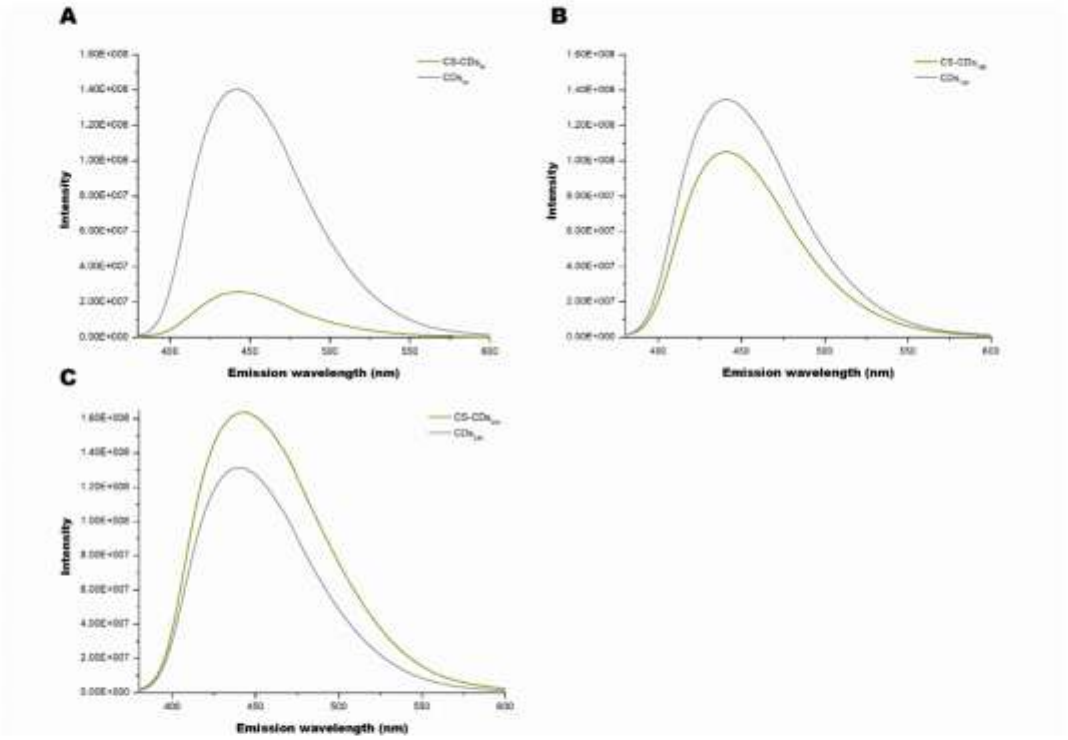

Figure S9. Emission spectra of CS-CDs$_{4h}$ and CDs$_{4h}$ at different reaction times, 4h (A), 16h (B), and 24h (C). The excitation wavelength was 350 nm, except for CS-CDs$_{4h}$ (355nm) and CS-CDs$_{24h}$ (360nm). Water was the solvent used in all analyses.

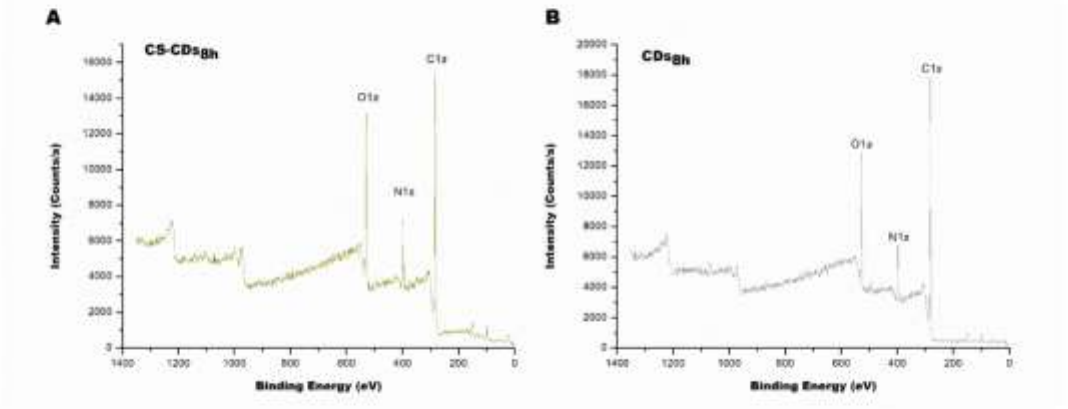

Figure S10. XPS Survey of CS-CDs$_{8h}$ (A) and CDs$_{8h}$ (B).

Table S3. XPS data.

CDs	C1*s*	N1*s*	O1*s*
CS-CDs$_{8h}$	70.0	11.6	18.5
CDs$_{8h}$	74.4	10.1	15.5

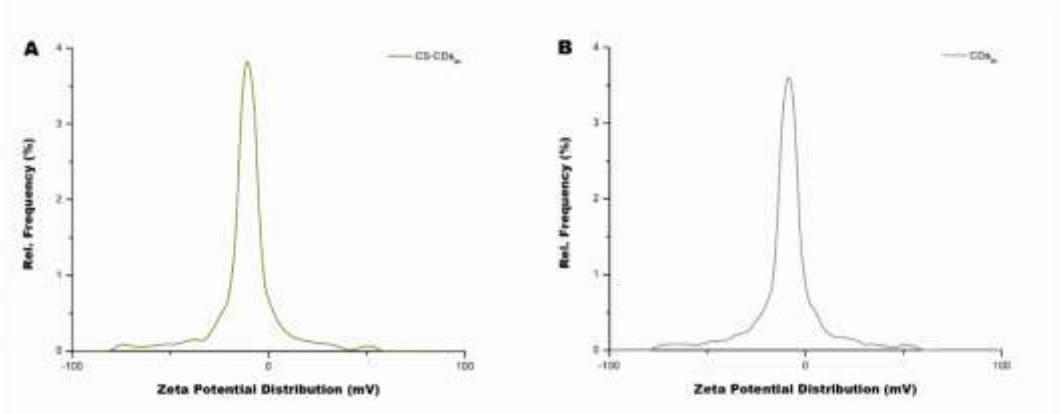

Figure S11. Zeta Potential curve of CS-CDs$_{8h}$ (A) and CDs$_{8h}$ (B).

2.2. Life Cycle Assessment

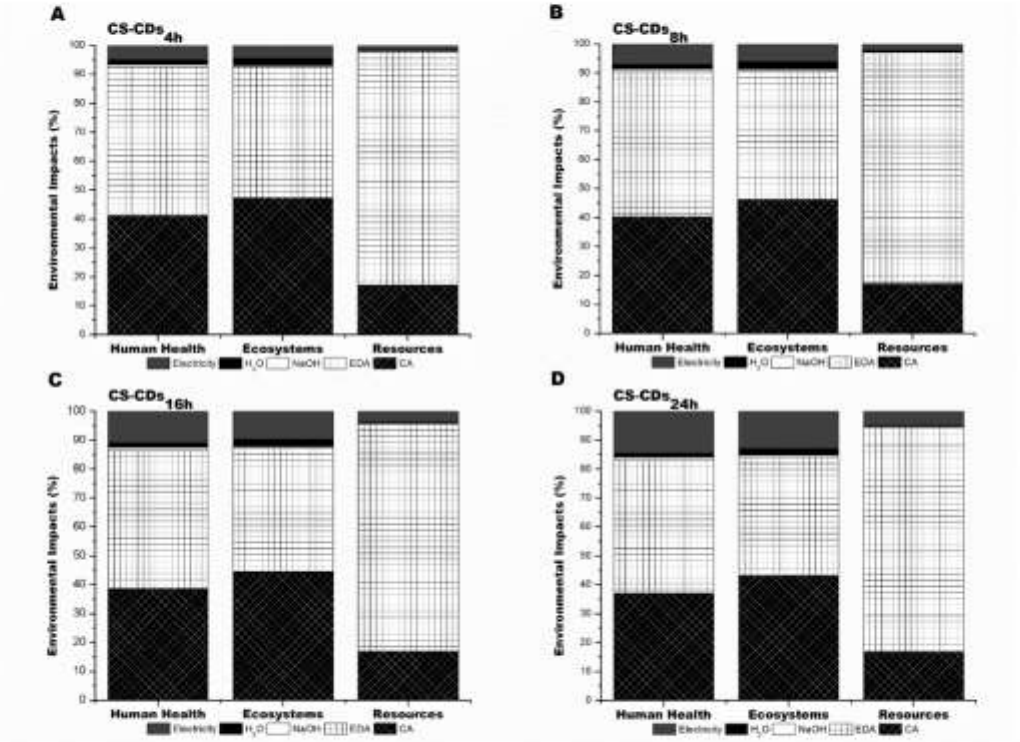

Figure S12. Relative potential environmental impacts for CS-CDs$_{4h}$ (A), CS-CDs$_{8h}$ (B), CS-CDs$_{16h}$ (C), and CS-CDs$_{24h}$ (D).

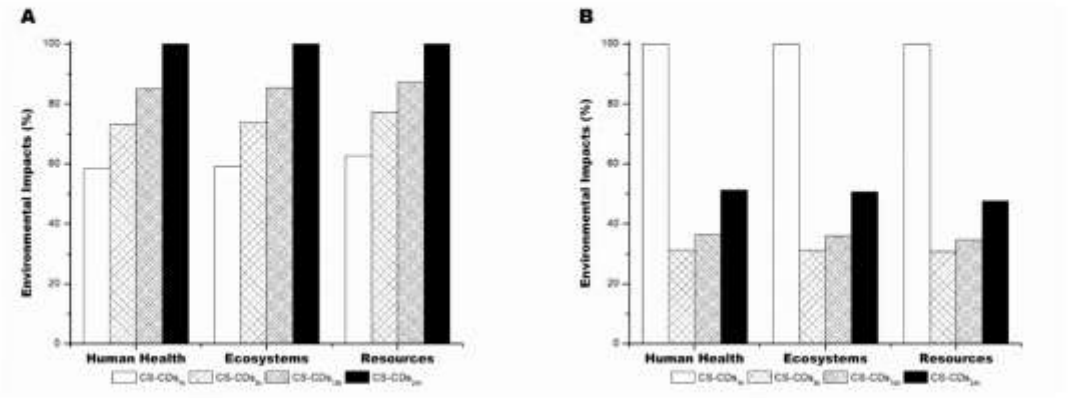

Figure S13. Comparison of relative environmental impacts of corn stover CDs by 100 L (A) and by QY_{FL} (B).

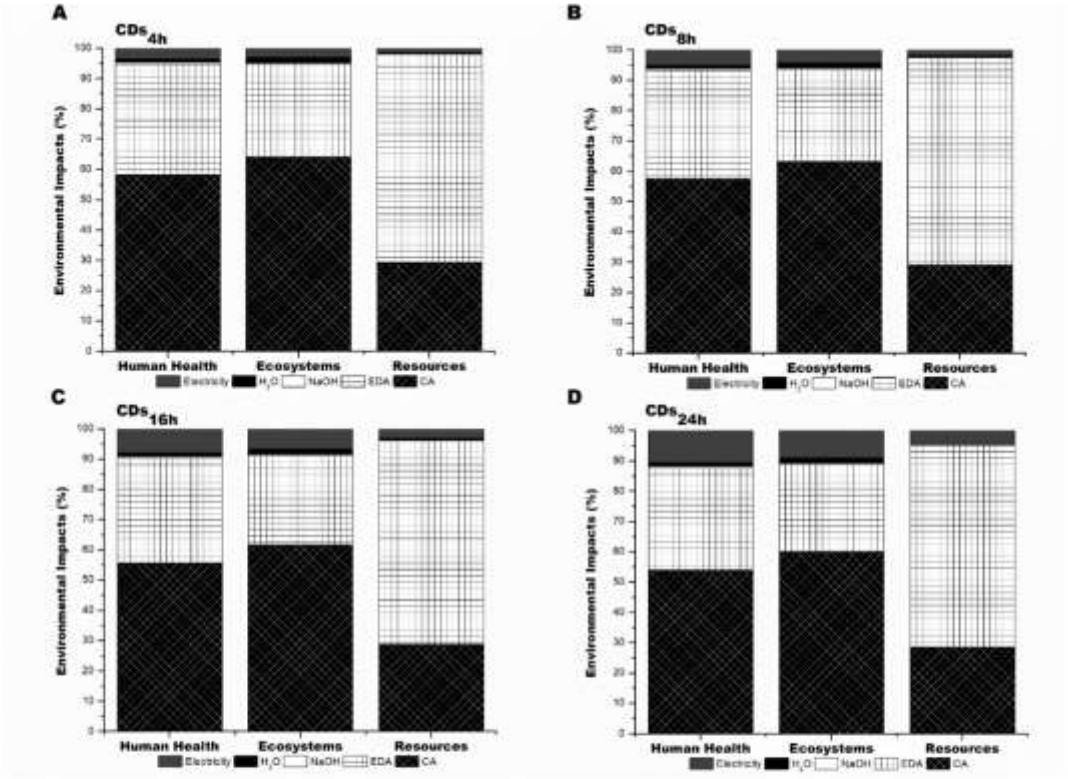

Figure S14. Relative potential environmental impacts for CDs_{4h} (A), CDs_{8h} (B), CDs_{16h} (C), and CDs_{24h} (D).

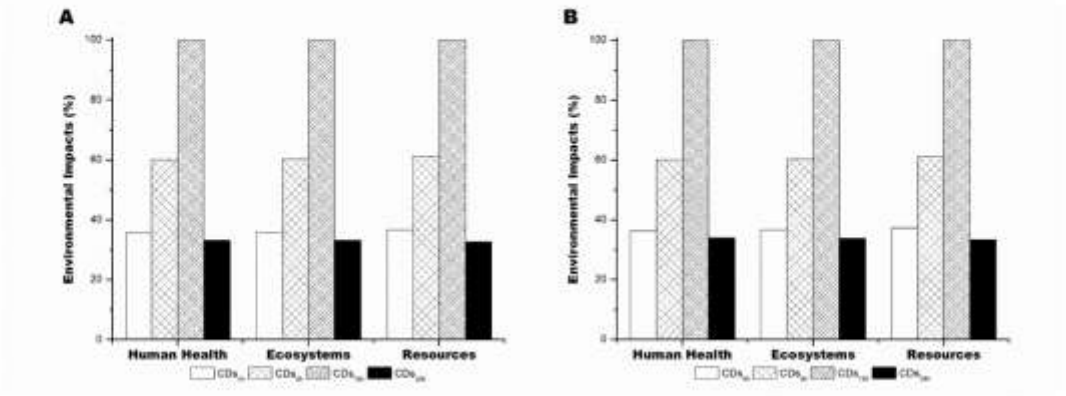

Figure S15. Comparison of relative environmental impacts of CDs without corn stover by 100 L (A) and by QY_{FL} (B).

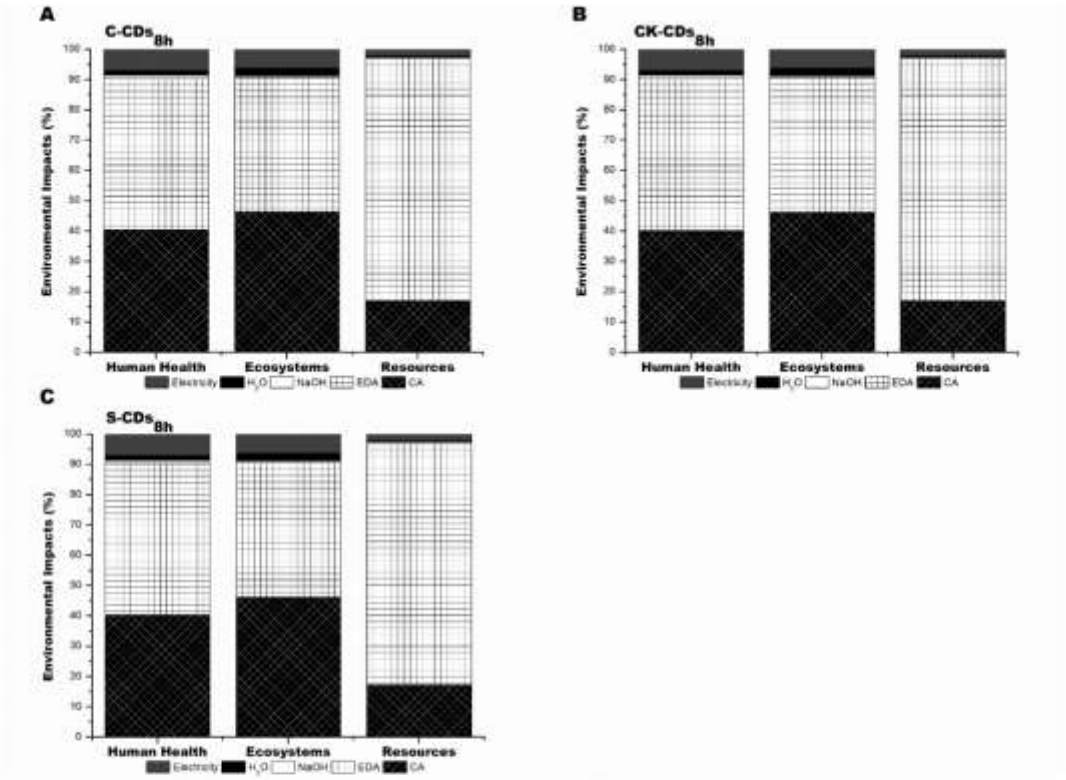

Figure S16. Relative potential environmental impacts for C-CDs_{8h} (A), CK-CDs_{8h} (B), and S-CDs_{8h} (C).

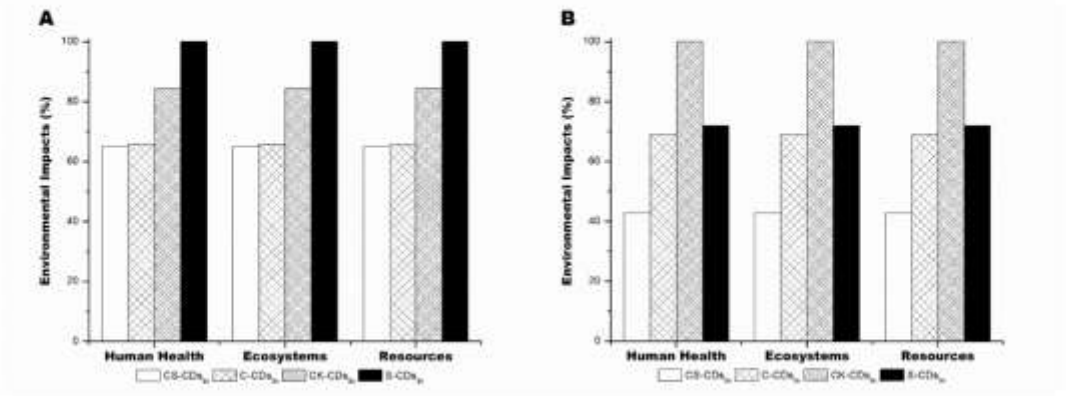

Figure S17. Comparison of relative environmental impacts of CS-CDs$_{EH}$ with CDs with other organic waste using a 100 L (A) and by QY_{FL} (B) FU.

References

[1] J.R. Lakowicz, *Principles of Fluorescence Spectroscopy*, Springer New York, NY, New York, **2006,** XXVI, 954.

[2] A.T.R. Williams, S.A. Winfield, and J.N. Miller, Analyst. **1983**, 108, 1067-1071, 10.1039/an9830801067.

[3] W. Melhuish, J. Phys. Chem. **1961**, 65, 10.1021/j100820a009.

[4] X.-Y. Jiao, L.-s. Li, S. Qin, Y. Zhang, K. Huang, and L. Xu, Colloids and Surfaces A: Physicochemical and Engineering Aspects. **2019**, 577, 306-314, 10.1016/j.colsurfa.2019.05.073.

[5] *Atomic, molecular, and optical physics* in *Handbook of chemistry and physics*, W.M. Haynes, Editor. 2014-2015, CRC Press.

[6] S. Feijoo, S. González-García, Y. Moldes-Diz, C. Vazquez-Vazquez, G. Feijoo, and M.T. Moreira, J. Clean. Prod. **2017**, 143, 528-538, 10.1016/j.jclepro.2016.12.079.

[7] R. Hischier and T. Walser, Sci. Total Environ. **2012**, 425, 271-82, 10.1016/j.scitotenv.2012.03.001.

[8] J. Liu, R. Li, and B. Yang, ACS Cent. Sci. **2020**, 6, 2179-2195, 10.1021/acscentsci.0c01306.

[9] S. Fernandes, J.C.G. Esteves da Silva, and L. Pinto da Silva, Materials (Basel). **2022**, 15, 10.3390/ma15103446.

[10] S. Fernandes, J.C.G. Esteves da Silva, and L. Pinto da Silva, NanoImpact. **2021**, 23, 100332, 10.1016/j.impact.2021.100332.

[11] M.A.J. Huijbregts, Z.J.N. Steinmann, P.M.F. Elshout, G. Stam, F. Verones, M. Vieira, M. Zijp, A. Hollander, and R. van Zelm, Int. J. Life Cycle Assess. **2016**, 22, 138-147, 10.1007/s11367-016-1246-y.

[12] F. Piccinno, R. Hischier, S. Seeger, and C. Som, J. Clean. Prod. **2016**, 135, 1085-1097, 10.1016/j.jclepro.2016.06.164.

[13] R. Sendão, M.d.V.M.d. Yuso, M. Algarra, J.C.G. Esteves da Silva, and L. Pinto da Silva, J. Clean. Prod. **2020**, 254, 10.1016/j.jclepro.2020.120080.

[14] D.M.A. Crista, J.C.G. Esteves da Silva, and L. Pinto da Silva, Nanomaterials (Basel). **2020**, 10, 10.3390/nano10071316.

[15] S. Christé, J.C.G. Esteves da Silva, and L. Pinto da Silva, Materials (Basel). **2020**, 13, 10.3390/ma13030504.

[16] H.K. Sadhanala, S. Pagidi, and A. Gedanken, J. Mater. Chem. C. **2021**, 9, 1632-1640, 10.1039/d0tc05081d.

[17] J. Liao, Z. Cheng, and L. Zhou, ACS Sustainable Chem. Eng. **2016**, 4, 3053-3061, 10.1021/acssuschemeng.6b00018.

[18] Y. Deng, J. Qian, Y. Zhou, and Y. Niu, RSC Adv. **2021**, 11, 10922-10928, 10.1039/d0ra10766b.

[19] A. Wang, F. Kang, Z. Wang, Q. Shao, Z. Li, G. Zhu, J. Lu, and Y.Y. Li, Adv. Sustain. Syst. **2018**, 3, 10.1002/adsu.201800132.

[20] A. Gouda, J. Manioudakis, R. Naccache, F. Soavi, and C. Santato, Adv. Sustain. Syst. **2021**, 5, 10.1002/adsu.202100152.

[21] D. Crista, M. Algarra, M.V. Martinez de Yuso, J.C.G. Esteves da Silva, and L. Pinto da Silva, J. Mater. Chem. B. **2023**, 11, 1131-1143, 10.1039/d2tb02318k.

[22] J. Zhou, H. Zhou, J. Tang, S. Deng, F. Yan, W. Li, and M. Qu, Mikrochim. Acta. **2016**, 184, 343-368, 10.1007/s00604-016-2043-9.

[23] Z. Pan, R. Zhang, and S. Zicari, *Integrated Processing Technologies for Food and Agricultural By-Products,* Academic Press, **2019,** 444.

[24] S. Kim and B.E. Dale, Biomass and Bioenergy. **2004**, 26, 361-375, 10.1016/j.biombioe.2003.08.002.

[25] W. Zhao, Y. Cui, X. Sun, H. Wang, and X. Teng, Sci. Total Environ. **2021**, 758, 143883, 10.1016/j.scitotenv.2020.143883.

[26] W. Kasprzyk, T. Swiergosz, S. Bednarz, K. Walas, N.V. Bashmakova, and D. Bogdal, Nanoscale. **2018**, 10, 13889-13894, 10.1039/c8nr03602k.

[27] T. Wang, H. Luo, X. Jing, J. Yang, M. Huo, and Y. Wang, Molecules. **2021**, 26, 10.3390/molecules26051246.

[28] M. Zhang, X. Long, Y. Ma, and S. Wu, Opt. Mater. **2023**, 135, 10.1016/j.optmat.2022.113311.

[29] N.K.R. Bogireddy, J. Lara, L.R. Fragoso, and V. Agarwal, Chem. Eng. J. **2020**, 401, 10.1016/j.cej.2020.126097.

[30] B. Vercelli, R. Donnini, F. Ghezzi, A. Sansonetti, U. Giovanella, and B. La Ferla, Electrochim. Acta. **2021**, 387, 10.1016/j.electacta.2021.138557.

[31] C. Olla, A. Cappai, S. Porcu, L. Stagi, M. Fantauzzi, M.F. Casula, F. Mocci, R. Corpino, D. Chiriu, P.C. Ricci, and C.M. Carbonaro, Nanomaterials (Basel). **2023**, 13, 10.3390/nano13081344.

3.1.3. Conclusion

This study demonstrates that brightly fluorescent CDs can be successfully synthesized through a simple, scalable, and environmentally benign hydrothermal route using a variety of organic waste materials as carbon precursors. The combined use of citric acid and ethylenediamine enabled consistent nitrogen incorporation and effective surface passivation, leading to enhanced photoluminescence despite the intrinsic compositional variability of waste-derived feedstocks.

The results confirm that waste valorization can be effectively integrated into CDs synthesis without compromising optical performance, supporting the feasibility of transforming low-value residues into functional luminescent nanomaterials. This outcome highlights the potential of waste-derived precursors as viable alternatives to conventional molecular sources, in alignment with green chemistry principles and circular economy strategies.

Within the context of this thesis, this work provides an experimental complement to the life cycle-oriented analysis presented in Article I. While LCA emphasizes the role of energy demand and process complexity in determining environmental impacts, the findings reported here demonstrate that precursor sustainability and feedstock selection are equally critical factors in shaping the overall sustainability profile of CDs production.

Comprehensive structural, chemical, and optical characterization confirmed that high photoluminescence efficiency can be achieved under mild reaction conditions, without reliance on energy-intensive or chemically aggressive synthesis routes. Moreover, the systematic evaluation of different waste precursors provided insight into the relationship between precursor chemistry, synthesis conditions, and photophysical behavior, contributing to a deeper understanding of structure-property relationships in CDs.

Beyond lighting-oriented applications, related work (Appendix 2) has demonstrated the potential of waste-derived CDs for advanced biomedical applications, highlighting the versatility and functional relevance of sustainably synthesized CDs.

Overall, this work shows that simple and green synthetic strategies can deliver CDs with competitive fluorescence performance, while maintaining environmental responsibility. These findings support the development of scalable and sustainable production routes for functional carbon-based nanomaterials and provide a solid foundation for the rational design of environmentally conscious CDs synthesis strategies.

3.2. Exploratory studies on emission modulation of waste-derived Carbon Dots

Beyond the synthesis strategy presented in Article II (Section 3.1), several exploratory studies were conducted to assess the feasibility of tuning the photoluminescence of waste-derived CDs toward longer wavelengths. These investigations were motivated by the limited emission tunability observed for CDs synthesized from biomass precursors under mild and environmentally benign conditions.

Initial tests indicated that partial red-shifting of the emission toward the green region could be achieved when hydrochloric acid was employed during synthesis, leading to emission maxima close to 500 nm for corn stover-derived CDs (Figure 13). However, these procedures suffered from practical limitations, including reproducibility issues and material loss during reactor cooling, and relied on acidic conditions that are not aligned with green chemistry principles. For these reasons, this approach was not pursued further.

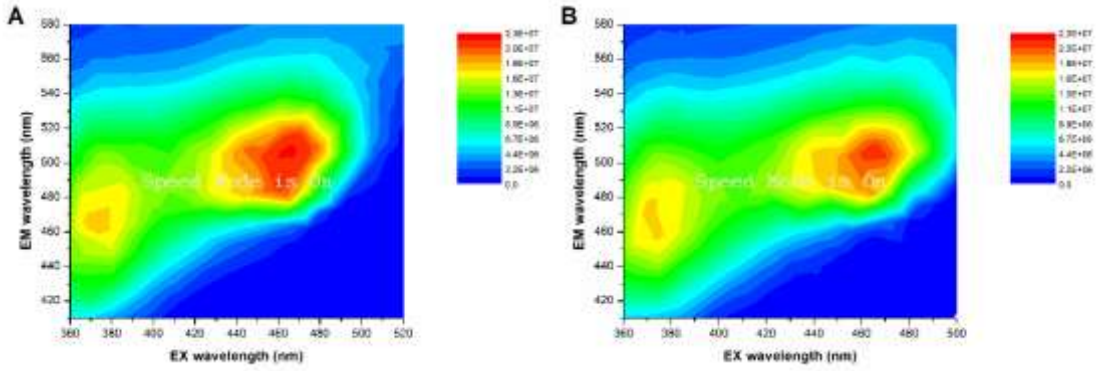

Figure 13. 2D excitation-emission contour plots (EECP) of CDs with corn stover (CS), citric acid (CA), ethylenediamine (EDA) and HCl solution. (A) 0.35M HCl and (B) 0.40M HCl.

Subsequently, alternative strategies were explored, focusing on parameters more compatible with sustainable synthesis. These investigations focused on strategies commonly reported in the literature included variations in solvent environment, reaction time, and precursor composition, as well as the use of different lignocellulosic residues and biomass pre-treatments. Despite these efforts, the resulting CDs consistently exhibited blue photoluminescence, indicating a strong tendency for waste-derived CDs to favor blue-emissive surface states.

Notably, green emission was only observed when replicating a literature-reported synthesis that employed molecular precursors rather than biomass-derived feedstocks [131]. Although the emission maximum differed from the reported values, this result

further highlighted the contrast between conventional precursors and complex waste materials in controlling emission wavelength.

Collectively, these exploratory studies demonstrate that achieving long-wavelength emission from waste-derived CDs under sustainable synthesis conditions remains challenging. Importantly, these findings directly motivated the focused investigation of heteroatom chemistry, particularly the role of sulfur-containing precursors, which is addressed in Chapter 4 to elucidate the mechanisms governing photoluminescence modulation.

4. Heteroatom doping, influence of Sulfur in doped CDs

4.1. **Article III**: Insights into the role of common sulfur precursors in hydrothermally synthesized N,S-doped Carbon Dots: Fluorescence modulation *via* surface oxidation rather than sulfur doping

Sónia Fernandes, Manuel Algarra, Ana T.S.C. Brandão, Antonio Gil, Carlos M. Pereira, Joaquim C.G. Esteves da Silva and Luís Pinto da Silva

4.1.1. Contextualization and author contributions

Heteroatom doping is widely employed to tailor the photoluminescent properties of CDs, with nitrogen and sulfur among the most frequently explored elements due to their ability to modify the electronic structure, surface chemistry, and radiative recombination pathways of carbon-based nanomaterials [182, 184, 208, 266]. Although numerous studies report enhanced QY_{FL} upon heteroatom incorporation, the mechanistic origin of these improvements remains under debate, particularly regarding the distinction between effective lattice doping and surface-related or precursor-induced chemical modifications [182, 184].

The investigation of sulfur-containing precursors emerged from earlier observations in this thesis, where attempts to modulate emission color through waste-derived carbon sources consistently resulted in blue-emissive CDs, in contrast with several reports in literature. These observations highlighted the limitations of precursor-based emission tuning and motivated a focused mechanistic study on the role of heteroatom chemistry in fluorescence modulation.

Sulfur-containing precursors are commonly employed in combination with nitrogen sources to produce N,S-modified CDs, often under the assumption that sulfur atoms are incorporated into the carbon framework and directly contribute to photoluminescence enhancement [176, 247, 267]. However, increasing evidence suggests that certain sulfur precursors may primarily act as oxidizing or surface-modifying agents rather than as true dopants, influencing surface states and non-radiative recombination pathways without significant sulfur incorporation into the carbon core [244, 268].

Within this context, the present work systematically investigates the influence of sulfur-containing precursors on the structural and photophysical properties of nitrogen-

modified CDs. By comparing N-CDs and N,S-CDs synthesized under identical hydrothermal conditions, this study aims to clarify whether the observed changes in photoluminescence originate from genuine sulfur doping or from indirect effects associated with surface oxidation and defect formation. A comprehensive set of optical, structural, and surface-sensitive characterization techniques is employed to establish robust structure-property relationships and to provide a critical assessment of sulfur-based heteroatom modification strategies in CDs synthesis.

I conducted all CDs syntheses and was responsible for the optical characterization, including fluorescence quenching, photostability, and solvent-dependent emission studies, as well as data analysis and interpretation, under the supervision of Professor Dr. Luís Pinto da Silva. XPS and XRD analyses were performed by the research group of Dr. Manuel Algarra. AFM measurements were carried out by the research team of Professor Dr. Carlos Pereira, namely Dr. Ana Brandão. FT-IR, dynamic light scattering (DLS), and zeta potential measurements were conducted in collaboration with the Lab&Services team, while electron paramagnetic resonance (EPR) measurements were performed at CEMUP.

The interpretation and discussion of the structural, chemical, and optical results were carried out by me under the supervision of Professor Dr. Luís Pinto da Silva. I prepared the initial manuscript draft in collaboration with Dr. Manuel Algarra, which was subsequently reviewed and revised by all co-authors.

Nanoscale

ROYAL SOCIETY OF CHEMISTRY

PAPER

View Article Online
View Journal | View Issue

Cite this: Nanoscale, 2026, 18, 9894

Insights into the role of common sulfur precursors in hydrothermally synthesized N,S-doped carbon dots: fluorescence modulation *via* surface oxidation rather than sulfur doping

Sónia Fernandes, [a] Manuel Algarra, *[b] Ana T. S. C. Brandão, [c] Antonio Gil, [b] Carlos M. Pereira, [c] Joaquim C. G. Esteves da Silva [a] and Luís Pinto da Silva *[a]

Received 2nd December 2025,
Accepted 20th March 2026

DOI: 10.1039/d5nr05082k

rsc.li/nanoscale

While heteroatom doping is widely used to enhance the fluorescence of carbon dots, the actual mechanism underlying this claimed enhancement remains unclear. Herein, we report a systematic comparison between nitrogen-doped carbon dots (N-CDs) and nitrogen/sulfur co-doped carbon dots (N,S-CDs) synthesized hydrothermally, with ethylenediamine and sodium thiosulfate as the N- and S-dopants, respectively. Contrary to expectations, the inclusion of the S-precursor significantly reduced the quantum yield by 63%, from 35.9% to 13.2%, while leaving the emission profile and response largely unchanged. Characterization assays revealed that S-doping in N,S-CDs was residual, whereas the surface oxygen content increased markedly, indicating surface oxidation. The data suggest that sodium thiosulfate acted not as a dopant but overall as an oxidant, generating oxygen-based surface defects that introduced nonradiative recombination pathways. Thus, our findings show that co-doping with this S-precursor can decrease the quantum yield by promoting surface oxidation and the effective formation of more oxidized N-CDs, rather than heteroatom incorporation and production of co-doped CDs. This decreasing effect on the quantum yield was also observed when using thiourea as the S-precursor. Future work should include the study of other common S-precursors. In conclusion, our research shows that specific heteroatom-based precursors can alter the optical characteristics of CDs through redox/surface-modification effects instead of actual compositional doping, and thus, claims based on heteroatom doping may need closer examination.

Introduction

Carbon dots (CDs) are a type of carbon-based nanomaterial, with sizes typically lower than 10 nm, and known for their fluorescence, biocompatibility, (photo)chemical stability, water solubility, and tunability.[1–3] These characteristics make CDs highly attractive for a range of applications, including in light-emitting devices, bioimaging, photocatalysis, and sensing.[4–6]

Another attractive feature of CDs is that they can potentially be generated from a variety of renewable carbon sources using environmentally friendly and non-toxic bottom-up routes.[7] This is particularly relevant when considering the development of engineered nanomaterials with a "sustainable-by-design" approach, given that the fabrication stage of nanomaterials has been identified as a potential environmental concern.[8–11] More specifically, CDs can be obtained from a wide variety of organic waste, such as agricultural (*e.g.*, corn stover and rice husks), food (*e.g.*, fruit peels and nut shells), urban waste (*e.g.*, spent coffee grounds), forestry residues (*e.g.*, eucalyptus leaves), and industrial byproducts (*e.g.*, sugarcane bagasse, olive pit liquor, and seafood shells).[5,12–15]

While CDs are known for their fluorescence and are used in fluorescence-based applications, their intrinsic quantum yield can be low (for both waste- and non-waste-based CDs).[16–20] Thus, CD synthesis processes typically involve heteroatom-doping strategies, in which compounds containing desired heteroatoms (such as N, S, P, and B) are added as dopants, resulting in the incorporation of these elements into the resulting nanoparticles.[21,22] The rationale behind this type of strategy is that heteroatom doping generates additional electron lone pairs, defect sites, and active centers, which facilitate radiative recombination and markedly enhance the fluorescence efficiency of CDs.[23–25]

[a]Chemistry Research Unit (CIQUP), Institute of Molecular Sciences (IMS), Department of Geosciences, Environment and Spatial Plannings, Faculty of Sciences, University of Porto, R. Campo Alegre s/n, 4169-007 Porto, Portugal. E-mail: luis.silva@fc.up.pt
[b]INAMAT²-Institute for Advanced Materials and Mathematics, Department of Science, Public University of Navarra, Campus of Arrosadía, 31006 Pamplona, Spain
[c]Chemistry Research Unit (CIQUP), Institute of Molecular Sciences (IMS), Department of Chemistry and Biochemistry, Faculty of Sciences, University of Porto, R. Campo Alegre s/n, 4169-007 Porto, Portugal

Among the various possible options, the most common doping strategies are arguably N-doping and N,S-doping, with S-doping being less employed.[21–24,26] Commonly used N-dopants are urea, ethylenediamine (EDA), and phenylenediamine, among others.[19,27–29] Regarding S-dopants, typical ones are $Na_2S_2O_3$, H_2SO_4, and Na_2S, among others.[21,22,30] Besides binary dopant systems (such as phenylenediamine/$Na_2S_2O_3$, urea/H_2SO_4, and EDA/H_2SO_4), single-source N,S-dopants (*e.g.*, cysteine and thiourea) can also be used.[31–34] Relevantly, both N- and N,S-doping strategies have been associated with high fluorescence quantum yields (QY_{FL}) and even red-shifted emission.[24,26,35–38]

However, despite these apparently promising reports of the potential of heteroatom-doping strategies for QY_{FL} enhancement, there are still unclarified issues that prevent their rational use in the fabrication of suitable and sustainable CDs for commercial/industrial applications.

For one, while different authors claim that N-doping is a suitable strategy for enhancing the QY_{FL} of CDs, there are different studies that either did not find any clear relationship between N-doping and the resulting QY_{FL} or concluded that N-doping alone is not enough for QY_{FL} enhancement.[4,39–41] Furthermore, studies that associate higher QY_{FL} with N-doping tend not to synthesize and study the corresponding non-N-doped CDs.[42,43] Without this comparison, it is ambiguous whether the observed high QY_{FL} values are related to the inclusion of nitrogen heteroatoms in the structure of CDs. Finally, it is known that bottom-up synthesis routes used to produce CDs can also generate highly fluorescent molecular by-products,[44–46] which can mask the luminescence of CDs. Furthermore, dialysis is considered an essential step to separate these by-products from CDs.[45,47,48] Despite this, several studies reporting N-CDs with elevated QY_{FL} did not incorporate adequate purification methods, and so, it is possible that the observed yields are not from CDs but from molecular fluorophores present in solution.[37,49,50]

Thus, the literature indicates that despite the widespread use of N-doping as a strategy for enhancing QY_{FL}, there are significant doubts about its overall success and potential, as well as its actual mechanism of action. Relevantly, while the N,S-doping strategy is relatively less used and studied than N-doping, there are some indications that the efficiency of the former as a general strategy should be equally questioned.

For one, there are also reports of highly emissive N,S-CDs (over 50%), but they did not include proper purification (as by dialysis).[51–54] This means that there is a question of whether the high QY_{FL} results from the N,S-CDs or from fluorescent molecular by-products. Some studies that also report highly emissive N,S-CDs did not include comparison with mono-doped and/or undoped CDs. Thus, it is also unclear whether the observed values result from synergistic effects of combining S- with N-doping.[52,55,56] Finally, there are also a number of synthesized N,S-CDs whose QY_{FL} values are still low ($\lesssim$~10%).[57–60] Therefore, there are discrepancies between the expected benefits of N,S-doping and the observed results.

Herein, we report the systematic characterization and comparison of N,S-CDs and N-CDs obtained from the hydrothermal treatment of sawdust and citric acid (as co-carbon precursors), EDA (as the N-dopant), and $Na_2S_2O_3$ (as the S-dopant). Our main goal is to gain insight into the role of combined N,S-doping regarding the optical properties and composition of CDs. The resulting data are essential to understand the true impact of N,S-doping as a QY_{FL}-enhancement strategy, with the systematic comparison with N-CDs allowing for the evaluation of whether combined doping results in any synergistic or additive effects. To this end, we performed comprehensive optical, microscopic, and structural characterization of both CDs, by using atomic force microscopy (AFM), X-ray photoelectron (XPS), Fourier-transform infrared (FTIR), X-ray diffraction (XRD), electron paramagnetic resonance (EPR), UV-Vis spectroscopy, steady-state fluorescence spectroscopy, and dynamic light scattering (DLS).

Notably, our results indicate that, contrary to potential expectations, combined N,S-doping reduces the QY_{FL} from 35.9% to 13.2% (a ~63% reduction) when compared with N-CDs. Despite these large alterations in QY_{FL}, the optical properties of both CDs (studied in different media and in the presence of different quenchers) were rather similar, which indicates that including $Na_2S_2O_3$ as a co-dopant had a limited effect. Finally, it was observed that the incorporation of S into the CDs was not effective and that $Na_2S_2O_3$ did not act as a true S-dopant (contrary to expectations). However, its use had an oxidative effect, resulting in surface oxidation of the CDs and a lower QY_{FL}. Thus, this study provided new insight into the efficiency of N,S-doping strategies for QY_{FL} enhancement, as well as some mechanistic insight into the role of dopant precursors in the synthesis of CDs and how they can modulate the nanomaterials' properties in unexpected ways.

Results and discussion

In this study, CDs were obtained through the hydrothermal treatment of the precursor mixture, which requires mild experimental conditions, is easy to operate, and is safe and low-cost.[12,61] It can be regarded as a representative method for creating these nanomaterials since it is also a common synthesis pathway for the creation of CDs.[13,15,20,23,57]

Citric acid was chosen as a co-carbon precursor, as it is arguably one of the most widely used traditional carbon sources for CD production.[25,27,37,41,62] Sawdust, a residue of the wood industry, was included as a co-carbon precursor, in a 50 : 50 mass ratio with citric acid. Its inclusion allowed for replacing half of the commercial carbon source with organic waste, which has already been shown to be an effective method for mitigating the environmental effects of CD manufacturing.[12,13] Both EDA and $Na_2S_2O_3$ are common N- and S-dopants,[26,34,40,63] respectively, and they were used as a binary doping system to generate N,S-CDs. For N-CDs, only EDA was used.

It is worth highlighting that we have selected widely used synthesis routes and common precursors to ensure that the conclusions obtained here are not limited to highly specific

conditions but instead provide insights that are broadly relevant to this field of research. The synthesis procedures here used are also based on a synthesis strategy developed previously by us for the generation of brightly fluorescent waste-based CDs.[12] The details of the synthesis procedures are provided in the Experimental section.

Optical characterization of CDs

The study began with a comparative characterization of the optical properties of N,S-CDs and N-CDs, toward understanding the resulting effect of S-inclusion on bi-doped CDs.

The fluorescence of both CDs was initially analyzed by measuring their 2D excitation–emission contour plots (EECPs), which are shown in Fig. 1. Interestingly, the two CDs exhibit a similar fluorescence profile, with the EECPs exhibiting a well-defined and single luminescent center, characterized by an emission maximum at ~440 nm and an excitation maximum at ~350 nm. This indicates that going from mono- to bi-doped CDs, with inclusion of S, had a limited effect on the properties of CDs. Moreover, and contrary to potential expectations, the inclusion of an S-dopant did not lead to a red-shifted emission.[24,26]

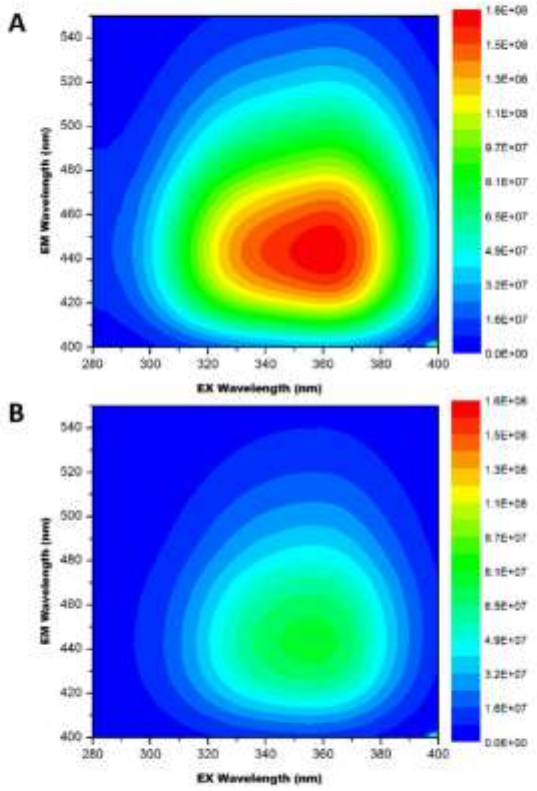

Fig. 1 EECPs of N-CDs (A) and N,S-CDs (B) in water.

The emission spectrum of each CD, measured at an excitation wavelength of 350 nm, is also presented (Fig. 2). The spectral shapes (Fig. 2A) are similar between CDs and are consistent with published spectra for this type of nanomaterial.[12] The emission spectrum of N-CDs is slightly broader than that of N,S-CDs (Fig. 2B), as can be seen from their full width at half maximum (FWHM) values of 79.4 and 73.5 nm, respectively. Nevertheless, this difference is rather modest. Interestingly, we can still see that the fluorescence intensity of N,S-CDs is lower than that of N-CDs, at the same concentration (Fig. 2A).

The UV-Vis spectra of the CDs were also recorded (Fig. 2C). The spectrum of N-CDs exhibited an absorption band with a maximum at 350 nm (attributed to $n \rightarrow \pi^*$ transitions) and two small shoulders at ~240 nm and ~280 nm that were associated with $\pi \rightarrow \pi^*$ transitions. Interestingly, the spectrum of N,S-CDs did show some relevant differences. Namely, while still present, the relative intensity of the 350 nm band is greatly reduced, and the shoulder at 240 nm is now not clearly visible. The shoulder at ~280 nm is still seen, nevertheless. Thus, the data indicate that the addition of an S-dopant affects the surface or structural features of these CDs.

The QY_{FL} values of the CDs were also determined by a relative method using quinine sulfate as a reference and were found to be 35.9% and 13.2% for N-CDs and N,S-CDs, respectively. It should be noted that the QY_{FL} obtained for N-CDs is relatively high, given that waste-based CDs tend to have a relatively low QY_{FL} (below 20%).[17–20] Thus, the followed synthesis strategy was useful for obtaining brightly emissive waste-based CDs.[12] Nevertheless, the co-addition of an S-dopant did not result in the predicted effect.[21,30–34,52,53,57,58] That is, in a QY_{FL} enhancement. In contrast, the use of an S-dopant decreased the QY_{FL} by 63%. Furthermore, even when considering just the QY_{FL} of N,S-CDs, a value of 13.2% is rather modest. Thus, for this system, adding an S-dopant in a binary system with an N-dopant not only does not produce brightly emissive CDs but also impairs fluorescence efficiency. This adds more doubts about the true benefits of heteroatom-doping strategies as a general solution for enhancing the QY_{FL} of CDs.

We also examined the relationship between the absorbance at 350 nm and the mass concentration of each CD (Fig. 2D). The variation was more significant for N-CDs than for N,S-CDs, which indicates that the former are stronger absorbers on a mass basis. Thus, not only does co-S-doping reduce the QY_{FL}, but it may also impair fluorescence intensity by reducing the light-absorption potential of the CDs.

In summary, so far, while co-S-doping has had little effect on the emission band position and shape, it has impaired the fluorescence efficiency of the CDs, while also affecting their surface/structural features. To gain further insight into the effects of this co-doping strategy on the optical properties of CDs, we performed additional fluorescence assays under various conditions.

In the initial assays, we aimed to investigate the fluorescence behavior of the CDs by measuring their emission intensity in water/methanol and water/glycerol mixtures with

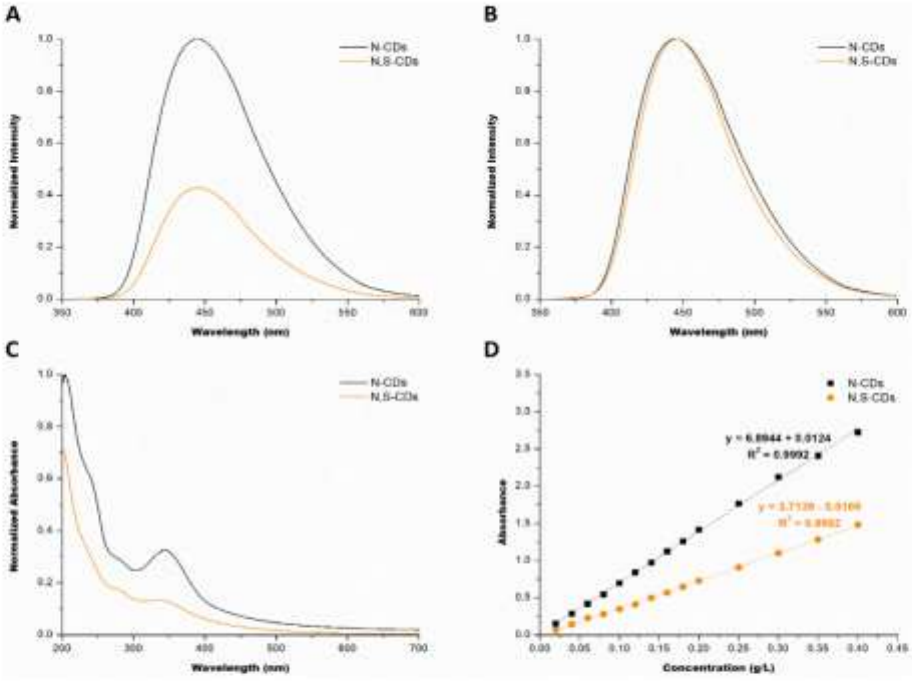

Fig. 2 Emission (A) and normalized emission (B) spectra of N-CDs and N,S-CDs; UV-Vis spectra of N-CDs and N,S-CDs (C); and absorbance as a function of concentration for both CDs (D).

increasing water content (Fig. 3). With these mixtures, we tried to probe the effect exerted by solvent polarity and viscosity (respectively). Interestingly, both CDs had the same behavior in these scenarios. That is, increasing the water percentage in both mixtures did not have a significant alteration in the fluorescence intensities of the nanoparticles, except just in both pure methanol and glycerol, but even then, the difference compared to pure water is somewhat modest. Therefore, these data indicate that the excited states of N-CDs are not strongly affected by solvent polarity and that nonradiative decay due to intramolecular motion does not appear to be relevant.[64–66] Additionally, co-S-doping did not alter these outcomes.

We subsequently evaluated the effects exerted by KI and KNO_3 on the fluorescence of N-CDs and N,S-CDs (Fig. 4). KI is a well-known heavy-atom quencher, given that its addition can result in fluorescence quenching by enhancing intersystem crossing in organic fluorophores.[62,67,68] KNO_3 was selected to evaluate the potential effect of another small ionic compound that shares the same counter-cation as KI but has different characteristics. Specifically, while KI can act as a hole scavenger, KNO_3 is known to function as an electron scavenger.[69,70]

Both ionic compounds induced quenching in the two CDs, and the resulting Stern–Volmer plots (Fig. 4) showed a linear relationship, which is usually associated with dynamic quenching. However, the quenching was rather limited in both cases, given that the obtained Stern–Volmer constants (K_{SV}) were only 5.1–6.7 × 10^{-3} and 3–5 × 10^{-4} mM^{-1}, in the presence of KI and KNO_3, respectively. Nevertheless, these assays did allow us to make two conclusions: (1) the CDs are more sensitive to KI than to KNO_3, probably due to the heavy-atom quenching effect of the former;[62,71] and (2) the fluorescence of N,S-CDs appears to be more sensitive to both quenchers than that of N-CDs (Fig. 4), which indicates some effect exerted by the co-S-doping.

In Fig. S1A, the relationship between fluorescence intensity and absorbance for N-CDs and N,S-CDs is presented. Both CDs showed the trend of a general increase in fluorescence intensity with increasing absorbance, which is not an unexpected behavior. Nevertheless, some studies have shown a decrease in fluorescence intensity with increasing concentration of CDs, which is attributed to aggregation-caused quenching (ACQ) and self-absorption quenching.[72,73] Thus, these results indicate that neither ACQ nor self-absorption quenching plays a relevant role within this absorbance range.

The photostability of the CDs was also tested by continuous irradiation at 365 nm for 30 minutes (Fig. S1B). Interestingly, both CDs were found to be photostable, with F/F_0 remaining constant throughout the assays. This stability suggests their suitability for optical applications, where sustained fluorescence is required under prolonged exposure to light.

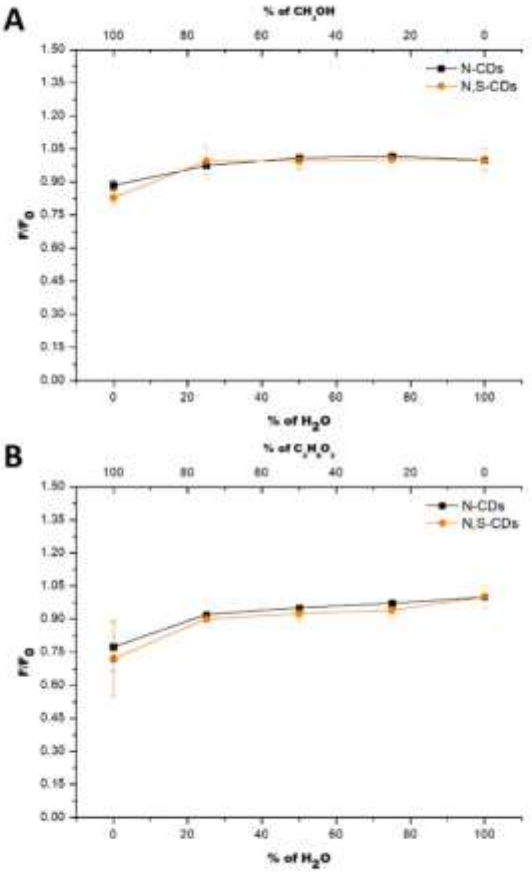

Fig. 3 Variation in fluorescence emission intensity in water/methanol (A) and water/glycerol (B) mixtures for N-CDs and N,S-CDs. Excitation at 350 nm.

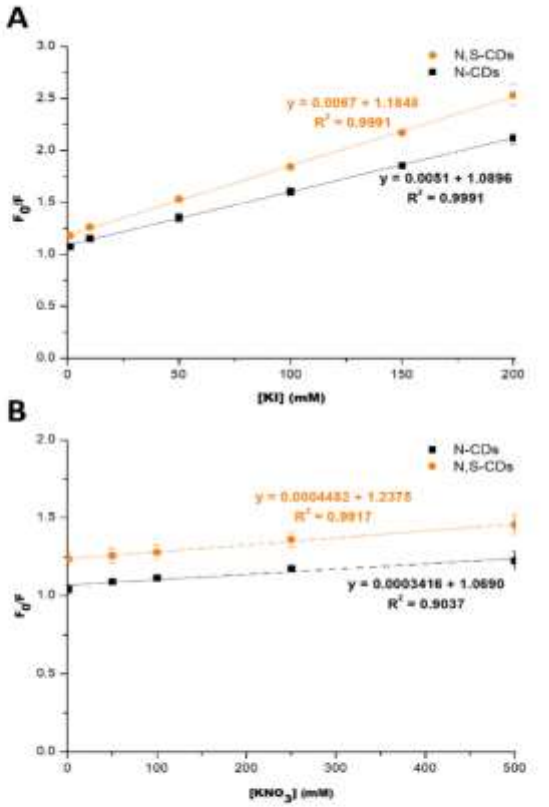

Fig. 4 Stern–Volmer plots for different quenchers: KI (A) and KNO_3 (B), for both CDs.

Furthermore, the behavior of both CDs was identical, meaning that co-S-doping had no effect on this characteristic.

The influence of the solvent on the fluorescence of the CDs was further probed through assays in water, methanol, ethanol, acetonitrile, and dimethylformamide (DMF), as presented in Fig. 5. Fig. 5A and C enable the measurement of the shift in the emission wavelength maximum caused by the solvent for N-CDs and N,S-CDs, respectively. Specifically, there is a little blue shift of about 10 nm from water to acetonitrile/DMF in both CDs. The variations in fluorescence intensity with solvent can be better observed in Fig. 5B (N-CDs) and Fig. 5D (N,S-CDs). Once again, the CDs behave similarly, with an ~20% (slightly higher for N,S-CDs) decrease in intensity from water to acetonitrile/DMF. These changes can be attributed to the different hydrogen-bonding interactions that the CDs can make with the solvent. That is, we observed variations associated with changing from protic to aprotic solvents, and there are reports in the literature that indicate that the fluorescence of CDs can be more significantly modulated by hydrogen bonding than by solvent polarity.[74]

Furthermore, the fluorescence emission behavior of both CDs was also analyzed in the same solvents using the Reichardt solvent polarity scale, ET(30). The results indicate that both N-CD and N,S-CD samples exhibit similar emission maxima (Fig. S2A) across different solvents, suggesting a limited solvatochromic effect. Fig. S2B shows comparable trends in fluorescence intensity ratios (F/F_{H_2O}). Additionally, the regression slopes observed in Fig. S2B indicate that both samples respond similarly to changes in solvent polarity, with only minor variations in fluorescence intensity.

One matter of debate regarding CDs is the origin of their fluorescence, and the relative relevance between core and surface states in their emission.[75–77] Here, we performed a comprehensive analysis of the fluorescence of the two CDs studied, specifically, by assessing their responses to external stimuli (ionic quenchers) and modifications in the external media (solvent polarity, hydrogen bonding, and viscosity). It is interesting to note that we have discovered that both CDs are virtually unaffected by these variations, exhibiting only slight

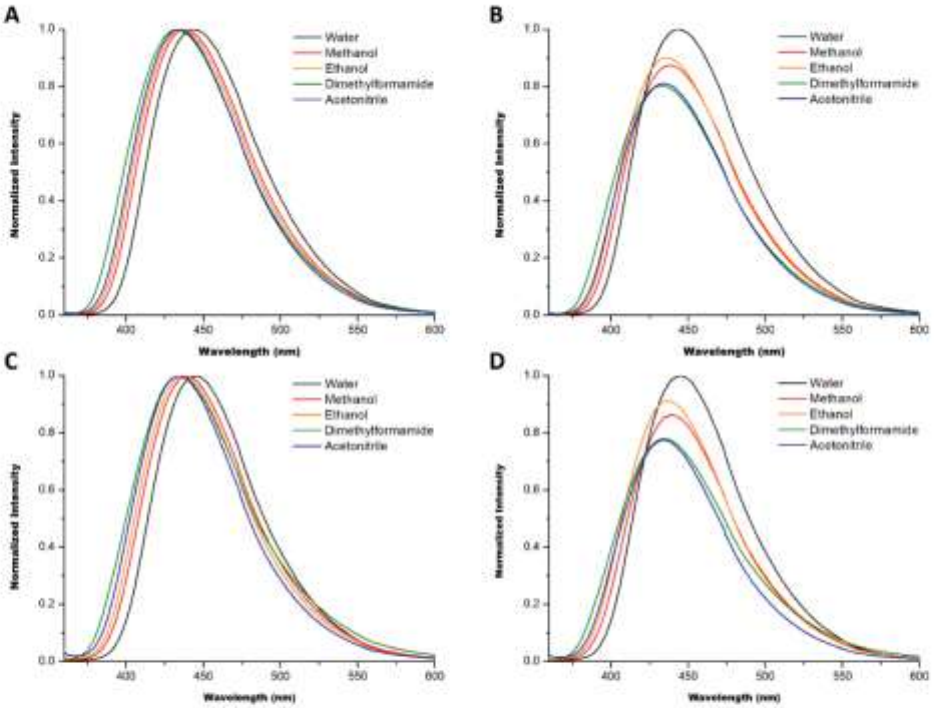

Fig. 5 Normalized emission spectra for evaluation of maximum emission wavelength and emission intensity of N-CDs (A and B, respectively) and N,S-CDs (C and D, respectively) in different solvents.

alterations. This suggests that their fluorescent moieties are partially protected from outside stimuli and media. This implies that their predominant emissive states are probably connected to core or protected states rather than less accessible surface-related ones.[4]

It should be noted that while N,S-CDs are, to a great extent, almost as unresponsive as N-CDs to these stimuli/changes, the resulting variations are slightly more relevant. Thus, it appears that the fluorescent moieties of N,S-CDs are somewhat less protected from the external environment, but co-S-doping does not change the overall situation.

Therefore, the emission of N,S-CDs appears to have a greater contribution from more surface-accessible states, indicating some changes in the surface/structure of these CDs with the addition of the S-dopant. This is consistent with their light absorption data (Fig. 2C).

Microscopy, structural and surface characterization of CDs

After analyzing the optical properties of both CDs, it is important to perform their microscopy, structural and surface characterization. More specifically, the focus is on performing a comparative analysis to gain insight into the changes induced by co-S-doping and how they can account for the reduction in QY_{FL}.

AFM height analysis of the topography of both samples showed distinct and separated objects with sub-10 nm particle height (Fig. 6). This indicates that N-CDs and N,S-CDs possess a nanosize nature, consistent with the literature reports for CDs.[78–80]

The CDs were also studied by DLS at two different mass concentrations (0.06 and 0.14 g L^{-1}) (Fig. S3 and S4). Their hydrodynamic diameters and mean ζ potentials are presented in Table 1. Regarding the latter, we can see that N,S-CDs have higher ζ potentials at both concentrations and, therefore, should be more stable in solution (Fig. S3B).

DLS analysis of N-CDs and N,S-CDs at concentrations of 0.06 g L^{-1} and 0.14 g L^{-1} reveals significant differences in size distribution and aggregation behavior (Table 1 and Fig. S4).

The intensity-weighted data (Fig. S4A) indicate that at 0.06 g L^{-1}, N-CDs exhibit a bimodal distribution with peaks at approximately 0.3 μm and 14 μm. However, at 0.14 g L^{-1} (Fig. S4B), the bimodal distribution transitions to a single peak around 0.5 μm, accompanied by an increase in hydrodynamic diameter from 0.3949 μm at 0.06 g L^{-1} to 0.7199 μm at 0.14 g L^{-1}, suggesting increased aggregation at higher concentrations. In contrast, N,S-CDs exhibit a bimodal distribution at both concentrations, with peaks at approximately 0.2 μm and 5 μm at 0.06 g L^{-1}, and at approximately 0.2 μm and 14 μm at 0.14 g L^{-1}. The hydrodynamic diameter of N,S-CDs decreases from 0.3652 μm at 0.06 g L^{-1} to 0.2826 μm at 0.14 g L^{-1}, suggesting improved colloidal stability with increasing concen-

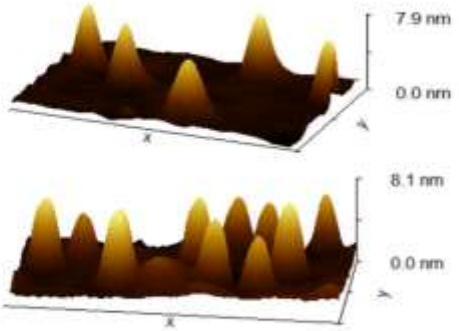

Fig. 6 AFM analysis of N-CDs (top) and N,S-CDs (bottom), showing representative 3D height images selected from full 10 × 10 μm (N-CDs) and 5 × 5 μm (N,S-CDs) scans. Z-Scale: 7.9 nm (N-CDs, top) and 8.1 nm (N,S-CDs, bottom).

Table 1 Results of DLS and ζ potential of N-CDs and N,S-CDs at different concentrations

CDs	Hydrodynamic diameter (μm)	Mean ζ potential (mV)
N-CDs 0.06 g L^{-1}	0.3949	−11.9
N-CDs 0.14 g L^{-1}	0.7199	−12.4
N,S-CDs 0.06 g L^{-1}	0.3652	−16.6
N,S-CDs 0.14 g L^{-1}	0.2826	−18.1

tration. The number-weighted distribution (Fig. S3A) further highlights key differences in particle size. At 0.06 g L^{-1}, N-CDs predominantly exhibit particle sizes with a peak at ≈0.07 μm, whereas at 0.14 g L^{-1}, the peak shifts to ≈0.03 μm, confirming a reduction in primary particle size with increasing concentration. In contrast, N,S-CDs maintain a relatively stable size distribution across both concentrations, with a consistent peak at 0.11 μm. These findings suggest that the tendency for aggregation is strongly dependent on particle composition, as N-CDs show a reduction in primary particle size with increasing concentration, whereas N,S-CDs maintain a stable size distribution, indicating higher colloidal stability. These differences in aggregation behavior for the CDs are in line with their respective mean ζ potentials.

Two additional topics should be addressed when discussing DLS data. One is that while the hydrodynamic diameters of the CDs (a few hundred nanometers) are significantly higher than the particle height estimated by AFM (sub-10 nm), this difference is actually in line with the literature.[81] That is, due to their functionalized surface, the particles are capable of interacting between themselves *via* hydrogen bonding and electrostatic interactions, leading to their aggregation in solution.[82]

Another noteworthy aspect is that the variation in hydrodynamic diameter with concentration (Table 1) indicates that N-CDs aggregate with increasing concentration, while N,S-CDs become less aggregated. However, despite this different behavior, Fig. S1A shows that the fluorescence of both CDs increases with concentration. Furthermore, the fluorescence increase is more pronounced for N-CDs, whereas their aggregation behavior would suggest the opposite. Given this, N-CDs appear to exhibit aggregation-induced emission behavior.[83,84] Meanwhile, co-S-doping decreased the aggregation potential of the CDs, which could be due to changes in surface functionalization of the nanoparticles. This is in line with the expected incorporation of additional functional groups in heteroatom-doping strategies and aligns with the data presented so far.

The XRD patterns of N-CDs and N,S-CDs are depicted in Fig. 7. In both XRD patterns, characteristic wide peaks near $2\theta \sim 25.0°$ (002 plane) and around 39.1° (100 planes) are observed, which reflect the presence of amorphous carbon.[85,86] The occurrence of oxygen-bearing functional groups that resemble amorphous carbon phases justifies this wide band.[87] The peak below 10.0° is ascribed to the (001) plane, to the presence of N and O groups and to the presence of organic compounds in the structure.[88] CDs having an amorphous nature are consistent with previous studies.[89–91]

EPR analysis of N-CDs and N,S-CDs (Fig. S5) did not reveal distinct peaks within the measured magnetic field range (2500 to 4500 G), indicating the absence of strongly detectable paramagnetic species. The lack of significant EPR signals suggests that unpaired electrons are either absent or present at concentrations too low to be detected under these conditions. This result highlights that the introduction of sulfur into the carbon dot structure does not induce notable paramagnetic behavior.

The CDs were also analyzed by FT-IR (Fig. 8), to gain valuable insights into how co-S-doping affects the functional groups present in the CDs. The obtained spectra are typical of doped CDs, with a broad band in the 2500–3500 cm^{-1} range, which demonstrates overlapping O–H and N–H stretching vibration modes.[12,28,92] Other relevant and common peaks can be found at ~1548/1557 cm^{-1} (N-CDs/N,S-CDs), ~1384 cm^{-1}, and ~1043/1039 cm^{-1} (N-CDs/N,S-CDs). According to previous studies, these peaks can be attributed to C=C/N–H, C–H/O–H, and C–O groups, respectively.[30,57,93–95]

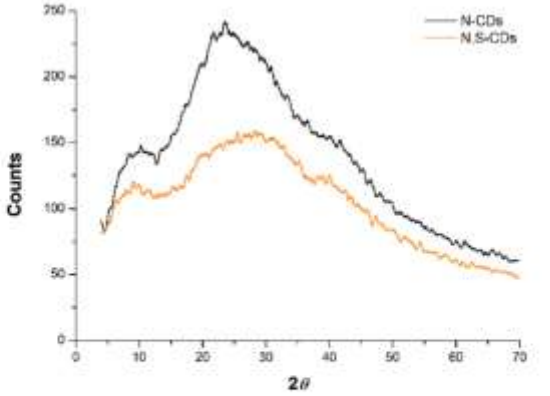

Fig. 7 XRD patterns of both CDs.

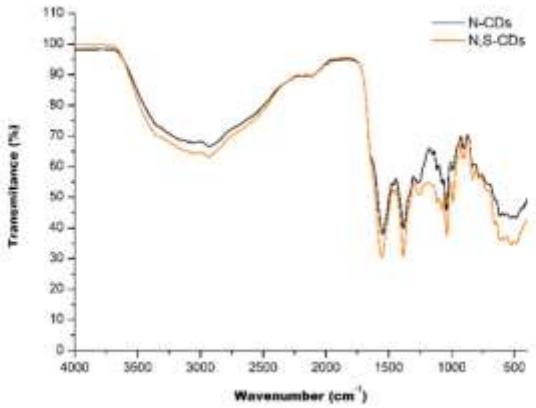

Fig. 8 FT-IR spectra of both CDs.

Given the use of an S-dopant to produce N,S-CDs, we would expect the presence of groups such as C–S, S–H, and O=S=O.[30,57,95–97] Some studies have indicated that C–S groups are associated with peaks at 690,[97] 713,[57] 1198 (ref. 30) and 1317 cm^{-1}.[95] S–H groups have been associated with bands at ~2500 cm^{-1},[97] while O=S=O with peaks between 1000 and 1180 cm^{-1} (1009, 1036, 1126, and 1176 cm^{-1}).[96] Unexpectedly, we did not find any particular peak in the FTIR spectrum of N, S-CDs that could be associated with S-based groups (Fig. 8), or that differed from what was found for N-CDs. In fact, the spectra of both CDs are quite identical in peak position and shape (Fig. 8), which indicates that the identity of the functional groups that they are composed of is very similar. Given this, the FTIR data suggest that despite the relevant effect that S-dopant addition had on the QY_{FL} of N,S-CDs, S-doping might not have been particularly efficient.

The surface composition of both CDs was investigated by XPS. The survey XPS results (Fig. S6) indicate that N-CDs are composed mainly of C (69.45%), O (19.26%), and N (11.30%). High-resolution spectra for the C 1*s*, N 1*s*, and O 1*s* levels were obtained for the N-CDs. To determine the functional groups on the surface of the CDs, the corresponding deconvolution, chemical state, and quantitative analyses were carried out. The C 1*s* spectrum of N-CDs (Fig. 9A) consists of four contributions: 284.5, 286.2, 287.9, and 289.32 eV. The produced graphitic structure carbon is responsible for the main contribution at 284.5 eV. The contributions at 286.2, 287.9, and 289.2 eV are due to the presence of C–O/C–N, C=O, and O–C=O groups, respectively. The N 1*s* spectrum (Fig. 9B) reveals three peaks, with their full width at half maximum (FWHM) values given in parentheses: 398.4 (1.85), 399.4(2), and 401.0 eV (2), which are ascribed to the pyridinic, pyrrolic, and quaternary N atoms, respectively.[98] The O 1*s* spectrum showed two contributions at 531.2 eV (C=O) and 532.8 eV (C–O) (Fig. 9C).

The survey XPS results reveal that N,S-CDs are superficially composed of C (63.70%), O (21.82%), N (10.14%), and S (1.67%), respectively, as shown in the full-scan spectrum (Fig. S6). The deconvoluted C 1*s* spectrum (Fig. 9D) shows three peaks: at 284.8 eV, attributed to C=C/C–C; at 285.9 eV, attributed to C–O/C–N/C–S; at 287.6 eV, attributed to C=O groups. The N 1*s* spectrum (Fig. 9E) showed a complex of 4 different contributions: 398.5 eV (2.7), 399.96 eV (1.97), 401.52 eV (2.03), and 402.5 eV (2.29), corresponding to pyridinic N, pyrrolic N, quaternary N, and oxidized N, respectively. The O 1*s* spectrum showed three contributions at 531, 532.6, and

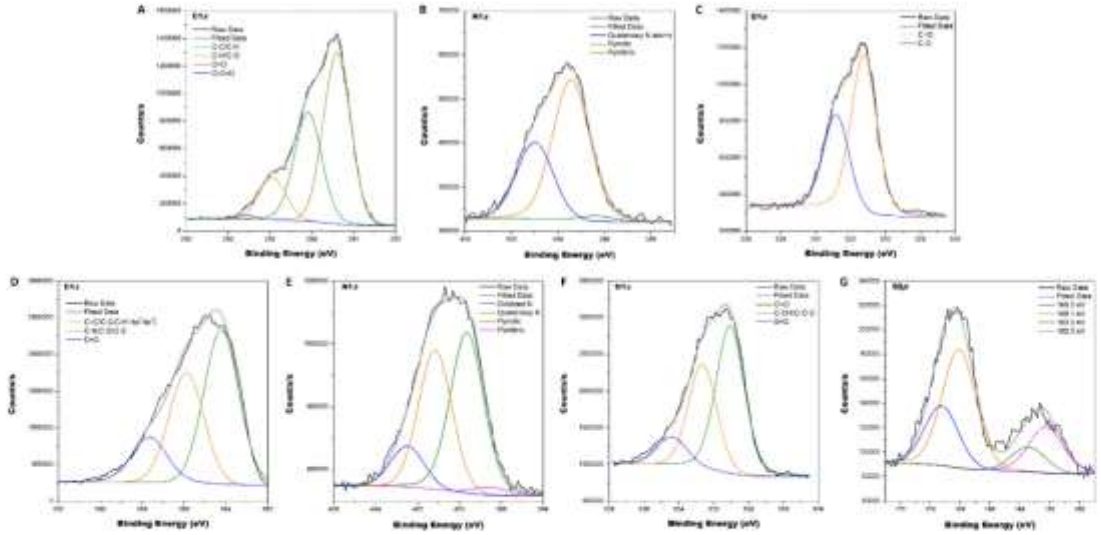

Fig. 9 XPS core-level spectra of N-CDs: C 1*s* (A), N 1*s* (B), and O 1*s* (C); and of N,S-CDs: C 1*s* (D), N 1*s* (E), O 1*s* (F), and S 2*p* (G).

534.4 eV, which are assigned to C=O, C–OH/C–O–C, and O–C/O–S bonds (Fig. 9F).[99] The S 2*p* spectrum is shown in Fig. 9G and consists of two distinct doublets: one at 162.3/163.5 eV and the other at 168.1/169.3 eV. The former is indicative of reduced sulfur species, such as thiophene-like or sulfide groups. The latter is characteristic of oxidized sulfur forms, such as C-SO_X groups. This spectrum is consistent with that observed for S-doped CDs. However, the higher intensity of the 168.1/169.3 eV doublet and the presence of a Na signal in the XPS survey (Fig. S6) could also indicate the presence of residual thiosulfate.

Postulated mechanism for QY_{FL}-reduction

Consistent with FTIR, the XPS results reveal that S surface incorporation is residual and that the main compositional difference between N-CDs and N,S-CDs lies in surface oxidation rather than S content. Specifically, N,S-CDs exhibit a lower C content (~64% *vs.* ~70%) and a higher O content (22% *vs.* ~19%), which corresponds to an ~24% increase in the O : C ratio (from 0.27 to 0.34). Meanwhile, the S content was below 2%, despite the addition of $Na_2S_2O_3$ in a 1 : 1 : 1 mass ratio with the N-dopant and the combined carbon precursors. This indicates that $Na_2S_2O_3$ did not act as an effective dopant under the employed conditions.

This last finding is surprising given the marked decrease of QY_{FL} observed for N,S-CDs (by 63%), which appears to be too large a variation to be caused by such residual co-S-doping. Nevertheless, the low S ratio in N,S-CDs helps explain why their optical properties (besides QY_{FL}) are quite similar to those of N-CDs.

As stated in the Introduction section, while different researchers have claimed that heteroatom doping has some QY_{FL}-changing properties,[24,26,35–38] it is still not proven that the measured effects are truly due to the inclusion of those heteroatoms.[4,39–41] Given this, it is possible that the QY_{FL} decrease is not due to the (residual) S-doping here achieved.

Nevertheless, any difference between N-CDs and N,S-CDs results, in a way or another, from the inclusion of $Na_2S_2O_3$ in the synthesis mixture of the latter.

Repeated syntheses of N,S-CDs consistently produced a "rotten-egg" odor upon opening the hydrothermal reactor, suggesting the release of reduced sulfur species.[100] This observation, together with previous reports of $Na_2S_2O_3$ decomposition and disproportionation in aqueous solutions under heating,[101–104] indicates that this compound was not inert but chemically transformed during the reaction. Thus, the measured compositional changes between N-CDs and N,S-CDs are most likely due to (secondary) redox effects arising from thiosulfate decomposition, rather than surface S-doping.

In fact, the observed increase in the O : C ratio in XPS demonstrates that $Na_2S_2O_3$ addition promoted surface oxidation of the CDs, producing a more oxygenated material. This was achieved while the CDs maintained an identical N : C ratio of ~0.16. Consequently, the N,S-CDs here obtained can be interpreted as oxidized N-CDs rather than as true co-doped nanomaterials. Interestingly, this oxidant-like role of $Na_2S_2O_3$ was described before.[105]

Finally, the observation that N,S-CDs are more akin to an oxidized version of N-CDs, rather than an actual co-doped nanomaterial, helps to explain the measured QY_{FL} reduction. Specifically, Chahal *et al.*[41] have claimed that QY_{FL} is correlated with the O : C ratio and that N-doping is insufficient to increase QY_{FL}. This is in line with our data, as the N : C ratio difference between N-CDs and N,S-CDs is negligible, while the latter nanoparticles are more oxidized than the former (O : C ratio is increased by ~24%). Previous authors have also correlated lower QY_{FL} with higher oxidation degrees.[106,107] This can be explained by the formation of oxygen-based surface defects that act as non-radiative centers, thereby allowing for non-radiative relaxation pathways.[108,109] This is compatible with our data, especially considering the fact that despite the QY_{FL} being markedly lower in N,S-CDs, their emission band position and shape remained mainly unchanged (when compared with N-CDs). Furthermore, the fluorescence of N,S-CDs presented a similar variation to external media/stimuli as N-CDs, with some apparent contribution from more surface-accessible states.

It should be noted that the potential presence of residual thiosulfate (Fig. 9G and S6) could raise the question of whether the QY_{FL} decrease could be attributed to it instead (by quenching effects). To investigate this, we measured the potential quenching effect of $Na_2S_2O_3$ toward N-CDs and N,S-CDs, at quencher concentrations up to 100 mM (Fig. S8). The quenching effect was found to range from negligible to small. Specifically, at 30 mM, the F_0/F ratio for N-CDs was still ~1 and just ~1.20 for N,S-CDs. These small effects are unlikely to account for the observed 63% decrease in QY_{FL}, especially given that the residual concentration of potential thiosulfate should be significantly lower than the range investigated here (mM levels). Finally, it should also be said that even if residual thiosulfate is present, it still supports our conclusion that $Na_2S_2O_3$ did not act as an effective dopant under these conditions.

To better assess the extension of our conclusions, we also synthesized two additional CDs: N,S-$CDs_{thiourea}$ and N,S-CDs_{half}. The former was produced in the same way as N,S-CDs, except that $Na_2S_2O_3$ was replaced with thiourea. N,S-CDs_{half} were produced with $Na_2S_2O_3$ but in a 1 : 1 : 0.5 mass ratio (C, N and S sources, respectively), that is, half the amount of $Na_2S_2O_3$ used to produce N,S-CDs. Their EECPs are shown in Fig. S9, and their QYs_{FL} are 3.8% (N,S-$CDs_{thiourea}$) and 34.1% (N,S-CDs_{half}).

This shows that the use of thiourea has also resulted in a significant decrease in QY_{FL} (by 89%), when compared with N-CDs. This indicates that the detrimental effect attributed to the S-precursors is not limited to $Na_2S_2O_3$. Regarding N,S-CDs_{half}, their QY_{FL} is actually similar to that of N-CDs (5% decrease). This indicates that the detrimental effect of $Na_2S_2O_3$ is concentration-dependent, which is expected for redox/surface-modification routes. Furthermore, while similar, the QY_{FL} is still inferior to that of N-CDs. Thus, it is another

example where co-S-doping does not provide a visible performance enhancement over N-doped CDs.

Overall, our data show that the co-addition of $Na_2S_2O_3$ during hydrothermal synthesis does not lead to effective S surface incorporation but instead promotes oxidation of the carbon surface. The resulting N,S-CDs are therefore best described as oxidized N-CDs with a higher O : C ratio, where oxygen-based surface traps are hypothesized to account for the observed 63% decrease in quantum yield. This finding highlights the possibility that some S-precursors commonly used for S-doping may act primarily as redox modifiers rather than dopants, emphasizing the need for careful surface-composition correlation when interpreting QY_{FL} changes in doped CDs.

Beyond this specific case, our results may reveal a broader issue in CD research. While many studies attribute optical property modulation to heteroatom doping, in the field there is a limited quantitative assessment of heteroatom incorporation into CDs and how it correlates with the observed changes. Given this, the role of "dopants" may be misinterpreted, and non-doping surface oxidation/modification effects may be overlooked. Compounds intended as dopants may in fact act primarily as redox-active agents, catalysts, or surface modifiers. Hence, there is a need for systematic compositional analysis and mechanistic validation when evaluating the true impact of doping strategies on CD emission. Nevertheless, it should be noted that our work focused solely on hydrothermal reactions and not on other synthesis routes (such as microwave-assisted or dry-heating). It was also focused on $Na_2S_2O_3$ rather than other common S-precursors (such as cysteine). Therefore, future work is needed to properly assess the impact of our results in the field of CDs.

Experimental

Carbon dot synthesis procedures

N-CDs and N,S-CDs were produced by following a general hydrothermal treatment route previously developed by us for the synthesis of brightly emissive waste-based CDs.[12] Specifically, the precursor mixtures for both CDs were prepared in a NaOH (0.01 M) solution, with the final reaction volume being 10 mL. For N-CDs, the precursor mixture consisted of the carbon precursors citric acid and sawdust (the waste material), in a 50 : 50 mass ratio (total 0.15 g), and the N-dopant (EDA, 0.15 g). N,S-CDs were prepared from a similar mixture, with the difference being the addition of also 0.15 g of $Na_2S_2O_3$ pentahydrate as an S-dopant. Both reaction mixtures were placed in a 25 mL Teflon-lined reactor with a stainless-steel shell from Cambridge Energy Solutions (CES) and then heated at 200 °C for 8 h in a D-6450 Hanau oven from Heraeus. Afterwards, the resulting CD solutions were placed in an ultrasonic bath from VWR, model USC100TH, for 20 minutes. Later, the samples were centrifuged for 30 minutes at 6000 rpm through a MIKRO 220R from Hettich to remove suspended particles. The precipitate was discarded, and the supernatant was further purified. The CDs were subsequently subjected to dialysis for 24 hours, using a Float-A-Lyzer®G2 dialysis device, MWCO: 3500 Da. The commercial chemicals used in the synthesis were citric acid anhydrous (>99%), EDA (≥99%), and NaOH (≥97%) from Sigma-Aldrich, as well as $Na_2S_2O_3$ from Merck. The sawdust was supplied by a Portuguese company specializing in timber trading and the production of derivative products. The efficiency of the dialysis process was assessed by measuring the absorbance of the dialysate solutions at 350 nm (the excitation wavelength of the CDs), at the first cycle of water replacement and at the end of the 24 h dialysis (Fig. S7). While the absorbance at the end of the first cycle was 0.116–0.123, at 24 h, only basal absorbance values were observed for both CDs (0.003–0.007). These decreases correspond to almost 100% (~95% for N-CDs and ~97% for N,S-CDs) and support the adequacy of our dialysis conditions.

Characterization techniques

Fluorescence measurements were performed using a Horiba Jobin Yvon Fluoromax-4 spectrofluorometer, using a standard 10 mm fluorescence quartz cell. The fluorescence spectra were acquired with slit widths set to 2 nm. Samples were analyzed at a fixed concentration of 0.1 g L^{-1}, except in concentration-dependent assays. Absorbance spectra were recorded using a UV-3100PC spectrophotometer from VWR, using quartz cells.

Dynamic light scattering (DLS) and ζ-potential measurements were conducted using an Anton Paar Litesizer™ 500 particle analyzer. ζ-Potential measurements were performed using a polycarbonate Omega cuvette, and size measurements (by DLS) were carried out using a disposable polystyrene cuvette.

Fourier transform infrared (FT-IR) spectroscopy was conducted using a PerkinElmer Spectrum Two FT-IR spectrometer (ATR module) and Spectrum software. The analysis included 4 scans per spectrum and covered a wavenumber range from 4000 to 400 cm^{-1}.

Using monochromatic Al-K_α radiation (49.1 W, 15 kV, and 1486.6 eV), X-ray photoelectron spectroscopy (XPS) was conducted on a Physical Electronics PHI VersaProbe II spectrometer to analyze the core-level signals of the components of interest using a hemispherical multichannel detector. Over a circular analysis region of 200 μm in diameter, the sample spectra were recorded with a constant pass energy value of 29.35 eV. PHI SmartSoft software was used to analyze the acquired XPS spectra, and MultiPak 9.3 was used for processing. The adventitious carbon C 1*s* signal (284.8 eV) served as the reference for the binding energy measurements. The binding energies were found using Gaussian-Lorentzian curves and Shirley-type backgrounds.

Laboratory X-ray powder diffraction (XRPD) patterns were collected using a PANalytical EMPYREAN automated diffractometer. Powder patterns were recorded in Bragg–Brentano reflection configuration by using a PIXcel 3D detector with a step size of 0.01° (2θ). The powder patterns were recorded between 5 and 70 in 2θ with a total measurement time of 60 min.

Electron paramagnetic resonance (EPR) spectra were recorded using a Bruker Elexys III E580 spectrometer, which operates in the X-band (9.5 GHz).

Atomic force microscopy (AFM) analysis was conducted with a Nano-Observer AFM (CSInstruments AFM Microscopes, Les Ulis, France). For this purpose, a mica substrate treated with 0.01% poly-L-lysine hydrobromide was used to deposit the sample, and measurements were carried out using a sharp Si N-type probe with a resistance of 0.01–0.025 Ω cm and a resonance frequency of 200–400 kHz. Samples were prepared by drop evaporation of a diluted CD solution, and Gwyddion software was used for AFM data analysis.

Fluorescence quantum yield

The fluorescence quantum yield (QY_{FL}) was determined following a standard methodology, which involves comparing the integrated luminescence intensities and absorbance values of the sample (in this case, the CDs) to those of a reference fluorophore, quinine sulfate (QS). The calculation of QY_{FL} is based on the following equation,

$$QY_{FL} = QY_{FL_{QS}} \times \frac{Grad_{sample}}{Grad_{QS}} \times \frac{\eta_{sample}^2}{\eta_{QS}^2} \times 100$$

where "Grad" represents the gradient derived from the plot of integrated fluorescence intensity *versus* absorbance and "η" denotes the refractive index.

In this study, QS was utilized as the reference fluorophore due to its established QY_{FL} of 0.54. QS is commonly used for QY_{FL} determination of CDs because it absorbs at the selected excitation wavelength and emits in a spectral region comparable to that of typical CDs, including the ones analyzed in this study. The refractive index of the reference (QS) was 1.33 (0.1 M H_2SO_4), and the sample (CDs) was 1.34 (H_2O). To minimize reabsorption effects, the absorbance at the excitation wavelength was kept below 0.1.

Conclusions

In summary, this study provided a comprehensive and comparative characterization of N-CDs and N,S-CDs synthesized from sawdust, citric acid, EDA, and $Na_2S_2O_3$ under hydrothermal conditions. More specifically, while heteroatom-doping strategies are widely used to enhance the QY_{FL} of CDs, there is a limited understanding of the mechanism behind it. In fact, it is still unclear how truly effective these strategies are. One example is the lack of a comprehensive demonstration that co-N,S-doping provides additional advantages over single N-doping approaches. Herein, our study aimed to provide insight into these processes by focusing on commonly used precursors, N- and S-dopants, and synthesis strategies, thereby ensuring a broader generalization of the conclusions within this research field.

Despite the broadly claimed benefits of co-N,S-doping and the common use of $Na_2S_2O_3$ as an S-dopant, the results revealed that its inclusion markedly reduced the QY_{FL} of N,S-CDs by 63%. Detailed microscopic and spectroscopic analyses indicate that this loss in QY_{FL} is not due to successful S-doping, but rather to a more oxidized surface, as evidenced by the higher O : C ratio measured by XPS. These findings suggest that the inclusion of $Na_2S_2O_3$ had a primarily oxidizing effect during the synthesis rather than the compound acting as a dopant, promoting oxygen-based surface defects that introduce nonradiative traps. In other words, the addition of $Na_2S_2O_3$ resulted in more oxidized N-CDs rather than co-doped N,S-CDs. It should be noted that thiourea was also found to cause a marked reduction in QY_{FL}.

Beyond this specific case, this study highlights the possibility that heteroatom-containing compounds can behave as redox-active modifiers rather than true dopants. As such, future studies should perform more quantitative assessments and validation of heteroatom incorporation into the resulting CDs, to better distinguish between real doping effects and surface modifications mediated by heteroatom-based compounds. Furthermore, S-precursors (*e.g.*, cysteine), which are also commonly used, should be specifically investigated to assess whether they induce this QY_{FL}-reducing effect, at least under some experimental conditions. Thus, this study provides valuable insight into the use of heteroatom precursors, which can inform a more rational design of better-performing CDs.

Author contributions

Conceptualization: LPS; investigation: SF, MA, and AB; visualization: SF and MA; supervision: LPS, JES, and CMP; funding acquisition: LPS, CMP, JES, and MA; writing – original draft: SF and MA; and writing – revision: LPS, MA, AG, AB, CMP, and JES.

Conflicts of interest

There are no conflicts to declare.

Data availability

The data supporting this article have been included as part of the supplementary information (SI). Supplementary information: emission intensity *vs* absorbance, photostability and ET(30) assays, DLS number- and intensity-weighted size distributions, EPR assay, XPS survey spectra, dialysis absorbance data of the external solution (350 nm) after 24h purification for both CDs, Stern-Volmer plots for the potential quenching effect of $Na_2S_{2.1}$, and EECPs of N,S-CDs_{half} and N,S-$CDs_{thiourea}$. See DOI: https://doi.org/10.1039/d5nr05082k.

Acknowledgements

"Fundação para a Ciência e a Tecnologia" (FCT, Portugal, https://ror.org/00snfqn58) is acknowledged for funding the

R&D Unit CIQUP (UID/00081/2025), project 2023.13127.PEX and the Associated Laboratory IMS (LA/P/0056/2020). The NORTE2030 program is also acknowledged for funding the project NORTE2030-FEDER-02706400 (iChem4M). Luís Pinto da Silva acknowledges funding from the FCT under the Scientific Employment Stimulus (CEECINST/00069/2021). Sónia Fernandes also acknowledges the FCT for funding her Ph.D. grant (2021.05479.BD). For the purpose of Open Access, the authors have applied a CC-BY public copyright license to any Author Accepted Manuscript (AAM) version arising from this submission. The authors also acknowledge the Lab&Services of the Chemistry and Biochemistry Department of the Faculty of Sciences of Porto University (FCUP|DQB – Lab&Services) and CEMUP (Materials Centre of the University of Porto). Manuel Algarra thanks the projects MCIN/AEI/10.13039/501100011033 and PID2021-122613OB-I00.

References

1 S. Dua, P. Kumar, B. Pani, A. Kaur, M. Khanna and G. Bhatt, *RSC Adv.*, 2023, **13**(20), 13845–13861, DOI: 10.1039/d2ra07180k.
2 J. Liu, R. Li and B. Yang, *ACS Cent. Sci.*, 2020, **6**(12), 2179–2195, DOI: 10.1021/acscentsci.0c01306.
3 R. M. S. Sendão, J. C. G. Esteves da Silva and L. Pinto da Silva, *Chemosphere*, 2022, **301**, 134731, DOI: 10.1016/j.chemosphere.2022.134731.
4 D. Crista, M. Algarra, M. V. Martinez de Yuso, J. C. G. Esteves da Silva and L. Pinto da Silva, *J. Mater. Chem. B*, 2023, **11**(5), 1131–1143, DOI: 10.1039/d2tb02318k.
5 G. Rodríguez-Carballo, R. Moreno-Tost, S. Fernandes, J. C. G. Esteves da Silva, L. Pinto da Silva, E. C. Galiano and M. Algarra, *J. Cleaner Prod.*, 2023, **423**, 138728, DOI: 10.1016/j.jclepro.2023.138728.
6 C. M. Magalhães, E. Ribeiro, S. Fernandes, J. C. G. Esteves da Silva, N. Vale and L. Pinto da Silva, *Cancers*, 2024, **16**(19), 3332, DOI: 10.3390/cancers16193332.
7 Y. Wang and A. Hu, *J. Mater. Chem. C*, 2014, **2**(34), 6921, DOI: 10.1039/c4tc00988f.
8 A. Bafana, S. V. Kumar, S. Temizel-Sekeryan, S. A. Dahoumane, L. Haselbach and C. S. Jeffryes, *Sci. Total Environ.*, 2018, **636**, 936–943, DOI: 10.1016/j.scitotenv.2018.04.345.
9 M. J. Eckelman, J. B. Zimmerman and P. T. Anastas, *J. Ind. Ecol.*, 2008, **12**(3), 316–328, DOI: 10.1111/j.1530-9290.2008.00043.x.
10 S. Fernandes, J. C. G. Esteves da Silva and L. Pinto da Silva, *NanoImpact*, 2021, **23**, 100332, DOI: 10.1016/j.impact.2021.100332.
11 L. Pourzahedi and M. J. Eckelman, *Environ. Sci.:Nano*, 2015, **2**(4), 361–369, DOI: 10.1039/c5en00075k.
12 S. Fernandes, M. Algarra, A. Gil, J. C. G. Esteves da Silva and L. Pinto da Silva, *ChemSusChem*, 2025, **18**(2), e202401702, DOI: 10.1002/cssc.202401702.
13 A. Johny, L. Pinto da Silva, C. M. Pereira and J. C. G. Esteves da Silva, *Environments*, 2024, **11**(1), 6, DOI: 10.3390/environments11010006.
14 D. M. A. Crista, A. El Mragui, M. Algarra, J. C. G. Esteves da Silva, R. Luque and L. Pinto da Silva, *Nanomaterials*, 2020, **10**(6), 1316, DOI: 10.3390/nano10061209.
15 F. Aldakhil, N. A. Alarfaj, S. A. Al-Tamimi and M. F. El-Tohamy, *RSC Adv.*, 2024, **14**(28), 19969–19982, DOI: 10.1039/d4ra02398f.
16 S. Zhu, Y. Song, X. Zhao, J. Shao, J. Zhang and B. Yang, *Nano Res.*, 2015, **8**(2), 355–381, DOI: 10.1007/s12274-014-0644-3.
17 C. Kang, Y. Huang, H. Yang, X. F. Yan and Z. P. Chen, *Nanomaterials*, 2020, **10**(11), 2316, DOI: 10.3390/nano10112316.
18 J. R. Bhamore, S. Jha, R. K. Singhal, T. J. Park and S. K. Kailasa, *J. Mol. Liq.*, 2018, **264**, 9–16, DOI: 10.1016/j.molliq.2018.05.041.
19 R. Atchudan, T. N. J. I. Edison, D. Chakradhar, S. Perumal, J.-J. Shim and Y. R. Lee, *Sens. Actuators, B*, 2017, **246**, 497–509, DOI: 10.1016/j.snb.2017.02.119.
20 A. M. Senol and E. Bozkurt, *Microchem. J.*, 2020, **159**, 105357, DOI: 10.1016/j.microc.2020.105357.
21 Q. Xu, P. Pu, J. Zhao, C. Dong, C. Gao, Y. Chen, J. Chen, Y. Liu and H. Zhou, *J. Mater. Chem. A*, 2015, **3**(2), 542–546, DOI: 10.1039/c4ta05483k.
22 C. Wang, Y. Wang, H. Shi, Y. Yan, E. Liu, X. Hu and J. Fan, *Mater. Chem. Phys.*, 2019, **232**, 145–151, DOI: 10.1016/j.matchemphys.2019.04.071.
23 Q. Xu, J. Zhao, Y. Liu, P. Pu, X. Wang, Y. Chen, C. Gao, J. Chen and H. Zhou, *J. Mater. Sci.*, 2015, **50**(6), 2571–2576, DOI: 10.1007/s10853-015-8822-6.
24 G. Somaraj, S. Mathew, T. Abraham, K. G. Ambady, C. Mohan and B. Mathew, *ChemistrySelect*, 2022, **7**(19), e202200473, DOI: 10.1002/slct.202200473.
25 A. Nasrin, M. Hassan, G. Mann and V. G. Gomes, *J. Lumin.*, 2020, **217**, 116811, DOI: 10.1016/j.jlumin.2019.116811.
26 M. L. Liu, B. B. Chen, C. M. Li and C. Z. Huang, *Green Chem.*, 2019, **21**(3), 449–471, DOI: 10.1039/c8gc02736f.
27 H. Qi, L. Qiu, X. Zhang, T. Yi, J. Jing, R. Sami, S. F. Alanazi, Z. Alqahtani, M. D. Aljabri and M. M. Rahman, *RSC Adv.*, 2023, **13**(4), 2663–2671, DOI: 10.1039/d2ra07150a.
28 T. T. A. Do, K. Wicaksono, A. Soendoro, T. Imae, M. J. Garcia-Celma and S. Grijalvo, *J. Funct. Biomater.*, 2022, **13**(4), 219, DOI: 10.3390/jfb13040219.
29 H. Song, Y. Li, L. Shang, Z. Tang, T. Zhang and S. Lu, *Nano Energy*, 2020, **72**, 104730, DOI: 10.1016/j.nanoen.2020.104730.
30 A. G. Kolekar, S. P. Pawar, D. B. Gunjal, O. S. Nille, P. V. Anbhule, S. V. Koparde, N. Q. Nguyen, D. Sohn, G. B. Kolekar, G. S. Gokavi and V. R. More, *RSC Adv.*, 2024, **14**(5), 3473–3479, DOI: 10.1039/d3ra07545a.
31 H. Wang, W. Mu, S. Wang, L. Shi, T. Ma and Y. Lu, *Spectrochim. Acta, Part A*, 2024, **305**, 123460, DOI: 10.1016/j.saa.2023.123460.

32 C. Cheng, M. Xing and Q. Wu, *Mater. Sci. Eng., C*, 2019, **99**, 611–619, DOI: 10.1016/j.msec.2019.02.003.
33 Y. Venkatesh, P. V. S. Naidu, M. Ramanjaneyulu, P. A. Rao and D. B. Kundrapu, *J. Nanopart. Res.*, 2025, **27**(3), 62, DOI: 10.1007/s11051-025-06260-y.
34 A. Saengsrichan, C. Saikate, P. Silasana, P. Khemthong, W. Wanmolee, J. Phanthasri, S. Youngjan, P. Posoknistakul, S. Ratchahat, N. Laosiripojana, K. C. Wu and C. Sakdaronnarong, *Int. J. Mol. Sci.*, 2022, **23**(9), 5001, DOI: 10.3390/ijms23095001.
35 Y. Li, Y. Zhao, H. Cheng, Y. Hu, G. Shi, L. Dai and L. Qu, *J. Am. Chem. Soc.*, 2012, **134**(1), 15–18, DOI: 10.1021/ja206030c.
36 M. Yang, X. Meng, B. Li, S. Ge and Y. Lu, *J. Nanopart. Res.*, 2017, **19**(6), 217, DOI: 10.1007/s11051-017-3914-7.
37 D. Qu, M. Zheng, L. Zhang, H. Zhao, Z. Xie, X. Jing, R. E. Haddad, H. Fan and Z. Sun, *Sci. Rep.*, 2014, **4**, 5294, DOI: 10.1038/srep05294.
38 W. Zou, J. Li and X. Gong, *Mater. Today Chem.*, 2024, **37**, 102001, DOI: 10.1016/j.mtchem.2024.102001.
39 D. M. A. Crista, J. C. G. Esteves da Silva and L. Pinto da Silva, *Nanomaterials*, 2020, **10**(7), 1316, DOI: 10.3390/nano10071316.
40 S. Christe, J. C. G. Esteves da Silva and L. Pinto da Silva, *Materials*, 2020, **13**(3), 504, DOI: 10.3390/ma13030504.
41 S. Chahal, N. Yousefi and N. Tufenkji, *ACS Sustainable Chem. Eng.*, 2020, **8**(14), 5566–5575, DOI: 10.1021/acssuschemeng.9b07463.
42 Z. Yi, X. Li, H. Zhang, X. Ji, W. Sun, Y. Yu, Y. Liu, J. Huang, Z. Sarshar and M. Sain, *Talanta*, 2021, **222**, 121663, DOI: 10.1016/j.talanta.2020.121663.
43 Y. Liu, L. Jiang, B. Li, X. Fan, W. Wang, P. Liu, S. Xu and X. Luo, *J. Mater. Chem. B*, 2019, **7**(19), 3053–3058, DOI: 10.1039/c9tb00021f.
44 J. B. Essner, J. A. Kist, L. Polo-Parada and G. A. Baker, *Chem. Mater.*, 2018, **30**(6), 1878–1887, DOI: 10.1021/acs.chemmater.7b04446.
45 N. Ullal, R. Mehta and D. Sunil, *Analyst*, 2024, **149**(6), 1680–1700, DOI: 10.1039/d3an02134c.
46 D. A. Sousa, M. N. Berberan-Santos and J. V. Prata, *Chemistry*, 2024, **30**(3), e202302955, DOI: 10.1002/chem.202302955.
47 Y. Hu, O. Seivert, Y. Tang, H. E. Karahan and A. Bianco, *Angew. Chem., Int. Ed.*, 2024, **63**(48), e202412341, DOI: 10.1002/anie.202412341.
48 H. Li, J. Xiao, J. Cao, J. Pan, C. Li and Y. Zheng, *J. Nanopart. Res.*, 2025, **27**(5), 140, DOI: 10.1007/s11051-025-06332-z.
49 P. Liu, C. Zhang, X. Liu and P. Cui, *Appl. Surf. Sci.*, 2016, **368**, 122–128, DOI: 10.1016/j.apsusc.2016.01.278.
50 J. Zheng, Y. Xie, Y. Wei, Y. Yang, X. Liu, Y. Chen and B. Xu, *Nanomaterials*, 2020, **10**(1), 82, DOI: 10.3390/nano10010082.
51 A. Abdel-Hakim, F. Belal, M. A. Hammad and M. El-Maghrabey, *Methods Appl. Fluoresc.*, 2023, **11**(4), 045007, DOI: 10.1088/2050-6120/acf119.
52 H. P. Dang, V. T. N. Thuy, B. T. Diem, N. Q. Thang and N. T. M. Tho, *Opt. Quantum Electron.*, 2025, **57**(5), 291, DOI: 10.1007/s11082-025-08185-1.
53 Q. Xu, Y. Liu, C. Gao, J. Wei, H. Zhou, Y. Chen, C. Dong, T. S. Sreeprasad, N. Li and Z. Xia, *J. Mater. Chem. C*, 2015, **3**(38), 9885–9893, DOI: 10.1039/c5tc01912e.
54 D. Qu, M. Zheng, P. Du, Y. Zhou, L. Zhang, D. Li, H. Tan, Z. Zhao, Z. Xie and Z. Sun, *Nanoscale*, 2013, **5**(24), 12272–12277, DOI: 10.1039/c3nr04402e.
55 S. Chen, W. Ouyang, Y. Zhu, L. He, L. Zou, X. Ao, S. Liu, Y. Yang and J. Li, *Foods*, 2022, **11**(16), 2414, DOI: 10.3390/foods11162414.
56 R. Tamizhselvi, K. S. Velu, A. A. Napoleon, M. S. Akhtar, N. Ahmad, S. Palanisamy, S. You, S. Mohandoss and S.-C. Kim, *Inorg. Chem. Commun.*, 2025, **172**, 113662, DOI: 10.1016/j.inoche.2024.113662.
57 O. A. Aladesuyi and O. S. Oluwafemi, *Inorg. Chem. Commun.*, 2023, **153**, 110843, DOI: 10.1016/j.inoche.2023.110843.
58 M. Hamid, S. Humaidi, H. Wijoyo, I. Isnaeni, I. R. Saragi, C. Simanjuntak, N. H. M. Kaus, M. M. A. Kechik, A. Nurbillah, Y. Yaakob and T. I. Nasution, *Case Stud. Chem. Environ. Eng.*, 2024, **10**, 100832, DOI: 10.1016/j.cscee.2024.100832.
59 J. Wang, Z. Wu, S. Chen, R. Yuan and L. Dong, *Microchem. J.*, 2019, **151**, 104246, DOI: 10.1016/j.microc.2019.104246.
60 J. Zhang, Z. Xu, C. Shi and X. Yang, *Sustainability*, 2021, **13**(15), 8255, DOI: 10.3390/su13158255.
61 H. K. M. Ng, G. K. Lim and C. P. Leo, *Microchem. J.*, 2021, **165**, 106116, DOI: 10.1016/j.microc.2021.106116.
62 A. O. Aswathy, S. M. Anju, J. Jayakrishna, N. S. Vijila, J. S. Anjali Devi, B. Anjitha and S. George, *J. Fluoresc.*, 2020, **30**(6), 1337–1344, DOI: 10.1007/s10895-020-02607-x.
63 S. R. Kamali, C.-N. Chen, D. C. Agrawal and T.-H. Wei, *J. Anal. Sci. Technol.*, 2021, **12**(1), 48, DOI: 10.1186/s40543-021-00298-y.
64 J. Guo, L. Fan, Q. Zan, J. Wang, Z. Yang, W. Lu, Y. Yang, X. Yang, C. Dong and S. Shuang, *Anal. Chem.*, 2023, **95**(32), 12139–12151, DOI: 10.1021/acs.analchem.3c02381.
65 V. I. Stsiapura, A. A. Maskevich, V. A. Kuzmitsky, V. N. Uversky, I. M. Kuznetsova and K. K. Turoverov, *J. Phys. Chem. B*, 2008, **112**(49), 15893–15902, DOI: 10.1021/jp805822c.
66 A. Neerkattil, M. M. Bijeesh, K. K. Ghosh, P. Padmanabhan, B. Gulyas, V. M. Murukeshan and J. Bhattacharyya, *Nanoscale Adv.*, 2025, **7**(9), 2686–2694, DOI: 10.1039/d5na00061k.
67 A. Chmyrov, T. Sanden and J. Widengren, *J. Phys. Chem. B*, 2010, **114**(34), 11282–11291, DOI: 10.1021/jp103837f.
68 K. E. Guðmundsson, G. Marteinsdóttir, K. Kristbergsson and Á. Kvaran, *Chem. Pap.*, 2022, **76**(8), 5253–5265, DOI: 10.1007/s11696-022-02222-z.
69 R. M. S. Sendão, M. Algarra, J. Lázaro-Martínez, A. T. S. C. Brandão, A. Gil, C. Pereira, J. C. G. Esteves da Silva and L. Pinto da Silva, *Colloids Surf., A*, 2025, **713**, 36475, DOI: 10.1016/j.colsurfa.2025.136475.
70 R. M. S. Sendão, M. Algarra, E. Ribeiro, M. Pereira, A. Gil, N. Vale, J. C. G. Esteves da Silva and L. Pinto da Silva, *Adv.*

Sustainable Syst., 2023, **8**(1), 2300317, DOI: 10.1002/adsu.202300317.
71 Y.-C. Wang, F. Zhu, J.-Y. Zhang and T.-M. Geng, *Microchem. J.*, 2025, **209**, 112739, DOI: 10.1016/j.microc.2025.112739.
72 J. Cao, X. An and S. Han, *Colloids Surf., A*, 2020, **586**, 124201, DOI: 10.1016/j.colsurfa.2019.124201.
73 Y. Song, S. Zhu, S. Xiang, X. Zhao, J. Zhang, H. Zhang, Y. Fu and B. Yang, *Nanoscale*, 2014, **6**(9), 4676–4682, DOI: 10.1039/c4nr00029c.
74 X. Ren, L. Guan, W. Shi, J. Zhang, M. Chen, T. Luo, C. Liu, Y. Lan, Z. Chen, X. Chen and X. Li, *J. Mol. Liq.*, 2024, **403**, 124872, DOI: 10.1016/j.molliq.2024.124872.
75 A. Das, D. Roy, C. K. De and P. K. Mandal, *Phys. Chem. Chem. Phys.*, 2018, **20**(4), 2251–2259, DOI: 10.1039/c7cp07411e.
76 J. Ren, F. Weber, F. Weigert, Y. Wang, S. Choudhury, J. Xiao, I. Lauermann, U. Resch-Genger, A. Bande and T. Petit, *Nanoscale*, 2019, **11**(4), 2056–2064, DOI: 10.1039/c8nr08595a.
77 P. K. Sarswat and M. L. Free, *Phys. Chem. Chem. Phys.*, 2015, **17**(41), 27642–27652, DOI: 10.1039/c5cp04782j.
78 A. Ventrella, A. Camisasca, A. Fontana and S. Giordani, *RSC Adv.*, 2020, **10**(60), 36404–36412, DOI: 10.1039/d0ra06172g.
79 F. Olia, F. Fiori and P. Innocenzi, *Next Mater.*, 2025, **8**, 100756, DOI: 10.1016/j.nxmate.2025.100756.
80 A. Wibrianto, S. Q. Khairunisa, S. C. W. Sakti, Y. L. Ni'mah, B. Purwanto and M. Z. Fahmi, *RSC Adv.*, 2020, **11**(2), 1098–1108, DOI: 10.1039/d0ra09403j.
81 R. M. F. Cardoso, I. M. F. Cardoso, L. Pinto da Silva and J. C. G. Esteves da Silva, *Nanomaterials*, 2022, **12**(7), DOI: 10.3390/nano12071211.
82 Y. Ru, G. I. N. Waterhouse and S. Lu, *Aggregate*, 2022, **3**(6), e296, DOI: 10.1002/agt2.296.
83 Z. X. Liu, Z. L. Wu, M. X. Gao, H. Liu and C. Z. Huang, *Chem. Commun.*, 2016, **52**(10), 2063–2066, DOI: 10.1039/c5cc08635c.
84 R. Guo, Z. Ling, B. Zheng, X. Sun, Z. Yuan and H. Li, *J. Phys. Chem. Lett.*, 2025, **16**(1), 140–147, DOI: 10.1021/acs.jpclett.4c03058.
85 R. Atchudan, T. Edison, K. R. Aseer, S. Perumal, N. Karthik and Y. R. Lee, *Biosens. Bioelectron.*, 2018, **99**, 303–311, DOI: 10.1016/j.bios.2017.07.076.
86 X. Teng, C. Ma, C. Ge, M. Yan, J. Yang, Y. Zhang, P. C. Morais and H. Bi, *J. Mater. Chem. B*, 2014, **2**(29), 4631–4639, DOI: 10.1039/c4tb00368c.
87 B. De and N. Karak, *RSC Adv.*, 2013, **3**(22), 8286–8290, DOI: 10.1039/c3ra00088e.
88 H. S. Tohamy, M. El-Sakhawy and S. Kamel, *Sci. Rep.*, 2023, **13**(1), 11306, DOI: 10.1038/s41598-023-37894-4.
89 K. J. Mintz, M. Bartoli, M. Rovere, Y. Zhou, S. D. Hettiarachchi, S. Paudyal, J. Chen, J. B. Domena, P. Y. Liyanage, R. Sampson, D. Khadka, R. R. Pandey, S. Huang, C. C. Chusuei, A. Tagliaferro and R. M. Leblanc, *Carbon*, 2021, **173**, 433–447, DOI: 10.1016/j.carbon.2020.11.017.
90 A. B. Siddique, A. K. Pramanick, S. Chatterjee and M. Ray, *Sci. Rep.*, 2018, **8**(1), 9770, DOI: 10.1038/s41598-018-28021-9.
91 E. Sturabotti, V. Di Lisio, L. Cardo, A. Camilli, E. Moretón Alfonsín, D. Cangialosi, A. Iturrospe Ibarra, A. Arbe and M. Prato, *Adv. Mater.*, 2025, DOI: 10.1002/adma.202510992.
92 M. B. Prado, N. T. Truong and A. K. Wanekaya, *Sensors Actuators Rep.*, 2023, **6**, 100165, DOI: 10.1016/j.snr.2023.100165.
93 A. Hemmati, H. Emadi and S. R. Nabavi, *ACS Omega*, 2023, **8**(23), 20987–20999, DOI: 10.1021/acsomega.3c01795.
94 C. Sun, Y. Zhang, P. Wang, Y. Yang, Y. Wang, J. Xu, Y. Wang and W. W. Yu, *Nanoscale Res. Lett.*, 2016, **11**(1), 110, DOI: 10.1186/s11671-016-1326-8.
95 Y. Xu, D. Li, M. Liu, F. Niu, J. Liu and E. Wang, *Sci. Rep.*, 2017, **7**(1), 4499, DOI: 10.1038/s41598-017-04754-x.
96 N. A. Travlou, D. A. Giannakoudakis, M. Algarra, A. M. Labella, E. Rodríguez-Castellón and T. J. Bandosz, *Carbon*, 2018, **135**, 104–111, DOI: 10.1016/j.carbon.2018.04.018.
97 T. Teymoorian, N. Hashemi, M. H. Mousazadeh and Z. Entezarian, *SN Appl. Sci.*, 2021, **3**(3), 305, DOI: 10.1007/s42452-021-04287-z.
98 J. F. Moulder, W. F. Stickle, P. E. Sobol and K. D. Bomben, *Handbook of X Ray Photoelectron Spectroscopy: A reference book of standard spectra for identification and interpretation of XPS Data*, Physical Electronics, Eden Prairie, Minn, 1995.
99 A. Bunge, L. Magerusan, I. Morjan, R. Turcu, G. Borodi and J. Liebscher, *J. Nanopart. Res.*, 2015, **17**(9), 379, DOI: 10.1007/s11051-015-3167-2.
100 D. Benchoam, E. Cuevasanta, M. N. Moller and B. Alvarez, *Antioxidants*, 2019, **8**(2), 48, DOI: 10.3390/antiox8020048.
101 W. A. Pryor, *J. Am. Chem. Soc.*, 2002, **82**(18), 4794–4797, DOI: 10.1021/ja01503a010.
102 W. F. Giggenbach, *Inorg. Chem.*, 2002, **13**(7), 1730–1733, DOI: 10.1021/ic50137a039.
103 D. A. Islam, K. Barman, S. Jasimuddin and H. Acharya, *Nanoscale*, 2019, **11**(16), 7560–7566, DOI: 10.1039/c9nr00782b.
104 D. Macabrey, J. Joniova, Q. Gasser, C. Bechelli, A. Longchamp, S. Urfer, M. Lambelet, C. Y. Fu, G. Schwarz, G. Wagnieres, S. Deglise and F. Allagnat, *Front. Cardiovasc. Med.*, 2022, **9**, 965965, DOI: 10.3389/fcvm.2022.965965.
105 X.-L. Wei, Q.-L. Shi, L. Jiang and Y. Qin, *New J. Chem.*, 2023, **47**(33), 15525–15533, DOI: 10.1039/d3nj02694a.
106 Y. Xu, M. Wu, X. Z. Feng, X. B. Yin, X. W. He and Y. K. Zhang, *Chemistry*, 2013, **19**(20), 6282–6288, DOI: 10.1002/chem.201204372.
107 H. Zheng, Q. Wang, Y. Long, H. Zhang, X. Huang and R. Zhu, *Chem. Commun.*, 2011, **47**(38), 10650–10652, DOI: 10.1039/c1cc14741b.
108 Y. Lou, X. Hao, L. Liao, K. Zhang, S. Chen, Z. Li, J. Ou, A. Qin and Z. Li, *Nano Sel.*, 2021, **2**(6), 1117–1145, DOI: 10.1002/nano.202000232.
109 C. Deeney, S. Wang, S. A. Belhout, A. Gowen, B. J. Rodriguez, G. Redmond and S. J. Quinn, *RSC Adv.*, 2018, **8**(23), 12907–12917, DOI: 10.1039/c7ra13383a.

4.1.2. Supporting Information

Supplementary Information

Insights into the Role of Common Sulfur Precursors in Hydrothermally Synthesized N,S-Doped Carbon Dots: Fluorescence Modulation via Surface Oxidation Rather Than Sulfur Doping

Sónia Fernandes [a], Manuel Algarra [b], Ana Brandão [c], Antonio Gil [b], Carlos M. Pereira [c], Joaquim C.G Esteves da Silva [a] and Luis Pinto da Silva [a*]

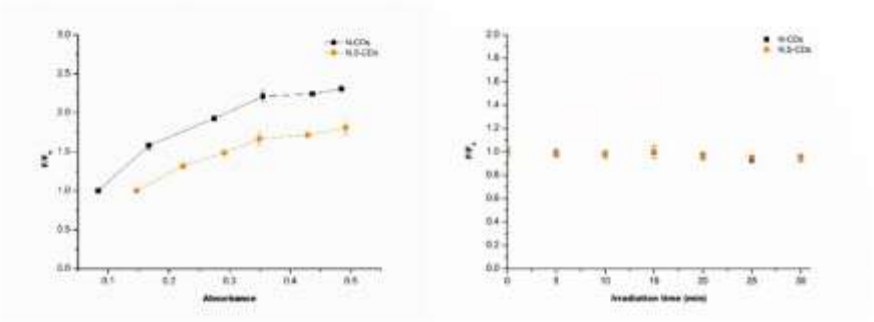

Figure S1. Emission intensity as a function of absorbance (A) and photostability assays (B) for both CDs.

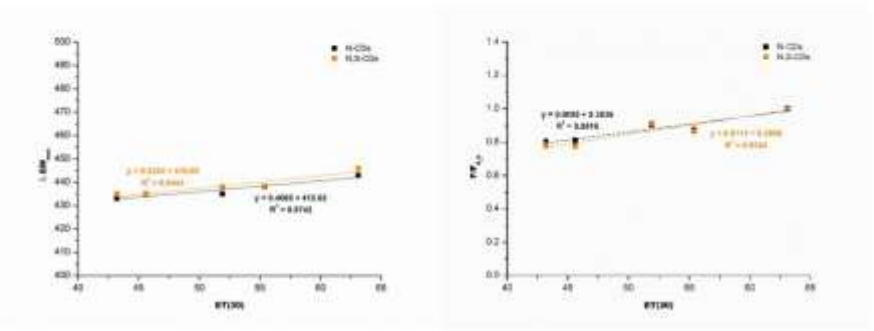

Figure S2. ET(30) considering maximum emission wavelength (A) and emission intensity (B) for both CDs.

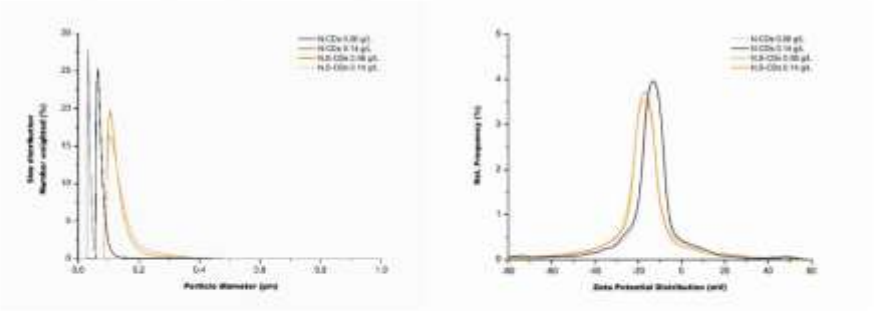

Figure S3. DLS considering a number weighted size distribution for both CDs at 0.06 g/L and 0.14 g/L (A), and ζ potential for both CDs at 0.06 g/L and 0.14 g/L (B).

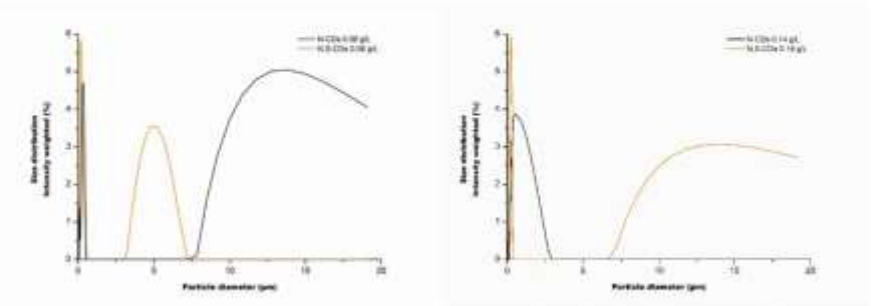

Figure S4. DLS considering an intensity weighted size distribution for both CDs at 0.06 g/L (A) and 0.14 g/L (B).

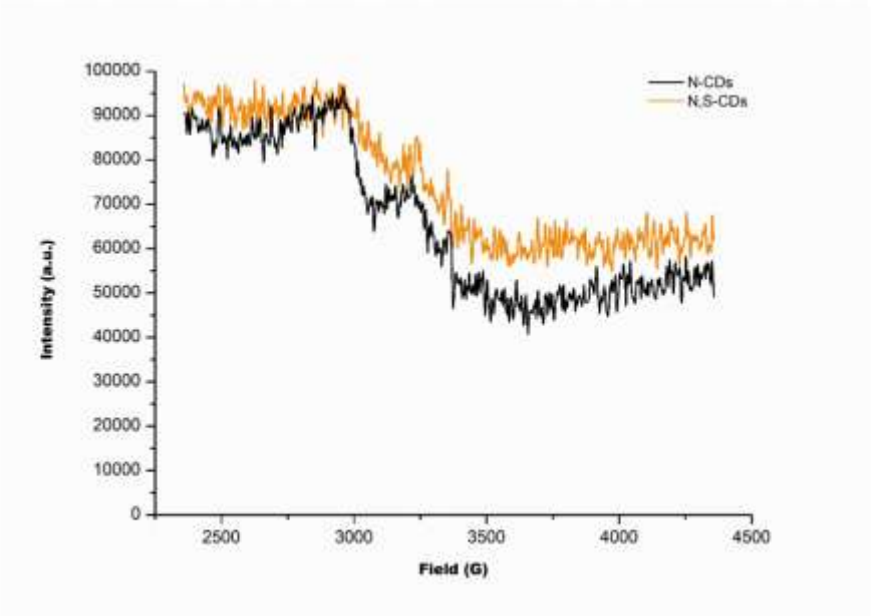

Figure S5. EPR spetra for both CDs.

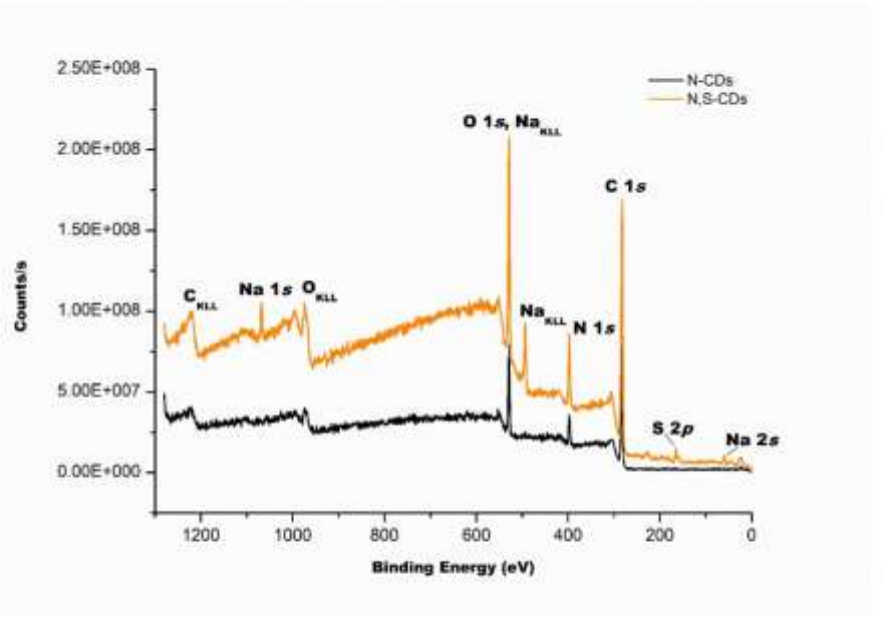

Figure S6. XPS survey for both CDs.

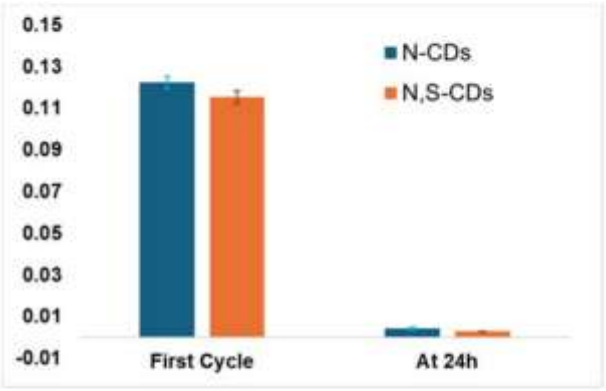

Figure S7. Absorbance of the dialysis external solution at the first cycle of water replacement and at the end of the 24 h dialysis processes for the purification of N-CDs and N,S-CDs, measured at 350 nm (the excitation wavelength of the CDs).

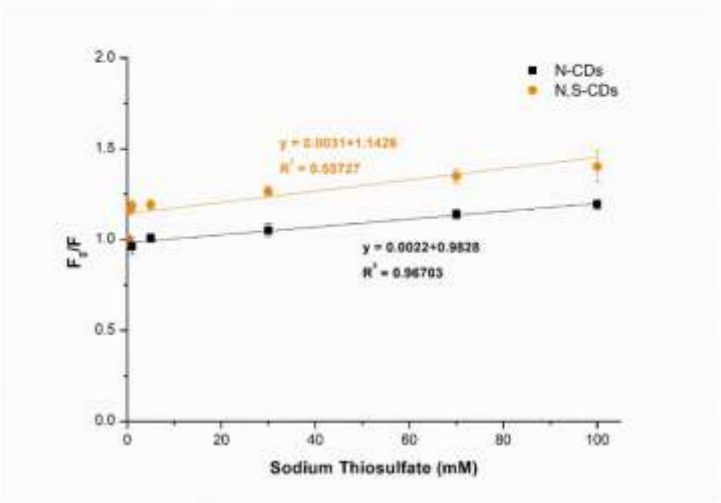

Figure S8. Stern-Volmer plots for the investigation of sodium thiosulfate as potential quencher for N-CDs and N,S-CDs.

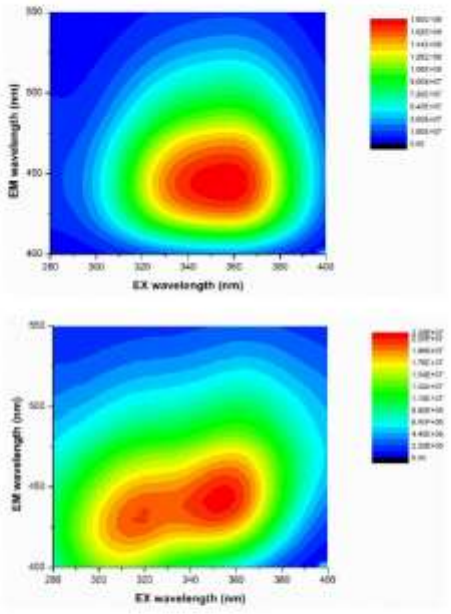

Figure S9. EECPs for N,S-CDs$_{sal}$ (top) and N,S-CDs$_{thiourea}$ (bottom), in water.

4.1.3. Conclusions

This study provides a critical assessment of the role of sulfur-containing precursors in the synthesis of nitrogen- and nitrogen/sulfur-modified CDs, offering new insights into the mechanisms governing their photoluminescent behavior. Contrary to the common assumption that sulfur precursors directly enhance fluorescence through effective heteroatom incorporation, the results demonstrate that the inclusion of sodium thiosulfate leads to a significant reduction in QY_{FL}, despite preserving the emission profile and excitation-dependent behavior.

Comprehensive structural and surface analyses reveal that sulfur incorporation into the carbon framework is minimal, while the surface oxygen content increases markedly in N,S-CDs. These findings indicate that the sulfur precursor primarily acts as an oxidizing agent, promoting the formation of oxygen-related surface defects that introduce non-radiative recombination pathways. As a result, the reduced photoluminescence efficiency is attributed to surface oxidation effects rather than to successful sulfur doping.

By distinguishing between true heteroatom doping and precursor-induced surface modification, this work highlights the need for caution when interpreting fluorescence enhancement claims based solely on the use of heteroatom-containing precursors. More broadly, the findings emphasize the importance of mechanistic understanding and comprehensive characterization in the rational design of CDs with controlled optical properties. Within the scope of this thesis, this work complements the preceding studies by deepening the understanding of structure-property relationships in CDs and reinforcing the importance of precursor chemistry in determining photophysical performance.

5. Conclusions and future perspectives

5.1. Conclusions

This thesis investigated CDs as sustainable luminescent nanomaterials by integrating LCA, green synthesis strategies, and fundamental studies of photoluminescence modulation. The work was developed within the broader context of climate change mitigation, energy efficiency, and responsible resource utilization, with a particular focus on bottom-up synthesis approaches compatible with environmentally benign conditions.

The LCA conducted in this thesis demonstrated that higher synthesis yields do not inherently correspond to improved environmental performance. While high-yield routes enhance material efficiency, their benefits are frequently counterbalanced by increased energy demand, longer reaction times, and additional chemical inputs. Simpler bottom-up approaches, combining moderate-to-high yields with lower process complexity, were identified as more balanced and environmentally favorable options. These results emphasize the necessity of adopting a life cycle perspective when evaluating the sustainability of nanomaterial synthesis routes.

From a materials development perspective, this thesis showed that waste-derived carbon sources can be successfully employed to produce brightly fluorescent CDs through facile and green hydrothermal strategy. The incorporation of organic residues, combined with controlled nitrogen doping and surface passivation, enabled the production of CDs with high photoluminescence efficiencies while maintaining synthesis simplicity and environmental compatibility. These findings support the feasibility of waste valorization as a viable pathway for sustainable CDs production.

Despite systematic efforts to tune the emission toward longer wavelengths, the incorporation of waste-derived precursors consistently resulted in blue-emissive CDs under the explored synthesis conditions. This behavior highlights intrinsic constraints associated with the complex and heterogeneous nature of waste feedstocks, which tend to favor the formation of high-energy emissive surface states. Rather than representing a limitation of the approach, this observation provides valuable insight into the dominant role of precursor chemistry and surface-state formation in governing CDs photoluminescence.

This challenge directly motivated a focused investigation into the role of heteroatom chemistry in fluorescence modulation. The study of sulfur-containing precursors revealed that emission tuning in N,S-CDs is primarily governed by surface

oxidation processes rather than by sulfur incorporation into the carbon core. This mechanistic insight helps reconcile discrepancies in the literature regarding sulfur doping and clarifies the pathways through which photoluminescence modulation occurs in CDs.

Overall, the results of this thesis demonstrate that sustainable CDs design requires a careful balance between environmental performance, precursor selection, and control over surface chemistry. By combining LCA with experimental synthesis and photophysical analysis, this work establishes a comprehensive framework for the rational development of environmentally responsible and optically functional CDs.

5.2. Future Perspectives

The findings of this thesis open several paths for future research aimed at advancing the sustainable development and application of CDs. In particular, achieving controlled green and red emission from waste-derived CDs remains an open challenge. Future studies should explore alternative strategies such as precursor pre-treatment, decoupling carbonization and surface-state formation, post-synthetic surface engineering, or hybrid approaches that combine waste-derived carbons with molecular emissive centers.

Further integration of LCA into early-stage material design could support the development of synthesis routes that simultaneously optimize optical performance and environmental sustainability. Expanding LCA to include scale-up scenarios and device-level integration would provide additional insight into the real-world impacts of CDs-based technologies.

From a fundamental perspective, advanced spectroscopic and theoretical studies could further elucidate the interplay between surface oxidation, heteroatom chemistry, and emissive states. Such efforts would contribute to resolving remaining ambiguities in the structure-property relationships governing CDs photoluminescence.

Finally, while this thesis focused on material-level design, the integration of sustainably synthesized CDs into WLEDs devices represents a natural continuation of this work. The design principles established here provide a solid foundation for future research targeting the development of efficient, environmentally responsible lighting technologies based on CDs.

References

[1] (WCED), W.C.o.E.a.D., *Our common future*. 1987: Oxford. p. 300.
[2] Purvis, B., Y. Mao, and D. Robinson, *Three pillars of sustainability: in search of conceptual origins.* Sustainability Science, 2018. **14**(3): p. 681-695.
[3] Daly, H.E., *Toward some operational principles of sustainable development.* Ecological Economics, 1990. **2**(1): p. 1-6.
[4] Missimer, M., K.-H. Robèrt, and G. Broman, *A strategic approach to social sustainability – Part 1: exploring the social system.* Journal of Cleaner Production, 2017. **140**: p. 32-41.
[5] Costanza, R., L. Fioramonti, and I. Kubiszewski, *The UN Sustainable Development Goals and the dynamics of well-being.* Frontiers in Ecology and the Environment, 2016. **14**(2): p. 59-59.
[6] IPCC, *Climate Change 2023: Synthesis Report. Contribution of Working Groups I, II and III to the Sixth Assessment Report of the Intergovernmental Panel on Climate Change* H.L.a.J. Romero, Editor. 2023: Geneva, Switzerland.
[7] (UNEP), U.N.E.P., *Emissions Gap Report 2022: The Closing Window - Climate Crisis Calls for Rapid Transformation of Societies*. 2022, Nairobi.
[8] Nations, U., *Transforming our world: the 2030 Agenda for Sustainable Development* U.G. Assembly, Editor. 2015.
[9] Griggs, D., et al., *Policy: Sustainable development goals for people and planet.* Nature, 2013. **495**(7441): p. 305-7.
[10] Kates;, R.W., et al., *Sustainability Science* Vol. 98(17) 2001.
[11] Singh, R.K., et al., *An overview of sustainability assessment methodologies.* Ecological Indicators, 2012. **15**(1): p. 281-299.
[12] Gibson, B., S. Hassan, and J. Tansey, *Sustainability Assessment: Criteria and Processses*. 1st Edition ed. 2013, London: Earthscan.
[13] Cash, D.W., et al., *Scale and Cross-Scale Dynamics: Governance and Information in a Multilevel World.* Ecology and Society, 2006. **11**(2).
[14] Barbier, E.B., *The Concept of Sustainable Economic Development.* Environmental Conservation, 1987. **14**(2): p. 101-110.
[15] Meadowcroft, J., *What about the politics? Sustainable development, transition management, and long term energy transitions.* Policy Sciences, 2009. **42**(4): p. 323-340.
[16] Melissa Leach, I.S., Andy Stirling, *Dynamic Sustainabilities: Technology, Environment, Social Justice*. 1st Edition ed. 2010: Earthscan.
[17] IPCC, *Climate Change 2021: The Physical Science Basis. Contribution of Working Group I to the Sixth Assessment Report of the Intergovernmental Panel on Climate Change*, P.Z. V. Masson-Delmotte, A. Pirani, S.L. Connors, C. Péan; and N.C. S. Berger, Y. Chen, L. Goldfarb, M.I. Gomis, M. Huang, K. Leitzell, E. Lonnoy, J.B.R., Matthews, T.K. Maycock, T. Waterfield, O. Yelekçi, R. Yu, and B. Zhou, Editors. 2021: Cambridge, United Kingdom and New York, NY, USA. p. 2391.
[18] W.V. Sweet, B.D.H., R.E. Kopp, C.P. Weaver, P.L. Barnard, D. Bekaert, W. Brooks, M. Craghan, G. Dusek, T. Frederikse, G. Garner, A.S. Genz, J.P. Krasting, E. Larour, D. Marcy, J.J. Marra, J. Obeysekera, M. Osler, M. Pendleton, D. Roman, L. Schmied, W. Veatch, K.D. White, and C. Zuzak,, *Global and Regional Sea Level Rise Scenarios for the United States: Updated Mean Projections and Extreme Water Level Probabilities Along U.S. Coastlines. NOAA Technical Report NOS 01.* 2022. p. 111.
[19] IPCC, *Summary for Policymakers*, in *IPCC Special Report on the Ocean and Cryosphere in a Changing Climate*, D.C.R. H.-O. Pörtner, V. Masson-Delmotte, P. Zhai, M. Tignor, E. Poloczanska, K. Mintenbeck, A. Alegría, M. Nicolai, A.

Okem, J. Petzold, B. Rama, and N.M. Weyer, Editor. 2019: Cambridge, UK and New York, NY, USA. p. 3-35.
[20] WMO, *State of the Global Climate 2020*. 2021, World Meteorological Organization (WMO): Geneva. p. 56.
[21] WMO, *State of the Global Climate 2024*. 2025, World Meteorological Organization (WMO): Geneva. p. 42.
[22] WMO, *State of the Global Climate 2021*. 2022, World Meteorological Organization (WMO): Geneva. p. 57.
[23] IPCC, *Chapter 2: High Mountain Areas*, in *IPCC Special Report on the Ocean and Cryosphere in a Changing Climate*, D.C.R. H.-O. Pörtner, V. Masson-Delmotte, P. Zhai, M. Tignor, E. Poloczanska, K. Mintenbeck, A. Alegría, M. Nicolai, A. Okem, J. Petzold, B. Rama, and N.M. Weyer, Editor. 2019: Cambridge, UK and New York, NY, USA. p. 131-202.
[24] Zemp, M., et al., *Global glacier mass changes and their contributions to sea-level rise from 1961 to 2016.* Nature, 2019. **568**(7752): p. 382-386.
[25] B. Bolin, B.R.D., J. Jäger, R. A. Warrick, *The greenhouse effect, climatic change and ecosystems*. 1986, Chichester, UK: John Wiley & Sons. 541.
[26] S. H. Schneider, *The greenhouse effect: science and policy.* Science, 1989. **243**(4892): p. 771-81.
[27] WMO, *The State of Greenhouse Gases in the Atmosphere Based on Global Observations through 2024*. 2025: Geneva. p. 10.
[28] Gerlach, T., *Volcanic versus anthropogenic carbon dioxide.* Eos, Transactions American Geophysical Union, 2011. **92**(24): p. 201-202.
[29] M. Saunois, A.R.S., B. Poulter, P. Bousquet, J.G. Canadell, R.B. Jackson, P.A. Raymond, E.J. Dlugokencky, S. Houweling, P.K. Patra, P. Ciais, V.K. Arora, D. Bastviken, P. Bergamaschi, D.R. Blake, G. Brailsford, L. Bruhwiler, K.M. Carlson, M. Carrol, S. Castaldi, N. Chandra, C. Crevoisier, P.M. Crill, K. Covey, C.L. Curry, G. Etiope, C. Frankenberg, N. Gedney, M.I. Hegglin, L. Höglund-Isaksson, G. Hugelius, M. Ishizawa, A. Ito, G. Janssens-Maenhout, K.M. Jensen, F. Joos, T. Kleinen, P.B Krummel, R.L. Langenfelds, G.G. Laruelle, L. Liu, T. Machida, S. Maksyutov, K. C. McDonald, J. McNorton, P.A. Miller, J.R. Melton, I. Morino, J. Müller, F. Murguia-Flores, V. Naik, Y. Niwa, S. Noce, S. O'Doherty, R.J. Parker, C. Peng, S. Peng, G.P. Peters, C. Prigent, R. Prinn, M. Ramonet, P. Regnier, W.J. Riley, J.A. Rosentreter, A. Segers, I.J. Simpson, H. Shi, S.J. Smith, L.P. Steele, B.F. Thornton, H. Tian, Y. Tohjima, F.N. Tubiello, A. Tsuruta, N. Viovy, A. Voulgarakis, T.S. Weber, M. vanWeele, G.R. van der Werf, R.F. Weiss, D. Worthy, D. Wunch, Y. Yin, Y. Yoshida, W. Zhang, Z. Zhang, Y. Zhao, B. Zheng, Q. Zhu, Q. Zhu, Q. Zhuang, , *The Global Methane Budget 2000–2017.* Earth System Science Data, 2020. **12**(3): p. 1561-1623.
[30] Zhu, Z., et al., *Greening of the Earth and its drivers.* Nature Climate Change, 2016. **6**(8): p. 791-795.
[31] Keenan, T.F., et al., *Increase in forest water-use efficiency as atmospheric carbon dioxide concentrations rise.* Nature, 2013. **499**(7458): p. 324-7.
[32] Terrer, C., et al., *Nitrogen and phosphorus constrain the CO2 fertilization of global plant biomass.* Nature Climate Change, 2019. **9**(9): p. 684-689.
[33] M. Crippa, D.G., F. Pagani, M. Banja, M. Muntean, E. Schaaf, R. Quadrelli, A. Risquez Martin, P. Taghavi-Moharamli, J. Köykkä, G. Grassi, S. Rossi, J. Melo, D. Oom, A. Branco, M. Suárez-Moreno, F. Sedano, J. San-Miguel, G. Manca, E. Pisoni, F. Pekar *GHG emissions of all world countries - 2025 Report*, J.I. Report, Editor. 2025, Publications Office of the European Union: Luxembourg.
[34] Labuschagne, C., A.C. Brent, and R.P.G. van Erck, *Assessing the sustainability performances of industries.* Journal of Cleaner Production, 2005. **13**(4): p. 373-385.

[35] Jiang, P., et al., *Analysis of the co-benefits of climate change mitigation and air pollution reduction in China.* Journal of Cleaner Production, 2013. **58**: p. 130-137.
[36] Wei, J., et al., *Industrial SO2 pollution and agricultural losses in China: evidence from heavy air polluters.* Journal of Cleaner Production, 2014. **64**: p. 404-413.
[37] AlFaris, F., A. Juaidi, and F. Manzano-Agugliaro, *Energy retrofit strategies for housing sector in the arid climate.* Energy and Buildings, 2016. **131**: p. 158-171.
[38] Kim, G., H.S. Lim, and J.T. Kim, *Sustainable lighting performance of refurbished glazed walls for old residential buildings.* Energy and Buildings, 2015. **91**: p. 163-169.
[39] Lowry, G., *Energy saving claims for lighting controls in commercial buildings.* Energy and Buildings, 2016. **133**: p. 489-497.
[40] Chen, Y., et al., *Experimental and simulation study on the performance of daylighting in an industrial building and its energy saving potential.* Energy and Buildings, 2014. **73**: p. 184-191.
[41] Wang, L., et al., *Lighting system design based on a sensor network for energy savings in large industrial buildings.* Energy and Buildings, 2015. **105**: p. 226-235.
[42] de Almeida Guimarães, V. and I.C. Leal Junior, *Performance assessment and evaluation method for passenger transportation: a step toward sustainability.* Journal of Cleaner Production, 2017. **142**: p. 297-307.
[43] Amber, K.P., M.W. Aslam, and S.K. Hussain, *Electricity consumption forecasting models for administration buildings of the UK higher education sector.* Energy and Buildings, 2015. **90**: p. 127-136.
[44] Klein-Vielhauer, S., *Framework model to assess leisure and tourism sustainability.* Journal of Cleaner Production, 2009. **17**(4): p. 447-454.
[45] Robèrt, K.-H., *Tools and concepts for sustainable development, how do they relate to a general framework for sustainable development, and to each other?* Journal of Cleaner Production, 2000. **8**(3): p. 243-254.
[46] Bocken, N.M.P., et al., *A literature and practice review to develop sustainable business model archetypes.* Journal of Cleaner Production, 2014. **65**: p. 42-56.
[47] Baños, R., et al., *Optimization methods applied to renewable and sustainable energy: A review.* Renewable and Sustainable Energy Reviews, 2011. **15**(4): p. 1753-1766.
[48] Fernández-García, A., et al., *A parabolic-trough collector for cleaner industrial process heat.* Journal of Cleaner Production, 2015. **89**: p. 272-285.
[49] (IEA), I.E.A., *World Energy Outlook*. 2024.
[50] Attia, S., M. Hamdy, and S. Ezzeldin, *Twenty-year tracking of lighting savings and power density in the residential sector.* Energy and Buildings, 2017. **154**: p. 113-126.
[51] Enongene, K.E., et al., *Energy savings and economic benefits of transition towards efficient lighting in residential buildings in Cameroon.* Renewable and Sustainable Energy Reviews, 2017. **78**: p. 731-742.
[52] Baloch, A.A., et al., *Simulation tools application for artificial lighting in buildings.* Renewable and Sustainable Energy Reviews, 2018. **82**: p. 3007-3026.
[53] Aman, M.M., et al., *Analysis of the performance of domestic lighting lamps.* Energy Policy, 2013. **52**: p. 482-500.
[54] Yadav, V.K., et al., *A Review on Light-Emitting-Diodes Characteristics*, in *2022 International Conference on Intelligent Controller and Computing for Smart Power (ICICCSP)*. 2022. p. 1-6.
[55] Weinold, M.P., S. Kolesnikov, and L.D. Anadón, *Rapid technological progress in white light-emitting diodes and its source in innovation and technology spillovers.* Nature Energy, 2025. **10**(5): p. 616-629.
[56] Morgan Pattison, P., M. Hansen, and J.Y. Tsao, *LED lighting efficacy: Status and directions.* Comptes Rendus. Physique, 2017. **19**(3): p. 134-145.

[57] Agrawal, D.C., H.S. Leff, and V.J. Menon, *Efficiency and efficacy of incandescent lamps.* American Journal of Physics, 1996. **64**(5): p. 649-654.
[58] Robert Friedel, P.I., Bernard S. Finn., *Edison's Electric Light, Biography of an Invention*. 1986: Rutgers University Press. 263.
[59] Waymouth, J.F., *Electric discharge lamps*. 1971, Cambridge: Cambridge, Mass., M.I.T. Press.
[60] Planck, M., *The Theory of Heat Radiation*. 1989, Melville, NY: American Institute of Physics. 470.
[61] (IESNA), I.E.S.o.N.A., *The IESNA lighting handbook : reference & application*, ed. M.S. Rea. 1950, New York: Illuminating Engineering Society of North America.
[62] DiLaura, D., *A Brief History of Lighting.* Optics and Photonics News, 2008. **19**(9).
[63] Maxson, P., M. Bender, and A. Culver, *Mercury in Fluorescent Lighting, Unnecessary health risks and actionable solutions*, A. Carreño, Editor. 2021.
[64] Tan, Q., Q. Song, and J. Li, *The environmental performance of fluorescent lamps in China, assessed with the LCA method.* The International Journal of Life Cycle Assessment, 2015. **20**(6): p. 807-818.
[65] Li, Z., et al., *Mercury Pollution, Treatment and Solutions in Spent Fluorescent Lamps in Mainland China.* Int J Environ Res Public Health, 2018. **15**(12).
[66] Iqbal, A., et al., *Effects of Using Fluorescent and Compact Fluorescent Lamps on Environment and Health-A Critical View.* i-manager's Journal on Future Engineering and Technology, 2015. **10**(4): p. 28-37.
[67] Tony Furfari, F.A. and H. Wallace, *History: A Different Kind of Chemistry: A History of Tungsten Halogen Lamps.* IEEE Industry Applications Magazine, 2001. **7**(6): p. 10-17.
[68] Wagner, T.P., *Compact fluorescent lights and the impact of convenience and knowledge on household recycling rates.* Waste Manag, 2011. **31**(6): p. 1300-6.
[69] Wang, Y., J.M. Alonso, and X. Ruan, *A Review of LED Drivers and Related Technologies.* IEEE Transactions on Industrial Electronics, 2017. **64**(7): p. 5754-5765.
[70] Ji, C., et al., *Light of carbon: Recent advancements of carbon dots for LEDs.* Nano Energy, 2023. **114**.
[71] Reineke, S., et al., *White organic light-emitting diodes: Status and perspective.* Reviews of Modern Physics, 2013. **85**(3): p. 1245-1293.
[72] Schubert, E.F. and J.K. Kim, *Solid-state light sources getting smart.* Science, 2005. **308**(5726): p. 1274-8.
[73] Cho, J., et al., *White light-emitting diodes: History, progress, and future.* Laser & Photonics Reviews, 2017. **11**(2).
[74] Chang, M.-H., et al., *Light emitting diodes reliability review.* Microelectronics Reliability, 2012. **52**(5): p. 762-782.
[75] Sun, C.-C., et al., *Packaging efficiency in phosphor-converted white LEDs and its impact to the limit of luminous efficacy.* Journal of Solid State Lighting, 2014. **1**(1).
[76] Wang, R., et al., *Energy Regulation in White-Light-Emitting Diodes.* ACS Energy Letters, 2022. **7**(6): p. 2173-2188.
[77] Huang, Y., et al., *Mini-LED, Micro-LED and OLED displays: present status and future perspectives.* Light Sci Appl, 2020. **9**: p. 105.
[78] Wu, Y., et al., *Full-Color Realization of Micro-LED Displays.* Nanomaterials (Basel), 2020. **10**(12).
[79] Sze, S.M. and K.K. Ng, *Physics of Semiconductor Devices*. 2006.
[80] Streetman, B.G. and S.K. Banerjee, *Solid State electronic devices*. Seventh edition Global edition. 2015, England: Pearson Education Limited.
[81] Schubert, E.F., *Light-Emitting Diodes*. 2012.
[82] Singh, J., *Semiconductor optoelectronics : physics and technology*. 1995, New York: McGraw-Hill.
[83] Hummel, R.E., *Electronic Properties of Materials*. 1993.

[84] Pimputkar, S., et al., *Prospects for LED lighting.* Nature Photonics, 2009. **3**(4): p. 180-182.
[85] Meretska, M.L., et al., *Systematic Design of the Color Point of a White LED.* ACS Photonics, 2019. **6**(12): p. 3070-3075.
[86] Islam, N.U., et al., *Review—White Light-Emitting Diodes: Past, Present, and Future.* ECS Journal of Solid State Science and Technology, 2021. **10**(10).
[87] Parauha, Y.R., et al., *Review on advancements in white light phosphor matrices for energy-efficient lighting.* Materials Science in Semiconductor Processing, 2024. **184**.
[88] Cesaria, M. and B. Di Bartolo, *Nanophosphors-Based White Light Sources.* Nanomaterials (Basel), 2019. **9**(7).
[89] Ye, S., et al., *Phosphors in phosphor-converted white light-emitting diodes: Recent advances in materials, techniques and properties.* Materials Science and Engineering: R: Reports, 2010. **71**(1): p. 1-34.
[90] Scholand, M. and H. Dillon, *Life-Cycle Assessment of Energy and Environmental Impacts of LED Lighting Products. Part 2: LED Manufacturing and Performance*. 2012.
[91] Gao, W., et al., *Green manufacturing evaluation of light-emitting diodes lamps production: Resource and environmental assessment.* Renewable and Sustainable Energy Reviews, 2025. **211**.
[92] Lim, S.R., et al., *Potential environmental impacts from the metals in incandescent, compact fluorescent lamp (CFL), and light-emitting diode (LED) bulbs.* Environ Sci Technol, 2013. **47**(2): p. 1040-7.
[93] Vinhal, J.T., et al., *Characterization of end-of-life LEDs: Mapping critical, valuable and hazardous elements in different devices.* Waste Manag, 2022. **151**: p. 113-122.
[94] Binnemans, K., et al., *Recycling of rare earths: a critical review.* Journal of Cleaner Production, 2013. **51**: p. 1-22.
[95] Zhang, H., J. Burr, and F. Zhao, *A comparative life cycle assessment (LCA) of lighting technologies for greenhouse crop production.* Journal of Cleaner Production, 2017. **140**: p. 705-713.
[96] Zamprogno Rebello, R., et al., *Characterization of end-of-life LED lamps for the recovery of precious metals and rare earth elements.* Resources, Conservation and Recycling, 2020. **153**.
[97] Cajochen, C., et al., *High sensitivity of human melatonin, alertness, thermoregulation, and heart rate to short wavelength light.* J Clin Endocrinol Metab, 2005. **90**(3): p. 1311-6.
[98] Falchi, F., et al., *The new world atlas of artificial night sky brightness.* Sci Adv, 2016. **2**(6): p. e1600377.
[99] Yuan, T., et al., *The emergence and prospects of carbon dots with solid-state photoluminescence for light-emitting diodes.* Mater Horiz, 2024. **11**(1): p. 102-112.
[100] Esteves da Silva, J.C.G. and H.M.R. Gonçalves, *Analytical and bioanalytical applications of carbon dots.* TrAC Trends in Analytical Chemistry, 2011. **30**(8): p. 1327-1336.
[101] Wang, R., et al., *Recent progress in carbon quantum dots: synthesis, properties and applications in photocatalysis.* Journal of Materials Chemistry A, 2017. **5**(8): p. 3717-3734.
[102] Zhou, J., et al., *Carbon dots doped with heteroatoms for fluorescent bioimaging: a review.* Microchimica Acta, 2016. **184**(2): p. 343-368.
[103] Xu, X., et al., *Electrophoretic analysis and purification of fluorescent single-walled carbon nanotube fragments.* J Am Chem Soc, 2004. **126**(40): p. 12736-7.
[104] Sun, Y.P., et al., *Quantum-sized carbon dots for bright and colorful photoluminescence.* J Am Chem Soc, 2006. **128**(24): p. 7756-7.

[105] Amir, D., et al., *Oncometabolite Fingerprinting Using Fluorescent Single-Walled Carbon Nanotubes.* Advanced Materials Interfaces, 2021. **9**(4).
[106] Abdullah, T.A., et al., *Functionalized multi-walled carbon nanotubes for oil spill cleanup from water.* Clean Technologies and Environmental Policy, 2021. **24**(2): p. 519-541.
[107] Norouzi, A., et al., *Functionalized nanodiamonds in polyurethane mixed matrix membranes for carbon dioxide separation.* Results in Materials, 2022. **13**.
[108] Chhetri, K., et al., *Hollow Carbon Nanofibers with Inside-outside Decoration of Bi-metallic MOF Derived Ni-Fe Phosphides as Electrode Materials for Asymmetric Supercapacitors.* Chemical Engineering Journal, 2022. **450**.
[109] Lu, D., et al., *Graphene coated sand for smart cement composites.* Construction and Building Materials, 2022. **346**.
[110] Jayanand, K., et al., *Sc3N@C80 and La@C82 doped graphene for a new class of optoelectronic devices.* Journal of Materials Chemistry C, 2020. **8**(12): p. 3970-3981.
[111] Simoes, E.F.C., et al., *Hypochlorite fluorescence sensing by phenylboronic acid-alizarin adduct based carbon dots.* Talanta, 2020. **208**: p. 120447.
[112] Wang, B., et al., *Carbon Dot Based Multicolor Electroluminescent LEDs with Nearly 100% Exciton Utilization Efficiency.* Nano Lett, 2023. **23**(18): p. 8794-8800.
[113] Yuan, F., et al., *Engineering triangular carbon quantum dots with unprecedented narrow bandwidth emission for multicolored LEDs.* Nat Commun, 2018. **9**(1): p. 2249.
[114] Crista, D., et al., *Investigation of the role of pH and the stoichiometry of the N-dopant in the luminescence, composition and synthesis yield of carbon dots.* J Mater Chem B, 2023. **11**(5): p. 1131-1143.
[115] Sendão, R.M.S., et al., *Carbon Dots–TiO2 Nanocomposites for the Enhanced Visible-Light Driven Photodegradation of Methylene Blue.* Advanced Sustainable Systems, 2023. **8**(1).
[116] Fernandes, S., et al., *Development of a Facile and Green Synthesis Strategy for Brightly Fluorescent Carbon Dots from Various Waste Materials.* ChemSusChem, 2025. **18**(2): p. e202401702.
[117] Jiang, L., et al., *UV-Vis-NIR Full-Range Responsive Carbon Dots with Large Multiphoton Absorption Cross Sections and Deep-Red Fluorescence at Nucleoli and In Vivo.* Small, 2020. **16**(19): p. e2000680.
[118] Algarra, M., et al., *Insights into the formation of N doped 3D-graphene quantum dots. Spectroscopic and computational approach.* J Colloid Interface Sci, 2020. **561**: p. 678-686.
[119] Sendao, R.M.S., et al., *Insight into the hybrid luminescence showed by carbon dots and molecular fluorophores in solution.* Phys Chem Chem Phys, 2019. **21**(37): p. 20919-20926.
[120] Kozák, O., et al., *Surfactant-Derived Amphiphilic Carbon Dots with Tunable Photoluminescence.* The Journal of Physical Chemistry C, 2013. **117**(47): p. 24991-24996.
[121] Vale, N., et al., *Normal breast epithelial MCF-10A cells to evaluate the safety of carbon dots.* RSC Med Chem, 2021. **12**(2): p. 245-253.
[122] Wang, K., et al., *Systematic safety evaluation on photoluminescent carbon dots.* Nanoscale Res Lett, 2013. **8**(1): p. 122.
[123] Crista, D.M.A., et al., *3-Hydroxyphenylboronic Acid-Based Carbon Dot Sensors for Fructose Sensing.* J Fluoresc, 2019. **29**(1): p. 265-270.
[124] Liu, Q., et al., *Synthesis of highly fluorescent carbon dots as a dual-excitation rationmetric fluorescent probe for the fast detection of chlorogenic acid.* Talanta, 2021. **221**: p. 121372.
[125] Mello, G.P.C., et al., *Glucose Sensing by Fluorescent Nanomaterials.* Crit Rev Anal Chem, 2019. **49**(6): p. 542-552.

[126] Qiu, Y., et al., *Facile, green and energy-efficient preparation of fluorescent carbon dots from processed traditional Chinese medicine and their applications for on-site semi-quantitative visual detection of Cr(VI).* Sensors and Actuators B: Chemical, 2020. **324**.
[127] Afonso, A.C.P., et al., *An Active Surface Preservation Strategy for the Rational Development of Carbon Dots as pH-Responsive Fluorescent Nanosensors.* Chemosensors, 2021. **9**(8).
[128] Kang, Y.F., et al., *Carbon Quantum Dots for Zebrafish Fluorescence Imaging.* Sci Rep, 2015. **5**: p. 11835.
[129] Bogireddy, N.K.R., et al., *One-step hydrothermal preparation of highly stable N doped oxidized carbon dots for toxic organic pollutants sensing and bioimaging.* Chemical Engineering Journal, 2020. **401**.
[130] Ding, Y., et al., *Serratia marcescens-derived fluorescent carbon dots as a platform toward multi-mode bioimaging and detection of p-nitrophenol.* Analyst, 2021. **146**(2): p. 683-690.
[131] Zhang, H., et al., *One step synthesis of efficient red emissive carbon dots and their bovine serum albumin composites with enhanced multi-photon fluorescence for in vivo bioimaging.* Light Sci Appl, 2022. **11**(1): p. 113.
[132] Li, D., et al., *Synthesis of a carbon dots modified g-C(3)N(4)/SnO(2) Z-scheme photocatalyst with superior photocatalytic activity for PPCPs degradation under visible light irradiation.* J Hazard Mater, 2021. **401**: p. 123257.
[133] Zhu, Z., et al., *Synthesis of carbon dots with high photocatalytic reactivity by tailoring heteroatom doping.* J Colloid Interface Sci, 2022. **605**: p. 330-341.
[134] Sendão, R.M.S., et al., *Visible-light-driven photocatalytic degradation of organic dyes using a TiO2 and waste-based carbon dots nanocomposite.* Colloids and Surfaces A: Physicochemical and Engineering Aspects, 2025. **713**.
[135] Wang, Y., et al., *High color rendering index trichromatic white and red LEDs prepared from silane-functionalized carbon dots.* Journal of Materials Chemistry C, 2017. **5**(37): p. 9629-9637.
[136] Wang, C., et al., *Polymer-Assisted Self-Assembly of Multicolor Carbon Dots as Solid-State Phosphors for Fabrication of Warm, High-Quality, and Temperature-Responsive White-Light-Emitting Devices.* ACS Appl Mater Interfaces, 2019. **11**(25): p. 22332-22338.
[137] An, Y., et al., *Preparation of Multicolour Solid Fluorescent Carbon Dots for Light-Emitting Diodes Using Phenylethylamine as a Co-Carbonization Agent.* Int J Mol Sci, 2022. **23**(19).
[138] Yuan, F., et al., *Bright high-colour-purity deep-blue carbon dot light-emitting diodes via efficient edge amination.* Nature Photonics, 2019. **14**(3): p. 171-176.
[139] Hettiarachchi, S.D., et al., *Triple conjugated carbon dots as a nano-drug delivery model for glioblastoma brain tumors.* Nanoscale, 2019. **11**(13): p. 6192-6205.
[140] Kong, T., et al., *Doxorubicin conjugated carbon dots as a drug delivery system for human breast cancer therapy.* Cell Prolif, 2018. **51**(5): p. e12488.
[141] Yan, L., et al., *Synthesis of carbon quantum dots by chemical vapor deposition approach for use in polymer solar cell as the electrode buffer layer.* Carbon, 2016. **109**: p. 598-607.
[142] Huang, P., et al., *Green carbon dots based ultraviolet photovoltaic window with high transparence to visible light.* International Journal of Energy Research, 2021. **45**(12): p. 17709-17720.
[143] Knoblauch, R. and C.D. Geddes, *Carbon Nanodots in Photodynamic Antimicrobial Therapy: A Review.* Materials (Basel), 2020. **13**(18).
[144] He, H., et al., *Diketopyrrolopyrrole-based carbon dots for photodynamic therapy.* Nanoscale, 2018. **10**(23): p. 10991-10998.

[145] Yang, K., et al., *Bioluminescence-initiated photodynamic therapy bridged on high-luminescent carbon dots-conjugated protoporphyrin IX.* Journal of Materials Science, 2018. **54**(4): p. 3383-3391.
[146] Magalhaes, C.M., et al., *Safety Evaluation of Carbon Dots in UM-UC-5 and A549 Cells for Biomedical Applications.* Cancers (Basel), 2024. **16**(19).
[147] Sen, S. and A. Bose, *Carbon dots: A review of innovations, applications, challenges, and future prospects.* Inorganic Chemistry Communications, 2025. **173**.
[148] Dey, S., et al., *Luminescence properties of boron and nitrogen doped graphene quantum dots prepared from arc-discharge-generated doped graphene samples.* Chemical Physics Letters, 2014. **595-596**: p. 203-208.
[149] Nguyen, V., et al., *Double-pulse femtosecond laser ablation for synthesis of ultrasmall carbon nanodots.* Materials Research Express, 2020. **7**(1).
[150] Gu, S., et al., *Optimization of graphene quantum dots by chemical exfoliation from graphite powders and carbon nanotubes.* Materials Chemistry and Physics, 2018. **215**: p. 104-111.
[151] Zhu, Y., et al., *One-step ultrasonic synthesis of graphene quantum dots with high quantum yield and their application in sensing alkaline phosphatase.* Chem Commun (Camb), 2015. **51**(5): p. 948-51.
[152] Joseph, J. and A.A. Anappara, *White-Light-Emitting Carbon Dots Prepared by the Electrochemical Exfoliation of Graphite.* Chemphyschem, 2017. **18**(3): p. 292-298.
[153] Ozyurt, D., et al., *Properties, synthesis, and applications of carbon dots: A review.* Carbon Trends, 2023. **12**.
[154] Sciortino, A., A. Cannizzo, and F. Messina, *Carbon Nanodots: A Review—From the Current Understanding of the Fundamental Photophysics to the Full Control of the Optical Response.* C, 2018. **4**(4).
[155] Tajik, S., et al., *Carbon and graphene quantum dots: a review on syntheses, characterization, biological and sensing applications for neurotransmitter determination.* RSC Adv, 2020. **10**(26): p. 15406-15429.
[156] Li, L., et al., *Kilogram-Scale Synthesis and Functionalization of Carbon Dots for Superior Electrochemical Potassium Storage.* ACS Nano, 2021. **15**(4): p. 6872-6885.
[157] Christe, S., J.C.G. Esteves da Silva, and L. Pinto da Silva, *Evaluation of the Environmental Impact and Efficiency of N-Doping Strategies in the Synthesis of Carbon Dots.* Materials (Basel), 2020. **13**(3).
[158] Wang, C., et al., *A strong blue fluorescent nanoprobe for highly sensitive and selective detection of mercury(II) based on sulfur doped carbon quantum dots.* Materials Chemistry and Physics, 2019. **232**: p. 145-151.
[159] Xu, Q., et al., *Preparation of highly photoluminescent sulfur-doped carbon dots for Fe(iii) detection.* Journal of Materials Chemistry A, 2015. **3**(2): p. 542-546.
[160] Somaraj, G., et al., *Nitrogen and Sulfur Co‐Doped Carbon Quantum Dots for Sensing Applications: A Review.* ChemistrySelect, 2022. **7**(19).
[161] Qiao, Z.A., et al., *Commercially activated carbon as the source for producing multicolor photoluminescent carbon dots by chemical oxidation.* Chem Commun (Camb), 2010. **46**(46): p. 8812-4.
[162] Li, H., et al., *Water-soluble fluorescent carbon quantum dots and photocatalyst design.* Angew Chem Int Ed Engl, 2010. **49**(26): p. 4430-4.
[163] Peng, J., et al., *Graphene quantum dots derived from carbon fibers.* Nano Lett, 2012. **12**(2): p. 844-9.
[164] Liu, H., T. Ye, and C. Mao, *Fluorescent carbon nanoparticles derived from candle soot.* Angew Chem Int Ed Engl, 2007. **46**(34): p. 6473-5.

[165] Shinde, D.B. and V.K. Pillai, *Electrochemical preparation of luminescent graphene quantum dots from multiwalled carbon nanotubes.* Chemistry, 2012. **18**(39): p. 12522-8.
[166] Dong, Y., et al., *One-step and high yield simultaneous preparation of single- and multi-layer graphene quantum dots from CX-72 carbon black.* Journal of Materials Chemistry, 2012. **22**(18).
[167] Chu, K.W., et al., *Recent Progress of Carbon Dot Precursors and Photocatalysis Applications.* Polymers (Basel), 2019. **11**(4).
[168] Crista, D.M.A., J.C.G. Esteves da Silva, and L. Pinto da Silva, *Evaluation of Different Bottom-up Routes for the Fabrication of Carbon Dots.* Nanomaterials (Basel), 2020. **10**(7).
[169] Zhou, Y., et al., *Photoluminescent Carbon Dots: A Mixture of Heterogeneous Fractions.* Chemphyschem, 2018. **19**(19): p. 2589-2597.
[170] Sahiner, N., et al., *Nitrogen and Sulfur Doped Carbon Dots from Amino Acids for Potential Biomedical Applications.* J Fluoresc, 2019. **29**(5): p. 1191-1200.
[171] Ding, H., et al., *Large scale synthesis of full-color emissive carbon dots from a single carbon source by a solvent-free method.* Nano Research, 2021. **15**(4): p. 3548-3555.
[172] Cailotto, S., et al., *Carbon Dots from Sugars and Ascorbic Acid: Role of the Precursors on Morphology, Properties, Toxicity, and Drug Uptake.* ACS Med Chem Lett, 2018. **9**(8): p. 832-837.
[173] Cardoso, R.M.F., et al., *Copper(II)-Doped Carbon Dots as Catalyst for Ozone Degradation of Textile Dyes.* Nanomaterials (Basel), 2022. **12**(7).
[174] Johny, A., et al., *Sustainability Assessment of Highly Fluorescent Carbon Dots Derived from Eucalyptus Leaves.* Environments, 2024. **11**(1).
[175] Zhang, Z., W. Sun, and P. Wu, *Highly Photoluminescent Carbon Dots Derived from Egg White: Facile and Green Synthesis, Photoluminescence Properties, and Multiple Applications.* ACS Sustainable Chemistry & Engineering, 2015. **3**(7): p. 1412-1418.
[176] Aldakhil, F., et al., *Hydrothermal synthesis of modified lignin-based carbon dots derived from biomass waste for fluorescence determination of valsartan.* RSC Adv, 2024. **14**(28): p. 19969-19982.
[177] Lim, S.Y., W. Shen, and Z. Gao, *Carbon quantum dots and their applications.* Chem Soc Rev, 2015. **44**(1): p. 362-81.
[178] Baker, S.N. and G.A. Baker, *Luminescent carbon nanodots: emergent nanolights.* Angew Chem Int Ed Engl, 2010. **49**(38): p. 6726-44.
[179] Xie, R., et al., *Graphene quantum dots as smart probes for biosensing.* Analytical Methods, 2016. **8**(20): p. 4001-4016.
[180] Sagbas, S. and N. Sahiner, *Carbon dots: preparation, properties, and application*, in *Nanocarbon and its Composites*. 2019. p. 651-676.
[181] Sadjadi, S., *The utility of carbon dots for photocatalysis*, in *Emerging Carbon Materials for Catalysis*. 2021. p. 123-160.
[182] Liu, J., R. Li, and B. Yang, *Carbon Dots: A New Type of Carbon-Based Nanomaterial with Wide Applications.* ACS Cent Sci, 2020. **6**(12): p. 2179-2195.
[183] Benner, D., P. Yadav, and D. Bhatia, *Red emitting carbon dots: surface modifications and bioapplications.* Nanoscale Adv, 2023. **5**(17): p. 4337-4353.
[184] Zhu, S., et al., *The photoluminescence mechanism in carbon dots (graphene quantum dots, carbon nanodots, and polymer dots): current state and future perspective.* Nano Research, 2015. **8**(2): p. 355-381.
[185] Park, Y., et al., *Improving the functionality of carbon nanodots: doping and surface functionalization.* Journal of Materials Chemistry A, 2016. **4**(30): p. 11582-11603.
[186] Shanmugasundaram, E., et al., *Heteroatom (boron, nitrogen, and fluorine) quantum dot-doped polyaniline-photoactive film preparation and characterization*

for organic solar cell applications. New Journal of Chemistry, 2023. **47**(28): p. 13127-13137.
[187] Wibrianto, A., et al., *Comparison of the effects of synthesis methods of B, N, S, and P-doped carbon dots with high photoluminescence properties on HeLa tumor cells.* RSC Adv, 2020. **11**(2): p. 1098-1108.
[188] Wibrianto, A., et al., *Naproxen release aspect from boron-doped carbon nanodots as a bifunctional agent in cancer therapy.* RSC Adv, 2021. **11**(59): p. 37375-37382.
[189] Yu, J., et al., *Theoretical Understanding of Structure-Property Relationships in Luminescence of Carbon Dots.* J Phys Chem Lett, 2021. **12**(32): p. 7671-7687.
[190] Yu, R., et al., *Metal and non-metal doped carbon dots: properties and applications.* Light: Advanced Manufacturing, 2024. **5**(4).
[191] Kajani, A.A., et al., *Heteroatom-doped magneto-fluorescent carbon dots, a potent agent for multimodal imaging.* Sci Rep, 2024. **14**(1): p. 29111.
[192] De, B., *Carbon Dots and Their Polymeric Nanocomposites*, in *Nanomaterials and Polymer Nanocomposites*. 2019. p. 217-260.
[193] Yadegari, A., et al., *Bottom-up synthesis of nitrogen and oxygen co-decorated carbon quantum dots with enhanced DNA plasmid expression.* Colloids Surf B Biointerfaces, 2019. **184**: p. 110543.
[194] Bao, H., et al., *Luminescence of carbon quantum dots and their application in biochemistry.* Heliyon, 2023. **9**(10): p. e20317.
[195] Shamsipur, M., A. Barati, and S. Karami, *Long-wavelength, multicolor, and white-light emitting carbon-based dots: Achievements made, challenges remaining, and applications.* Carbon, 2017. **124**: p. 429-472.
[196] Liu, M.L., et al., *Carbon dots: synthesis, formation mechanism, fluorescence origin and sensing applications.* Green Chemistry, 2019. **21**(3): p. 449-471.
[197] Wang, Q., et al., *Microwave–hydrothermal synthesis of fluorescent carbon dots from graphite oxide.* Carbon, 2011. **49**(9): p. 3134-3140.
[198] Xu, Q., et al., *Enhancing the luminescence of carbon dots by doping nitrogen element and its application in the detection of Fe(III).* Journal of Materials Science, 2015. **50**(6): p. 2571-2576.
[199] Nasrin, A., et al., *Conjugated ternary doped carbon dots from vitamin B derivative: Multispectral nanoprobes for targeted melanoma bioimaging and photosensitization.* Journal of Luminescence, 2020. **217**.
[200] Atchudan, R., et al., *Facile green synthesis of nitrogen-doped carbon dots using Chionanthus retusus fruit extract and investigation of their suitability for metal ion sensing and biological applications.* Sensors and Actuators B: Chemical, 2017. **246**: p. 497-509.
[201] Qi, H., et al., *Novel N-doped carbon dots derived from citric acid and urea: fluorescent sensing for determination of metronidazole and cytotoxicity studies.* RSC Adv, 2023. **13**(4): p. 2663-2671.
[202] Do, T.T.A., et al., *Complexation Nanoarchitectonics of Carbon Dots with Doxorubicin toward Photodynamic Anti-Cancer Therapy.* J Funct Biomater, 2022. **13**(4).
[203] Song, H., et al., *Designed controllable nitrogen-doped carbon-dots-loaded MoP nanoparticles for boosting hydrogen evolution reaction in alkaline medium.* Nano Energy, 2020. **72**.
[204] Kolekar, A.G., et al., *Facile synthesis of sulphur-doped carbon dots (S-CDs) using a hydrothermal method for the selective sensing of Cr(6+) and Fe(3+) ions: application to environmental water sample analysis.* RSC Adv, 2024. **14**(5): p. 3473-3479.
[205] Zhang, Q., et al., *Photoluminescence mechanism of carbon dots: triggering high-color-purity red fluorescence emission through edge amino protonation.* Nat Commun, 2021. **12**(1): p. 6856.

[206] Ma, Z., et al., *Research on light-responsive luminescence properties of carbon dots and their applications.* Mater Horiz, 2025. **12**(17): p. 6558-6586.
[207] Liu, M., *Optical Properties of Carbon Dots: A Review.* Nanoarchitectonics, 2020. **1**(1): p. 1-12.
[208] Wang, Y. and A. Hu, *Carbon quantum dots: synthesis, properties and applications.* Journal of Materials Chemistry C, 2014. **2**(34).
[209] John, B.K., T. Abraham, and B. Mathew, *A Review on Characterization Techniques for Carbon Quantum Dots and Their Applications in Agrochemical Residue Detection.* J Fluoresc, 2022. **32**(2): p. 449-471.
[210] Huo, X., et al., *Solvent Effects on Fluorescence Properties of Carbon Dots: Implications for Multicolor Imaging.* ACS Omega, 2021. **6**(40): p. 26499-26508.
[211] Yoshinaga, T., et al., *Glycothermally Synthesized Carbon Dots with Narrow-Bandwidth and Color-Tunable Solvatochromic Fluorescence for Wide-Color-Gamut Displays.* ACS Omega, 2021. **6**(2): p. 1741-1750.
[212] Mohammad-Jafarieh, P., et al., *Solvent effect on the absorption and emission spectra of carbon dots: evaluation of ground and excited state dipole moment.* BMC Chem, 2021. **15**(1): p. 53.
[213] He, Z., et al., *Recent advances of solvent-engineered carbon dots: A review.* Carbon, 2023. **204**: p. 76-93.
[214] Rao, L., et al., *Multicolor Luminescent Carbon Dots: Tunable Photoluminescence, Excellent Stability, and Their Application in Light-Emitting Diodes.* Nanomaterials (Basel), 2022. **12**(18).
[215] Zheng, B., *A Review of the Application of Green Solvents in Organic Synthesis.* Theoretical and Natural Science, 2025. **119**(1): p. 16-24.
[216] Maki, M.A.A., et al., *Green solvents as a sustainable strategy to reduce the impact of hazardous waste on human health.* Discover Chemistry, 2025. **2**(1).
[217] Santos M, A.A., Lopes C, Oliveira T. *Toxicidade dos Solventes em Contexto Laboral*. Revista Portuguesa de Saúde Ocupacional, 2019. **2**, 1-22 DOI: 10.31252/RPSO/05.10.2019.
[218] Nam, N.N., et al., *Design Strategy and Application of Deep Eutectic Solvents for Green Synthesis of Nanomaterials.* Nanomaterials (Basel), 2023. **13**(7).
[219] Wang, Z., et al., *A review of designable deep eutectic solvents for green fabrication of advanced functional materials.* RSC Sustainability, 2025. **3**(2): p. 738-756.
[220] Zhou, Y., et al., *Deep eutectic-like solvents: Promising green media for biomass treatment and preparation of nanomaterials.* BioResources, 2022. **17**(3): p. 5485-5509.
[221] Eckelman, M.J., J.B. Zimmerman, and P.T. Anastas, *Toward Green Nano.* Journal of Industrial Ecology, 2008. **12**(3): p. 316-328.
[222] Bafana, A., et al., *Evaluating microwave-synthesized silver nanoparticles from silver nitrate with life cycle assessment techniques.* Sci Total Environ, 2018. **636**: p. 936-943.
[223] Chahal, S., et al., *Green synthesis of carbon dots and their applications.* RSC Adv, 2021. **11**(41): p. 25354-25363.
[224] Fernandes, S., J.C.G. Esteves da Silva, and L. Pinto da Silva, *Life Cycle Assessment-Based Comparative Study between High-Yield and "Standard" Bottom-Up Procedures for the Fabrication of Carbon Dots.* Materials (Basel), 2022. **15**(10).
[225] Salieri, B., et al., *Life cycle assessment of manufactured nanomaterials: Where are we?* NanoImpact, 2018. **10**: p. 108-120.
[226] Pourzahedi, L. and M.J. Eckelman, *Comparative life cycle assessment of silver nanoparticle synthesis routes.* Environmental Science: Nano, 2015. **2**(4): p. 361-369.

[227] Fernandes, S., J.C.G. Esteves da Silva, and L. Pinto da Silva, *Comparative life cycle assessment of high-yield synthesis routes for carbon dots.* NanoImpact, 2021. **23**: p. 100332.
[228] Ramos, A., C. Afonso Teixeira, and A. Rouboa, *Environmental Analysis of Waste-to-Energy—A Portuguese Case Study.* Energies, 2018. **11**(3).
[229] Ramos, A., C.A. Teixeira, and A. Rouboa, *Assessment study of an advanced gasification strategy at low temperature for syngas generation.* International Journal of Hydrogen Energy, 2018. **43**(21): p. 10155-10166.
[230] Hischier, R. and T. Walser, *Life cycle assessment of engineered nanomaterials: state of the art and strategies to overcome existing gaps.* Sci Total Environ, 2012. **425**: p. 271-82.
[231] Feijoo, S., et al., *Comparative life cycle assessment of different synthesis routes of magnetic nanoparticles.* Journal of Cleaner Production, 2017. **143**: p. 528-538.
[232] Pu, Y., et al., *Fate and Characterization Factors of Nanoparticles in Seventeen Subcontinental Freshwaters: A Case Study on Copper Nanoparticles.* Environ Sci Technol, 2016. **50**(17): p. 9370-9.
[233] Piccinno, F., et al., *Predicting the environmental impact of a future nanocellulose production at industrial scale: Application of the life cycle assessment scale-up framework.* Journal of Cleaner Production, 2018. **174**: p. 283-295.
[234] Teah, H.Y., et al., *Life Cycle Greenhouse Gas Emissions of Long and Pure Carbon Nanotubes Synthesized via On-Substrate and Fluidized-Bed Chemical Vapor Deposition.* ACS Sustainable Chemistry & Engineering, 2020. **8**(4): p. 1730-1740.
[235] Temizel-Sekeryan, S. and A.L. Hicks, *Global environmental impacts of silver nanoparticle production methods supported by life cycle assessment.* Resources, Conservation and Recycling, 2020. **156**.
[236] Temizel-Sekeryan, S., F. Wu, and A.L. Hicks, *Global scale life cycle environmental impacts of single- and multi-walled carbon nanotube synthesis processes.* The International Journal of Life Cycle Assessment, 2021. **26**(4): p. 656-672.
[237] Upadhyayula, V.K.K., et al., *Life cycle assessment as a tool to enhance the environmental performance of carbon nanotube products: a review.* Journal of Cleaner Production, 2012. **26**: p. 37-47.
[238] Deng, Y., et al., *Deriving characterization factors on freshwater ecotoxicity of graphene oxide nanomaterial for life cycle impact assessment.* The International Journal of Life Cycle Assessment, 2016. **22**(2): p. 222-236.
[239] Celik, I., et al., *Environmental Impacts from Photovoltaic Solar Cells Made with Single Walled Carbon Nanotubes.* Environ Sci Technol, 2017. **51**(8): p. 4722-4732.
[240] Fernandes, S., J.C.G. Esteves da Silva, and L. Pinto da Silva, *Life Cycle Assessment of the Sustainability of Enhancing the Photodegradation Activity of TiO(2) with Metal-Doping.* Materials (Basel), 2020. **13**(7).
[241] Sendão, R., et al., *Comparative life cycle assessment of bottom-up synthesis routes for carbon dots derived from citric acid and urea.* Journal of Cleaner Production, 2020. **254**.
[242] Pini, M., et al., *Assessment of Environmental Performance of TiO2 Nanoparticles Coated Self-Cleaning Float Glass.* Coatings, 2017. **7**(1).
[243] Zhang, B., et al., *Sustainable Synthesis of Bright Green Fluorescent Nitrogen-Doped Carbon Quantum Dots from Alkali Lignin.* ChemSusChem, 2019. **12**(18): p. 4202-4210.
[244] Crista, D.M.A., et al., *Turning Spent Coffee Grounds into Sustainable Precursors for the Fabrication of Carbon Dots.* Nanomaterials (Basel), 2020. **10**(6).
[245] Xie, Y., et al., *Green Hydrothermal Synthesis of N-doped Carbon Dots from Biomass Highland Barley for the Detection of Hg(2).* Sensors (Basel), 2019. **19**(14).

[246] Algarra, M., et al., *Sustainable Production of Carbon Nanoparticles from Olive Pit Biomass: Understanding Proton Transfer in the Excited State on Carbon Dots.* ACS Sustainable Chemistry & Engineering, 2019. **7**(12): p. 10493-10500.
[247] Bhamore, J.R., et al., *Facile green synthesis of carbon dots from Pyrus pyrifolia fruit for assaying of Al3+ ion via chelation enhanced fluorescence mechanism.* Journal of Molecular Liquids, 2018. **264**: p. 9-16.
[248] Atchudan, R., et al., *Hydrophilic nitrogen-doped carbon dots from biowaste using dwarf banana peel for environmental and biological applications.* Fuel, 2020. **275**.
[249] Li, Z., et al., *A fluorescence probe based on the nitrogen-doped carbon dots prepared from orange juice for detecting Hg 2+ in water.* Journal of Luminescence, 2017. **187**: p. 274-280.
[250] Senol, A.M. and E. Bozkurt, *Facile green and one-pot synthesis of seville orange derived carbon dots as a fluorescent sensor for Fe3+ ions.* Microchemical Journal, 2020. **159**.
[251] Sharma, S., et al., *Fluorescent spongy carbon nanoglobules derived from pineapple juice: A potential sensing probe for specific and selective detection of chromium (VI) ions.* Ceramics International, 2017. **43**(9): p. 7011-7019.
[252] Lu, M., et al., *Green preparation of versatile nitrogen-doped carbon quantum dots from watermelon juice for cell imaging, detection of Fe3+ ions and cysteine, and optical thermometry.* Journal of Molecular Liquids, 2018. **269**: p. 766-774.
[253] Hoan, B.T., et al., *A green luminescence of lemon derived carbon quantum dots and their applications for sensing of V5+ ions.* Materials Science and Engineering: B, 2019. **251**.
[254] Luo, P.G., et al., *Carbon-based quantum dots for fluorescence imaging of cells and tissues.* RSC Advances, 2014. **4**(21).
[255] Damera, D.P., et al., *Green Synthesis of Full-Color Fluorescent Carbon Nanoparticles from Eucalyptus Twigs for Sensing the Synthetic Food Colorant and Bioimaging.* ACS Omega, 2020. **5**(31): p. 19905-19918.
[256] Salimi Shahraki, H., Qurtulen, and A. Ahmad, *Synthesis, characterization of carbon dots from onion peel and their application as absorbent and anticancer activity.* Inorganic Chemistry Communications, 2023. **150**.
[257] Ruan, Z., et al., *Corn*, in *Integrated Processing Technologies for Food and Agricultural By-Products*. 2019. p. 59-72.
[258] Kim, S. and B.E. Dale, *Global potential bioethanol production from wasted crops and crop residues.* Biomass and Bioenergy, 2004. **26**(4): p. 361-375.
[259] Zhao, W., et al., *Corn stover biochar increased edible safety of spinach by reducing the migration of mercury from soil to spinach.* Sci Total Environ, 2021. **758**: p. 143883.
[260] Han, Q., et al., *Multicolor Carbon Dots for Warm White Light-Emitting Diodes with a High Color Rendering Index of 93.2.* ACS Applied Nano Materials, 2023. **6**(18): p. 16373-16382.
[261] Zhou, L., et al., *White light emitting diodes with a high colour rendering index of 98.3 using blue emissive carbon dots.* Journal of Materials Chemistry C, 2023. **11**(45): p. 15926-15933.
[262] Yuan, T., et al., *Fluorescence-phosphorescence dual emissive carbon nitride quantum dots show 25% white emission efficiency enabling single-component WLEDs.* Chem Sci, 2019. **10**(42): p. 9801-9806.
[263] He, P., et al., *Recent advances in white light-emitting diodes of carbon quantum dots.* Nanoscale, 2020. **12**(8): p. 4826-4832.
[264] Jing, S., et al., *Facile and High-Yield Synthesis of Carbon Quantum Dots from Biomass-Derived Carbons at Mild Condition.* ACS Sustainable Chemistry & Engineering, 2019. **7**(8): p. 7833-7843.
[265] Li, L., et al., *A high-yield and versatile method for the synthesis of carbon dots for bioimaging applications.* J Mater Chem B, 2017. **5**(10): p. 1935-1942.

[266] Dua, S., et al., *Stability of carbon quantum dots: a critical review.* RSC Adv., 2023. **13**(20): p. 13845-13861.
[267] Kang, C., et al., *A Review of Carbon Dots Produced from Biomass Wastes.* Nanomaterials (Basel), 2020. **10**(11).
[268] Sendão, R.M.S., J.C.G. Esteves da Silva, and L. Pinto da Silva, *Photocatalytic removal of pharmaceutical water pollutants by TiO(2) - Carbon dots nanocomposites: A review.* Chemosphere, 2022. **301**: p. 134731.

Appendices

Appendix 1

A1.1. **Article IV**: Nitrogen doped carbon dots as a photocatalyst based on biomass. A life cycle assessment

Gabriela Rodríguez-Carballo, Ramón Moreno-Tost, Sónia Fernandes, Joaquim C. G. Esteves da Silva, Luís Pinto da Silva, Eulogio Castro Galiano, Manuel Algarra

Journal of Cleaner Production 423 (2023) 138728

Contents lists available at ScienceDirect

Journal of Cleaner Production

journal homepage: www.elsevier.com/locate/jclepro

Nitrogen doped carbon dots as a photocatalyst based on biomass. A life cycle assessment

Gabriela Rodríguez-Carballo [a], Ramón Moreno-Tost [a,**], Sónia Fernandes [b], Joaquim C. G. Esteves da Silva [b,c], Luís Pinto da Silva [b,c], Eulogio Castro Galiano [d], Manuel Algarra [e,*]

[a] Universidad de Málaga, Departamento de Química Inorgánica, Cristalografía y Mineralogía, Facultad de Ciencias, Campus de Teatinos, (Unidad Asociada al ICP-CSIC), 29071, Málaga, Spain
[b] Chemistry Research Unit (CIQUP), Institute of Molecular Sciences (IMS), Department of Geosciences, Environment and Territorial Planning, Faculty of Sciences, University of Porto, Rua do Campo Alegre s/n, 4169-007, Porto, Portugal
[c] LACOMEPHI, GreenUPorto, Department of Geosciences, Environment and Territorial Planning, Faculty of Sciences, University of Porto, Rua do Campo Alegre s/n, 4169-007, Porto, Portugal
[d] Department of Chemical, Environmental and Materials Engineering, Centre for Advanced Studies in Earth Sciences, Energy and Environment (CEACTEMA), University of Jaén, Jaén, 23071, Spain
[e] INAMAT², Institute for Advanced Materials and Mathematics, Department of Sciences, Public University of Navarre, Campus de Arrosadía, 31006, Pamplona, Spain

ARTICLE INFO

Handling Editor: Jin-Kuk Kim

Keywords:
Carbon dots
Xylose
Acid catalyst
Biomass
Nanoparticles
Hydrothermal synthesis
Photoluminescence
Photocatalysis
Life cycle assessment

ABSTRACT

The effectiveness of various transition metal phosphate-based acid catalysts, including vanadium and niobium, in the hydrothermal synthesis of carbon dots (CDs), has been assessed. Two sources of carbohydrates were employed for this: commercial xylose and liquor of xylose produced by processing olive pits. Catalysts were identified using the NH_3-TPD, DTA/TG, XRD, and XPS techniques. The reaction was conducted for 4 h at a temperature of 180 °C. The existence of such nanoparticles, regardless of the carbohydrate source, was confirmed by an analysis of the features and characteristics of CDs nanoparticles. N-doped CDs with increased fluorescence were also created at the same time using a similar hydrothermal technique, and their photocatalytic activity was investigated. A Life Cycle Assessment (LCA) was conducted for both syntheses with the goal of comparing the environmental effects of the synthesis from commercial xylose to the synthesis from biomass. It was revealed that, although energy is the primary driver of both synthesis pathways' effect categories, the fundamental variations that seem to determine their relative sustainability are connected to the nature of the carbon precursor. Regarding the latter, it is determined that electricity has the greatest environmental impact.

1. Introduction

CDs are recently discovered nanoparticles and present unique properties. Each nanoparticle consists of a graphitic lattice core covered by a functionalized surface composed by several polar functional groups attached (Hola et al., 2014; Zhu et al., 2020), making these nanoparticles extremely soluble in aqueous solutions. CDs can be obtained via two main synthetic approaches: from small molecules aggregation, the bottom-up route, or from larger carbon structures such as graphite, graphene or nanotubes, the top-down route (Tajik et al., 2020).

A current tendency for obtaining CDs is the pursuit of a synthesis method that fulfils the requirements of green chemistry but keeps production costs low. Therefore, CDs obtained from green precursors coming from biomass is an emergent research topic (Rodriguez-Padrón et al., 2018; Algarra et al., 2019; Sim et al., 2019; Crista et al., 2020; Y. Wu et al., 2021; El-Shahawy et al., 2021; Kurian and Paul, 2021). The most frequent and best-known method for CDs production is hydrothermal or solvothermal method (Sim et al., 2019; Zhu et al., 2020; Kurian and Paul, 2021; Yin et al., 2021). This method requires acidic conditions commonly achieved using mineral acids such as HCl, nonetheless, the hydrothermal method is compatible with heterogeneous catalysis, providing that the selected catalysts are in the acid environment to promote successive dehydration, condensation and superior aggregation processes leading to the generation of CDs (Xiong et al., 2021; Singh et al., 2023).

Due to admitting functionalization on their surface, CDs exhibit

* Corresponding author.
** Corresponding author.
E-mail addresses: rmtost@uma.es (R. Moreno-Tost), manuel.algarra@unavarra.es (M. Algarra).

https://doi.org/10.1016/j.jclepro.2023.138728
Received 22 May 2023; Received in revised form 1 September 2023; Accepted 5 September 2023
Available online 10 September 2023

photoinduced electronic transference, fluorescence, and up-conversion photoluminescence (Sim et al., 2019). CDs have raised increasing attention for their undemanding synthesis procedure combined with the fact that they have been proved to be non-toxic and can be modified to reach satisfactory quantum yield values (Kaur et al., 2021). CDs photoluminescence presents variation with size, showing a strong dependency on the energy gap between valence and conduction bands, that corresponds to the HOMO-LUMO (the highest occupied molecular orbital and lowest unoccupied molecular orbital, respectively) gap, as size increases, gap decreases (Macairan et al., 2022). As CDs are functionalized by a great variety of groups, these nanoparticles exhibit surface state photoluminescence, considering that the functional groups on their surface have multiple energy levels that can interact and result in emissive traps, thus dominating the emission. The surface state is a synergetic contribution of all groups conforming the surface of the CDs that hybridize with the outer graphitic core. This interaction between the core and the functional groups should not be mistaken as molecular state. Molecule state refers to the photoluminescence expected when an organic fluorophore is attached to the surface of the CDs. These CDs show exceedingly high quantum yields and strong photoluminescence, whereas when surface state is the predominant effect causing emission, CDs tend to exhibit much lower photoluminescence, but higher photostability (Zhu et al., 2015).

Several materials have been proposed as semiconductors to carry out photochemical reactions for a wide variety of purposes. The materials put to the test have mostly been metal-based. Currently, the novel trend is the utilization of metal nanoparticles, such as quantum dots (QDs). Despite its great performance in vacancy generation and electron movement, their production method is still costly and time consuming. Furthermore, metal-based photocatalysts will lead to unavoidable metal leakage in time (Zhu et al., 2022). Because of their photoluminescence and electron transfer properties, CDs can work as electron mediators, photosensitizers, as well as photocatalysts by themselves (Khan et al., 2022). It has been proved that CDs when photo excited are outstandingly good electron donors and electron acceptors, since either electron acceptors or electron donors are able to quench the photoluminescence emitted by CDs effectively (Dhamodharan et al., 2022). CDs provide an environmentally friendly alternative to their metal analogues. A variety of techniques can be used over virgin carbon nanoparticles to achieve an improvement in its photocatalytic and emissive features, such as surface functionalization and doping. Using CDs as catalysts in photoreactions bring some advantages along. CDs exceed by far other conventional catalyst such as TiO_2, ZnO and CdS in terms of solubility in aqueous solutions, chemo-stability, and toxicity. Surface of CDs can be modified to tune the absorbance of CDs and up-converted fluorescence that can help increasing the effectiveness of the absorption of sunlight of semiconductors from infrared to visible regions of the spectrum (Jung et al., 2022).

CDs are exceedingly versatile nanoparticles that find application in diverse fields such as bioimaging (Hola et al., 2014), biological (Wang et al., 2021), chemical sensors (Campos et al., 2016; Li et al., 2017, 2018), photocatalysis (Brumbaiah et al., 2021; Q. Wu et al., 2021), drug delivery (Nocito et al., 2021), next generation light emitting devices (Perikala and Bhardwaj, 2021), and immunoassays (Sharma et al., 2021). They are usually prepared from biomass and exhibit considerably low quantum yield (<10%). As a result, doping has emerged as a promising strategy to improve CDs quantum yields, reaching values near 60% (Liao, Cheng, and Zhou, 2016). Nitrogen is a frequent dopant of CDs, as N doped CDs have abundant surface-state defects (Zheng et al., 2021). Up until now, three aromatic N species have been identified to always appear in CDs framework: pyridinic, pyrrolic and graphitic nitrogen (Hao et al., 2021). CDs provide an environmentally friendly alternative to their metallic analogues. To the best of our knowledge, almost all catalysts assayed in CDs heterogeneous-catalysed production are metal oxides. Since vanadium phosphate (VPO) catalysts and their Nb analogues are known for being capable of promoting carbohydrates further dehydration into platform chemicals, such as 5-hydroxymethylfurfural (HMF) and furfural, they were selected as catalysts for a novel CDs production method, as one of the main steps of CDs synthesis involves the dehydration and further condensation and aggregation of the precursors (Xiong et al., 2021; Yin et al., 2021). Hydrothermal method also enables the simultaneous heteroatom doping and generation of CDs via a one-pot synthesis with a dopant (Sim et al., 2019; Zheng et al., 2021).

One of the most appropriated approaches to understand the associated environmental impacts of given products/processes is life cycle assessment (LCA). This tool can characterize the potential environmental impacts of a given system during its entire life cycle. More specifically, this can be achieved through the identification and quantification of potential impacts from raw materials extraction until to end-of-life, including the manufacturing/use stage (Ramos, Texeira and Roubia, 2018; Sendão et al., 2020; Fernandez, Esteves da Silva and Pinto da Silva 2021). It is noteworthy that an LCA study can provide multiple impact categories for evaluation of target products/systems (Marras et al., 2015). LCA approaches has already been used to evaluate the environmental impacts associated with different systems such as wind farms (Bi et al., 2021), dairy products [Kumar, et al., 2021), ceramic industry (Monteiro, Cruz, and Moura, 2022) and different types of engineered nanomaterials (Crista et al., 2020; Christé, Esteves da Silva and Pinto da Silva, 2020). In fact, members of this team have been focused on the evaluation, through LCA studies, of the environmental sustainability of fabricating CDs (Crista, Esteves da Silva and Pinto da Silva 2020; Sendão et al., 2020; Christé, Esteves da Silva and Pinto da Silva, 2020; Fernandez, Esteves da Silva and Pinto da Silva 2021; Fernandez, Esteves da Silva and Pinto da Silva 2021).

In this research, we successfully produced CDs utilizing a hydrothermal technique with commercial xylose and olive pit biomass as carbonous feedstock, as well as $VOPO_4$ and $NbOPO_4$ as catalysts. Then, the produced CDs were examined using TEM, XPS, and a confocal photoluminescence microscope to characterize them. The environmental sustainability of the synthetic CDs made using commercial xylose and olive pit biomass as carbonous feedstock was assessed using life cycle assessment (LCA). The resulting CDs were then successfully used in the photocatalyst-based degradation of methyl orange.

2. Materials methods

2.1. Materials

Vanadium (V) oxide, V_2O_5 (Aldrich Chemie, >99,6%); niobium oxalate monooxalate adduct, $Nb(HC_2O_4)_5$ (ABCR); Xylose (Millipore, >98%); orthophosphoric acid, H_3PO_4 (Panreac, >85%); ammonium chloride, NH_4Cl (Sigma-Aldrich, >99,5%); nitric acid, HNO_3 (VWR, >65%).

2.2. Synthesis

2.2.1. Catalyst

2.2.1.1. Preparation of the catalyst. Both $VOPO_4$ and $NbPO_4$ catalysts were prepared according to previously described methods (Luo et al., 2015; Zhu et al., 2020). Briefly, $VOPO_4$ was prepared from 1.93 g of V_2O_5 stirred magnetically with H_3PO_4 (10.5 mL), V:P molar ratio of 1; H_2O (22 mL) and concentrated HNO_3 (2 mL) and kept under reflux conditions for 2 h at 105 °C, then the yellow solid was filtrated and left to dry in the stove overnight at 60 °C. $NbOPO_4$ was obtained following a similar method, starting from 2.78 g of $Nb(HC_2O_4)_5$, stirred magnetically with 20 mL of deionized water and 2.2 mL of phosphoric acid, being the Nb:P molar ratio of 1, at 115 °C for 48 h. The white solid was separated from the solution by centrifugation, and it was left to dry overnight at room conditions. Characterization based in XRD, Raman,

TPD is found in Supplementary Information (S.I) Figures S11-3.

2.2.2. Synthesis of carbon dots (CDs)

Two sources of xylose were selected for the CDs synthesis: commercial xylose and xylose contained in the liquor prepared from olive pits treatment (see below). The preparation of CDs (Scheme 1) from commercial xylose involved 50 mL of 0.75 M solution of xylose and 100 mg of catalyst $VOPO_4$ or $NbOPO_4$ that were added into a hydrothermal Teflon-lined steel reactor. After catalyst addition, the pH of the suspension was measured and varied from 2 to 3.5, depending on the catalyst. The reaction was kept at 180 °C and the reaction time was set at 4 h, respectively. The product obtained following the centrifugation and filtration of the reaction solution was a vibrant yellowish orange solution and when irradiated under UV light showed modest fluorescence. This solution was further purified to obtain a clean solution of CDs. In this regard, the yellowish orange solution of CDs underwent a treatment including three steps. First, the solution was centrifuged along with 10 mL of a pH 4.7 buffer solution (Afonso et al., 2021). Next, the solution was dialyzed *v*. H_2O (1 L). After 48 h of dialysis, a CDs pale yellow solution was obtained, and its photoluminescence was tested under UV lamp to ensure the dialysis was performed correctly. Finally, the dialysed solutions were treated with $N_{2,\ liq}$ (−196 °C) in constant stirring, when all solution was frozen, it was lyophilized in a Scanvac Coolsafe 110-4 Pro during 48 h. Synthesis of CDs from biomass liquor was essentially like that of commercial xylose. In Table 1 are shown the main characteristics of the liquor obtained from olive pits. The xylose-enriched liquor from olive pits was produced in an autoclave. Briefly, 1500 g of crushed olive pits were soaked with 1500 g of a 2% sulfuric acid solution and put into a crystal bottle inside the autoclave. Target temperature was set at 125 °C for 30 min once this temperature was attained (in the used device, heating time was approximately 20 min and cooling time also 20 min). After this time, solids and liquid fractions were separated by vacuum filtration.

The autoclave treatment resulted in a high dissolution of the hemicellulose fraction of olive pits, with xylose as the main sugar. Once the liquor was obtained, the CDs synthesis was carried out following the same procedure as it was mentioned before, the liquor was transferred along with 100 mg of catalysts into the hydrothermal reactor and pH was measured providing values from 1 to 1.3, substantially lower than with commercial xylose since biomass liquor was prepared from acid itself. Both temperature and reaction time were the same as with commercial xylose. Furthermore, the CDs was also submitted to the purification steps previously described.

2.2.3. CDs doping with N

CDs doped with nitrogen moieties (N-CDs) were synthesized via a one-step hydrothermal method as well. 100 mg of $VOPO_4$ or $NbOPO_4$ catalyst, 25 mL of 0.75 M xylose and NH_4Cl (5 g and 7.5 g) as dopants were added into a Teflon lined stainless steel reactor. pH was measured to ensure that acidic conditions were appropriate for the reaction to proceed, obtaining values from 2.3 to 2.5 for nitrogen solution.

Table 1
Composition of biomass liquor (g/L).

Sugars		Other compounds	
Glucose	4.19	Formic acid	1.10
Xylose	69.97	Acetic acid	17.58
Galactose	8.19	HMF	0.13
Mannose	0.404	Furfural	0.21
Arabinose	9.86		

2.3. Liquor aging

With the aim of studying the effect of further degradation of liquor in the obtention of biomass CDs, the liquor was left to age for different time periods: a day, a week, and two weeks. Aging the liquor did not worsen its characteristics and properties, that were measured by means of HPLC.

2.4. Characterization

Transmission Electron Microscopy (TEM) was performed in a FEI-Talos F200X equipped with FEG 200 kV electron gun, four STEM detectors and four FEG detector and Thermo Scientific-FEI Tecnai G2 20 Twin Transmission Electron Microscope equipped with LaB_6 filament, tomography software, cryo-transmission system and EDS/EDX (Energy Dispersive X-ray Spectroscopy) elemental analyzer used to carry out the superficial analysis of CDs. The optical properties of the CDs were evaluated by photoluminescence measurements using a LabRAM Odyssey PL microscope (Horiba). Zeta potential (ζ) was measured aiming an evaluation of the superficial electric charge of CDs nanoparticles Measurements were performed using a 4mWHeNe Laser Doppler Velocimetry laser working at a fixed wavelength of 633 nm via an automatized procedure in a Malvern Zetasizer Nano ZS. The superficial composition of the CDs was analyzed by XPS This analysis was conducted in a Physical Electronics PHI5700 spectrometer using monochromatic MgK_α radiation of 300 W, 15 kV and 1253.6 eV with a multichannel detector. Analysis zone comprised an area of 720 μm of diameter and constant pass energy mode was set at 29.35 eV. The spectrum obtained was processed using MultiPak *v*.9.3 software. The XPS analysis was carried out to the lyophilized samples. All values were referenced to adventitious carbon (C 1s at 284.8 eV). Functional groups were studied by means of FTIR using a Shimadzu FTIR-8300 infrared spectrophotometer for the case of CDs that were shaped into wafers along with KBr and irradiated under a 0.5 mW power IR-beam at a fixed

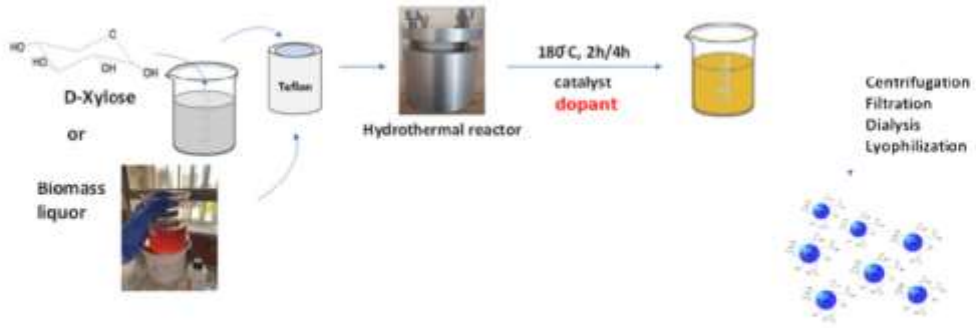

Scheme 1. Hydrothermal synthesis of CDs from commercial xylose and biomass liquor.

wavelength of 632.8 nm. Whereas N-CDs were also lyophilized but the solid was analyzed by means of FTIR-ATR using a Jasco Analytics 6800FV infrared spectrophotometer coupled with an ATR ProOne accesory. The remaining xylose in reaction samples was controlled using HPLC instrument (JASCO) equipped with an autoinjector (AS-2055) which injects 6 μL of the sample in a Phenomenex Rezex RCM-Monosaccharide Ca^{2+} (8%) (300 mm × 7.8 mm, 5 μm) column. The mobile phase (deionized and degassed water) was pumped by a quaternary gradient pump (PU-2089) at 0.4 mL/min flow rate to the column. The column is thermostatic at 70 °C.

2.5. Photocatalytic activity

N doped CDs (0.05 g) were added into 500 mL of 5 ppm methyl orange (MO) ethanol-water solution. Samples were irradiated by visible light inside photoreactor (Luzchem Model CCP-4V 220 V 50 Hz 3 A) with mechanical stirring and equipped with fourteen white visible lamps. Aliquots were taken after 5, 10, 20, 30, 60 and 80 min to study MO photodegradation. The photodegradation of MO was followed by Spectrophotometry UV (UV, 1800 SHIMADZU UV). Sample concentration was calculated by interpolation to the calibration curve obtained from standards measurements (2, 3, 4, 5 ppm and 0.2, 0.3, 0.4, 0.5 ppm) (Figure SI6). The total carbon and/or total nitrogen content of aqueous samples was analyzed by means of TOC Analyzer (Analytikjena multi-N/C 3100).

2.6. Life cycle assessment

This study consists in a cradle-to-gate LCA that intends to quantify and compare the potential environmental impacts associated with the synthesis of the two studied CDs (Scheme 2). More specifically, the present study is focused on the laboratory-scale synthesis of the target nanoparticles and considers the direct emissions from CDs production, as well as indirect impacts related with upstream resource extraction and energy generation. The environmental impacts were analyzed and compared by using a weight-based functional unit of 1 kg (kg). The environmental impacts related to the CDs syntheses were assessed based on inventory data from laboratory-scale synthesis procedures found in Ecoinvent® 3.5 database. Potential environmental impacts were assessed according to ReCiPe (2016) V1.03 endpoint method (Huijbregts et al., 2017) and the LCA study was performed using SimaPro 9.0.0.48 software. The environmental impacts under study were categorized in terms of Human Health, Ecosystems and Resources. Detail information about endpoint indicators is described in Supplementary Information.

2.6.1. Life cycle inventory data

The chemicals used as raw materials and the electricity used for the fabrication process constitutes the foreground system of the synthesis procedure. In this sense, the different processes, as well as the chemicals included in this study were modelled with the data present in the Ecoinvent® 3.5 database. As referred above, the electricity included was the required for the use of autoclave (power consumption of 3200 W and a vacuum pump with 180 W), centrifuge (power consumption of 500 W), heating and stirring plate (power consumption of 1000 W) and furnace (power consumption of 1800 W). For the xylose production it was considered the synthesis route described previously (Sharma et al., 2020). It is worth mentioning that for this LCA study it was not considered the catalysts used in the CDs production, since they are not consumed in these reactions. It should also be noted that olive pits in biomass liqueur production were also not considered in the inventory, as they are waste material that is generated because of the production of olive oil. Thus, in the framework of this study, we attributed the environmental impacts resulting from the production of olive pits to the olive oil industry and considered its use as precursor as the absence of the need to employ instead commercial precursors (Algarra et al., 2018). The used materials and electricity are reported in Table 2.

2.6.2. Sensitivity analysis

It was performed a sensitivity analysis by considering "What-if"

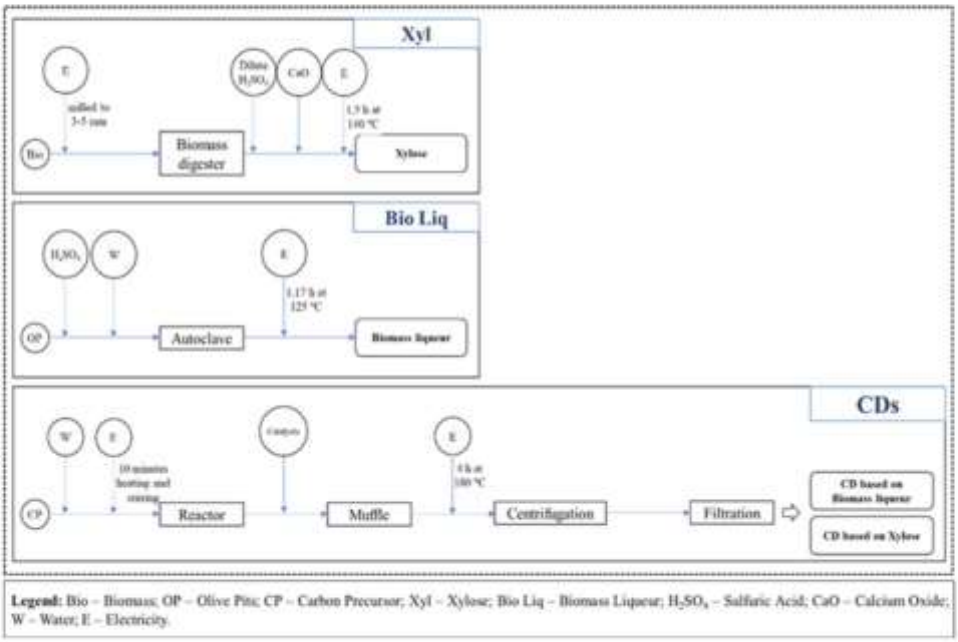

Scheme 2. Diagram for carbon precursors syntheses and CDs synthesis.

Table 2
Data inventory used from Ecoinvent® 3.5 database of raw materials for each CDs under study, in which quantities are referred to 1 kg of CDs. For xylose synthesis/raw materials it was considered the information provided previously (Sharma et al., 2021).

Raw Materials	Ecoinvent® 3.5 database	Amount
Biomass Liqueur		
Sulfuric Acid	Sulfuric acid (RER)	0.03 kg
Water	Water, deionized, from tap water, at user (Europe without Switzerland)	1.48 kg
Electricity	Electricity, medium voltage (ES)	3.82 kWh
Carbon Dots		
Carbon Precursor	Xylose or Biomass Liqueur	1.29 kg
Water	Water, deionized, from tap water, at user (Europe without Switzerland)	17.53 kg
Electricity	Electricity, medium voltage (ES)	7.42 kWh

scenarios (Pianosi et al., 2016), which consist of varying the amount and country origin of the required electricity. More specifically, in a first scenario was considered the variation of the amount of electricity for biomass liqueur. It was also considered a scenario related to the origin of electricity production (Spain, United States (USA) and Brazil (BR)) for both raw materials (xylose and biomass liqueur). This scenario intends to determine how the location of electricity production affects the environmental sustainability of the routes and the raw materials synthesis once each country has a specific energy matrix (Kumar et al., 2021). This analysis is not directly related with countries involved in olive oil industry but is instead with the evaluation of environmental impacts of employing electricity with different and known mixes of renewable/non-renewable energy.

3. Results and discussion

In previous works, we have demonstrated that CDs can be successfully synthesized by using heterogeneous catalysis, thus avoiding the CDs impurification with adatoms (Algarra et al., 2018, 2019; Rodriguez-Padrón et al., 2018). Here, we propose two solid acid catalysts, $VOPO_4{\cdot}2H_2O$ and $NbOPO_4{\times}H_2O$, for synthesizing CDs free of impurities. Afterwards, we will show that the CDs can be functionalized by heteroatoms (N) using those catalysts to modify their optical properties. As previously mentioned, those catalysts were both assayed in a hydrothermal heterogeneous catalysed synthesis of CDs from commercial xylose and biomass liquor.

The presence of CDs in the solution after reaction was confirmed visually through exposure to UV lamp (Figure SI7). The samples that did not show any fluorescence either had no catalyst (blank) or the reaction time was not enough to develop CDs and thus were discarded. Every sample treated with $VOPO_4$ or $NbOPO_4$ showed fluorescence, thus were analyzed by means of TEM. In addition, remaining xylose after reaction was controlled by HPLC for both CDs solutions from biomass and from commercial xylose. Conversion of commercial xylose was estimated at 77.7% ($VOPO_4$) and 65.3% ($NbOPO_4$) and for biomass 86.6% ($VOPO_4$). It must be noted that these conversions do not fully correspond to a real CDs yield, since not all the xylose that is reacting transforms into CDs.

3.1. Morphological analysis

TEM images for commercial xylose derived CDs presented homogeneous quasi spherical nanoparticles whose size range varied from 2 to 6 nm (Fig. 1A and B and Figures SI8A,B), irrespective of the catalyst they were obtained with and if they underwent doping or not. It was observed (Fig. 1B) that a major density of nanoparticles was obtained when working with $VOPO_4$ catalyst, NH_4Cl as dopant and commercial xylose for reaction time of 4 h. While for biomass carbon source, a major concentration was observed when working with $NbOPO_4$ catalyst (Figures SI8C,D). Biomass derived CDs were also notably bigger than the ones synthesized from commercial xylose, presenting an average size of 15 nm. Abundance was strongly affected by the catalyst for biomass liquors. While when performing the synthesis with $NbOPO_4$ a great quantity of CDs was obtained, when switching the catalyst to $VOPO_4$ in the same reaction conditions, a greater dispersion, and less quantity, either working with the absence of dopant (Fig. 1C) or with the presence of it (Fig. 1D). Fig. 2 shows an example of size histograms for commercial xylose N-CDs and biomass liquor N-CDs, due to the difficulty of

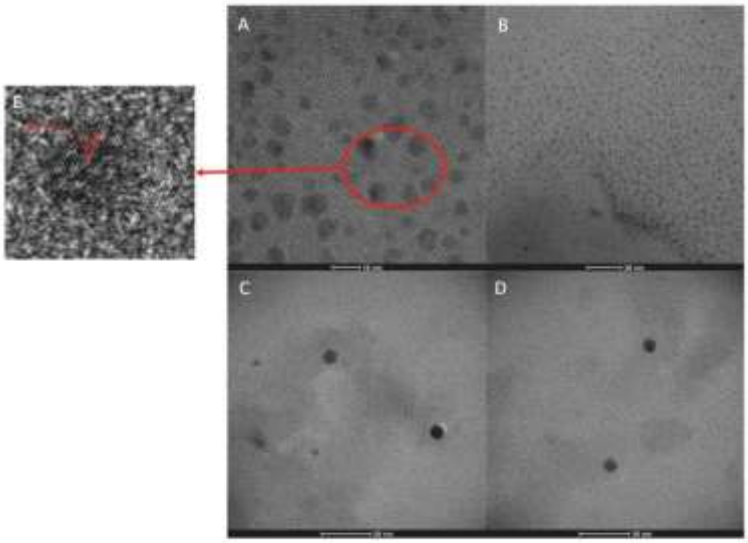

Fig. 1. TEM images of **(A)** Pristine CDs from xylose and $VOPO_4$ catalyst; **(B)** N-CDs from xylose and $VOPO_4$ catalyst; **(C)** CDs from biomass liquor and $VOPO_4$ catalyst; **(D)** N-CDs from biomass liquor and $VOPO_4$ catalyst and **(E)** Graphite spacing in CDs from commercial xylose and $VOPO_4$ catalyst.

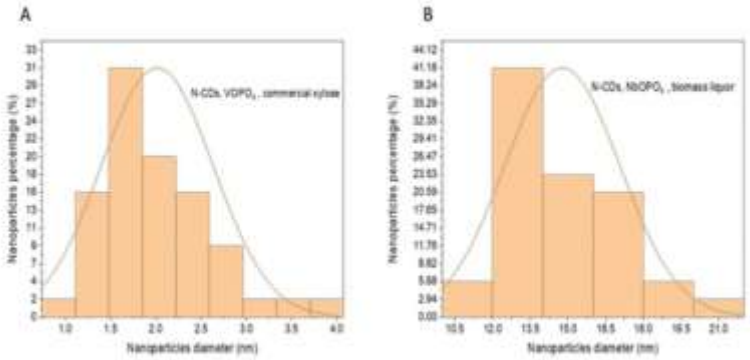

Fig. 2. (A) N-CDs from $VOPO_4$ and commercial xylose size histogram and (B) N-CDs from $NbOPO_4$ and biomass liquor size histogram (B).

measuring CDs when the outline of each nanoparticle is not completely defined, the size measurements were carried out on commercial xylose N-CDs from $VOPO_4$ catalyst and on biomass liquor N-CDs from $NbOPO_4$ catalyst, since for the rest of cases it was not possible to measure a representative number of nanoparticles for the size histogram. The use of analogue $VOPO_4$ and $NbOPO_4$ catalysts, provided analogue results in the synthesis, in particle size and shape.

Since biomass liquors CDs are full of different oxidation-prone compounds that cannot be separated from the reaction medium, $VOPO_4$ might be acting as a catalyst promotion further oxidation of other organic compounds rather than dehydration of xylose and subsequent aggregation into CDs. For further confirmation of the presence of CDs, the graphitic lattice was identified in HR-TEM images and the measurement of the spacing gave out a value of 0.314 nm (Fig. 1E) (Hembacher et al., 2003; Zheng et al., 2017). Similar found for CDs from xylose and $NbOPO_4$ catalyst (Figure SI8E).

3.2. Surface analysis

After having confirmed, by TEM, the existence of the CDs in the reaction solution, with the aim of confirming the functionalization in the surface of CDs, a XPS analysis was performed in a lyophilized sample of commercial xylose CDs (Fig. 3A). Samples after dialysis were cleaner of organic residues from reaction solution, hence the band that corresponds to C–C binding energy is more intense than those corresponding to –C═O and O–C═O binding energies, as it would be expected from CDs, since are mainly composed of graphitic carbon. The C1*s* core level spectrum obtained was deconvoluted into three mayor contributions (Table 3). The first band (248.8 eV) can be related to simple C–C bond (adventitious carbon), while second and third bands present maximums at 286.6 eV and 288.0 eV, respectively that can be related to carbonyl and carboxylate groups (Patra et al., 2023; Wang et al., 2023).

XPS analysis of commercial xylose N-doped samples confirmed N-doping was successful (Fig. 3B and C). Nitrogen atoms on CDs were

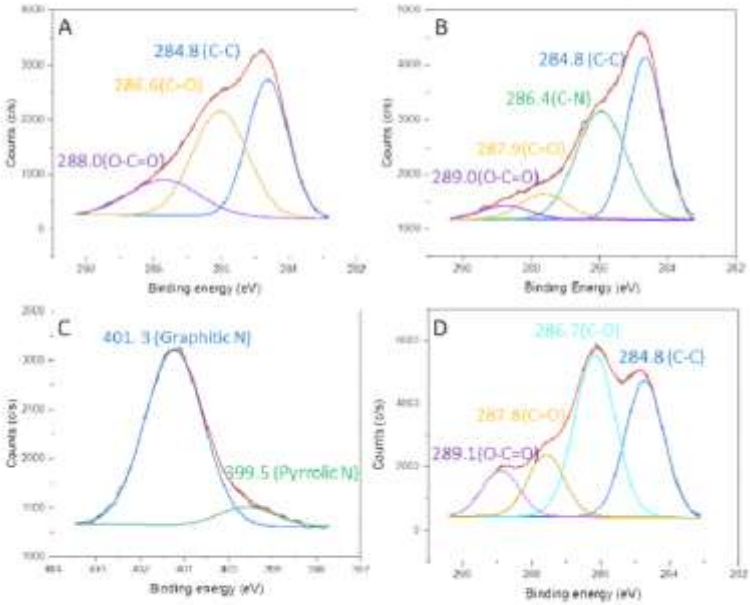

Fig. 3. XPS core level spectra for **(A)** C 1*s* of commercial xylose CDs. **(B)** C 1*s* of commercial xylose N-CDs; **(C)** N 1*s* of commercial xylose N-CDs; **(D)** C 1*s* of biomass liquor CDs.

Table 3
Assignation of the binding energies resulted from the deconvolution of C1s core level of CDs synthesized from commercial xylose and biomass liquor and $VOPO_4$ as catalyst.

	C1s (eV)	C assignation	N1s (eV)	N assignation
Commercial xylose CDs	284.8 (49.27%)	C–C	N/A	
	286.6 (34.54%)	C=O		
	288.0 (16.19%)	O–C=O		
Biomass liquor CDs	284.4 (34.65%)	C–C	N/A[a]	
	286.7 (38.50%)	C–O		
	287.8 (15.25%)	C=O		
	289.1 (11.60%)	O–C=O		
Commercial xylose, N-CDs	284.8 (53.22%)	C–C[		
	286.4 (32.46%)	C–N	401.3 (91.84%)	Graphitic N
	287.9 (8.51%)	C=O	399.5 (8.16%)	Pyrrolic N
	289.0 (5.81%)	O–C=O		

[a] Note: Biomass liquor N-CDs are not presented in this table due to the difficulty observed in obtaining and deconvoluting spectra data from these nanoparticles, since they cannot be totally separated from the rest of components of the reaction media.

mainly found as graphitic nitrogen, but there was also a small amount in the form of pyrrolic nitrogen (Table 3) (Huang et al., 2023). For the C1s core level, it was also possible to confirm the existence of the C–N bond (Table 3). Biomass liquor CDs were also analyzed by means of XPS (Fig. 3D). Obtaining the following deconvoluted spectrum for C 1s core level (Table 3). Generally, for CDs, the band for C–C bonding should be the highest band in intensity, due to the graphite carbon core of the CDs, but for biomass liquor, since it has many other substances that are impossible to separate from reaction medium, it can be seen in the XPS a major band for C–O whose contribution can be arose from those substances. Due to the difficulty of obtaining clear XPS spectra for biomass CDs samples in general, for those that were doped, the success of the inclusion of N atoms was confirmed by EDS (Figure SI9). All related survey spectra are presented in Figure SI10.

The survey and the XPS core level of C1s and C1s and the spectra binding energies for CDs from $NbOPO_4$ are also compiled in the SI (Figure SI11-12 and Table SI3). Additional FTIR analysis were carried out for further confirmation of the functional groups decorating the surface of the CDs (Figure SI13).

3.3. Photoluminescence (PL) analysis

PL is considerably higher for the solutions where catalysts were added and for those that were set at 4 h reaction time. A greater amount of PL registered can be related to a greater presence of nanoparticles in the solution, consequently the catalysts, as suspected in TEM, do stimulate the reaction. Similarly, to TEM results, samples where the selected catalyst was $VOPO_4$ exhibited slightly better results. CDs show hugely particular photoluminescence properties, thus are extremely sensitive to irradiation wavelength and its maximum emission peak is highly tuneable. Generally, if irradiated at longer wavelengths using low energy lasers, the maximum undergoes a bathochromic shift, that can be observed for CDs from commercial xylose as well as for biomass CDs (Fig. 4A and B).

Since CDs main applications in bioimaging, sensing and photocatalyst are strongly dependent on their capacity to produce a high amount of photoluminescent emission, it was necessary to perform photoluminescence measurements to confirm whether their photoluminescence emission was as expected and to know their wavelength of emission. Furthermore, since doping the CDs was pursued as a mean to improve the photoluminescence values, these measurements were carried out to corroborate whether the doping met the target. Wavelength emission values for CDs depend on several factors that can be sum up in two main categories: particle size and contributions from different functional groups. Since for the case of CDs coming from commercial xylose a greater homogeneity in size was observed, the bands appearing in the spectra can be related to different groups emitting, rather than to different size particles. These contributions can be explored carrying out a deconvolution of photoluminescence band. It was selected for deconvolution the band corresponding to the sample treated during 4 h with the addition of $VOPO_4$ catalyst (Fig. 4A). Two main contributions appeared on the spectrum, the first one around 500 nm, the second one near 600 nm. The main contribution (500 nm) can be assigned to the emission produced by simple C–O bonds, while the second contribution can be related to the emission of carbonylic groups (-C=O) (van Dam et al., 2017). Therefore, photoluminescence results suggested that the surface of the synthesized CDs might be functionalized by carboxylic acids, and it is possible to confirm that the PL effect is explained by the transitions $n \rightarrow \pi^*$ (Braeuer, 2015; Sun et al., 2018; Chen et al., 2021). The elucidation of the different contributions for the photoluminescence band of biomass CDs is difficult to perform, since not only the number of different groups functionalizing the surface is potentially bigger than for the case of commercial xylose CDs, but due to the greater heterogeneity in size. Although the bathochromic shift observed in biomass CDs band when compared to xylose photoluminescence band can be associated to a bigger size of the nanoparticles.

PL measurements of pristine CDs samples (Fig. 4B–D), as expected, were lower in intensity than those of doped CDs (Fig. 4E and F), since doping CDs generates defects in the surface that are highly emissive spots and since new N–C bonds are created with doping, there is also a contribution in the PL emission that comes from the variety of functional groups generated thanks to doping. Aging the biomass liquor neither improved nor worsened the results obtained from plain liquor (Fig. 4G), intensity values remained over the same units. The $VOPO_4$ catalyst activity after the second and third cycle was controlled by photoluminescence (Fig. 4H). Although with every cycle the spectra decreased in intensity, it remained emitting, indicating the presence of CDs. The catalyst, thus, can be reused at least for three reaction cycles until having to discard it. Similar tendency was observed when $NbOPO_4$ was recovered and reused in subsequent catalytic cycles (Figure SI14). Contrary to what it was expected, for the case of CDs from commercial xylose and $NbOPO_4$ the intensity of photoluminescent emission was lower than for their analogues obtained using $VOPO_4$ as catalyst, despite of the quantity of CDs being just slightly lower. This behaviour can be attributed to the fact that a greater aggregation is observed for the case of CDs from $NbOPO_4$ catalyst and thus, the effect of auto-absorption arouses (Albani, 2004; Gutiérrez et al., 2022). The greater tendency of aggregation of these CDs was further confirmed by ζ potential measurements.

The resulted value was −11.8 and −10.6 mV for $VOPO_4$ and $NbOPO_4$ respectively. When the obtained value result negative tends to imply that the surrounding electron cloud is dense. A high ζ potential, positive or negative, often involves excellent electrostatic stability and null tendency to form aggregates. Highly dispersed nanoparticles frequently present values ranging from −30 mV to 30 mV, while particles considered neutral go from −10 mV to 10 mV (Pudza et al., 2020). As the measured value is certainly near the neutral interval, the synthesized CDs might end up forming aggregate if conserved in solution, although no aggregate have been observed yet. ζ potential is also very sensitive to pH. As acidity increases it gradually acquire a more positive value. Since the pH in this reaction is set between 1 and 3.5, it seems only natural that

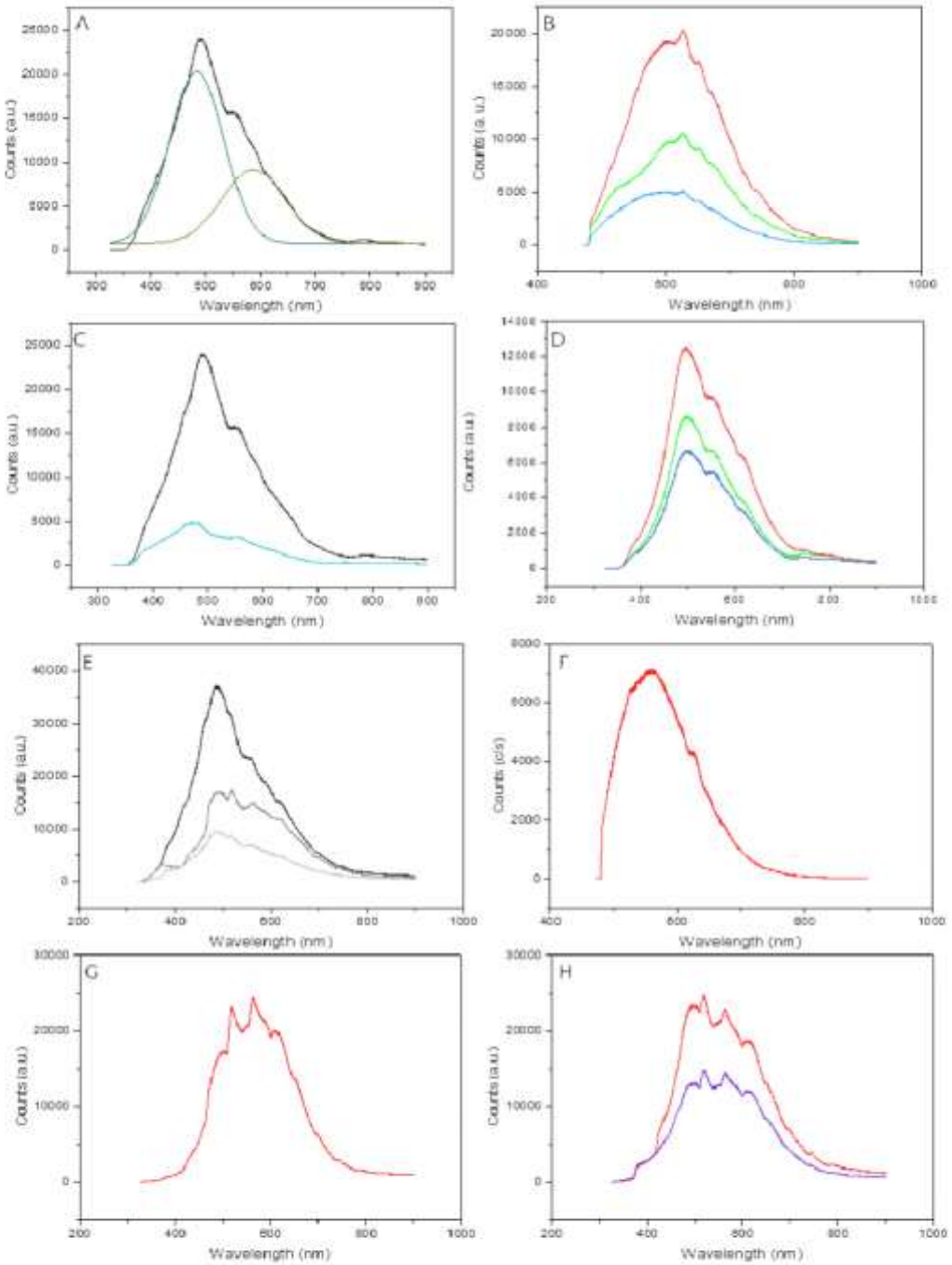

Fig. 4. Photoluminescent emission of **(A)** biomass CDs irradiated with 325 nm excitation laser **(B)** biomass CDs irradiated with 473 nm excitation laser; **(C)** commercial xylose CDs measured with 325 nm excitation laser; **(D)** Deconvolution of the band corresponding to CDs $VOPO_4$, 4 h, 0.75 M xylose, 180 °C; **(E)** N-doped commercial xylose CDs irradiated with 325 nm excitation laser; **(F)** N-doped biomass liquor CDs irradiated with 325 nm excitation laser; **(G)** Aged liquor and **(H)** Recycled $VOPO_4$ catalyst.

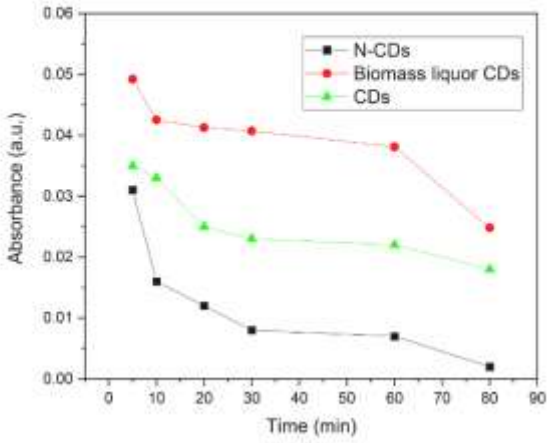

Fig. 5. (A) MO degradation catalysed by N-CDs from commercial xylose and VOPO4 as catalyst, pristine CDs from commercial xylose and $VOPO_4$ as catalyst and CDs from biomass liquor and $VOPO_4$ as catalyst.

ζ potential is not extremely negative. When working with biomass derived CDs, however, the quantity of CDs in the sample treated with $NbOPO_4$ as catalyst greatly exceeded the number of CDs present in its analogue sample with $VOPO_4$ as catalyst, but again, the aggregation is such that the auto-absorption effect is incredibly notable, diminishing the intensity of photoluminescence.

3.4. Photocatalytic degradation of methyl orange

The activity of N-doped and pristine CDs in the degradation of methyl orange was compared. N-CDs (Fig. 5A and SI.15A) presented a better yield in contrast to the yield observed for pristine CDs (Fig. 5 and SI.15B). The discoloration was moderate for the case of pristine CDs, while for N-CDs, a faster and more effective degradation was observed. For biomass derived CDs (Figure C), the yield was lower in comparison to CDs from commercial xylose, but still the degradation took place, at a slower rate and lower effectiveness. The differences between commercial CDs and biomass liquor CDs were related to the carbon precursor used that eventually leads to a major or minor formation of CDs, as it was seen in TEM with different qualities that can affect slightly in their performance.

The photocatalytic activity was therefore strongly related to the photoluminescence measurements because the surface state of the CDs is responsible for both their photoluminescent properties and their photocatalytic activity. The final concentration of MO in the solutions after less than 2 h was under the lowest limit of the calibration curved described by 0.1–0.4 ppm standards and it was not possible to determine. The real concentration was then studied by means of TOC.

To perform the TOC analysis and confirm the degradation of methyl orange, an aliquot of reaction medium, that included the presence of N-CDs from commercial source, was analyzed before and after reaction. Moreover, an aliquot of N-CDs to ensure they would not interfere in TOC results was also analyzed without MO. TOC proved that the discoloration observed in UV spectrophotometry was, indeed, a sign of degradation of MO. The analyses showed that the presence of organic compounds diminished after the use of CDs as catalyst for photodegradation and that a solution of CDs provided no signal in TOC, thus it did not interfere in the result of analysis. The TOC results showed (Table 4) that the carbon was reduced up to 99%. These results demonstrated the great photocatalytic activity of the CDs and their potential use in degradation of dyes. The final concentration of MO present (Table 4) in the solution after reaction can be related to what

Table 4
Methyl orange (MO) final concentration obtained from TOC determination.

Samples	MO concentration (ppm)
MO	4.34
N-CDs	0
MO + N-CDs before reaction	4.29
MO + N-CDs after reaction	0.0443

was obtained as final concentration in the study of discoloration in Spectrophotometry UV, having into accounts the limitations in the detection limits.

Furthermore, the results of TOC analysis confirmed that no adsorption of MO was detected in dark conditions, as in MO + CDs before reaction sample no alteration of the concentration was observed.

Based on the photocatalytic results, the photodegradation mechanism of MO is portrayed in Scheme 3, where CDs would act as photocatalysts and electron donors, as the carboxylic groups would enhance electron movement, while graphitic N would provide the electrons as the donors. Molecular oxygen is proposed as the acceptor and would then attack methyl orange, causing its degradation (Park et al., 2019; Zhao et al., 2019; Rajapandi et al., 2022).

3.5. LCA results

The comparison of potential environmental impacts between the syntheses under study was made by considering a weight-based functional unit of 1 kg of CDs (Fig. 6) (Crista et al., 2020; Crista, Esteves da Silva and Pinto da Silva 2020; Fernandes, Esteves da Silva and Pinto da Silva, 2021; Chritié, Esteves da Silva and Pinto da Silva 2020). Our objective is to compare the relative contributions of the input materials/energy involved in each synthesis for the different impact categories. Thus, we will not make quantitative appreciations of the environmental impacts. For both syntheses, electricity represents more than 68% of the potential environmental impacts in different categories, which identifies it as a main hotspot in both processes. On the other hand, the relative contributions of deionized water appear to be negligible in the two analyzed processes. The contributions of carbon precursor to the different impact categories (in both syntheses) are not negligible but appear to be significantly less relevant than that of electricity.

Comparing both syntheses, the immediate conclusion is that the CDs produced from xylose are associated with lower environmental impacts in all categories. This does not mean, however, that CDs from biomass liqueur should not be further explored. For the contrary, this LCA should be used to investigate why higher environmental impacts results from CDs Biomass Liqueur, in these conditions, so that we can address it and reduce the associated impacts. This should be pursued so that biomass waste can be properly valorised as a raw material.

While electricity is the main hotspot in both syntheses, its consumption is the same in both processes, and so, it cannot be the reason for the different relative environmental impacts (Table 2).

More specifically, the differences should be attributed to the carbon precursor (which is the different parameter between the syntheses). In fact, xylose in CDs Xylose contributes 12% for Human Health impacts, 13% for Ecosystems and 14% for the Resources category, while in CDs Biomass Liqueur the carbon precursor represents about 31% in both Human Health, Ecosystems and Resources. So, the carbon precursor appears to be a key parameter to determine the sustainability of these CDs syntheses. This finding is in line with previous LCA of fabrication routes for CDs (Fernandes, Esteves da Silva and Pinto da Silva, 2020; Sendão et al., 2020). Given this, reducing the environmental impacts associated with the production of the carbon precursor should the focus for increasing the environmental sustainability of CD Biomass Liqueur. To better understand how this can be achieved, the relative environmental impacts for the synthesis of xylose synthesis are shown in Fig. 7A, while the results obtained to produce biomass liqueur are found on

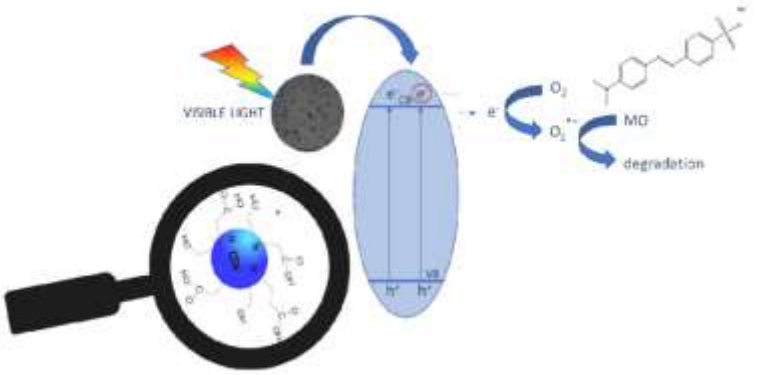

Scheme 3. Photocatalytic mechanism of MO degradation.

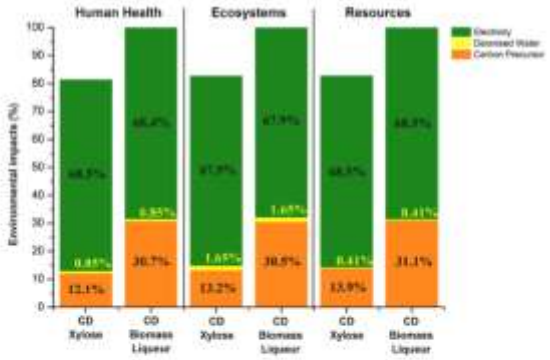

Fig. 6. Relative environmental impacts of both syntheses (CDs Xylose and CDs Biomass Liqueur). This graphic was obtained applying ReCiPe endpoint method.

Fig. 7B. According to Fig. 7A, the major contributor to the environmental impacts generated by xylose synthesis is electricity, as it presents contributions between 78% and 89%. Deionized water, sulfuric acid, and calcium oxide have a negligible influence on the associated potential environmental impacts. However, sugarcane represents about 9% in Ecosystem category and steam is responsible for approximately 20% of environmental impacts in Resources category.

On the other hand, the production of biomass liqueur appears to have only one parameter responsible for relevant environmental impacts, since electricity is responsible for about 98% contributions for the Resources category and 99% contribution for both Human Health and Ecosystems associated impacts. Thus, electricity appears to be the main hotspot in the synthesis of both carbon precursors, with higher relative contributions to produce biomass liqueur.

Given this, electricity should be the parameter to be focused on to reduce the environmental impacts associated with the production of biomass liqueur, and consequently of CDs Biomass Liqueur. In fact, we have used here data obtained at the laboratory-scale, in which the consumption of electricity from used equipment might not be the most efficiently scaled with the amount of generated materials. Therefore, optimization of the consumption of electricity should lead to lower environmental impacts associated with this process. To showcase this possibility, we performed a sensitivity analysis in which we varied the amount of consumed electricity (reduction of 2, 3 and 6 times the normal amount). Interestingly, the decrease of the amount of electricity in the production of biomass liqueur did lead to lower impacts than the synthesis of xylose. More specifically, the production of biomass liqueur would be more sustainable than the synthesis of xylose if the amount of used electricity was at least three times lower than the amount effectively used. To further understand the influence of electricity on the production of biomass liqueur we also performed a sensibility analysis, in which we varied the amount of used electricity (Figure SI16)

Considering this, it was performed an analysis to evaluate the differences between three countries regarding electricity production (Fig. 8). This analysis showed that for both carbon precursors, there is a

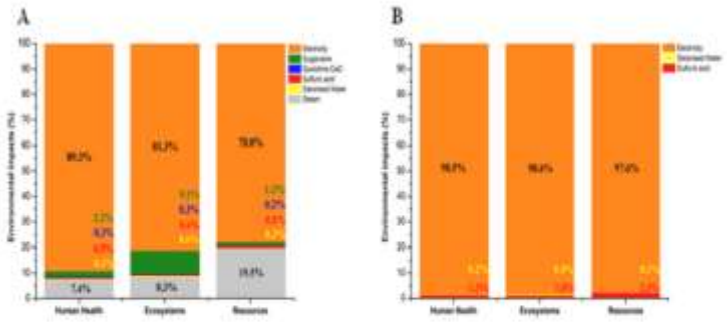

Fig. 7. (A) Relative environmental impacts of xylose. This graphic was obtained applying ReCiPe endpoint method. (B) Relative environmental impacts of biomass liqueur. This graphic was obtained applying ReCiPe endpoint method.

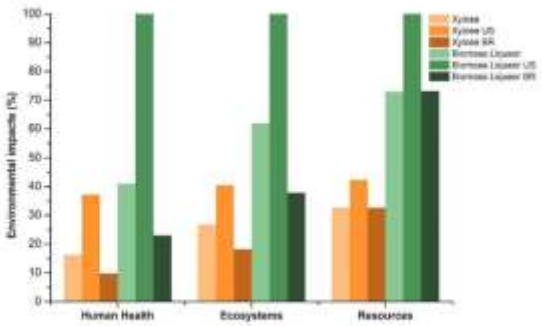

Fig. 8. Relative environmental impacts for sensibility analysis of both carbon precursors syntheses (xylose and biomass liqueur), considering electricity production from different countries. ES refers to Spain, US refers to United States and BR refers to Brazil. This graphic was obtained applying ReCiPe endpoint method.

trend regarding the electricity production in different countries (Brazil < Spain < USA).

That agrees with a study carried out by Ecoinvent database, in which was discovered that the impacts associated with energy production were smaller in all countries in the European Community than the impacts for scenarios for the US. This is justified because the energy matrix in the US is basically based on coal and natural gas, while in Europe the energy production is also reliant on coal, but many countries also have relevant sources of renewable energy. On the other hand, the impacts associated with energy production in Brazil were smaller because the energy matrix is basically composed of clean and renewable energy sources, such as hydroelectric dams (Zhao et al., 2019).

4. Conclusions

The capacity of both catalysts $VOPO_4$ and $NbOPO_4$ of promoting the synthesis of carbon nanoparticles have been proved, being optimal for $VOPO_4$ according to results obtained for xylose conversion, photoluminescence and TEM that indicated a greater quantity of nanoparticles present in the solution. Reaction time was also a determinant factor in the synthesis of CDs, being 4 h the one that showed to be the most fruitful. Nanoparticles' synthesis was feasible from commercial carbon precursor as well as from biomass precursor. The slight differences in results established between both carbon sources were almost certainly due to the concentration and composition difference. The synthesized nanoparticles stand out for their size homogeneity. Surface characterization proved that the synthesized CDs are functionalized by carboxylate groups that caused the emission observed when irradiated with UV. ζ potential analysis suggested a tendency to form aggregates, although in TEM images no aggregates were spotted, on the contrary, a great dispersion was observed, thus permitting the identification of graphitic lattice and the measurement of its spacing. Doped CDs, especially, N-doped CDs showed great potential in photoluminescent applications, since their emissive values exceeded greatly those obtained from pristine CDs. To check the photoactivity of the obtained CDs from xylose was tested in the photocatalytic degradation of methyl orange as probe and showed promising results, demonstrated that is possible the valorisation for further process of catalyst. A LCA was also performed to understand the environmental impacts associated with each synthesis route here studied. This was achieved by considering both the synthesis of CDs and the carbon precursor production. We have found that while electricity was found to be a major contributor to all categories for synthesis, the parameter that explain the differences in sustainability between these processes is the identity of the carbonous precursor. Following this, we have further analysis the sustainability of the production of each carbon precursor (xylose and biomass liqueur). This showed that electricity is a main hotspot in the current process to produce biomass liqueur.

Ethics approval and consent to participate

Not applicable.

Consent for publication

Not applicable.

CRediT authorship contribution statement

Gabriela Rodríguez-Carballo: Conceptualization, Formal analysis, Writing – original draft, Writing – review & editing, Methodology, Resources, Formal analysis, Writing – review & editing, Formal analysis, Writing – review & editing, Conceptualization, Resources, Formal analysis. **Ramón Moreno-Tost:** Conceptualization, Formal analysis, Writing – original draft, Writing – review & editing. **Sónia Fernandes:** Methodology, Resources, Formal analysis, Writing – review & editing, Formal analysis, Writing – review & editing, Conceptualization, Resources, Formal analysis. **Joaquim C.G. Esteves da Silva:** Methodology, Resources, Formal analysis, Writing – review & editing, Formal analysis, Writing – review & editing, Conceptualization, Resources, Formal analysis. **Luís Pinto da Silva:** Conceptualization, Formal analysis, Writing – original draft, Writing – review & editing. **Eulogio Castro Galiano:** Methodology, Resources, Formal analysis, Writing – review & editing, Formal analysis, Writing – review & editing, Conceptualization, Resources, Formal analysis. **Manuel Algarra:** Conceptualization, Formal analysis, Writing – original draft, Writing – review & editing.

Declaration of competing interest

The authors declare that they have no known competing financial interests or personal relationships that could have appeared to influence the work reported in this paper.

Data availability

No data was used for the research described in the article.

Acknowledgments

This research was funded by the Spanish Ministry of Science and Innovation (PID2021- 122736OB-C42), FEDER (European Union) funds (PID2021-122736OB-C42, P20-00375, UMA20- FEDERJA88). M.A thanks to the Spanish Ministry of Science and Innovation (MCIN/AEI/10.13039/501100011033) through project PID2021-122613OB-I00. This work was made in the framework of projects UIDB/00081/2020 (CIQUP), UIDB/05748/2020 (GreenUPorto), LA/P/00081/2020 (IMS), and PTDC/QUI-QFI/2870/2020, funded by the Portuguese Foundation for Science and Technology (FCT, Lisbon). Luís Pinto da Silva acknowledges funding from FCT under the Scientific Employment Stimulus (CEECINST/00069/2021), while S.F acknowledges FCT for funding of her Ph.D. grant (2021. 05479.BD). The Laboratory of Computational Modelling of Environmental Pollutants-Human Interactions (LACOMEPHI) is acknowledged. Open access funding provided by Universidad Pública de Navarra.

Appendix A. Supplementary data

Supplementary data to this article can be found online at https://doi.org/10.1016/j.jclepro.2023.138728.

References

Afonso, A.C.P., Correia, A.S., Duarte, D., Brandão, A.T.S.C., Martínez de Yuso, M.V., Jiménez- Jiménez, J., Vale, N., Pereira, C.M., Algarra, M., Pinto da Silva, L., 2021. An active surface preservation strategy for the rational development of carbon dots as pH-responsive fluorescent nanosensors. Chemosensors 9, 191. https://doi.org/10.3390/chemosensors9080191.

Albani, J.R., 2004. Fluorescence: Principles and Observables, en: Structure and Dynamics of Macromolecules: Absorption and Fluorescence Studies. Elsevier, pp. 55–98, 2004.

Algarra, M., González-Calabuig, A., Radotić, K., Mutavdzic, D., Ania, C.O., Lázaro-Martínez, J.M., Jiménez-Jiménez, J., Rodríguez-Castellón, E., del Valle, M., 2018. Enhanced electrochemical response of carbon quantum dot modified electrodes. Talanta 178, 679–685. https://doi.org/10.1016/j.talanta.2017.09.082.

Algarra, M., dos Orfãos, L., Alves, C.S., Moreno-Tost, R., Pino-González, M.S., Jiménez-Jiménez, J., Rodríguez-Castellón, E., Eliche-Quesada, D., Castro, E., Luque, R., 2019. Sustainable production of carbon nanoparticles from Olive pit biomass: understanding proton transfer in the excited state on carbon dots. ACS Sustain. Chem. Eng. 7, 10493–10500. https://doi.org/10.1021/acssuschemeng.9b00969.

Brueuer, A., 2015. Interaction of matter and electromagnetic radiation, en: In situ Spectroscopic Techniques at High Pressure. Elsevier, pp. 41–192.

Bramhaiah, K., Bhuyan, R., Mandal, S., Kar, S., Prabhu, R., John, N.S., Graeslich, M., Urban, A.S., Bhattacharyya, S., 2021. Molecular, aromatic, and amorphous domains of N-carbon dots: leading toward the competitive photoluminescence and photocatalytic properties. J. Phys. Chem. C Nanomater. Interfaces. 125, 4299–4309. https://doi.org/10.1021/acs.jpcc.1c00004.

Campos, B.B., Contreras-Cáceres, R., Bandosz, T.J., Jiménez-Jiménez, J., Rodríguez-Castellón, E., Esteves da Silva, J.C.G., Algarra, M., 2016. Carbon dots as fluorescent sensor for detection of explosive nitrocompounds. Carbon 106, 171–178. https://doi.org/10.1016/j.carbon.2016.05.030.

Chen, X., Wu, W., Zhang, W., Wang, Z., Fu, Z., Zhou, L., Yi, Z., Li, G., Zeng, L., 2021. Blue and green double band luminescent carbon quantum dots: synthesis, origin of photoluminescence, and application in white light-emitting devices. Appl. Phys. Lett. 118, 153102 https://doi.org/10.1063/5.0046495.

Christé, S., Esteves da Silva, J.C.G., Pinto da Silva, L., 2020. Evaluation of the environmental impact and efficiency of N-doping strategies in the synthesis of carbon dots. Materials 13, 504. https://doi.org/10.3390/ma13030504.

El-Shahawy, R.M., Farouk Elsadek, M., Mohamed Ahmed, B., Fawzy Farahat, M., Mosleh, K.N., Taher, M.M., 2021. Recent developments in carbon quantum dots: properties, fabrication techniques, and bio-applications. Processes 9, 388. https://doi.org/10.3390/pr9020388.

Fernandes, S., Esteves da Silva, J.C.G., Pinto da Silva, L., 2020. Life Cycle Assessment of the sustainability of enhancing the photodegradation activity of TiO_2 with metal-doping. Materials 13, 1487. https://doi.org/10.3390/ma13071487.

Fernandes, S., Esteves da Silva, J.C.G., Pinto da Silva, L., 2021. Comparative life cycle assessment of high-yield synthesis routes for carbon dots. NanoImpact 23, 100332. https://doi.org/10.1016/j.impact.2021.100332.

Gutiérrez, M., Zhang, Y., Tan, J.C., 2022. Confinement of luminescent guests in metal-organic frameworks: understanding pathways from synthesis and multimodal characterization to potential applications of LG@MOF systems. Chem. Rev. 122, 10438–10483. https://doi.org/10.1021/acs.chemrev.1c00980.

Hao, Q., Qiao, L., Shi, G., He, Y., Cui, Z., Fu, P., Liu, M., Qiao, X., Pang, X., 2021. Effect of nitrogen type on carbon dot photocatalysts for visible-light-induced atom transfer radical polymerization. Polym. Chem. 12, 3060–3066. https://doi.org/10.1039/d1py00148e.

Hembacher, S., Giessibl, F.J., Mannhart, J., Quate, C.F., 2003. Revealing the hidden atom in graphite by low-temperature atomic force microscopy. Proc. Natl. Acad. Sci. USA 100, 12539–12542. https://doi.org/10.1073/pnas.2134173100.

Hola, K., Zhang, Y., Wang, Y., Giannelis, E.P., Zboril, R., Rogach, A.L., 2014. Carbon dots- Emerging light emitters for bioimaging, cancer therapy and optoelectronics. Nano Today 9, 590–603. https://doi.org/10.1016/j.nantod.2014.09.004.

Huang, H., Shi, M., Zhai, H., Zhang, Y., Zhang, Y., Zhao, Y., 2023. Nitrogen-doped carbon dots as visible light initiators for 3D (Bio)Printing. Polym. Chem. 14, 268–276. https://doi.org/10.1039/d2py01324j.

Huijbregts, M.A.J., Steinmann, Z.J.N., Elshout, P.M.F., Stam, G., Verones, F., Vieira, M., Zijp, M., Hollander, A., van Zelm, R., 2017. ReCiPe2016: a harmonised life cycle impact assessment method at midpoint and endpoint level. Int. J. Life Cycle Assess. 22, 138–147. https://doi.org/10.1007/s11367-016-1246-y.

Jung, H., Sapner, V.S., Adhikari, A., Sathe, B.R., Patel, R., 2022. Recent progress on carbon quantum dots based photocatalysis. Front. Chem. 10, 881495 https://doi.org/10.3389/fchem.2022.881495.

Kaur, A., Gupta, U., Hasan, I., Muhammad, R., Ahmad Khan, R., 2021. Synthesis of highly fluorescent carbon dots from spices for determination of sunset yellow in beverages. Microchem. J. 170, 106720 https://doi.org/10.1016/j.microc.2021.106720.

Khan, M.E., Mohammad, A., Yoon, T., 2022. State-of-the-art developments in carbon quantum dots (CQDs): photo-catalysis, bio-imaging, and bio-sensing applications. Chemosphere 302, 134815. https://doi.org/10.1016/j.chemosphere.2022.134815.

Kumar, M., Choubey, V.K., Deepak, A., Gedam, V.V., Raut, R.D., 2021. Life cycle assessment (LCA) of dairy processing industry: a case study of North India. J. Clean. Prod. 326, 129331 https://doi.org/10.1016/j.jclepro.2021.129331.

Kurian, M., Paul, A., 2021. Recent trends in the use of green sources for carbon dot synthesis - a short review. Carbon Trends 3, 100032. https://doi.org/10.1016/j.cartre.2021.100032.

Li, J., Zuo, G., Qi, X., Wei, W., Pan, X., Su, T., Zhang, J., Dong, W., 2017. Selective determination of Ag^+ using Sidecan derived nitrogen doped carbon dots as a fluorescent probe. J. Mater. Sci. Eng. C 77, 508–512. https://doi.org/10.1016/j.msec.2017.04.007.

Li, J., Zuo, G., Pan, X., Wei, W., Qi, X., Su, T., Dong, W., 2018. Nitrogen-doped carbon dots as a fluorescent probe for the highly sensitive detection of Ag^+ and cell imaging. Luminescence 33, 243–248. https://doi.org/10.1002/bio.4236.

Luo, Z., Liu, E., Hu, T., Li, Z., Liu, T., 2015. Effect of synthetic methods on electrochemical performances of $VOPO_4{\cdot}2H_2O$ supercapacitor. Ionics 21, 289–294. https://doi.org/10.1007/s11581-014-1317-7.

Macairan, J.R., de Medeiros, T.V., Gazzetto, M., Yarur Villanueva, F., Cannizzo, A., Naccache, R., 2022. Elucidating the mechanism of dual-fluorescence in carbon dots. J. Colloid Interface Sci. 606, 67–76. https://doi.org/10.1016/j.jcis.2021.07.156.

Marras, Masia, S., Duce, P., Spano, D., Sirca, C., 2015. Carbon footprint assessment on a mature vineyard. Agric. For. Meteorol. 214–215, 350–356. https://doi.org/10.1016/j.agrformet.2015.09.270.

Nocito, G., Calabrese, G., Forte, S., Petralia, S., Puglisi, C., Campolo, M., Esposito, E., Conoci, S., 2021. Carbon Dots as promising tools for cancer diagnosis and therapy. Cancers 13, 1991. https://doi.org/10.3390/cancers13091991.

Park, C.H., Hira, S.A., Muthuchamy, N., Park, S., Park, K.H., 2019. Synthesis of silver nanostructures in ionic liquid media and their application to photodegradation of methyl orange. Nanomater. Nanotechnol. 9, 1847980419836500 https://doi.org/10.1177/1847980419836500.

Patra, S., Singh, M., Subudhi, S., Mandal, M., Nayak, A.K., Sahu, B.B., Mohanandia, P., 2023. One-step green synthesis of in-situ functionalized carbon quantum dots from Tagetes patula flowers: applications as a fluorescent probe for detecting Fe^{3+} ions and as an antifungal agent. J. Photochem. Photobiol. Chem. 442, 114779 https://doi.org/10.1016/j.jphotochem.2023.114779.

Perikala, M., Bhardwaj, A., 2021. Excellent color rendering index single system white light emitting carbon dots for next generation lighting devices. Sci. Rep. 11, 11594 https://doi.org/10.1038/s41598-021-91074-w.

Pianosi, F., Beven, K., Freer, J., Hall, J.W., Rougier, J., Stephenson, D.B., Wagener, T., 2016. Sensitivity analysis of environmental models: a systematic review with practical workflow. Environ. Model. Software 79, 214–232. https://doi.org/10.1016/j.envsoft.2016.02.008.

Podzia, M.Y., Zainal Abidin, Z., Abdul Rashid, S., Yusin, F.M., Noor, A.S.M., Issa, M.A., 2020. Eco-friendly sustainable fluorescent carbon dots for the adsorption of heavy metal ions in aqueous environment. Nanomaterials 10, 315. https://doi.org/10.3390/nano10020315.

Rajapandi, S., Pandeeswaran, M., Kousalya, G.N., 2022. Novel green synthesis of N-doped carbon dots from fruits of opuntia Ficus indica as an effective catalyst for the photocatalytic degradation of methyl orange dye and antibacterial studies. Inorg. Chem. Commun. 146, 110041 https://doi.org/10.1016/j.inoche.2022.110041.

Rodríguez-Padrón, D., Algarra, M., Tarelho, L.A.C., Frade, J., Franco, A., de Miguel, G., Jiménez, J., Rodríguez-Castellón, E., Luque, R., 2018. Catalyzed microwave-assisted preparation of carbon quantum dots from lignocellulosic residues. ACS Sustain. Chem. Eng. 6, 7200–7205. https://doi.org/10.1021/acssuschemeng.7b03848.

Sendão, R., Martínez de Yuso, M.V., Algarra, M., Esteves da Silva, J.C.G., Pinto da Silva, L., 2020. Comparative life cycle assessment of bottom-up synthesis routes for carbon dots derived from citric acid and urea. J. Clean. Prod. 254, 120080 https://doi.org/10.1016/j.jclepro.2020.120080.

Sharma, T., Dasgupta, D., Singh, J., Bhaskar, T., Ghosh, D., 2020. Yeast lipid-based biofuels and oleochemicals from lignocellulosic biomass: life cycle impact assessment, Sustain. Energy Fuels 4, 387–398. https://doi.org/10.1039/c9se00540d.

Sharma, S., Saini, S., Khangembam, M., Singh, V., 2021. Nanomaterials-based biosensors for COVID-19 detection-A review. IEEE Sensor. J. 21, 5598–5611. https://doi.org/10.1109/jsen.2020.3036748.

Sim, L.C., Tai, J.Y., Khor, J.M., Wong, J.L., Lee, J.Y., Leong, K.H., Saravanan, P., Aziz, A. A., 2019. Carbon dots synthesized from green precursors with an amplified photoluminescence: Synthesis, characterization, and its application, en: Plant Nanobiotics. Springer International Publishing, Cham, pp. 1–33.

Singh, P., Rani, N., Kumar, S., Kumar, P., Mohan, B., Pallavi, Bhankar, V., Kataria, N., Kumar, R., Kumar, K., 2023. Assessing the biomass-based carbon dots and their composites for photocatalytic treatment of wastewater. J. Clean. Prod. 413, 137474 https://doi.org/10.1016/j.jclepro.2023.137474.

Sun, Z., Li, X., Wu, Y., Wei, C., Zeng, H., 2018. Origin of green luminescence in carbon quantum dots: specific emission bands originate from oxidized carbon groups. New J. Chem. 42, 4603–4611. https://doi.org/10.1039/c7nj04762j.

Tajik, S., Dourandish, Z., Zhang, K., Beitollahi, H., Van Le, Q., Jang, H.W., Shokouhimehr, M., 2020. Carbon and graphene quantum dots: a review on syntheses, characterization, biological and sensing applications for neurotransmitter determination. RSC Adv. 10, 15406–15429. https://doi.org/10.1039/d0ra01709d.

Van Dam, B., Nie, H., Ju, B., Marino, E., Paulusse, J.M.J., Schall, P., Li, M., Dohnalová, K., 2017. Excitation-dependent photoluminescence from single-carbon dots. Small 13, 1702098. https://doi.org/10.1002/smll.201702098.

Wang, X., Wang, Y., Pan, W., Wang, J., Sun, X., 2021. Carbon-dot-based probe designed to detect intracellular pH in fungal cells for building its relationship with intracellular polysaccharide. ACS Sustain. Chem. Eng. 9, 3718–3726. https://doi.org/10.1021/acssuschemeng.0c08160.

Wang, Y., Wu, R., Zhang, Y., Cheng, S., Zhang, Y., 2023. High quantum yield nitrogen doped carbon dots for Ag^+ sensing and bioimaging. J. Mol. Struct. 1283, 135212 https://doi.org/10.1016/j.molstruc.2023.135212.

Wu, Y., Li, Y., Pan, X., Hu, C., Zhuang, J., Zhang, X., Lei, B., Liu, Y., 2021. Hemicellulose triggered high-yield synthesis of carbon dots from biomass. New J. Chem. 45, 5484–5490. https://doi.org/10.1039/d1nj00340h.

Wu, Q., Cao, J., Wang, X., Liu, Y., Zhao, Y., Wang, H., Liu, Y., Huang, H., Liao, F., Shao, M., Kang, Z., 2021. A metal-free photocatalyst for highly efficient hydrogen

peroxide photoproduction in real seawater. Nat. Commun. 12, 483. https://doi.org/10.1038/s41467-020-20823-8.

Xiong, H.F., An, B.L., Zhang, J.M., Yin, C.L., Wang, X.H., Wang, J.H., Xu, J.Q., 2021. Efficient one step synthesis of green carbon quantum dots catalyzed by tin oxide. Mater. Today Commun 26, 101762. https://doi.org/10.1016/j.mtcomm.2020.101762.

Yin, C.L., An, B.L., Li, J., Wang, X.H., Zhang, J.M., Xu, J.Q., 2021. High-efficient synthesis of bright yellow carbon quantum dots catalyzed by SnO_2 NPs. J. Lumin. 233, 117850 https://doi.org/10.1016/j.jlumin.2020.117850.

Zhao, B., Wang, B., Lu, H., Dai, S., Huang, Z., 2019. Tuning the visible-light photocatalytic degradation activity of thin nanosheets constructed porous g-C_3N_4 microspheres by decorating ionic liquid modified carbon dots: roles of heterojunctions and surface charges. New J. Chem. 43, 10141–10150. https://doi.org/10.1039/c9nj00308h.

Zheng, B., Chen, Y., Li, P., Wang, Z., Cao, B., Qi, F., Liu, J., Qiu, Z., Zhang, W., 2017. Ultrafast ammonia-driven, microwave-assisted synthesis of nitrogen-doped graphene quantum dots and their optical properties. Nanophotonics 6, 259–267. https://doi.org/10.1515/nanoph-2016-0102.

Zheng, S., Qin, F., Hu, C., Zhang, C., Ma, Y., Yang, R., Wei, L., Bao, L., 2021. Up-converted nitrogen-doped carbon quantum dots to accelerate charge transfer of dibismuth tetraoxide for enhanced full-spectrum photocatalytic activity. Colloids Surf. A Physicochem. Eng. Asp. 615, 126217 https://doi.org/10.1016/j.colsurfa.2021.126217.

Zhu, S., Song, Y., Zhao, X., Shao, J., Zhang, J., Yang, B., 2015. The photoluminescence mechanism in carbon dots (graphene quantum dots, carbon nanodots, and polymer dots): current state and future perspective. Nano Res. 8, 355–381. https://doi.org/10.1007/s12274-014-0644-3.

Zhu, L., Shen, D., Wu, C., Gu, S., 2020. State-of-the-art on the preparation, modification, and application of biomass-derived carbon quantum dots. Ind. Eng. Chem. Res. 59, 22017–22039. https://doi.org/10.1021/acs.iecr.0c04760.

Zhu, Z., Li, X., Luo, M., Chen, M., Chen, W., Yang, P., Zhou, X., 2022. Synthesis of carbon dots with high photocatalytic reactivity by tailoring heteroatom doping. J. Colloid Interface Sci. 605, 330–341. https://doi.org/10.1016/j.jcis.2021.07.016.

A1.1.1. Supporting Information

Supplementary Information

Nitrogen doped Carbon Dots as a Photocatalyst based on Biomass. A Life Cycle Assessment Analysis

Gabriela Rodríguez Carballo, Ramón Moreno Tost*, Sónia Fernandes, Joaquim C.G. Esteves da Silva, Luís Pinto da Silva, Eulogio Castro Galiano and Manuel Algarra*

The catalysts have been characterized by means of different analytical techniques to know their structural and acid properties. The diffraction patterns of both layered catalysts show the peaks corresponding to the crystalline phases of $VOPO_4 \cdot 2H_2O$ (PDF: 00-036-1472) and $NbOPO_4 \cdot xH_2O$ (PDF: 00-037-0378) (Figure SI.1) validating the synthesis procedure for both catalysts. However, the $NbOPO_4$ catalyst is also accompanied by a segregated phase of niobic acid (PDF: 00-061-0608. Both catalysts were further characterized by Raman spectroscopy to confirm the structure of the solids.

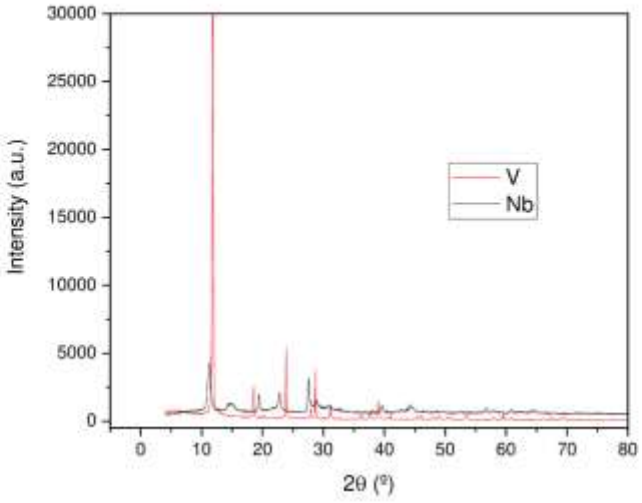

Figure SI.1. XRD patterns of the $VOPO_4 \cdot 2H_2O$ and NbOPO4·xH2O catalysts.

The Raman spectra (Figure SI.2) of $NbOPO_4$ show the symmetric stretching vibration of phosphate groups at 924 cm^{-1} [1,2,3] and the corresponding band to the disordered NbO_6 octahedra at 992 cm^{-1} [3,4,5,6] The band ascribed to Nb=O described in the bibliography at roughly 800 cm^{-1} [2,4,7,8] is absence in this solid since this band is sensitive to ordering and its intensity is lowered in disordered structures as McConnell *et al.* shown [6]. This was corroborated by XRD analysis showing a low crystallinity for this solid. The Raman spectra of the vanadium catalyst is like other published in bibliography [9, 10, 11, 12, 13]. Thus, the strong band at 925 cm^{-1} is due to the symmetric stretching vibration of phosphate groups. In addition, the bands corresponding the symmetric bending vibrations

Supplementary Information

at 536 and 576 cm^{-1} are observed [9]. Finally, the vanadyl stretching vibration lies on 1033 cm^{-1}.

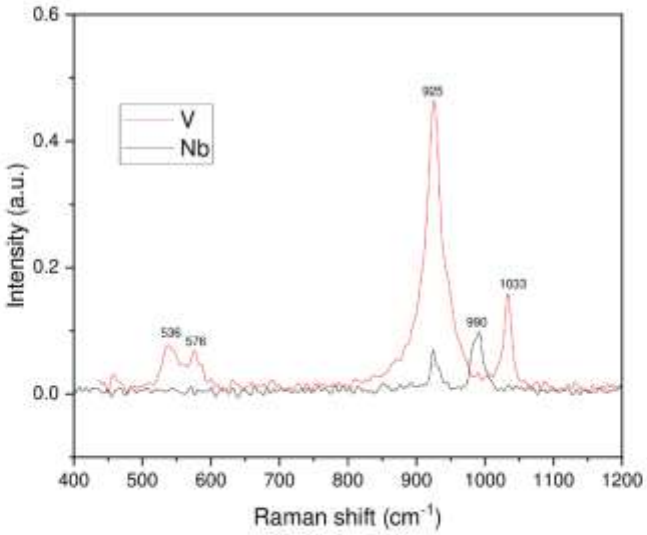

Figure SI.2. Raman spectra of the $VOPO_4 \cdot 2H_2O$ and $NbOPO_4 \cdot xH_2O$ catalysts.

As the synthesis of CDs requires acid conditions, so the acidity was evaluated by means of NH_3-TPD (Figure SI.3). Both catalysts show acid sites titrated by ammonia, the concentration of such sites is extremely high for the niobium catalyst (7.2 mmol NH_3/g) compared to vanadium catalyst (0.5 mmol NH_3/g). This fact could be due to the presence of the niobic acid which could contribute to the total acidity of the solid. Despite this difference on the acidity, the two catalysts are acid enough to carry out the reaction.

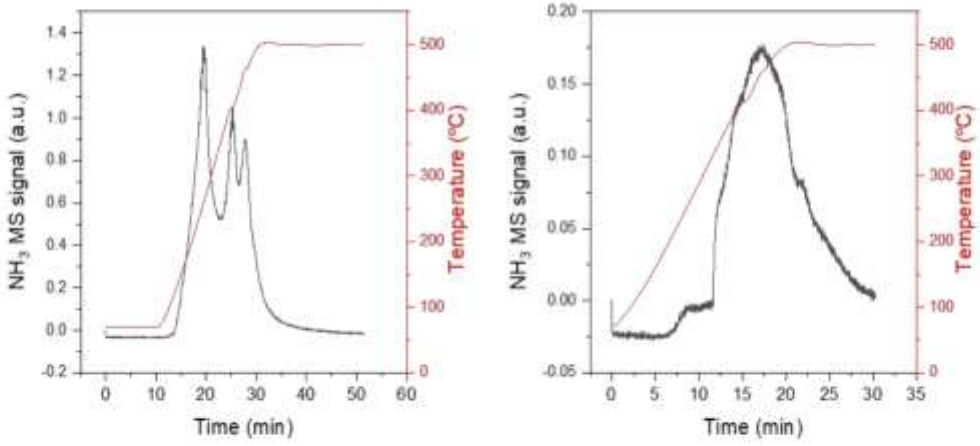

Figure SI.3. TPD of the $VOPO_4 \cdot 2H_2O$ and $NbOPO_4 \cdot xH_2O$ catalysts.

Supplementary Information

Catalysts were recovered partially from the bottom of the reactor once the reaction was completed and from centrifuging the resulting CDs solution. The solid obtained was left to dry overnight at 60ºC in stove and then calcined at 550 ºC for 4h in muffle furnace for the elimination of the residual carbon. Recovered catalyst was then used in a new cycle where its performance was studied. An XPS analysis was carried out for each catalyst to study the possible changes of the active surface. It is depicted in Figures SI.4 and SI.5 and Tables SI.1 and SI.2.The $VOPO_4 \cdot 2H_2O$ recovered catalyst was analyzed by XPS analysis. XPS atomic concentration showed that V/P superficial relationship remained the same after the reaction cycle and calcination (Table SI.1). Furthermore, V2*p* (Figure SI.10) band value can be associated to that of the V (V), no reduction was observed in the surface of the catalyst. Thus, indicating that it can be recovered and reused in a new cycle.

Table SI.1. Atomic concentration of V, C and P for $VOPO_4$.

Catalyst	V2*p* after reaction	V2*p* before reaction	C1*s* after reaction	C1*s* before reaction	P2*p* after reaction	P2*p* before reaction	V/P after reaction	V/P before reaction
$VOPO_4$	11.98	13.02	17.29	16.76	10.98	12.76	1.09	1.02

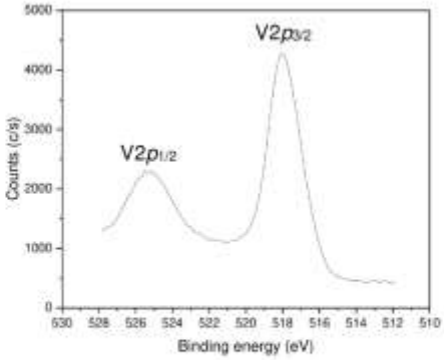

Figure SI.4. V 2*p* region of the catalyst after the reaction.

For $NbOPO_4$ (Table SI.2) catalyst, the Nb/P ratio also remained unchanged after reaction as the $VOPO_4$. The characteristic core level of Nb3*d* (Figure SI.11) showed a characteristic value of 208.5 eV Nb$3d_{5/2}$ related to Nb(V).

Table SI.2. Atomic concentration of Nb, C and P for $NbOPO_4$.

Catalyst	P2*p* after reaction	P2*p* before reaction	C1*s* after reaction	C1*s* before reaction	Nb3*d* after reaction	Nb3*d* before reaction	Nb/P after reaction	Nb/P before reaction

Supplementary Information

$NbOPO_4$	10.11	11.99	14.23	8.10	13.23	13.48	1.30	1.12

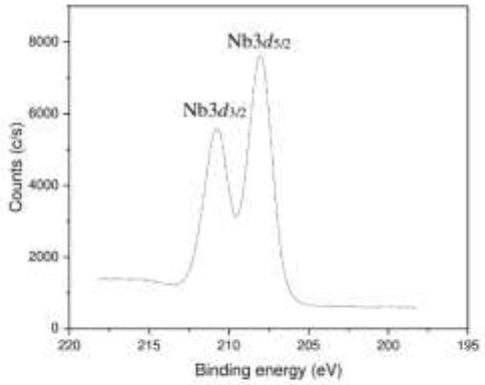

Figure SI.5. Energy binding spectrum of Nb3*d* core level in $NbOPO_4$.

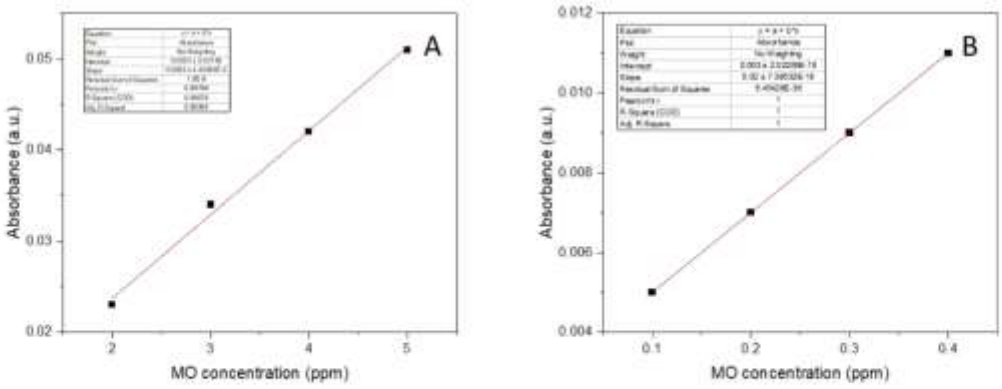

Figure SI.6. Calibration curves of standards for UV-vis spectrophotometry measurements.

Supplementary Information

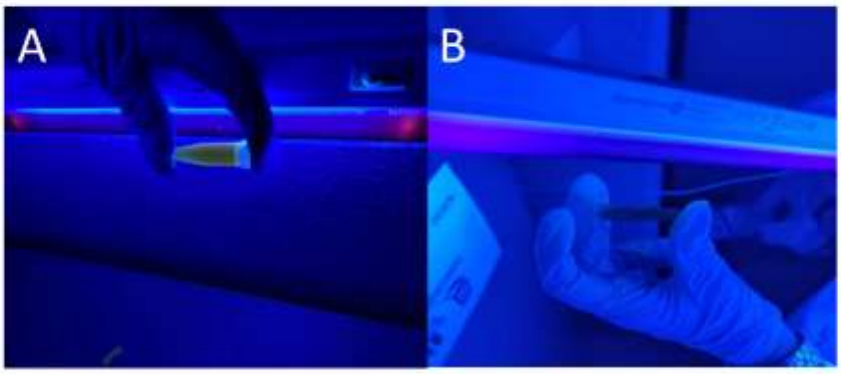

Figure SI.7. UV irradiation of a sample with (**A**) presence of CDs and (**B**) absence of CDs.

The graphite spacing of commercial xylose CDs (Figure SI.8) was also identified by means of TEM when the $NbOPO_4$ was used as catalyst, confirming that both methods were adequate routes for the obtention of CDs. XPS of xylose N-CDs (Figure SI.13.)

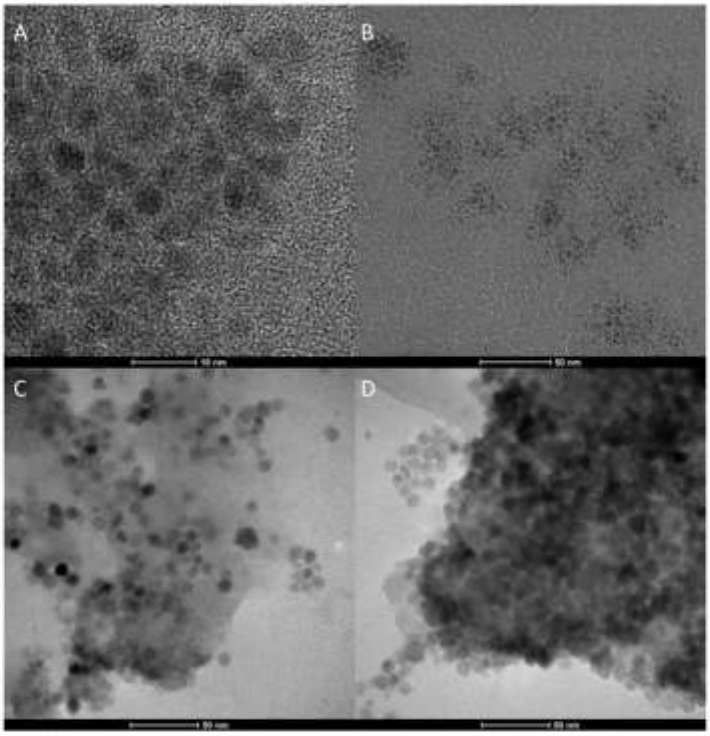

Figure SI.8. TEM images of **(A)** Pristine CDs from xylose and $NbOPO_4$ catalyst; **(B)** N-CDs from xylose and $NbOPO_4$ catalyst; **(C)** CDs from biomass liquor and $NbOPO_4$ catalyst; **(D)** N-CDs from biomass liquor and $NbOPO_4$ catalyst.

Supplementary Information

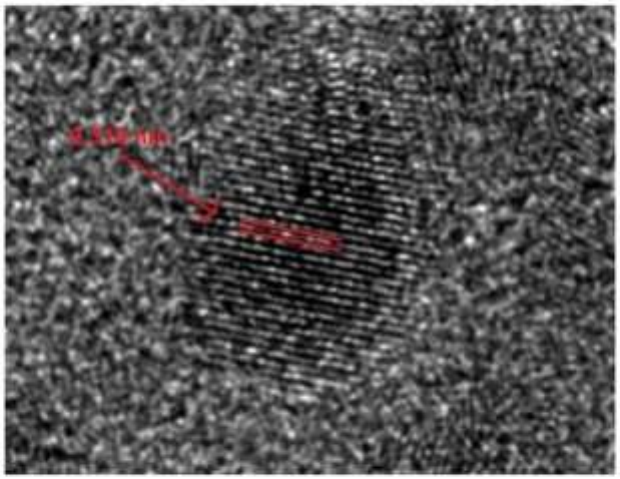

Figure SI.8E. Graphite spacing of CDs from $NbOPO_4$ catalyst.

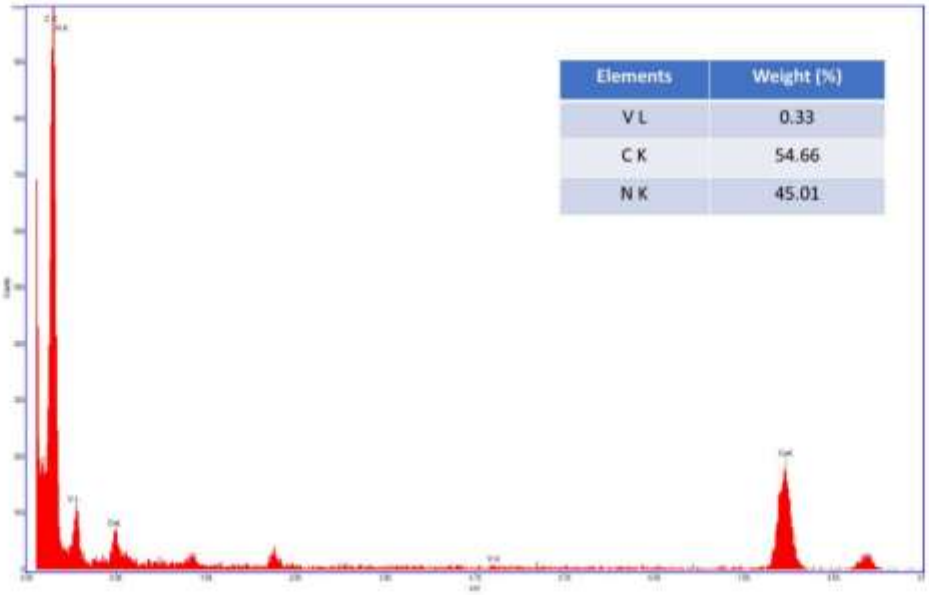

Figure SI.9. EDS analysis of biomass liquor N-CDs.

Supplementary Information

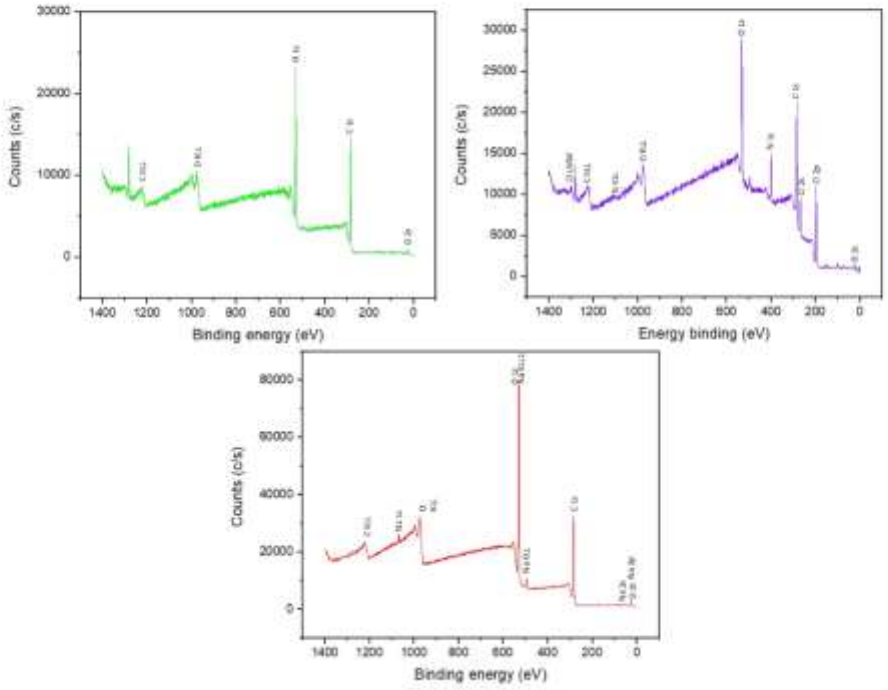

Figure SI.10. Survey XPS spectra of (**A**) commercial xylose CDs using $VOPO_4$ as catalys; (**B**) commercial xylose N-CDs using $VOPO_4$ as catalyst and (**C**) biomass liquor CDs using $VOPO_4$ as catalyst.

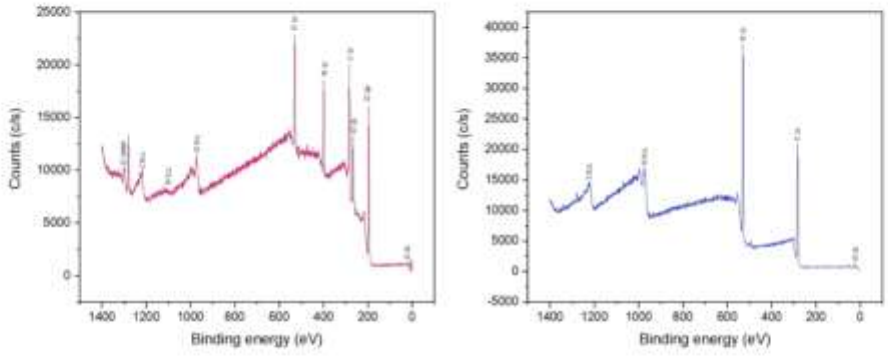

Figure SI.11. Survey XPS spectra of (**A**) commercial xylose CDs using $NbOPO_4$ as catalys; (**B**) commercial xylose N-CDs using $NbOPO_4$ as catalyst and (**C**) biomass liquor CDs using $NbOPO_4$ as catalyst.

Supplementary Information

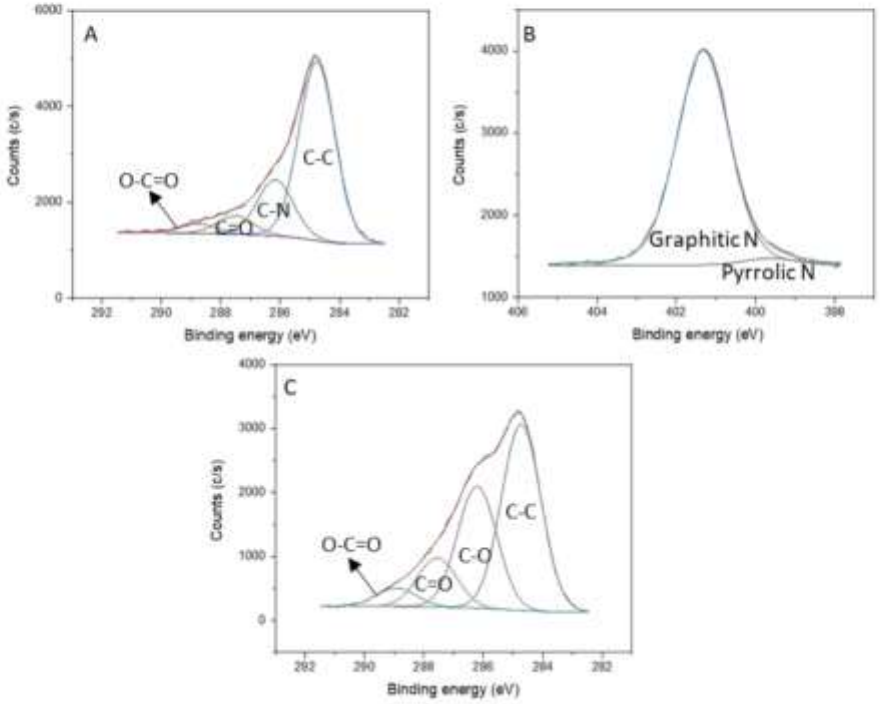

Figure SI.12. Deconvolution of the binding energy for **(A)** C 1*s* core level of commercial xylose N-CDs using $NbOPO_4$ as catalyst; **(B)** N 1*s* core level of commercial xylose N-CDs using $NbOPO_4$ as catalyst; **(C)** C 1*s* core level of commercial xylose CDs using $NbOPO_4$ as catalyst.

Table SI.3. Assignation of the binding energies resulted from the deconvolution of C1*s* core level of CDs synthesized from commercial xylose and $NbOPO_4$ as catalyst.

	C1*s* (eV)	C assignation	N1*s* (eV)	N assignation
Commercial xylose CDs	284.7 (48.13%)	C-C	N/A	
	286.1 (31.95%)	C-O		
	287.4 (14.51%)	C=O		
	288.7 (5.42%)	O-C=O		
Commercial xylose N-CDs	284.8 (67.00%)	C-C	399.5 (2.12%)	Pyrrolic N
	286.2 (21.71%)	C-N	401.3(97.88%)	Graphitic N
	287.5 (7.40%)	C=O	N/A	
	288.7 (3.89%)	O-C=O		

Supplementary Information

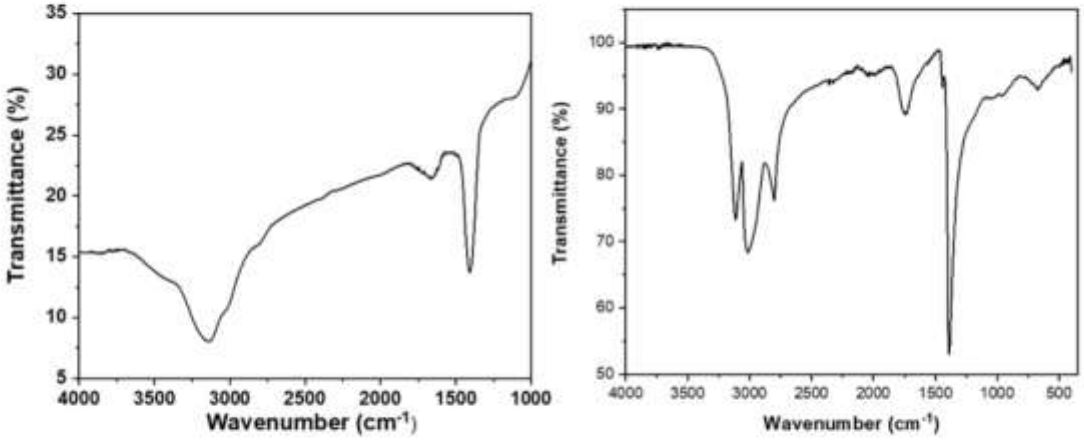

Figure SI.13. FTIR spectra of (**A**) commercial xylose CDs and (**B**) commercial xylose N-CDs.

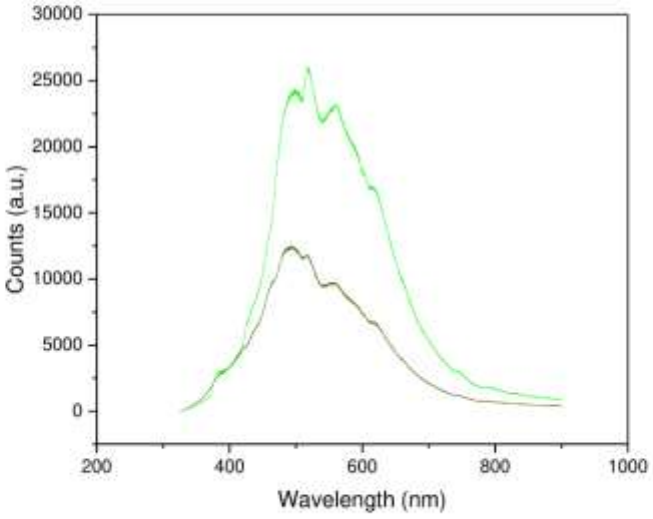

Figure SI.14. Photoluminescence spectra of recycled $NbOPO_4$ Catalyst.

Supplementary Information

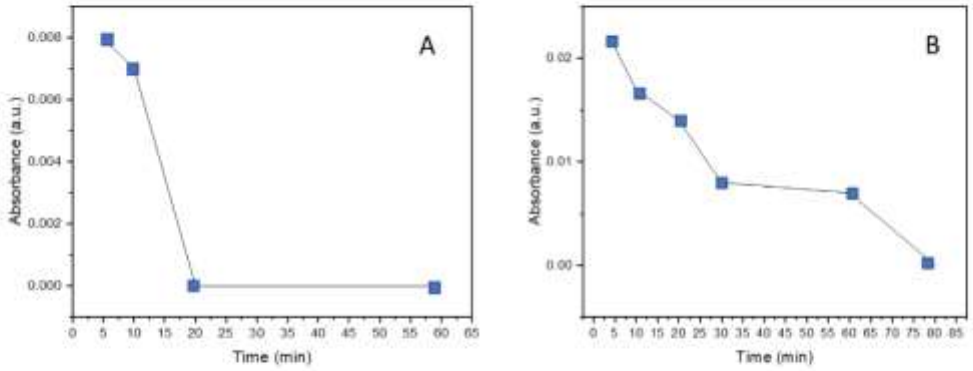

Figure SI.15. MO degradation catalysed by N-CDs from commercial xylose and $NbOPO_4$ as catalyst (**A**) and MO degradation catalysed by CDs from commercial xylose and $NbOPO_4$ as catalyst (**B**).

Life Cycle Impact Assessment

This LCA considered the characterization factors at endpoint level that correspond, according to ReCiPe method to three areas of protection (human health, ecosystems quality and resources scarcity). Human Health category considers the damage to human health, using the concept of disability-adjusted life years' (DALY), including years of life lost and years of life disabled to quantify the damage contributing to this area of protection [14]. This indicator combines mortality and morbidity. Ecosystems category, more specifically ecosystems quality, is described in terms of information flow at the species level, if the diversity of species properly represents the quality of ecosystems [14]. In this sense, this indicator has been represented by loss of species. Resources category is based on the geological distribution of mineral and fossil resources, considering that the use of these resources causes changes in the future resources extraction [14]. In this sense, this indicator reflects the increase of the extraction cost because of continuous resource extraction. These endpoint characterization factors are directly derived from the midpoint characterization factors [15].

Sensibility Analysis

In this sense, we evaluated if the decrease of the amount of used electricity (reduction of 2, 3 and 6 times the normal amount) in the production of biomass liqueur would lead to lower environmental impacts. The results can be observed on Figure SI.16. According to Figure 7 and as mentioned above the production of biomass liqueur presents higher impacts than xylose synthesis. However, the decrease of the amount of electricity in the production of biomass liqueur synthesis leads to lower impacts than the production of xylose. More specifically, the production of biomass liqueur would be more sustainable than the synthesis of xylose if the amount of used electricity was at least three times lower than the amount effectively used. This indicates that electricity is a hotspot regarding the environmental impacts associated with the production of biomass liqueur.

Supplementary Information

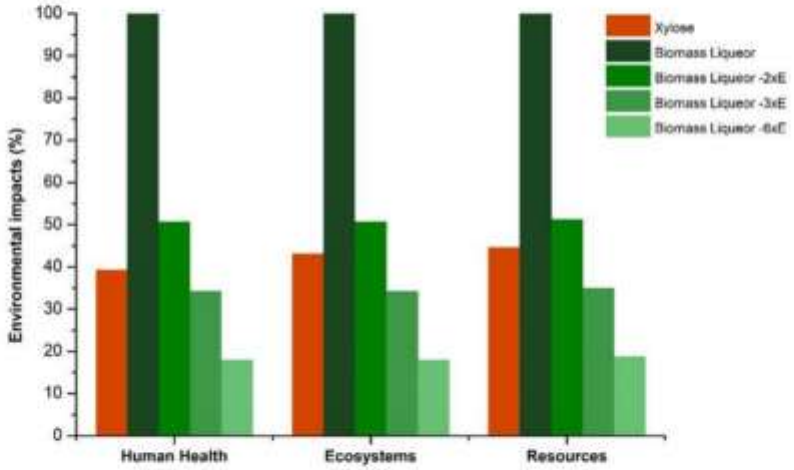

Figure SI.16. Relative environmental impacts for sensibility analysis of both carbon precursors syntheses (xylose and biomass liqueur), considering the decrease of electricity amount in biomass liqueur synthesis. E refers to electricity. This graphic was obtained applying ReCiPe endpoint method.

References

[1] Y. Zhu, Y. Qian, Z. Ju, Y. Ji, Y. Yan, Y. Liu, G. Yu, G. Understanding Charge Storage in Hydrated Layered Solids MOPO4 (M = V, Nb) with Tunable Interlayer Chemistry. ACS Nano 14 (2020) 13824-13833. https://doi.org/10.1021/acsnano.0c06193

[2] B. Wen, R. Guo, X. Liu, W. Luo, Q. He, C. Niu, J. Meng, Q. Li, Y. Zhao, L. Mai, Niobium Oxyphosphate Nanosheet Assembled Two-Dimensional Anode Material for Enhanced Lithium Storage. J. Energy Chem. 53 (2021) 268-275. https://doi.org/10.1016/j.jechem.2020.05.004

[3] J. Safaei, S.M.H. Mashkani, H. Tian, C. Ye, P. Xiong, G. Wang. Self-Assembled $NbOPO_4$ Nanosheet/Reduced Graphene Oxide Heterostructure for Capacitive Desalination. ACS Appl. Nano Mater. 4 (2021) 12629-12639. https://doi.org/10.1021/acsanm.1c03180

[4] G.T. Stranford, R.A. Condrate, A Raman Spectral Study of Hydrated Niobium Phosphate ($NbPO_5$) Phases. J. Solid State Chem. 76 (1988) 407-411. https://doi.org/10.1016/0022-4596(88)90235-6

[5] W. Weng, M. Davies, G. Whiting, B. Solsona, C.J. Kiely, A.F. Carley, S.H. Taylor, Niobium Phosphates as New Highly Selective Catalysts for the Oxidative

Supplementary Information

Dehydrogenation of Ethane. Phys. Chem. Chem. Phys. 13 (2011) 17395-17404. https://doi.org/10.1039/C1CP21136F

[6] A.A. McConnell, J.S. Aderson, C.N.R. Rao, Raman Spectra of Niobium Oxides. Spectrochim. Acta A 32 (1976) 1067-1076.https://doi.org/10.1016/0584-8539(76)80291-7

[7] F. Hardcastle, I. Wachs, I. Determination of Niobium-Oxygen Bond Distances and Bond Orders by Raman Spectroscopy. Solid State Ion. 45 (1991) 201-213. https://doi.org/10.1016/0167-2738(91)90153-3

[8] J. C. G.Da Silva, M.D. Vieira, W.D.O. Andrade, A. C. B. D. Santos. Chemical and Structural Aspects of a Layered Acid Niobium (V) Phosphate. J. Mater. Sci. 40 (2005) 4455-4460.https://doi.org/10.1007/s10853-005-2828-4

[9] M. Trchová, P. Čapková, P. Matějka, K, Melánová, L. Beneš, E. Uhlířová. Intercalation of Water into Anhydrous Vanadyl Phosphate Studied by the Infrared and Raman Spectroscopies. J. Solid State Chem. 148 (1999) 197-204. https://doi.org/10.1006/jssc.1999.8431

[10] Y. De Luna, N. Bensalah. Synthesis, characterization, and electrochemical evaluation of layered vanadium phosphates as cathode material for aqueous rechargeable Zn-ion batteries. Front. Mater. 8 (2021). https://doi.org/10.3389/fmats.2021.645915

[11] L. Griesel, J.K. Bartley, R.P.K. Wells, G.J. Hutchings, G. J. Preparation of Vanadium Phosphate Catalysts from VOPO4·2H2O: Effect of $VOPO_4{\cdot}2H_2O$ Preparation on Catalyst Performance. J. Mol. Catal. A Chem. 220 (2004) 113-119. https://doi.org/10.1016/j.molcata.2004.02.027

[12] M.R. Antonio, R.L. Barbour, P.R. Blum. Interlayer Coordination Environments of Iron, Cobalt, and Nickel in Vanadyl Phosphate Dihydrate, VOPO4.2H2O, Intercalation Compounds. Inorg. Chem. 26 (1987) 1235-1243. https://doi.org/10.1021/ic00255a012

[13] L. Beneš, K. Melánová, V. Zima, M. Trchová, P. Čapková, B. Koudelka. Vanadyl Phosphate Intercalated with Dimethyl Sulfoxide. J. Phys. Chem. Solids 67 (2006) 956-960. https://doi.org/10.1016/j.jpcs.2006.01.009

[14] Goedkoop, M., Heijungs, R., Huijbregts, M., De Schryver, A., Struijs, J., Van Zelm, R. ReCiPe 2008—A Life Cycle Impact AssessmentMethod Which Comprises Harmonised Category Indicators at the Midpoint and the Endpoint Level; VROM: Den Haag, The Netherlands, 2009; Volume 1, pp. 1–126

[15] Huijbregts M.A.J., Steinmann, Z.J.N., Elshout, P.M.F., Stam, G., Verones, F., Vieira, M., M. Zijp, M., Hollander, A., van Zelm, R. ReCiPe2016: a harmonised life cycle impact assessment method at midpoint and endpoint level. Int. J. Life Cycle Assess. 22 (2017), 138-147. https://doi.org/10.1007/s11367-016-1246-y.

Appendix 2

A2.1. **Article V**: Safety Evaluation of Carbon Dots in UM-UC-5 and A549 Cells for Biomedical Applications Introduction

Carla M. Magalhães, Eduarda Ribeiro, Sónia Fernandes, Joaquim Esteves da Silva, Nuno Vale, Luís Pinto da Silva

cancers

MDPI

Article

Safety Evaluation of Carbon Dots in UM-UC-5 and A549 Cells for Biomedical Applications

Carla M. Magalhães [1], Eduarda Ribeiro [2,3], Sónia Fernandes [1], Joaquim Esteves da Silva [1], Nuno Vale [2,3,4,*] and Luís Pinto da Silva [1,*]

[1] Chemistry Research Unit (CIQUP), Institute of Molecular Sciences, Department of Geosciences, Environment, and Spatial Plannings, Faculty of Sciences, University of Porto, Rua do Campo Alegre s/n, 4169-007 Porto, Portugal; up201201533@fc.up.pt (C.M.M.); up201708297@fc.up.pt (S.F.); jcsilva@fc.up.pt (J.E.d.S.)
[2] PerMed Research Group, Center for Health Technology and Services Research (CINTESIS), Rua Doutor Plácido da Costa, 4200-450 Porto, Portugal; eduardaprr@gmail.com
[3] CINTESIS@RISE, Faculty of Medicine, University of Porto, Alameda Hernâni Monteiro, 4200-319 Porto, Portugal
[4] Department of Community Medicine, Health Information and Decision (MEDCIDS), Faculty of Medicine, University of Porto, Rua Doutor Plácido da Costa, 4200-450 Porto, Portugal
* Correspondence: nunovale@med.up.pt (N.V.); luis.silva@fc.up.pt (L.P.d.S.)

Simple Summary: Carbon dots (CDs) are carbon-based nanomaterials with versatile applications, including fluorescence imaging, drug and gene transport, drug delivery, medical diagnosis, and biosensing. In this study, we successfully synthesized various CDs without significantly impacting the cell viability of cancer cells, which suggests the potential for future bioimaging and drug delivery applications. These findings contribute to advancing the potential of CDs in various biomedical research contexts.

Abstract: Backgroung: The rising complexity and associated side effects of cancer treatments highlight the need for safer and more effective therapeutic agents. Carbon-based nanomaterials such as CDs have been gaining prominence for their unique characteristics, opening avenues for diverse applications such as fluorescence imaging, drug and gene transport, controlled drug delivery, medical diagnosis, and biosensing. Despite promising advancements in research, it remains imperative to scrutinize the properties and potential cytotoxicity of newly developed CDs, ensuring their viability for these applications. Methods: We synthesized four N-doped CDs through a hydrothermal method. Cell viability assays were conducted on A549 and UM-UC-5 cancer cells at a range of concentrations and incubation times, both individually and with the chemotherapeutic agent 5-fluorouracil (5-FU). Results: The obtained results suggest that the newly developed CDs exhibit suitability for applications such as bioimaging, as no significant impact on cell viability was observed for CDs alone.

Keywords: nanomaterials; carbon dots; bioimaging; drug delivery; cancer cells; anticancer activity

Citation: Magalhães, C.M.; Ribeiro, E.; Fernandes, S.; Esteves da Silva, J.; Vale, N.; Pinto da Silva, L. Safety Evaluation of Carbon Dots in UM-UC-5 and A549 Cells for Biomedical Applications. *Cancers* **2024**, *16*, 3332. https://doi.org/10.3390/cancers16193332

Academic Editor: Stefano Leporatti

Received: 6 September 2024
Revised: 26 September 2024
Accepted: 26 September 2024
Published: 29 September 2024

1. Introduction

Cancer poses a formidable challenge due to the complexity of available treatments and associated side effects. In 2020 alone, there were 18.1 million reported cases worldwide, resulting in 10 million deaths [1]. Numerous research groups have been dedicated to advancing therapies, such as targeted therapy and immunotherapy, as well as developing novel chemotherapeutic agents [2–4]. Despite these efforts, the limitations of targeted therapies, which only address specific targets, and the occurrence of severe side effects, including skin reactions and autoimmune responses, contribute to suboptimal and inefficient cancer treatments for patients [5–7]. Hence, there is a crucial need for developing safer and more effective therapeutic agents, particularly those capable of precise delivery to the desired

target site. Over the past few decades, nanotechnology has emerged as a dominant force in cutting-edge research across different fields, including biomedicine, molecular diagnostics, pharmaceuticals, optoelectronics, and environmental preservation [8–13]. The prominently developed components involve nanoparticles, such as liposomes, solid lipid nanoparticles, dendrimers, polymers, and materials like silicon and carbon, characterized by sizes smaller than 100 nm [14–18].

Lately, significant focus has been directed towards carbon-based nanomaterials, including Carbon Dots (CDs), fullerenes, Carbon nanotubes (CNTs), and Graphene Quantum Dots (GQDs) [19–22]. CDs stand out as a type of carbon nanomaterial with sizes below 10 nm [23,24] and with a core that is thought to be composed of sp^2 carbon connected by sp^3 carbon atoms in between [25–27]. On their surface, different types of functional groups (such as carboxylic acids, alcohols, and amines) can be found whose identity depends on the type of precursor used and the synthesis route employed [28,29]. These nanomaterials boast unique properties such as high photoluminescence, cost-effective synthesis, chemical stability, and environmental friendliness. These distinctive properties enable diverse applications, including imaging, drug and gene transport through conjugation, controlled drug delivery, medical diagnosis, and biosensing [25–29]. CDs can be prepared through "top-down" and "bottom-up" strategies [11,25,28,30]. Top-down synthesis involves the breakdown of large carbon structures into smaller ones [27,30,31]. However, bottom-up synthesis is the more commonly applied method, where CDs are produced from smaller carbon structures (such as carbohydrates and citric acid) through processes like calcination, hydrothermal treatment, and microwave-assisted synthesis [30,32,33]. These pathways are often favored because they are a cost-effective, environmentally friendly, and non-toxic approach for CD production [34–36].

Citric acid emerges as the preferred precursor for CD synthesis due to its affordability, ready availability, and low carbonization temperature [16,28,32]. Nonetheless, using citric acid in the synthesis process tends to result in low photoluminescence [37,38]. Thus, to overcome this problem, heteroatom-doping of CDs (using N, S, P, and B) is employed to enhance the fluorescence quantum yield (QY_{FL}) [11,16,39]. The most commonly employed strategy is N-doping, where a nitrogen-rich molecule, such as urea [34,40,41] or ethylenediamine (EDA) [41,42], is added to the carbon precursor. Furthermore, an additional nitrogen atom offers five valence electrons for bonding with carbon atoms [43,44]. Indeed, when employing bottom-up strategies, a diverse range of precursors can be used, enabling the production of CDs without the need for sophisticated equipment [32,45]. CDs can be generated using various biomass or organic waste as precursors, facilitating the valorization of different residues within a circular economy framework [46,47].

Given the exponential development and study of new CDs, it is crucial to evaluate their biocompatibility to assess their potential applications and guide further application studies. Numerous researchers have been synthesizing CDs from several natural sources and investigating their applicability in cancer treatment and bioimaging. For instance, Li et al. extracted fluorescent CDs from ginger and tested them on different cancer cell lines, including the human lung cancer cell line (A549), human breast cancer cell line (MDA-MB-231), human cervical cancer cell line (HeLa), and human hepatocellular carcinoma cell line (HepG2). Their findings revealed a higher growth suppression effect in HepG2 cells [48]. In another study, Xie et al. used date pits to synthesize CDs and explored their impact on the growth of cancer cells, including A549 cancer cells, breast cancer (MCF-7), and prostate cancer (PC3) cells. The inhibition rates were reported as 52%, 65%, and 26%, respectively [49]. Additionally, Wang et al. combined Metformin (Met) and CDs for integrated tumor imaging and therapy, demonstrating a significant inhibitory effect on A549 cancer cells [50].

Despite these promising advancements and positive outcomes in existing research, it remains crucial to investigate the properties and potential cytotoxicity effects of newly developed CDs to determine their suitability for in vivo/vitro imaging and drug delivery applications. Hence, this study aims to assess the chemical properties and the biocompati-

bility of four N-doped CDs in A549 and UM-UC-5 cancer cell lines. To that end, these CDs were prepared through a hydrothermal approach based on routes previously documented by our research group [32,51]. Then, an MTT assay was performed to evaluate the cytotoxicity of CDs in A549 and UM-UC-5 cancer cell lines. Moreover, to gain additional insights into the potential application of these CDs in drug delivery, we explored their interactions in the presence of an anticancer drug, 5-Fluorouracil (5-FU) [52,53].

2. Materials and Methods

2.1. Synthesis of CDs

In this study, four CDs were synthesized, following previously described procedures [52,54]. The synthesis followed a hydrothermal methodology. In brief, for the synthesis of CD-1, CD-2, and CD-3, 0.075 g of citric acid (CA) and 0.075 g of corn stover (whereas for CD-4, 0.150 g of CA were used) were combined with ethylenediamine (EDA, 166.9 µL) and dissolved in 0.01 M NaOH (10 mL). This mixture was placed in a Teflon-lined container, then enclosed in a steel outer shell. The reaction proceeded for 4 h (CD-1), 16 h (CD-2), or 24 h (CD-3) at 200 °C in an oven (VWR DL 112 Prime oven, 2500 W power consumption, Avantor, PA, USA). Following this period, the container was allowed to cool to room temperature, and the reaction products underwent centrifugation (6000 rpm, 30 min) to eliminate insoluble components. Subsequently, dialysis was performed (24 h, molecular weight cutoff of 3.5 kDa) to remove soluble by-products formed during the synthesis that could impact the properties and photoreactivity of the nanoparticles [13]. Finally, to determine the mass concentration of the CDs, the purified CD solution underwent lyophilization, was weighed, and dissolved in deionized water (5 mL). The CDs were then stored in cold conditions (4 °C) until use. The synthesis yields obtained were 8.4%, 6.2%, 5.5%, and 2.4% for CD-1, CD-2, CD-3, and CD-4, respectively.

2.2. Characterization of CDs

AFM analysis was conducted by using the tapping mode with a Veeco Metrology Multimode/Nanoscope IVA. For this analysis, a silica plate was used to deposit the sample for analysis, and an AFM TESP-SS cantilever (curvature radius of 2 nm) was used. Samples were prepared via drop evaporation of the diluted CD solution, and NanoScope v. 1.40 was the software used for the AFM data analysis. Particle size measurements were made based on the height of the particles, and the average size was calculated by averaging the measurements of 100 individual particles. The absorption spectra were recorded using a VWR® UV3100PC spectrophotometer (with the UV–Vis Analyst software v.5.44) and standard 10 mm quartz cells. The fluorescence spectra of the CDs were obtained using a Horiba Jovin Yvon Fluoromax-4 spectrofluorimeter using the FluorEssence software v.3.9 to analyze the results. Slit widths of 5 nm or 2 nm were employed when obtaining 2D matrices and fluorescence spectra emission, respectively. Photostability was evaluated by exposing the CD sample to a continuous LED light source (OceanOptics, Orlando, FL, USA) of 365 nm. Then, fluorescence spectra were obtained at t = 10, 15, 20, and 30 min. Standard 10 mm fluorescence quartz cells were used. The Zeta Potential was measured by using a particle analyzer Anton Paar LitesizerTM 500 (Anton Paar, Graz, Austria) and a polycarbonate Omega Cuvette (Ref. 155765).

2.3. Fluorescence Quantum Yield (QY_{PL}) Calculations

The fluorescence quantum yield (QY_{FL}) was determined using a standard procedure that involved comparing the integrated photoluminescence intensities and absorbance values of the prepared CDs with those of a reference fluorophore. The QY_{FL} value, expressed as a percentage, is calculated using the following equation:

$$QY_{FL}^{Sample} = QY_{FL}^{Ref} \times \frac{Grad_{Sample}}{Grad_{Ref}} \times \frac{{\eta_{Sample}}^2}{{\eta_{Ref}}^2} \times 100$$

In the above equation, Grad corresponds to the gradient of the plot of integrated fluorescence intensity versus absorbance for both the sample and the reference fluorophore and η is the refractive index of the medium. Quinine sulphate was chosen as the reference fluorophore ($QYFL = 54\%$) for the quantum yield calculations due to the similarities of its photoluminescent properties to those of our CDs [54].

2.4. CDs Toxicity Assays

2.4.1. Cells, Medium, and Compounds

A549 adenocarcinoma human alveolar basal epithelial cancer cell and UM-UC-5 urothelial bladder cancer cell lines were obtained from the American Type Culture Collection (ATCC; Manassas, VA, USA). The cells were cultured in a humidified incubator with 5% CO_2 at 37 °C in DMEM medium (PAN-Biotech, Aidenbach, Germany), supplemented with 10% fetal bovine serum (FBS) and 1% penicillin–streptomycin (pen–strep) solution. These reagents were purchased from Millipore Sigma (Merck KGaA, Darmstadt, Germany). The medium was changed every 2–3 days.

2.4.2. Cell Viability Assays

Cell viability was assessed using the MTT (Thiazolyl blue tetrazolium bromide; cat. no. M5655; Sigma-Aldrich; Merck KGaA, Darmstadt, Germany) assay in 96-well plates. For the assay, 5000 cells in 200 µL of medium were seeded per well and incubated for 24 h at 37 °C. Subsequently, cells were treated with CDs at concentrations of 0.1, 0.8, 1.0, 1.5, 1.8, and 2.35 g/L. Control wells were treated with 0.1% H_2O and 0.1% DMSO (vehicle controls). After 24 h and 72 h of incubation at 37 °C, the media were aspirated and 100 µL of MTT solution (0.5 mg/mL in PBS) was added to each well. Following 3 h of incubation at 37 °C in the dark, the MTT solution was removed, and 100 µL of DMSO was added to solubilize the formazan crystals. Absorbance was measured using a Tecan Infinite M200 plate reader (Tecan Group Ltd., Männedorf, Switzerland) at 570 nm. Cell viability was calculated relative to the absorbance of vehicle controls. Average values were delivered from three independent experiments ($n = 3$).

2.4.3. Morphological Analysis

Changes in cell morphology were evaluated after cell treatment using a Leica DMI 6000B microscope equipped with a Leica DFC350 FX camera (Leica Microsystems, Wetzlar, Germany). Images were analyzed with the Leica LAS X imaging software (v3.7.4) (Leica Microsystems, Wetzlar, Germany).

2.4.4. Synergistic Effect Analysis

To evaluate the interaction between the chemotherapeutic drug and each carbon dot, we employed the Chou–Talalay method using the CompuSyn software (version 1.0; ComboSyn, Paramus, NJ, USA) to calculate the Combination Index (CI). CI values help classify the interactions: $CI < 1$ signifies synergism, $CI = 1$ denotes an additive effect, and $CI > 1$ indicates antagonism. These simulations were conducted using a non-fixed dose ratio, maintaining a constant concentration of the chemotherapeutic drug while varying the concentrations of each carbon dot.

2.4.5. Statistical Analysis

Cell viability graphs were obtained using the software GraphPad Prism 9 (GraphPad Software Inc., San Diego, CA, USA) after conducting three independent experiments ($n = 3$). Results are represented as the mean ± SD for n experiments performed. Statistical analysis was performed with one-way ANOVA tests by Dunnett's multiple comparisons between the control and treatment groups. Results were considered statistically significant for p values < 0.05.

3. Results and Discussion

3.1. Characterization of CDs

In the current study, four distinct CDs were synthesized using a hydrothermal methodology. Specifically, citric acid and corn stover were used as the carbon precursors (for CD-4, only citric acid was used), and EDA was used to achieve N-doping. The reaction times were set at 4 and 16 h for CD-1 and CD-2, respectively, and 24 h for CD-3 and CD-4. Size distributions were determined through AFM measurements (Figure 1). CD-1, CD-2, and CD-3 presented sizes of ~1 nm, typical of CDs. CD-4 was previously found to present a particle size of ~2 nm [55].

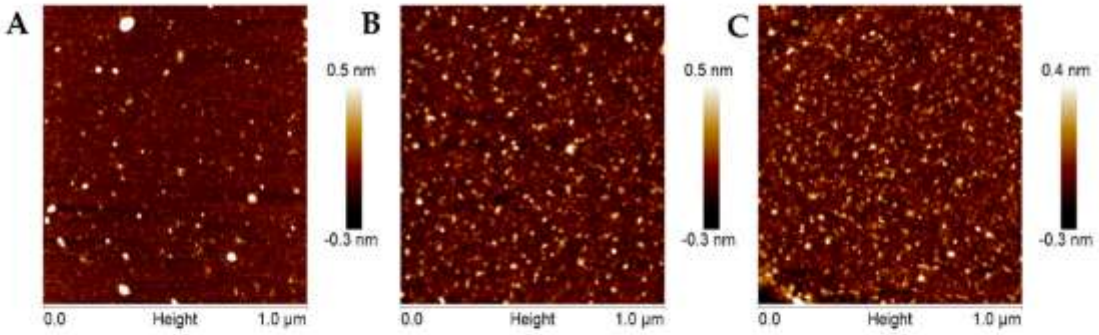

Figure 1. AFM images of CD−1 (**A**), CD−2 (**B**), CD−3 (**C**).

To assess the photoluminescent properties of CDs, 2D excitation–emission contour plots (EECP) were measured (Figure 2), demonstrating similar fluorescent properties between samples. Consistently with the previous analysis [55], CD-1/2/3 exhibited a single emissive center featuring an emission peak at 440 nm. The excitation maxima for these CDs are at ~350 nm. Additionally, we calculated the quantum yield of photoluminescence (QY_{PL}) using quinine sulfate as a reference [56]. The resulting values were 9.9%, 38.9%, and 33.1% for CD-1, CD-2, and CD-3, respectively. The absorption spectra of these CDs were also obtained (Figure 3). The results indicate that all three CDs share identical absorption spectra, characterized by a primary band at ~340 nm and a shoulder at ~230 nm. These features are attributed to n-π^* and π-π^* transitions, respectively [57–59]. These findings align with the previous features obtained for CDs [8,33,34,46,60], as well as our previous study of CD-4 [60]. These results are expected as the newly developed CDs are variations of CD-4, using corn stover in the synthesis process.

To gain insights into the ionization state of the nanoparticle surface, we measured the Zeta Potential of these CDs, yielding the following values: -5.9 ± 0.31, -6.3 ± 0.32, -4.2 ± 0.33, and -5.7 ± 0.35 mV for CD-1 to CD-4, respectively. These values collectively suggest that all four CDs display a negative Zeta Potential with no significant variations between them [49,50,52,61].

To understand the potential pH effect on the fluorescence of CDs, we have measured their emission spectra at pH 5 and 9 (Figure 4). The obtained results show that for all the CDs, either acidic or basic pH present the same maximum emission. More specifically, the maximum emission is ≈440 nm, irrespective of the pH of the media. Given this, all the CDs appear to be stable to pH variations.

We have also evaluated the photostability of CDs, under 30 min UV irradiation, by using an LED light source of 365 nm. More specifically, the photostability was monitored by measuring the emission spectra at t = 0, 10, 15, 20, and 30 min (Figure 5). For CD-1, there was a small increase in emission intensity after 10 min of irradiation, followed by a decrease in emission intensity onward. Nevertheless, this decrease (compared with t = 0 min) appears less relevant. A similar decrease was also seen for CD-2, with the

difference being the continuous decrease in emission intensity over time. On the contrary, CD-3 was found to be less photostable, with a decrease of emission intensity to ~50% over 30 min of irradiation, when compared with the values measured at t = 0 min. Finally, CD-4 presents a similar behavior to that of CD-1 and CD-2. Namely, a small decrease in emission intensity over 10/20 min of irradiation, followed by relative stabilization. Thus, CD-1, CD-2, and CD-4 appear to be relatively photostable, with CD-3 showing a significant reduction in emission intensity due to UV light irradiation.

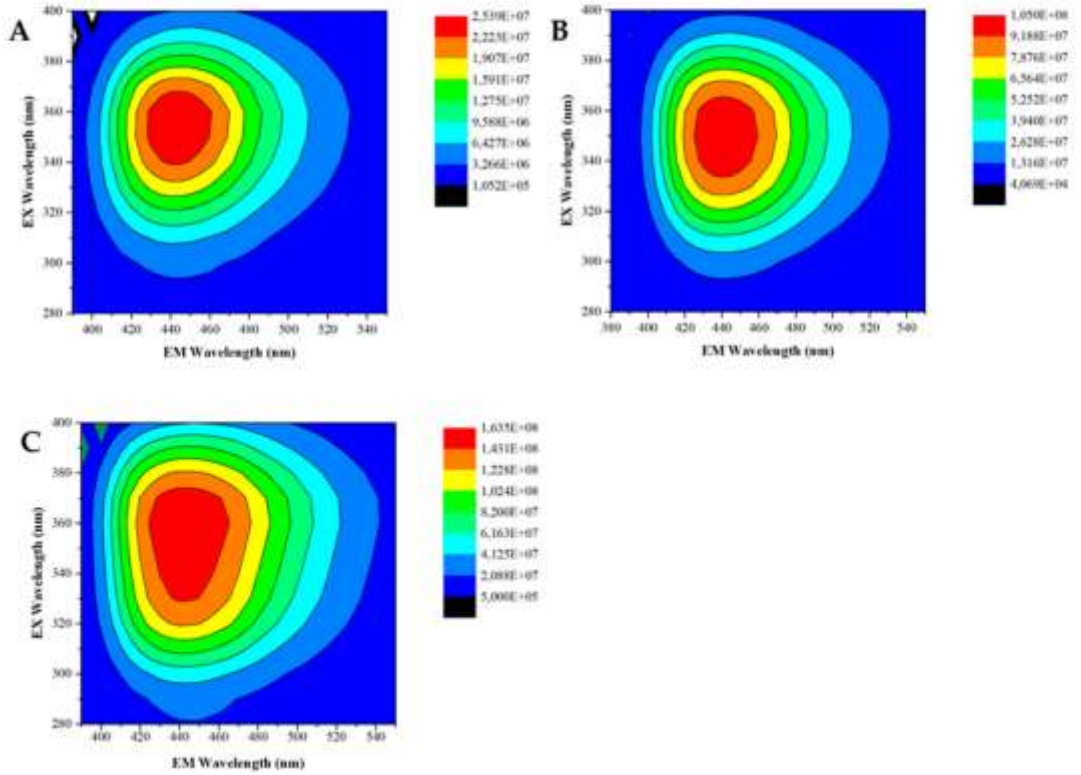

Figure 2. 2D fluorescence excitation–emission matrices of CD−1 (**A**), CD−2 (**B**), and CD−3 (**C**).

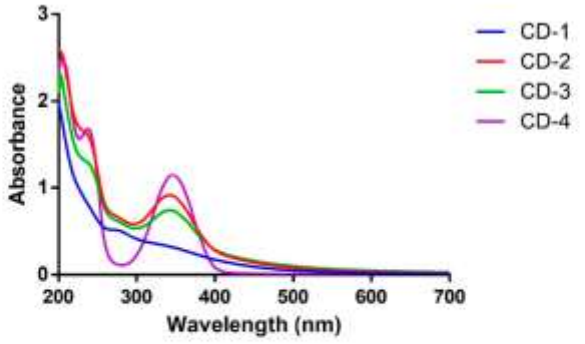

Figure 3. UV–Vis spectra of CDs.

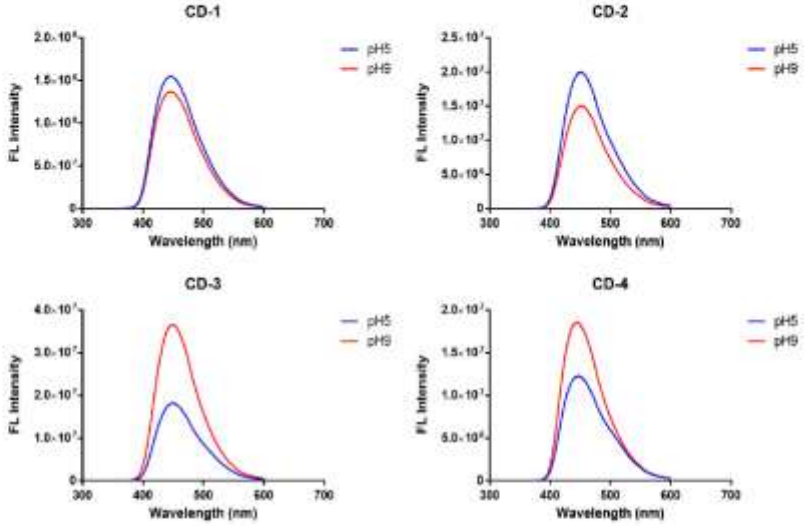

Figure 4. Emission spectra of CDs at pH 5 and 9, in aqueous solution.

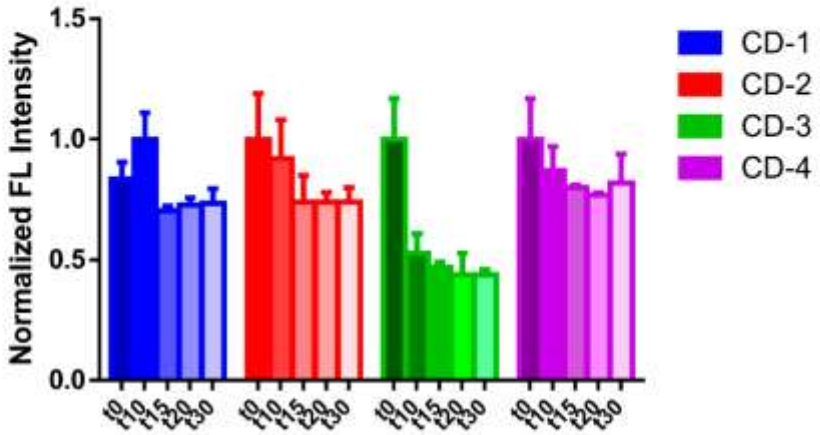

Figure 5. Normalized emission intensity of CDs under UV light irradiation, at t = 0, 10, 15, 20, and 30 min.

3.2. Cytotoxic Effect of CDs on A549 and UM-UC-5 Cell Lines

In our investigation to ascertain the suitability of these nanoparticles for applications in bioimaging and drug delivery, we assessed their potential effects when interacting with cancer cells. Specifically, we studied the cytotoxic effects of the four CDs on A549 and UM-UC-5 cancer cell lines. The cells were incubated with CDs within a 0.1–3.14 g/L concentration range for 24 and 72 h. When choosing these incubation times, we wanted to evaluate the long-term safety of these nanomaterials and ensure the absence of any associated cytotoxic effects. Additionally, we tested the impact of a standard chemotherapeutic agent, 5-fluorouracil (5-FU, Figure 6), and calculated IC50 for future combinations. To evaluate cell viability, we conducted the MTT assay. In this assessment, the control well signifies 100% viable cells, and the percentage of cell viability in each well is expressed relative to that of the control.

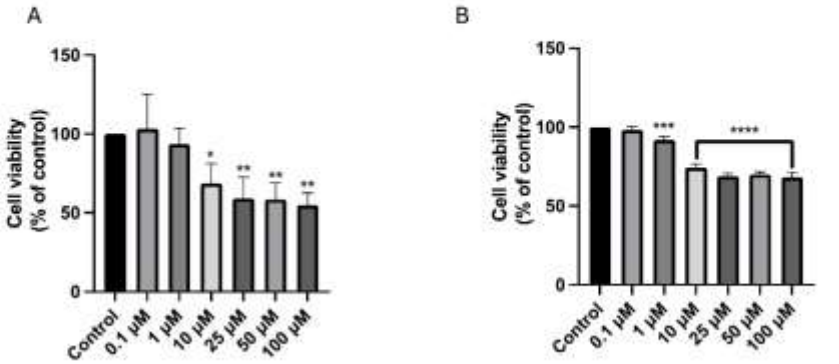

Figure 6. Cell viability of A549 (**A**) and UM-UC-5 (**B**) cancer cells treated with 5-FU for 48 h. Cultured cells were seeded in 96-well plates and treated with 5-FU (0.1–100 µM). Cells treated with vehicle (0.1% DMSO) were used as the control. Values are expressed as percentages of control and represent means ± SD. Each experiment was done three times independently ($n = 3$). * Statistically significant vs. control at $p < 0.1$. ** Statistically significant vs. control at $p < 0.01$. *** Statistically significant vs. control at $p < 0.001$. **** Statistically significant vs. control at $p < 0.0001$.

The IC50 value serves as a quantitative indicator of the drug's effectiveness in inhibiting cancer cell growth. Notably, 5-FU demonstrate significant cytotoxic effect to A549 cells above 10 µM, with only 2.42 µM of 5-FU necessary to reduce 50% of A549 cells viability (Figure 6A). UM-UC-5 cells exhibited a modest response to the cytotoxic effects of 5-FU, with concentrations above 1 µM exhibiting significant anti-cancer effects (Figure 6B). Consequently, a concentration of 2.42 and 4.21 µM of 5-FU was applied to A549 and UM-UC-5 cells, respectively, for further experimentation.

The results of the 24-h incubation period (Figure 7) indicate that, at this stage, the CDs exerted no discernible effect on either A549 (Figure 7A) or UM-UC-5 (Figure 7B) cancer cells. Cellular viability remained consistent across the tested concentrations. Notably, our team's previous evaluation of CD-4 on A549 cancer cells [55] also revealed no significant cytotoxic effects after 24 and 72 h of incubation. Thus, the cytotoxic effect of CD-1/2/3 in these cancer cells is consistent with previous results for CD-4. Curiously, CD-1 and CD-2 induced a significant increase in cell viability that could be attributed to either an elevated cell count in the well or increased metabolic activity of the cells. Variations in cellular metabolism or minor pipetting errors leading to slightly higher cell seeding in specific wells can result in samples exceeding 100% viability, which is considered normal. Our findings indicate that these CDs may also impact cell growth, as confirmed by cell counting with trypan blue.

Morphological evaluations were conducted to examine potential modifications in the phenotype of both A549 and UM-UC-5 cells (Figure 8). Consistently with cellular viability, at the 24-h incubation mark, no significant morphological alterations were detected for the tested nanoparticles. This observation suggests that, within this timeframe, the nanoparticles did not induce noticeable changes in the visual appearance or structure of the studied cancer cells. These findings collectively suggest that, within the investigated timeframe, the CDs did not induce significant cytotoxicity in the studied cancer cell lines.

Then, we extended the incubation time of this analysis to a period of 72 h when accessing the cell viability of A549 and UM-UC-5 cancer cells in the presence of CDs. The results (Figure 9) indicate that no effect was observed on cell viability for the A549 cancer cell line across the range of CD concentrations studied (Figure 9A). On the other hand, when analyzing the results for the UM-UC-5 cancer cell line (Figure 9B), CD-4 induced a decrease in cell viability across all studied concentrations.

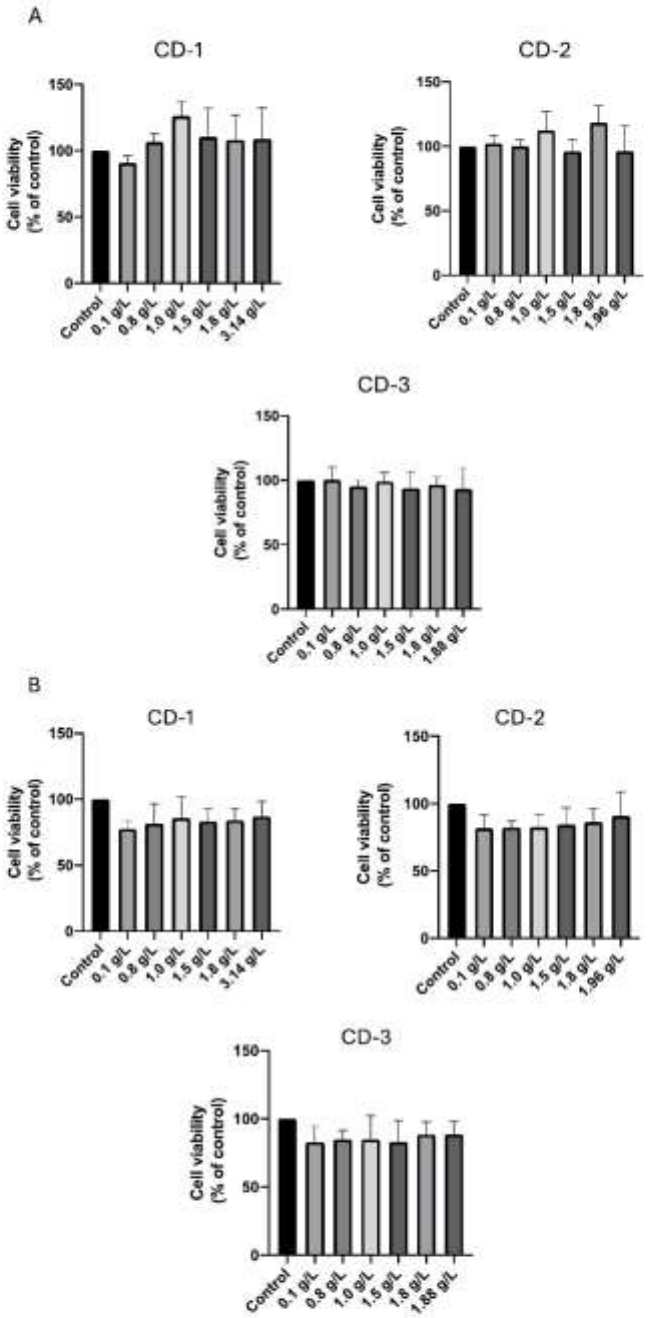

Figure 7. Cell viability of A549 (**A**) and UM-UC-5 (**B**) cancer cells treated with CD-1–3 for 24 h. Cultured cells were seeded in 96-well plates and treated with increasing concentrations of CD-1–3. Cells treated with vehicle (0.1% DMSO) were used as the control. Values are expressed as percentages of control and represent means ± SD. Each experiment was done three times independently ($n = 3$).

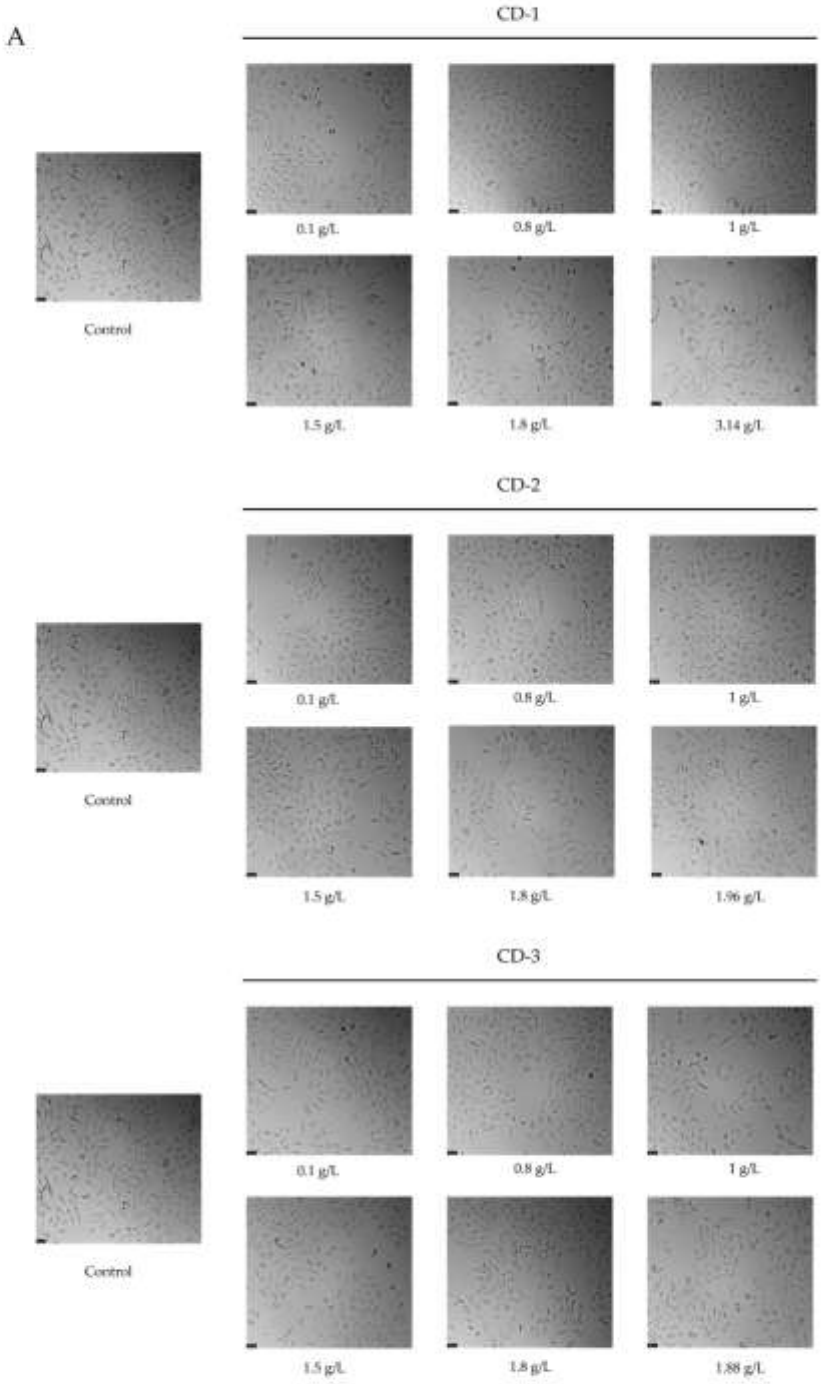

Figure 8. *Cont.*

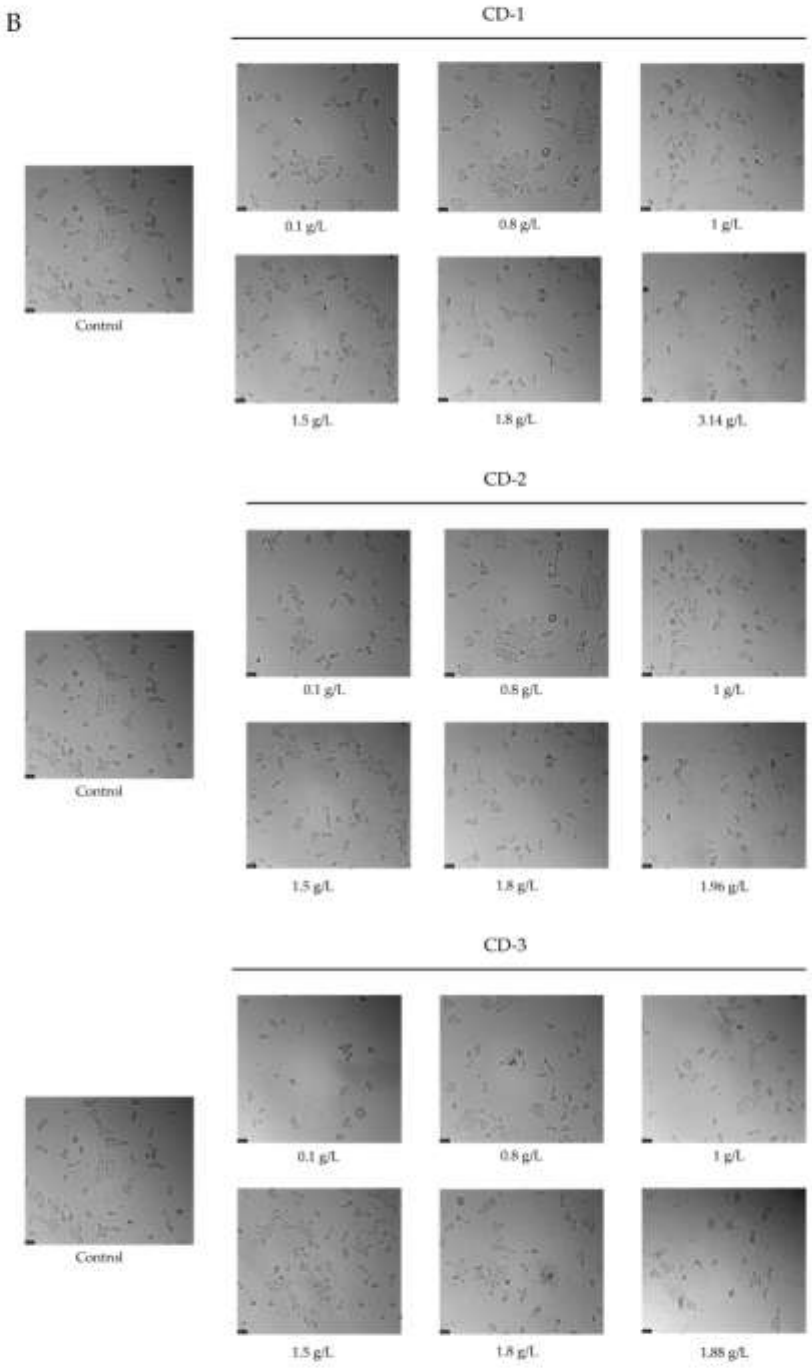

Figure 8. Morphological analysis of A549 (**A**) and UM-UC-5 (**B**) cancer cells treated with CDs for 24 h of incubation.

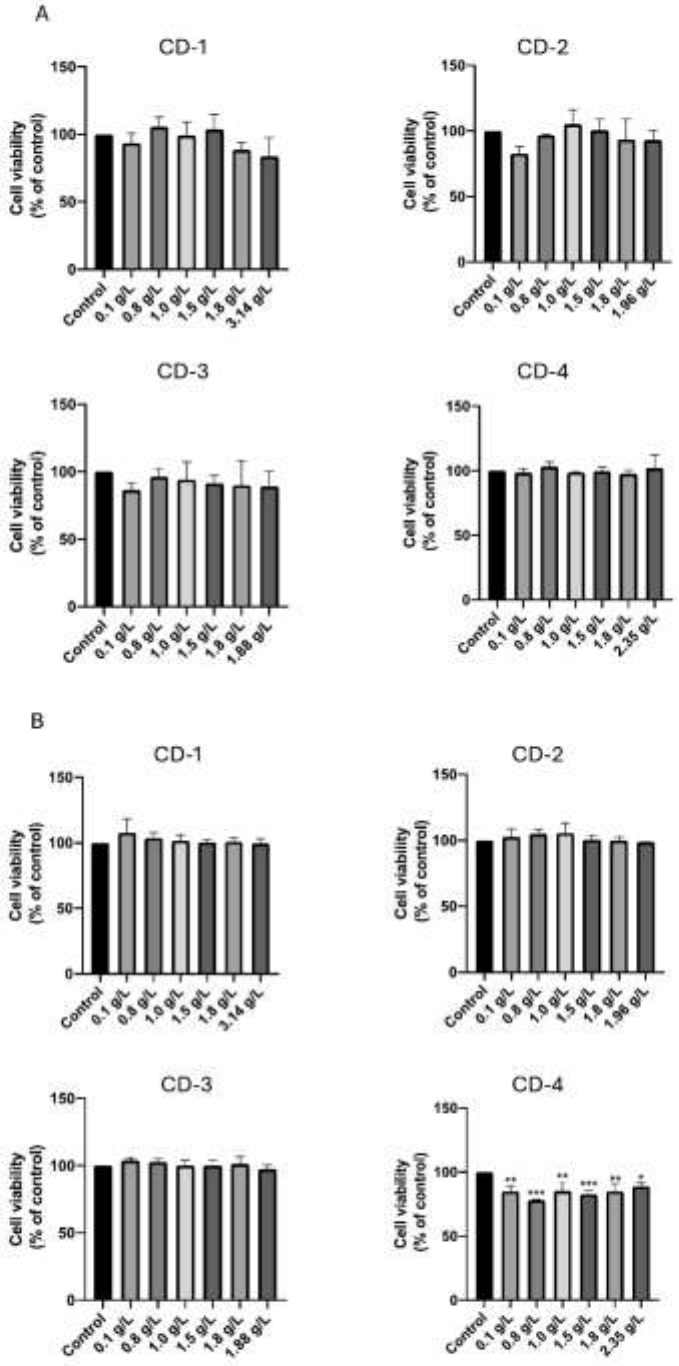

Figure 9. Cell viability of A549 (**A**) and UM-UC-5 (**B**) cancer cells treated with CD-1–4 for 72 h. Cultured cells were seeded in 96-well plates and treated with increasing concentrations of CD-1–4. Cells

treated with vehicle (0.1% DMSO) were used as the control. Values are expressed as percentages of control and represent means ± SD. Each experiment was done three times independently ($n = 3$). * Statistically significant vs. control at $p < 0.1$. ** Statistically significant vs. control at $p < 0.01$. *** Statistically significant vs. control at $p < 0.001$.

Unlike CD-1, CD-2, and CD-3, the results suggest that CD-4 may not be suitable for potential use in UM-UC-5 cancer cell lines due to its impact on cell viability. However, its application in A549 cancer cells appears to be fitting.

In addition, we report here a class of CDs, obtained from a synthesis that is simple and uses organic waste as precursors. These CDs present a safety profile for both A549 and UM-UC-5 cells for future biological applications at different times of incubation.

To gain further insights into the potential applicability of these CDs in drug delivery, we investigated their behavior in the presence of a drug used in cancer treatment, 5-FU [52,53]. We assessed the cell viability of A549 and UM-UC-5 cancer cells with increasing concentrations of CDs (0.1–3.14 g/L), in combination with the IC50 of 5-FU, for each cancer cell line (4.21 µM for UM-UC-5 and 2.42 µM for A549 cells) over 24 and 72 h of incubation. As depicted in Figure 10A, the combination of CD-1, CD-2, and CD-4 with 5-FU only decreased A549 cell viability at a CD concentration of 0.1 g/L. Similar effects were also observed for higher concentrations of CD-2 (1.96 g/L) and CD-4 (1.80 and 2.35 g/L). In contrast, for UM-UC-5 cells (Figure 10B), CDs in combination with 5-FU showed no significant impact on cell viability. Interestingly, with a 72-h incubation period (Figure 11), none of the CDs affected cell viability for both cancer cell lines. These findings suggest that the CDs are protecting the cells and mitigating the effects of 5-FU. This phenomenon could be explained by the CDs' ability to interact with the cells in a way that reduces the cytotoxicity of 5-FU [61,62]. The CDs might be facilitating a mechanism of cellular resistance or altering the uptake of 5-FU by the cancer cells. Another possibility is that the CDs possess antioxidant properties that help protect the cells from the adverse effects of 5-FU [63]. This means that these CDs are not suitable for acting as drug carriers for this type of drug, as they mitigate its therapeutic effect. However, they could be of use in potential applications in which there is a need to mitigate the toxic effects of chemotherapeutic agents.

3.3. Combination Index Evaluation in the Combination of Carbon Dots CD-1–CD-4 with 5-FU in A549 and UM-UC-5 Cancer Cell Lines

To explore the effects of combining the antineoplastic agent 5-FU with CD-1–CD-4 in A549 and UM-UC-5 cancer cell lines, we employed the Chou–Talalay method to calculate the combination index (CI). The CI plot for the combinations of 5-FU with CD-1–4 over 24 h and 72 h are shown in Figures 12 and 13, respectively and illustrate the CI values against the fractional effect (Fa). CI values above one indicates antagonism, values equal to one indicate additivity, and values below one indicate synergism. A Fa value of zero indicates no cell death, whereas a Fa value of one indicates complete cell death. These results are summarized in Table 1.

The combination index plot obtained for the combinations in A549 for 24 h demonstrates that all CI values obtained are above one, which indicates that all combinations present antagonistic interactions. Regarding the UM-UC-5 cell line, the results for the combination of 5-FU with CD-1, 3, and 4 show the same results as above. However, the combination with CD-2 shows synergistic interactions at all concentrations.

After 72 h of incubation, the combination index plot obtained for the combinations in A549 and the results for the A549 cell line remain similar, since almost all the combinations present antagonistic interactions (Table 2). In fact, there are two combinations (1.5 g/L CD-2 and 1.8 g/L CD-3) that come very close to an additive interaction (CI = 1). Regarding the UM-UC-5 cell line, the results for the combination of 5-FU with CDs present antagonistic interactions at all combinations, except for the CD-2 at a concentration of 1 g/L.

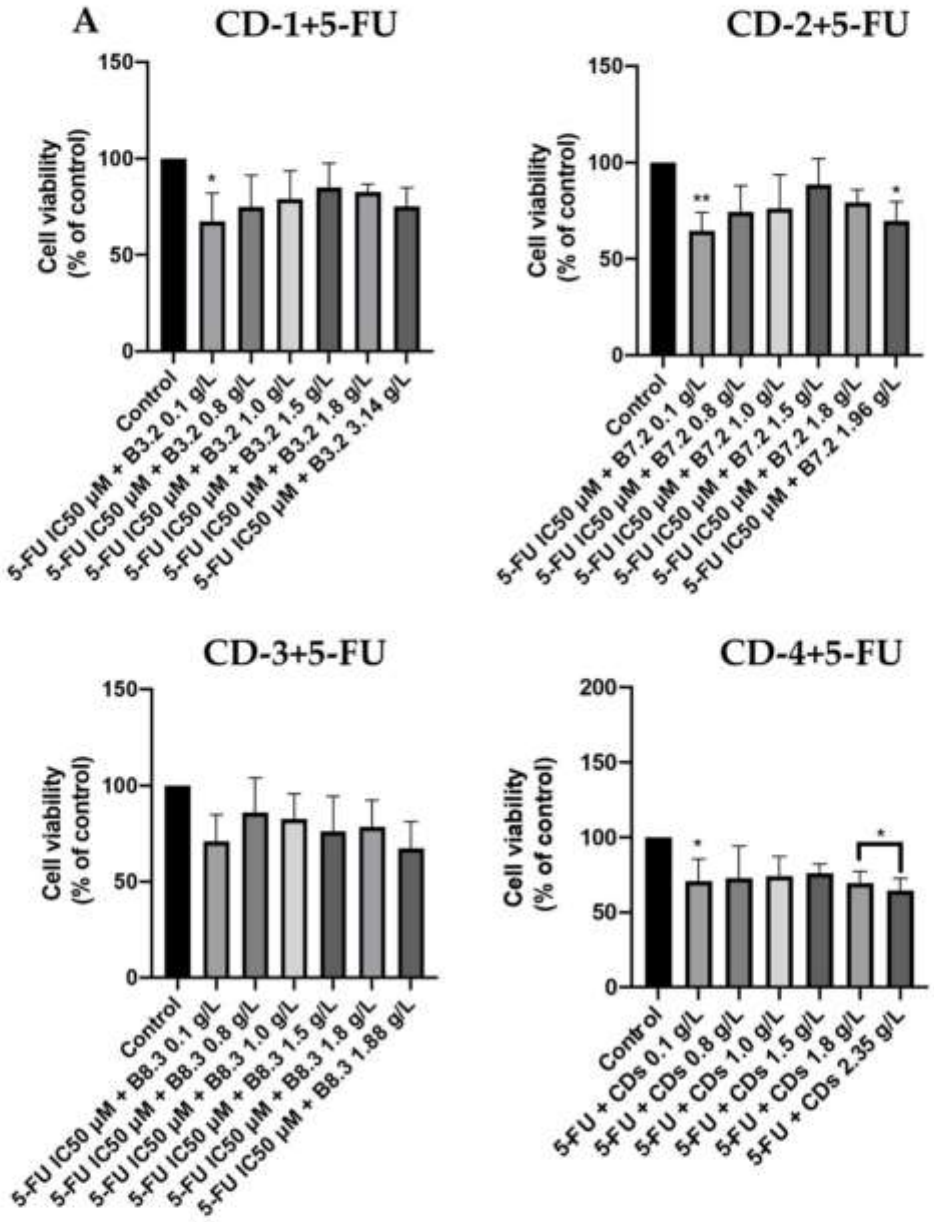

Figure 10. *Cont.*

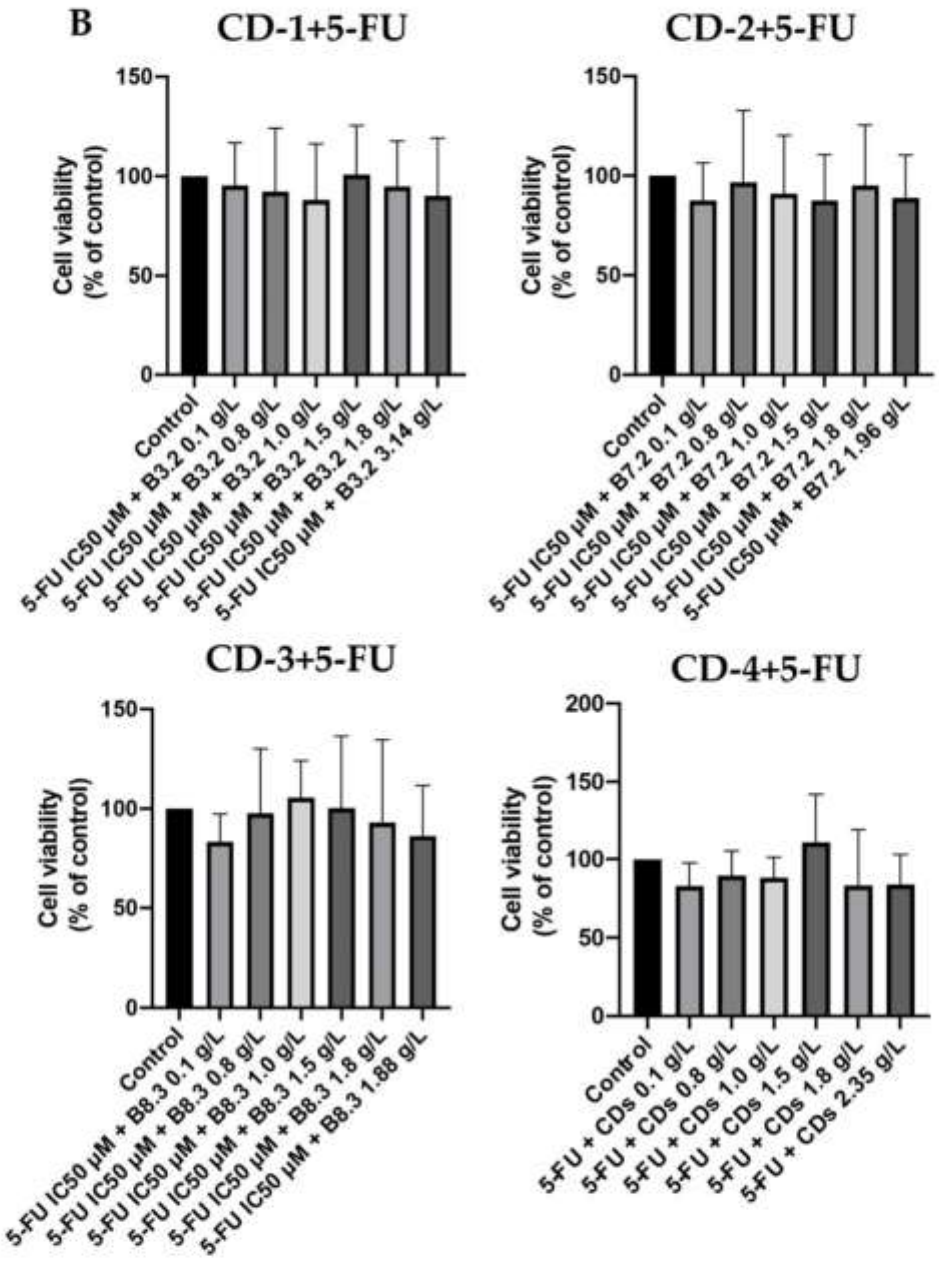

Figure 10. Cell viability of A549 (**A**) and UM-UC-5 (**B**) cancer cells treated with CD-1–4 (0.1–3.14 g/L) in combination with IC50 of 5-FU (4.21 µM for UM-UC-5 and 2.42 µM for A549 cells) for 24 h of incubation. Cells treated with vehicle (0.1% DMSO) were used as the control. Values are expressed as percentages of control and represent means ± SD. Each experiment was done three times independently ($n = 3$). * Statistically significant vs. control at $p < 0.1$. ** Statistically significant vs. control at $p < 0.01$.

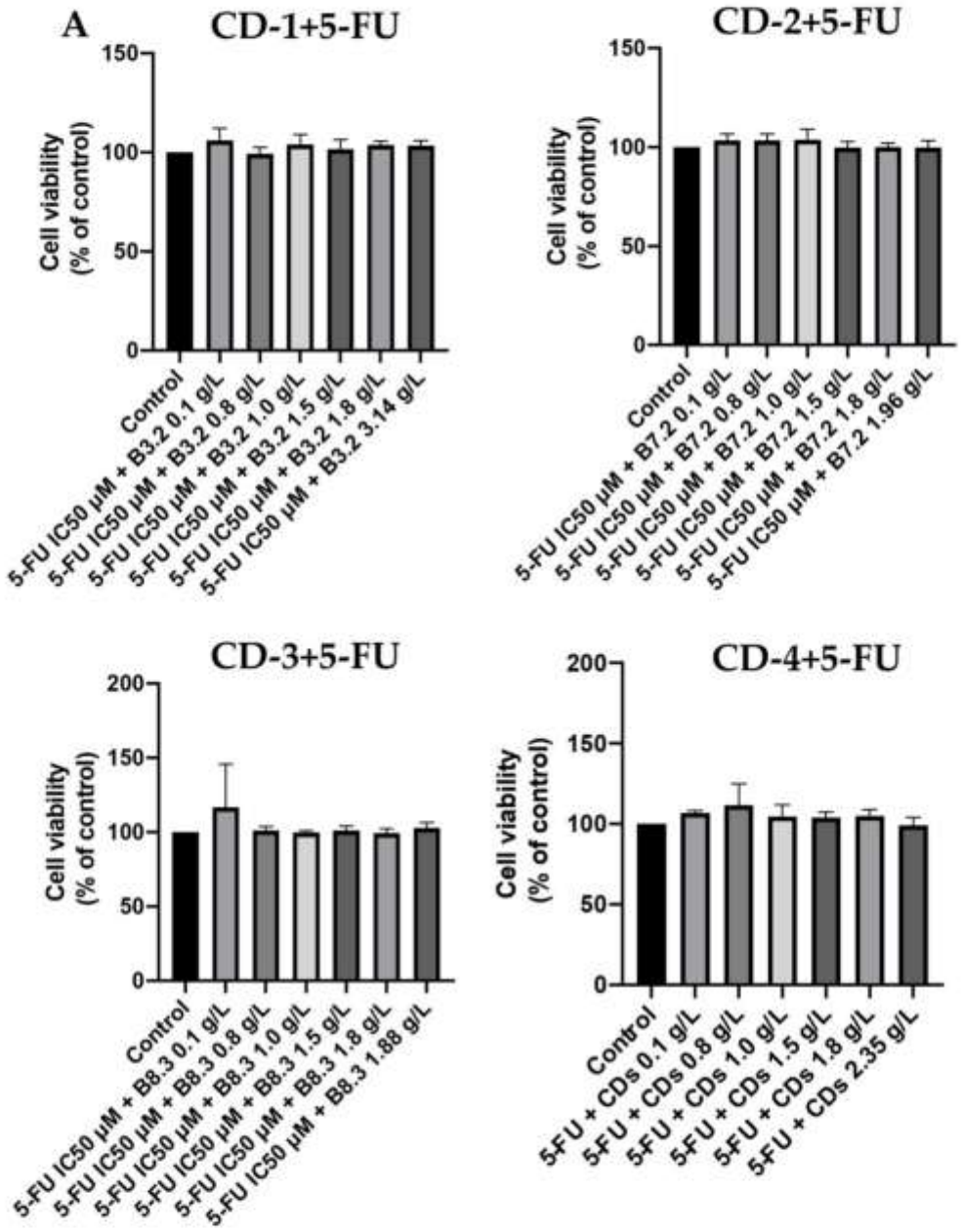

Figure 11. *Cont.*

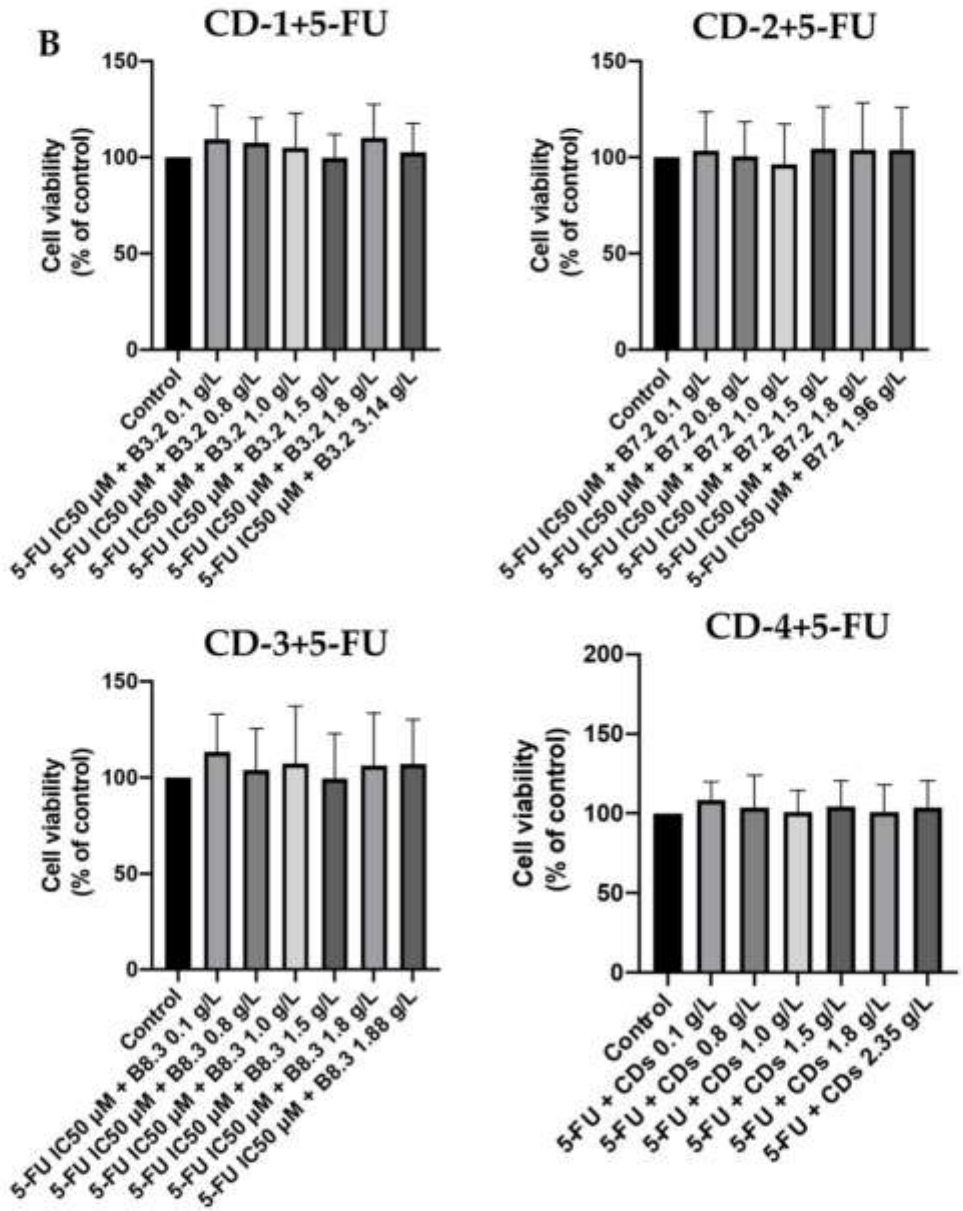

Figure 11. Cell viability of A549 (**A**) and UM-UC-5 (**B**) cancer cells treated with CD-1–4 (0.1–3.14 g/L) in combination with IC50 of 5-FU (4.21 µM for UM-UC-5 and 2.42 µM for A549 cells) for 72 h of incubation. Cells treated with vehicle (0.1% DMSO) were used as the control. Values are expressed as percentages of control and represent means ± SD. Each experiment was done three times independently ($n = 3$).

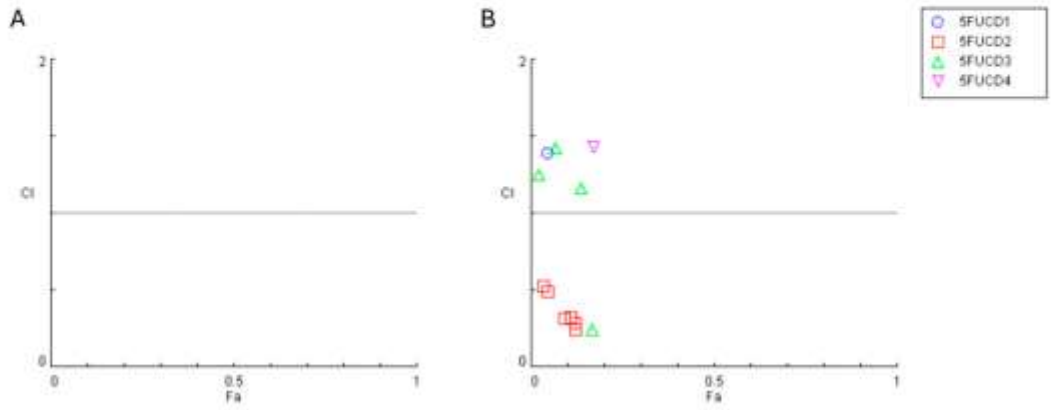

Figure 12. Graphical representation of combination index plot obtained from the CompuSyn Report for the combinations of IC50 5-FU with increasing concentrations of carbon dots 1–4, obtained using the Chou–Talalay method for (**A**) A549 cell line and (**B**) UM-UC-5 cell line for 24 h.

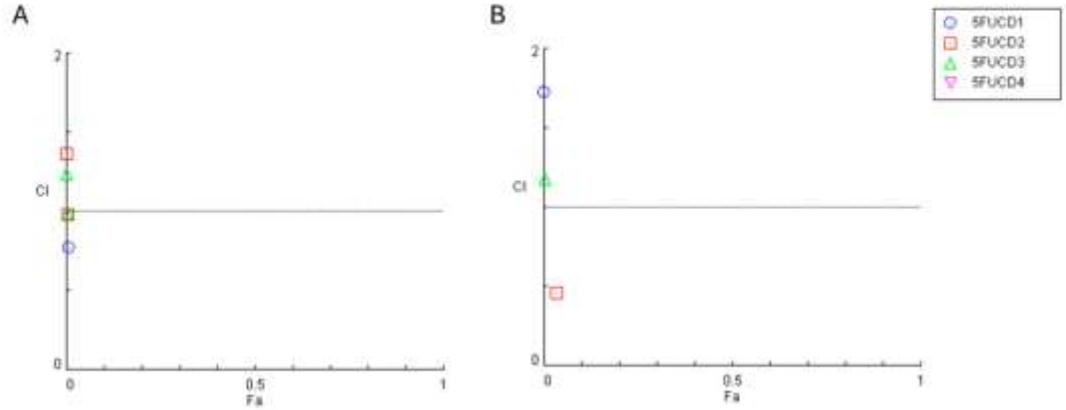

Figure 13. Graphical representation of combination index plot obtained from the CompuSyn Report for the combinations of IC50 5-FU with increasing concentrations of carbon dots 1–4, obtained using the Chou–Talalay method for (**A**) A549 cell line and (**B**) UM-UC-5 cell line for 72 h.

Table 1. Fa and CI values of carbon dots and 5-FU (2.42 μM for A549 or 4.21 for UM-UC-5) combinations for 24 h in A549 and UM-UC-5 cells. CI in bold indicates drug pairs that are synergic and addictive.

Cell Line	Carbon Dot (g/L)	CD-1		CD-2		CD-3		CD-4	
		Fa	CI	Fa	CI	Fa	CI	Fa	CI
A549	0.1	0.32571	>10	0.35358	4.07950	0.29050	>10	0.29327	>10
	0.8	0.25045	>10	0.25625	>10	0.14106	>10	0.27112	>10
	1.0	0.21080	>10	0.23775	>10	0.17399	>10	0.25960	>10
	1.5	0.14973	>10	0.11464	>10	0.24125	>10	0.23729	>10
	1.8	0.17149	>10	0.20749	>10	0.21533	>10	0.30515	>10
	3.14/1.96/1.88/2.35	0.24841	2.5×10^7	0.30239	>10	0.32533	>10	0.35487	2.0×10^7

Table 1. *Cont.*

Cell Line	Carbon Dot (g/L)	CD-1		CD-2		CD-3		CD-4	
UM-UC-5	0.1	0.04691	1.38739	0.12282	**0.24168**	0.16829	**0.24545**	0.17125	1.42858
	0.8	0.07871	9.49265	0.03349	**0.52381**	0.02238	1.25008	0.10344	6.23997
	1.0	0.12014	>10	0.09244	**0.31672**	1.0×10^{-6}	>10	0.11796	8.72487
	1.5	1.0×10^{-6}	>10	0.12338	**0.28694**	1.0×10^{-6}	>10	1.0×10^{-6}	>10
	1.8	0.05181	>10	0.04826	**0.48553**	0.06963	1.42030	0.16593	>10
	3.14/1.96/1.88/2.35	0.09961	>10	0.11033	**0.32097**	0.13757	1.16018	0.16034	>10

Table 2. Fractional effect (Fa) and CI values of carbon dots and 5-FU (2.42 µM for A549 or 4.21 for UM-UC-5) combinations for 72 h in A549 and UM-UC-5 cells. CI in bold indicates drug pairs that are synergic and addictive.

Cell Line	Carbon Dot (g/L)	CD-1		CD-2		CD-3		CD-4	
		Fa	CI	Fa	CI	Fa	CI	Fa	CI
A549	0.1	1.0×10^{-6}	>10	1.0×10^{-6}	>10	1.0×10^{-6}	>10	1.0×10^{-6}	>10
	0.8	0.00689	**0.76924**	1.0×10^{-6}	>10	1.0×10^{-6}	>10	1.0×10^{-6}	>10
	1.0	1.0×10^{-6}	>10	1.0×10^{-6}	>10	0.00228	1.23695	1.0×10^{-6}	>10
	1.5	1.0×10^{-6}	>10	0.00368	**0.98253**	1.0×10^{-6}	>10	1.0×10^{-6}	>10
	1.8	1.0×10^{-6}	>10	1.0×10^{-6}	>10	0.00365	**0.99106**	1.0×10^{-6}	>10
	3.14/1.96/1.88/2.35	1.0×10^{-6}	>10	0.00187	1.36813	1.0×10^{-6}	>10	0.00760	>10
UM-UC-5	0.1	1.0×10^{-6}	>10	1.0×10^{-6}	>10	1.0×10^{-6}	>10	1.0×10^{-6}	>10
	0.8	1.0×10^{-6}	>10	1.0×10^{-6}	>10	1.0×10^{-6}	>10	1.0×10^{-6}	>10
	1.0	1.0×10^{-6}	>10	0.03624	**0.45725**	1.0×10^{-6}	>10	1.0×10^{-6}	>10
	1.5	0.00255	1.73160	1.0×10^{-6}	>10	0.00554	1.17674	1.0×10^{-6}	>10
	1.8	1.0×10^{-6}	>10	1.0×10^{-6}	>10	1.0×10^{-6}	>10	1.0×10^{-6}	>10
	3.14/1.96/1.88/2.35	1.0×10^{-6}	>10	1.0×10^{-6}	>10	1.0×10^{-6}	>10	1.0×10^{-6}	>10

4. Conclusions

Recent research on carbon dots (CDs) has highlighted their potential as valuable assets for applications in bioimaging and drug delivery, among others. Considering this, in this study, we successfully synthesized four distinct N-doped CDs using a hydrothermal methodology. In addition, CDs were obtained from a "green" synthesis that is simple and uses organic waste as a precursor. In our investigation into the applicability of these nanoparticles for bioimaging and drug delivery, we examined their potential cytotoxic effects on A549 and UM-UC-5 cell lines. The 24-h incubation period showed no discernible effects on cellular viability, indicating that the CDs did not induce cytotoxicity within this timeframe. Morphological evaluations at 24 h revealed no notable changes in cell phenotype. Extended incubation periods of 72 h demonstrated that CD-4 might not be suitable for UM-UC-5 cancer cells due to its effects on cell viability and morphology. In contrast, all four nanoparticles proved promising for applications in A549 cancer cells, emphasizing their potential in different contexts using these cancer cells. Further exploration of combination assays with a chemotherapeutic drug (5-FU) revealed that the CDs protect the cells and mitigate the toxic effects of this drug. It was also observed that most CDs presented antagonistic interaction with 5-FU, except CD-2, which presented synergistic interaction, opening a new strategy for future studies in which CDs can be employed as chemoprotective agents.

Author Contributions: Conceptualization, L.P.d.S. and N.V.; investigation, C.M.M., E.R. and S.F.; writing—original draft preparation, C.M.M., E.R. and S.F.; writing—review and editing, L.P.d.S., J.E.d.S. and N.V.; visualization, C.M.M. and E.R.; supervision, L.P.d.S., N.V. and S.F.; funding acquisition, L.P.d.S., J.E.d.S. and N.V. All authors have read and agreed to the published version of the manuscript.

Funding: The Portuguese "Fundação para a Ciência e Tecnologia" (FCT, Lisbon) is acknowledged for funding of projects PTDC/QUI-QFI/2870/2020 (http://doi.org/10.54499/PTDC/QUI-QFI/2870/2020) and 2023.13127.PEX, R&D Units CIQUP (UIDB/00081/2020 and UIDP/00081/2020), and Associated Laboratory IMS (LA/P/0056/2020). Luís Pinto da Silva acknowledges funding from FCT under the Scientific Employment Stimulus (CEECINST/00069/2021). Carla Magalhães acknowledges FCT for funding her PhD grant (SFRH/143211/2019). NV acknowledges funding from FCT in the framework of projects IF/00092/2014/CP1255/CT0004 and CHAIR in Onco-Innovation.

Institutional Review Board Statement: Not applicable.

Informed Consent Statement: Not applicable.

Data Availability Statement: The original contributions presented in the study are included in the article, further inquiries can be directed to the corresponding author/s.

Acknowledgments: E.R. acknowledges CHAIR in Onco-Innovation for supporting her PhD project. CEMUP is acknowledged for AFM analysis, and FCUP|DQB—Lab&Services for Zeta Potential measurements.

Conflicts of Interest: The authors declare no conflict of interest.

References

1. Health Professional|Cancer Research UK. Available online: https://www.cancerresearchuk.org/health-professional/ (accessed on 24 October 2023).
2. Kreso, A.; Dick, J.E. Evolution of the Cancer Stem Cell Model. *Cell Stem Cell* **2014**, *14*, 275–291. [CrossRef] [PubMed]
3. Gavas, S.; Quazi, S.; Karpiński, T.M. Nanoparticles for Cancer Therapy: Current Progress and Challenges. *Nanoscale Res. Lett.* **2021**, *16*, 173. [CrossRef] [PubMed]
4. Carneiro, B.A.; El-Deiry, W.S. Targeting Apoptosis in Cancer Therapy. *Nat. Rev. Clin. Oncol.* **2020**, *17*, 395–417. [CrossRef] [PubMed]
5. Zhang, Q.-Y.; Wang, F.-X.; Jia, K.-K.; Kong, L.-D. Natural Product Interventions for Chemotherapy and Radiotherapy-Induced Side Effects. *Front. Pharmacol.* **2018**, *9*, 1253. [CrossRef] [PubMed]
6. Oun, R.; Moussa, Y.E.; Wheate, N.J. The Side Effects of Platinum-Based Chemotherapy Drugs: A Review for Chemists. *Dalton Trans.* **2018**, *47*, 6645–6653. [CrossRef] [PubMed]
7. Sterner, R.C.; Sterner, R.M. CAR-T Cell Therapy: Current Limitations and Potential Strategies. *Blood Cancer J.* **2021**, *11*, 69. [CrossRef]
8. Nocito, G.; Calabrese, G.; Forte, S.; Petralia, S.; Puglisi, C.; Campolo, M.; Esposito, E.; Conoci, S. Carbon Dots as Promising Tools for Cancer Diagnosis and Therapy. *Cancers* **2021**, *13*, 1991. [CrossRef] [PubMed]
9. Milewska, S.; Niemirowicz-Laskowska, K.; Siemiaszko, G.; Nowicki, P.; Wilczewska, A.Z.; Car, H. Current Trends and Challenges in Pharmacoeconomic Aspects of Nanocarriers as Drug Delivery Systems for Cancer Treatment. *Int. J. Nanomed.* **2021**, *16*, 6593–6644. [CrossRef]
10. Kirtane, A.R.; Verma, M.; Karandikar, P.; Furin, J.; Langer, R.; Traverso, G. Nanotechnology Approaches for Global Infectious Diseases. *Nat. Nanotechnol.* **2021**, *16*, 369–384. [CrossRef]
11. Liu, J.; Li, R.; Yang, B. Carbon Dots: A New Type of Carbon-Based Nanomaterial with Wide Applications. *ACS Cent. Sci.* **2020**, *6*, 2179–2195. [CrossRef]
12. Wang, H.; Zhou, L.; Yu, H.; Tang, X.; Xing, C.; Nie, G.; Akafzade, H.; Wang, S.; Chen, W. Exploration of Room-Temperature Phosphorescence and New Mechanism on Carbon Dots in a Polyacrylamide Platform and Their Applications for Anti-Counterfeiting and Information Encryption. *Adv. Opt. Mater.* **2022**, *10*, 2200678. [CrossRef]
13. Fang, M.; Wang, B.; Qu, X.; Li, S.; Huang, J.; Li, J.; Lu, S.; Zhou, N. State-of-the-Art of Biomass-Derived Carbon Dots: Preparation, Properties, and Applications. *Chin. Chem. Lett.* **2024**, *35*, 108423. [CrossRef]
14. Dang, Y.; Guan, J. Nanoparticle-Based Drug Delivery Systems for Cancer Therapy. *Smart Mater. Med.* **2020**, *1*, 10–19. [CrossRef] [PubMed]
15. Xin, Y.; Yin, M.; Zhao, L.; Meng, F.; Luo, L. Recent Progress on Nanoparticle-Based Drug Delivery Systems for Cancer Therapy. *Cancer Biol. Med.* **2017**, *14*, 228. [CrossRef]
16. Couvreur, P. Nanoparticles in Drug Delivery: Past, Present and Future. *Adv. Drug Deliv. Rev.* **2013**, *65*, 21–23. [CrossRef] [PubMed]
17. Cho, K.; Wang, X.; Nie, S.; Chen, Z.; Shin, D.M. Therapeutic Nanoparticles for Drug Delivery in Cancer. *Clin. Cancer Res.* **2008**, *14*, 1310–1316. [CrossRef] [PubMed]

18. Wilczewska, A.Z.; Niemirowicz, K.; Markiewicz, K.H.; Car, H. Nanoparticles as Drug Delivery Systems. *Pharmacol. Rep.* **2012**, *64*, 1020–1037. [CrossRef]
19. Adrita, S.; Tasnim, K.; Ryu, J.; Sharker, S. Nanotheranostic Carbon Dots as an Emerging Platform for Cancer Therapy. *J. Nanotheranostics* **2020**, *1*, 58–77. [CrossRef]
20. Rao, N.; Singh, R.; Bashambu, L. Carbon-Based Nanomaterials: Synthesis and Prospective Applications. *Mater. Today Proc.* **2021**, *44*, 608–614. [CrossRef]
21. Xie, P.; Yuan, W.; Liu, X.; Peng, Y.; Yin, Y.; Li, Y.; Wu, Z. Advanced Carbon Nanomaterials for State-of-the-Art Flexible Supercapacitors. *Energy Storage Mater.* **2021**, *36*, 56–76. [CrossRef]
22. Saleh, T.A. Nanomaterials: Classification, Properties, and Environmental Toxicities. *Environ. Technol. Innov.* **2020**, *20*, 101067. [CrossRef]
23. Su, W.; Wu, H.; Xu, H.; Zhang, Y.; Li, Y.; Li, X.; Fan, L. Carbon Dots: A Booming Material for Biomedical Applications. *Mater. Chem. Front.* **2020**, *4*, 821–836. [CrossRef]
24. Mikhraliieva, A.; Zaitsev, V.; Xing, Y.; Coelho-Júnior, H.; Sommer, R.L. Excitation-Independent Blue-Emitting Carbon Dots from Mesoporous Aminosilica Nanoreactor for Bioanalytical Application. *ACS Appl. Nano Mater.* **2020**, *3*, 3652–3664. [CrossRef]
25. Innocenzi, P.; Stagi, L. Carbon-Based Antiviral Nanomaterials: Graphene, C-Dots, and Fullerenes. A Perspective. *Chem. Sci.* **2020**, *11*, 6606–6622. [CrossRef]
26. Pandiyan, S.; Arumugam, L.; Srirengan, S.P.; Pitchan, R.; Sevugan, P.; Kannan, K.; Pitchan, G.; Hegde, T.A.; Gandhirajan, V. Biocompatible Carbon Quantum Dots Derived from Sugarcane Industrial Wastes for Effective Nonlinear Optical Behavior and Antimicrobial Activity Applications. *ACS Omega* **2020**, *5*, 30363–30372. [CrossRef]
27. Wang, B.; Song, H.; Qu, X.; Chang, J.; Yang, B.; Lu, S. Carbon Dots as a New Class of Nanomedicines: Opportunities and Challenges. *Coord. Chem. Rev.* **2021**, *442*, 214010. [CrossRef]
28. Xia, C.; Zhu, S.; Feng, T.; Yang, M.; Yang, B. Evolution and Synthesis of Carbon Dots: From Carbon Dots to Carbonized Polymer Dots. *Adv. Sci.* **2019**, *6*, 1901316. [CrossRef]
29. Ali, H.; Ghosh, S.; Jana, N.R. Fluorescent Carbon Dots as Intracellular Imaging Probes. *WIREs Nanomed. Nanobiotechnol.* **2020**, *12*, e1617. [CrossRef]
30. Kang, Z.; Lee, S.-T. Carbon Dots: Advances in Nanocarbon Applications. *Nanoscale* **2019**, *11*, 19214–19224. [CrossRef] [PubMed]
31. Vale, N.; Silva, S.; Duarte, D.; Crista, D.M.A.; Pinto da Silva, L.; Esteves da ValeVale, J.C.G. Normal Breast Epithelial MCF-10A Cells to Evaluate the Safety of Carbon Dots. *RSC Med. Chem.* **2021**, *12*, 245–253. [CrossRef]
32. Crista, D.M.A.; Esteves da Silva, J.C.G.; Pinto da Silva, L. Evaluation of Different Bottom-up Routes for the Fabrication of Carbon Dots. *Nanomaterials* **2020**, *10*, 1316. [CrossRef] [PubMed]
33. Sendão, R.M.S.; Crista, D.M.A.; Afonso, A.C.P.; Martinez de Yuso, M.D.V.; Algarra, M.; Esteves da Silva, J.C.G.; Pinto da Silva, L.P. Insight into the Hybrid Luminescence Showed by Carbon Dots and Molecular Fluorophores in Solution. *Phys. Chem. Chem. Phys.* **2019**, *21*, 20919–20926. [CrossRef]
34. Wang, Y.; Hu, A. Carbon Quantum Dots: Synthesis, Properties and Applications. *J. Mater. Chem. C Mater.* **2014**, *2*, 6921. [CrossRef]
35. Luo, P.G.; Yang, F.; Yang, S.-T.; Sonkar, S.K.; Yang, L.; Broglie, J.J.; Liu, Y.; Sun, Y.-P. Carbon-Based Quantum Dots for Fluorescence Imaging of Cells and Tissues. *RSC Adv.* **2014**, *4*, 10791. [CrossRef]
36. Jing, H.; Bardakci, F.; Akgöl, S.; Kusat, K.; Adnan, M.; Alam, M.; Gupta, R.; Sahreen, S.; Chen, Y.; Gopinath, S.; et al. Green Carbon Dots: Synthesis, Characterization, Properties and Biomedical Applications. *J. Funct. Biomater.* **2023**, *14*, 27. [CrossRef]
37. Carbonaro, C.M.; Chiriu, D.; Stagi, L.; Casula, M.F.; Thakkar, S.V.; Malfatti, L.; Suzuki, K.; Ricci, P.C.; Corpino, R. Carbon Dots in Water and Mesoporous Matrix: Chasing the Origin of Their Photoluminescence. *J. Phys. Chem. C* **2018**, *122*, 25638–25650. [CrossRef]
38. Zhang, Q.; Wang, R.; Feng, B.; Zhong, X.; Ostrikov, K. Photoluminescence Mechanism of Carbon Dots: Triggering High-Color-Purity Red Fluorescence Emission through Edge Amino Protonation. *Nat. Commun.* **2021**, *12*, 6856. [CrossRef]
39. Dong, X.; Liang, W.; Meziani, M.J.; Sun, Y.-P.; Yang, L. Carbon Dots as Potent Antimicrobial Agents. *Theranostics* **2020**, *10*, 671–686. [CrossRef] [PubMed]
40. Kasprzyk, W.; Świergosz, T.; Bednarz, S.; Walas, K.; Bashmakova, N.V.; Bogdał, D. Luminescence Phenomena of Carbon Dots Derived from Citric Acid and Urea—A Molecular Insight. *Nanoscale* **2018**, *10*, 13889–13894. [CrossRef]
41. Simões, E.F.C.; Esteves da Silva, J.C.G.; Leitão, J.M.M. Peroxynitrite and Nitric Oxide Fluorescence Sensing by Ethylenediamine Doped Carbon Dots. *Sens. Actuators B Chem.* **2015**, *220*, 1043–1049. [CrossRef]
42. Rao, L.; Tang, Y.; Lu, H.; Yu, S.; Ding, X.; Xu, K.; Li, Z.; Zhang, J. Highly Photoluminescent and Stable N-Doped Carbon Dots as Nanoprobes for Hg^{2+} Detection. *Nanomaterials* **2018**, *8*, 900. [CrossRef] [PubMed]
43. Zhou, J.; Zhou, H.; Tang, J.; Deng, S.; Yan, F.; Li, W.; Qu, M. Carbon Dots Doped with Heteroatoms for Fluorescent Bioimaging: A Review. *Microchim. Acta* **2017**, *184*, 343–368. [CrossRef]
44. Jiang, L.; Ding, H.; Lu, S.; Geng, T.; Xiao, G.; Zou, B.; Bi, H. Photoactivated Fluorescence Enhancement in F,N-Doped Carbon Dots with Piezochromic Behavior. *Angew. Chem.* **2020**, *132*, 10072–10077. [CrossRef]
45. Crista, D.M.A.; El Mragui, A.; Algarra, M.; Esteves da Silva, J.C.G.; Luque, R.; Pinto da Silva, L. Turning Spent Coffee Grounds into Sustainable Precursors for the Fabrication of Carbon Dots. *Nanomaterials* **2020**, *10*, 1209. [CrossRef]
46. John, B.K.; Abraham, T.; Mathew, B. A Review on Characterization Techniques for Carbon Quantum Dots and Their Applications in Agrochemical Residue Detection. *J. Fluoresc.* **2022**, *32*, 449–471. [CrossRef]

47. Long, W.-J.; Li, X.-Q.; Yu, Y.; He, C. Green Synthesis of Biomass-Derived Carbon Dots as an Efficient Corrosion Inhibitor. *J. Mol. Liq.* **2022**, *360*, 119522. [CrossRef]
48. Li, C.-L.; Ou, C.-M.; Huang, C.-C.; Wu, W.-C.; Chen, Y.-P.; Lin, T.-E.; Ho, L.-C.; Wang, C.-W.; Shih, C.-C.; Zhou, H.-C.; et al. Carbon Dots Prepared from Ginger Exhibiting Efficient Inhibition of Human Hepatocellular Carcinoma Cells. *J. Mater. Chem. B* **2014**, *2*, 4564. [CrossRef]
49. Xie, Y.; Filchakova, O.; Yang, Q.; Yesbolatov, Y.; Tursynkhan, D.; Kassymbek, A.; Bouhrara, M.; Wang, K.; Balanay, M.; Fan, H. Inhibition of Cancer Cell Proliferation by Carbon Dots Derived from Date Pits at Low-Dose. *ChemistrySelect* **2017**, *2*, 4079–4083. [CrossRef]
50. Wan, J.; Xu, S.; Li, J.; Yu, M.; Zhang, K.; Wei, G.; Su, Z. Facile Synthesis of Multifunctional Pharmaceutical Carbon Dots for Targeted Bioimaging and Chemotherapy of Tumors. *Nanoscale* **2022**, *14*, 11359–11368. [CrossRef]
51. Fernandes, S.; Algarra, M.; Gil, A.; Esteves da Silva, J.; Pinto da Silva, L. Development of a Facile and Green Synthesis Strategy for Brightly Fluorescent Carbon Dots from Various Waste Materials. *ChemSusChem* **2024**, e202401702. [CrossRef]
52. Katharotiya, K.; Shinde, G.; Katharotiya, D.; Shelke, S.; Patel, R.; Kulkarni, D.; Panzade, P. Development, Evaluation and Biodistribution of Stealth Liposomes of 5-Fluorouracil for Effective Treatment of Breast Cancer. *J. Liposome Res.* **2022**, *32*, 146–158. [CrossRef] [PubMed]
53. Mawalizadeh, F.; Mohammadzadeh, G.; Khedri, A.; Rashidi, M. Quercetin Potentiates the Chemosensitivity of MCF-7 Breast Cancer Cells to 5-Fluorouracil. *Mol. Biol. Rep.* **2021**, *48*, 7733–7742. [CrossRef] [PubMed]
54. Eaton, D.F. Reference Materials for Fluorescence Measurement. *Pure Appl. Chem.* **1988**, *60*, 1107–1114. [CrossRef]
55. Sendão, R.M.S.; Algarra, M.; Ribeiro, E.; Pereira, M.; Gil, A.; Vale, N.; Esteves da Silva, J.C.G.; Pinto da Silva, L. Carbon Dots–TiO_2 Nanocomposites for the Enhanced Visible-Light Driven Photodegradation of Methylene Blue. *Adv. Sustain. Syst.* **2023**. [CrossRef]
56. Melhuish, W.H. Quantum Efficiencies of Fluorescence of Organic Substances: Effect of Solvent and Concentration of the Fluorescent Solute. *J. Phys. Chem.* **1961**, *65*, 229–235. [CrossRef]
57. Sharma, A.; Gadly, T.; Gupta, A.; Ballal, A.; Ghosh, S.K.; Kumbhakar, M. Origin of Excitation Dependent Fluorescence in Carbon Nanodots. *J. Phys. Chem. Lett.* **2016**, *7*, 3695–3702. [CrossRef]
58. Wang, W.; Wang, B.; Embrechts, H.; Damm, C.; Cadranel, A.; Strauss, V.; Distaso, M.; Hinterberger, V.; Guldi, D.M.; Peukert, W. Shedding Light on the Effective Fluorophore Structure of High Fluorescence Quantum Yield Carbon Nanodots. *RSC Adv.* **2017**, *7*, 24771–24780. [CrossRef]
59. Christé, S.; Esteves da Silva, J.C.; Pinto da Silva, L. Evaluation of the Environmental Impact and Efficiency of N-Doping Strategies in the Synthesis of Carbon Dots. *Materials* **2020**, *13*, 504. [CrossRef]
60. Sendão, R.M.S.; Esteves da Silva, J.C.G.; Pinto da Silva, L. Photocatalytic Removal of Pharmaceutical Water Pollutants by TiO_2—Carbon Dots Nanocomposites: A Review. *Chemosphere* **2022**, *301*, 134731. [CrossRef]
61. Esfandiari, N.; Bagheri, Z.; Ehtesabi, H.; Fatahi, Z.; Tavana, H.; Latifi, H. Effect of Carbonization Degree of Carbon Dots on Cytotoxicity and Photo-Induced Toxicity to Cells. *Heliyon* **2019**, *5*, e02940. [CrossRef]
62. Kaurav, H.; Verma, D.; Bansal, A.; Kapoor, D.N.; Sheth, S. Progress in Drug Delivery and Diagnostic Applications of Carbon Dots: A Systematic Review. *Front. Chem.* **2023**, *11*, 1227843. [CrossRef] [PubMed]
63. Gao, F.; Liu, J.; Gong, P.; Yang, Y.; Jiang, Y. Carbon Dots as Potential Antioxidants for the Scavenging of Multi-Reactive Oxygen and Nitrogen Species. *Chem. Eng. J.* **2023**, *462*, 142338. [CrossRef]